THE
PHYSICAL REVIEW
A journal of experimental and theoretical physics established by E. L. Nichols in 1893

VOL. 62, NOS. 5 AND 6 SEPTEMBER 1 AND 15, 1942 SECOND SERIES

Nuclear Excitations Resulting from Radioactive Decay

E. H. PLESSET*
Randal Morgan Laboratory of Physics, University of Pennsylvania, Philadelphia, Pennsylvania
(Received May 29, 1942)

The radiations emitted by several radioactive nuclei have been investigated with a permanent β-ray magnet spectrograph. Four transitions have been found to result from the decay of Co^{57}. No internally converted radiation is emitted by Zn^{65} in the region 20–300 kev. A complicated spectrum is emitted by the products of deuteron bombardment of gold, which has been only partially resolved.

INTRODUCTION

A PERMANENT magnet β-ray spectrograph has been used to study internal conversion electrons and γ-rays. Photographic detection has been employed. Radii of electron curvature between 2.0 cm and 11.4 cm could be observed with deflecting fields ranging as high as 2300 oersteds. Field measurements are considered reliable to within $\frac{1}{2}$ percent.[1]

RADIOACTIVE COBALT

A. Assignment of Isotopes

The following assignments for the 72- and 270-day half-life activities have been proposed by J. J. Livingood and G. T. Seaborg,[2] assuming Co^{57} to be non-stable:[3]

Co^{58}: 72-day, β^+, range 0.12 g/cm² of Al;
Co^{57}: 270-day, β^+, range 0.06 g/cm² of Al;
Co^{56}: 72-day, β^+, range 0.5 g/cm² of Al.

Absorption measurements of the radiations from sources showing 72-day and 270-day half-lives have been carried out by the author.

The cobalt activities produced by high energy deuteron bombardment of iron (16 Mev), nickel (11 Mev), and α-particle bombardment of manganese (22 Mev) were examined. The following non-stable isotopes can be produced by the Fe (d, n) Co reaction:[2]

Co^{55} (from Fe^{54}, 6.04 percent), known 18.2-hr. activity;
Co^{57} (from Fe^{56}, 91.57 percent), 270-day;
Co^{58} (from Fe^{57}, 2.11 percent), 72-day;

and, the following, by Fe $(d, 2n)$ Co:[2]

Co^{54} (from Fe^{54}, 6.04 percent), not observed;
Co^{56} (from Fe^{56}, 91.57 percent), 72-day;
Co^{57} (from Fe^{57}, 2.11 percent), 270-day.

Bombardment of nickel may produce radioactive cobalt isotopes by (d, α) reactions. The products expected are:

Co^{56} (from Ni^{58}, 68 percent);
Co^{58} (from Ni^{60}, 27.2 percent);
Co^{60} (from Ni^{62}, 3.8 percent) (10.7 min., 5.3 years).

The 5.3-year activity is produced much less in-

* Now at David Taylor Model Basin, Navy Department, Washington, D. C.

[1] The magnet, the spectrograph, and the associated technique have been described in a paper submitted by E. H. Plesset, G. P. Harnwell, and F. G. P. Seidl to the Rev. Sci. Inst.

[2] J. J. Livingood and G. T. Seaborg, Phys. Rev. **60**, 913 (1941).

[3] J. J. Mitchell, H. S. Brown and R. D. Fowler, Phys. Rev. **60**, 359 (1940).

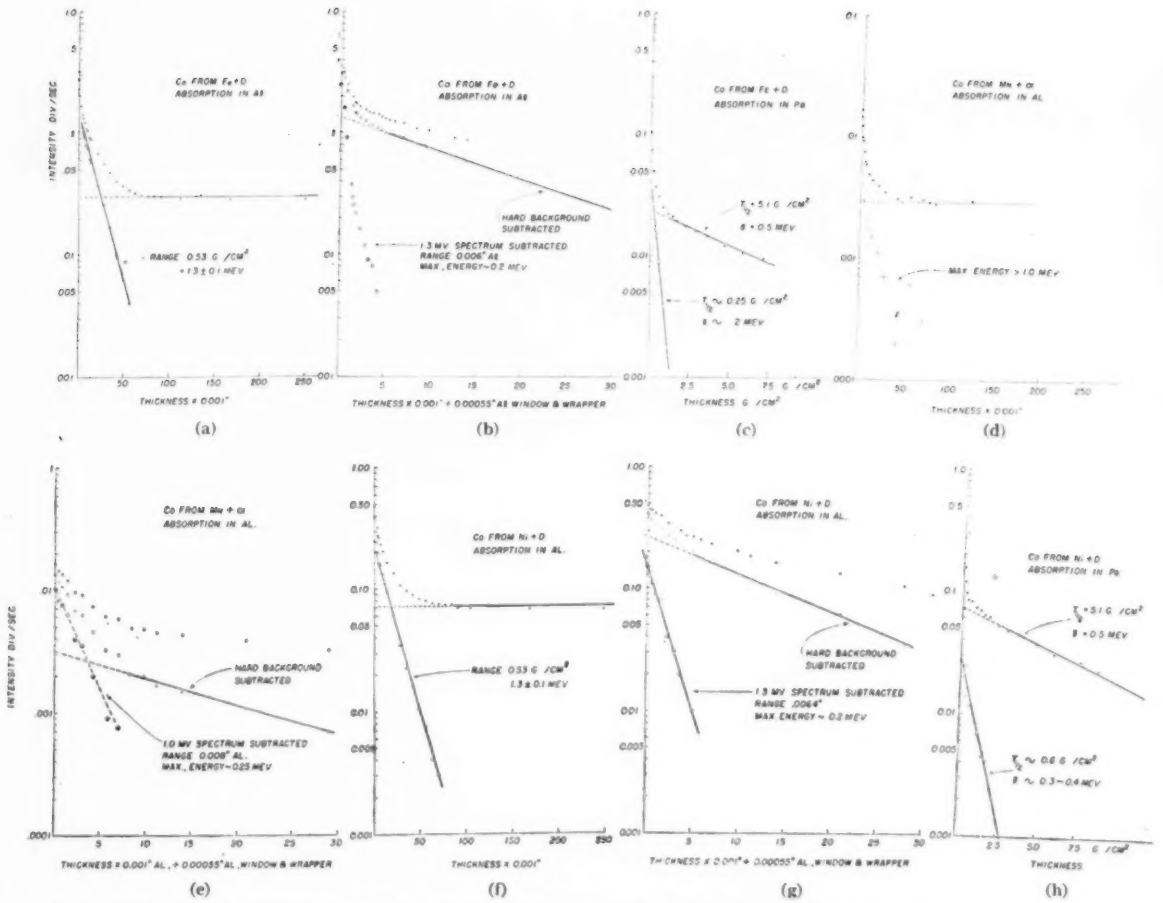

FIG. 1. Absorption in aluminum and lead of radiation from cobalt. The background of the Lauritsen type electroscope, 0.0040 div./sec., has been subtracted. The uppermost points are the observed intensities. (a), (d), and (f) The horizontal lines represent a hard component. The differences, obtained by subtraction of the hard component, represent positron spectra whose maximum energy is derived from Widdowson's and Champion's empirical formula. (b), (e), and (g) Portions of above with expanded thickness scale. The soft group shown in (b), of maximum energy 0.2 Mev, may be composed of positron spectra and internal conversion electrons. The soft group shown in (e), of maximum energy 0.25 Mev, may conceivably be due to the unlikely Mn $(\alpha, 2n)$ Co^{57} reaction, or to recoil electrons produced in the thick source. (c) and (h) The presence of 0.5-Mev annihilation radiation is confirmed. The γ-radiation of energy 0.2 Mev shown in (c) has been confirmed spectrographically.

tensely. α-particle bombardment of the single manganese isotope should produce Co^{58} alone, according to the reaction Mn^{55} (α, n) Co^{58}, unless particle energies >32 Mev are used, in which case Mn^{55} $(\alpha, 2n)$ Co^{57} conceivably occurs.

The present absorption curves, Fig. 1, do not permit conclusive assignment of maximum ranges. The 1.3 Mev β^+ spectrum indicated would be assignable to Co^{58} on the basis of absorption measurements of radiation from cobalt produced by $Mn+\alpha$.

B. Spectrograph Observations

The excitations resulting from the decay of the 70- and 270-day half-life isotopes of cobalt have been investigated spectrographically. Emission of radiation has been observed to follow the decay of the 270-day Co^{57}. The experimental method consisted in studying:

(1) sources containing Co^{56}, Co^{57}, and Co^{58} prepared by high energy deuteron bombardment of iron, (2) sources containing the two 70-day isotopes Co^{56} and Co^{58} prepared by the deuteron bombardment of nickel.

Observations of the two types of sources follow.

(1) *Sources Containing* Co^{56}, Co^{57}, *and* Co^{58}

The following transitions have been established:

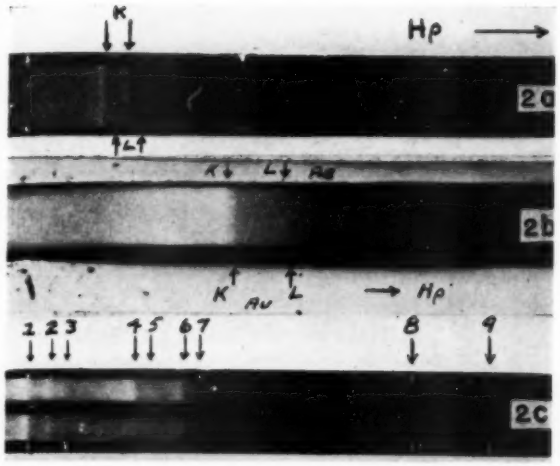

FIG. 2. (a) Transitions from Co^{57}, 270-day period. Contact print showing internal conversion in K and L shells of iron due to 0.117-Mev and 0.130-Mev transitions. (b) Transitions from Au^{198}. Thick source, half covered with lead foil, showing internal and photo-conversion within the gold source and photo-conversion in the lead foil. (c) Exposure to target, Au^{197+d}. First two of four exposures, Au 1_a and Au 1_b.

0.117±0.001 Mev, electric multipole transition = 3;
0.130±0.001 Mev, electric multipole transition = 3;
0.202±0.004 Mev, electric multipole transition = 3 or less; or magnetic multipole transition = 2 or less;
0.215±0.004 Mev, electric multipole transition = 3 or less; or magnetic multipole transition = 2 or less.

The first two transitions listed are about equally probable, each is highly converted in the K shell of iron and partially converted in the L shell, with $\alpha_K/\alpha_L = 7 \pm 1$.[4] The latter two transitions are also about equally probable; they are not converted to any significant extent. These latter were observed by photo-effect in lead. The transitions of higher energy appear to be roughly as frequent as those of lower energy.

The accuracy of the measurement of α_K/α_L was limited by the fact that thick sources were employed in order to obtain exposures in a reasonable time. Cobalt (5 mg/cm²) electroplated on one mm wide sources inclined at 60° required about one-week exposure. The higher energy transitions were observed when the source was covered by lead foil thick enough to absorb the known electrons. The observed $H\rho$ values are listed in Table I. The K–L energy difference corresponds closely to that anticipated for the end product of the decay, namely, iron. Contact prints and photometer prints appear in Fig. 2a and Fig. 3.

(2) *Sources Containing* Co^{56} *and* Co^{58}

Long exposures (as measured by the product intensity times time of exposure) were made. No internally converted nor photoelectrically con-

TABLE I. Transitions.

$H\rho$	Conversion in	Energy Mev
1168 K	Fe	0.110
1196 L	Fe	0.116
1258 K	Fe	0.124
1285 L	Fe	0.129
1205 K	Pb	
1280 K	Pb	

[4] Obtained by comparison of photometrically read densities, rather than opacities, cf. footnote 1.

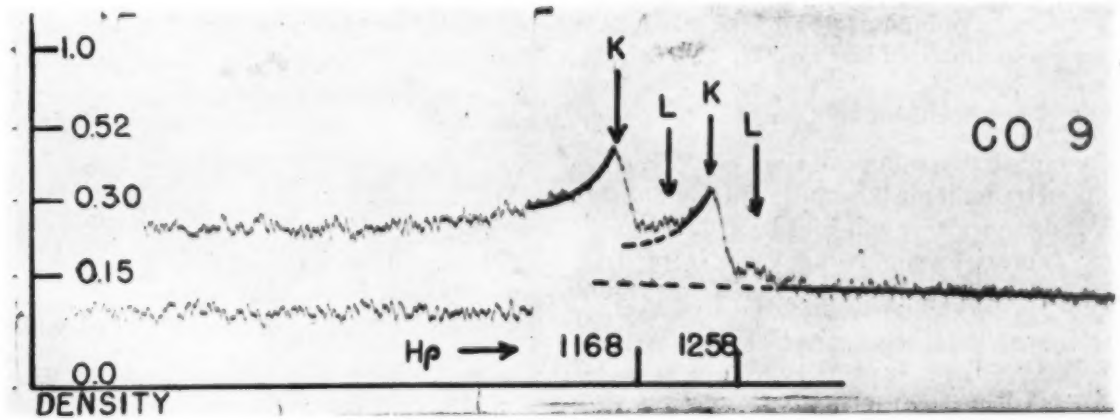

FIG. 3. Microphotometer trace of Fig. 2(a). Electron intensities have been deduced from the net densities of the lines. The net densities of the two K peaks are nearly the same.

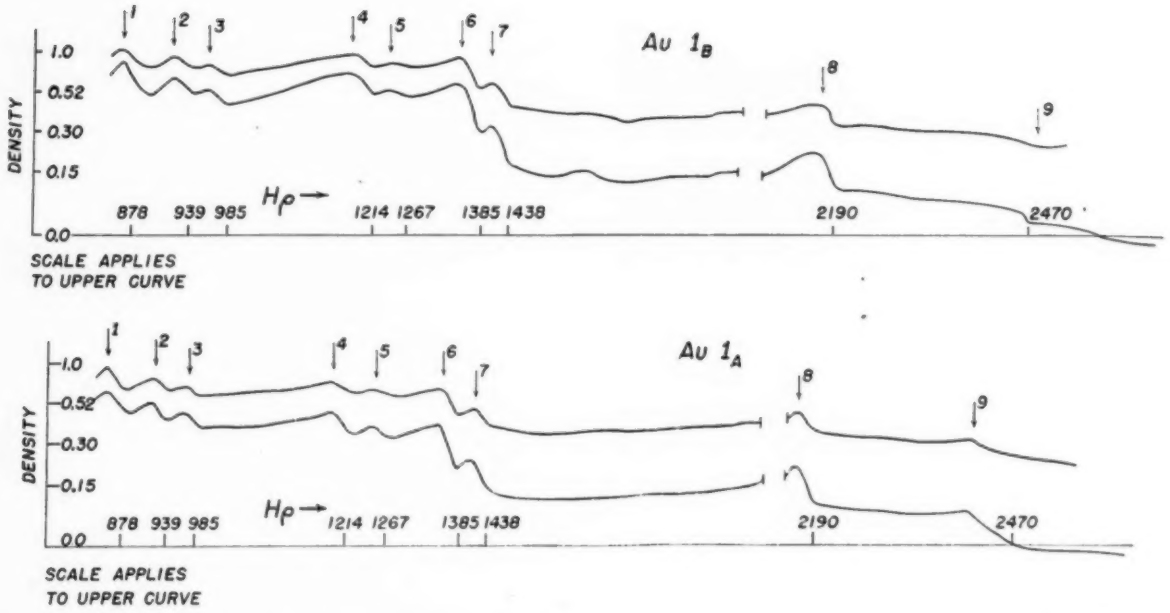

FIG. 4. Tracing of photometer prints. The density scale was expanded for the lower trace to assist in identification.

verted (in lead) electrons were found. The assignment of the transitions to the 270-day isotope Co^{57} is then quite definite.

A rough estimate of the internal conversion coefficient α_K of the 0.117-Mev and 0.130-Mev transitions was obtained by study of the photoelectric yield from lead. α_K appears to have at least the order of magnitude of 1. For the transitions of higher energy α_K is certainly less than 0.1, else these transitions would have been found directly. On a basis of these values and the theoretical values for α_K and α_K/α_L predicted by Hebb and Nelson[5] and Dancoff and Morrison,[6] and the computed lifetimes τ for such transitions[7] the l values have been assigned. The theoretical values are summarized in Table II.

RADIOACTIVE Zn^{65}

The radioactive isotope of zinc, $_{30}Zn^{65}$, may be produced by deuteron bombardment, Cu^{65} $(d, 2n)$ Zn^{65}. It decays with a half-life of 250 days largely by K capture.[8] Gamma-ray energies of 0.45, 0.65, and 1.0 Mev have been reported from cloud-chamber investigations. Absorption curves indicate the presence of soft electrons which have been assumed to be due to internally converted electrons.[9]

A source of practically pure Zn^{65}, having no visible or measurable thickness, was electroplated on a piece of copper by the rotating cathode method. A systematic search was made in the region 0.02–0.3 Mev for conversion electrons. No discrete group of electrons was found; the existence of internally converted electrons in any number is to be denied.

RADIATIONS FROM PRODUCTS OF $Au^{197}+d$

Observations have been made of the discrete electron spectrum emitted by gold which has

TABLE II. Summary of theoretical values.

l	Type transition	Energy Mev	α_K	α_K/α_L	τ
2	elec	0.117	0.2	9.8	0.01×10^{-6} sec.
3	elec	0.117	1.6	7.7	0.2 sec.
4	elec	0.117	13.	5.5	83 hr.
2	mag	0.117	.13	7.2	0.5 sec.
3	mag	0.117	6.6	6.6	510 hr.
2	elec	0.202	.02		0.001×10^{-6} sec.
3	elec	0.202	0.1		0.2 sec.
4	elec	0.202	0.5		83 hr.
2	mag	0.202	0.02		0.01 sec.
3	mag	0.202	0.14		7.6 hr.

[5] M. H. Hebb and E. Nelson, Phys. Rev. **58**, 486 (1940).
[6] S. M. Dancoff and P. Morrison, Phys. Rev. **55**, 122 (1939).
[7] M. H. Hebb and G. E. Uhlenbeck, Physica **5**, 605 (1938).
[8] J. J. Livingood and G. T. Seaborg, Phys. Rev. **55**, 457 (1939).
[9] G. T. Seaborg, Chem. Rev. **27**, 199 (1940).

been bombarded by 11-Mev deuterons. In addition to a mercury isotope of 43 minutes, whose effects were negligible because of the short half-life, two isotopes could be responsible for the spectrum observed:

(1) $_{79}Au^{198}$, from $_{79}Au^{197}$ (d, p), β^-, 65 hours.

(2) A 25-hour period isotope of mercury which may be due to Hg^{197},[10] or Hg^{198*}.[11] The Hg^{198*} would presumably be formed by the decay of the 65-hour Au^{198}. In the latter case, discrete electrons would not show simple 25-hour decay.

One transition of 0.402 ± 0.002 Mev has been established to have a 65-hour half-life. It has an internal conversion coefficient of about 0.04, which indicates that the transition may be adequately represented as an electric quadrupole. The transition doubtless arises from the decay of Au^{198}.[12] Seven additional lines have been observed:

(1) 0.0639; (2) 0.0725; (3) 0.0795; (4) 0.116; (5) 0.126; (6) 0.147; (7) 0.157 Mev.

The values given are probably correct to within 2 percent. Transitions have not been correlated with these lines. They do not have a simple 65-hour half-life, but appear to grow in intensity and have a decay period less than 65 hours.

Exposure to a thick target (0.002 in.) yielded the pair of edges of momenta 2185 $H\rho$ and 2465 $H\rho$ ascribed to 402 kev γ-ray. The energy difference corresponds to the $K-L$ difference for gold rather than mercury, since the more numerous photoelectrons of higher energies formed within the gold source itself mask the internally converted electrons. The internal conversion coefficient was deduced from an exposure in which half the source was covered with a known thickness of lead foil (see Fig. 2b). The intensities of the photoelectrons from the lead enabled computation of the relative number of γ-rays (from expected photo-yields) from the lead and gold, and hence the conversion coefficient. The value $\alpha_K=0.04$ is in good agreement with the values measured for naturally radioactive materials and the theoretically expected values for this region of the periodic table for an electric quadrupole.[13]

TABLE III. Data on observed lines. The upper figures in the columns Au 1_a through Au 2_b are photometrically read densities. The lower figures are the ratios of these densities referred to that of Au 1_a. The ratios are nominal. The figures in the last column give the intensity of the lines relative to line 1, Au 1_a. The solid angle correction is included. Electron intensities are here taken to be proportional to densities, cf. footnote 1.

Line	Momentum $H\rho$	Energy Mev	Au 1_a	Au 1_b	Au 2_a	Au 2_b	Rel. int.
1	878	0.0639	1.0 1.0	1.2 1.2	1.0 1.0	1.0 1.0	100
2	939	0.0725	0.77 1.0	0.96 1.3	0.65 0.85	0.76 1.0	80
3	985	0.0795	0.64 1.0	0.83 1.3	0.48 0.75	0.54 0.85	70
4	1214	0.116	0.72 1.0	0.96 1.3	0.43 0.60	0.59 0.82	100
5	1267	0.126	0.62 1.0	0.83 1.3	0.36 0.60	0.52 0.84	90
6	1385	0.147	0.63 1.0	0.89 1.4	0.38 0.60	0.51 0.81	100
7	1438	0.157	0.48 1.0	0.60 1.3	0.32 0.67	0.40 0.83	100
8	2190	0.323	0.43 1.0	0.48 1.1	0.40 1.0	0.40 1.0	110
9	2470	0.389	0.32 1.0	0.32 1.0	0.28 0.9	0.28 0.9	90
Continuous distribution	2650	0.430	0.16 1.0	0.17 1.0	0.17 1.0	0.17 1.0	50
Relative intensities for 65-hr. period			1.00	1.02	1.14	1.05	
Relative intensities for 25-hr. period growing from 65-hr. period			1.0	1.3	1.9	3.2	
Relative intensities for 25-hr. period			1.0	0.71	0.41	0.14	

Examination of a source 0.0003 in. thick (15 mg/cm^2) allowed better resolution; seven lines of lower energies were observed. Unfortunately this source was too thick to give sufficient resolution to enable deduction of net intensities necessary for complete inference of half-lives and responsible transitions. In an attempt to discover the

[10] Sherr, Bainbridge, and Anderson, Phys. Rev. **60**, 473 (1941).
[11] R. S. Krishnan, Proc. Camb. Phil. Soc. **37**, 186 (1941).
[12] A 410-Mev ray from Au^{198} has been reported by J. L. Lawson and J. M. Cork, Phys. Rev. **58**, 580 (1940).
[13] Hulme, Mott, Oppenheimer, and Taylor, Proc. Roy. Soc. **A155**, 315 (1936). In this paper α is taken $=N_e/(N_q+N_e)$, rather than the definition $\alpha=N_e/N_q$ used in this paper.

rate of decay of the observed lines, four exposures were made with the exposure times so adjusted that the density due to electrons of 65-hour half-life would be nearly the same in each exposure. By covering successive halves of the film, two exposures were made on each of two films. Relative intensities measured may not be correct even in order of magnitude, but can only indicate a trend. Prints (Fig. 2c) and traces (Fig. 4) are shown. Table III lists densities measured from the exposures. It is clear that lines numbered 8 and 9 show a simple 65-hour half-life; the lines of lower energy appear to experience growth and decay, with the possible exception of the line of lowest energy.

ACKNOWLEDGMENTS

The construction of the permanent magnet used in these experiments was made possible by a grant-in-aid-of-research to Professor G. P. Harnwell from the Penrose Fund of the American Philosophical Society. Radioactive cobalt, zinc, and gold were supplied by Drs. J. J. Livingood and B. R. Curtis. Dr. A. S. Jensen prepared a cobalt source from material supplied by Professor L. W. Alvarez. Dr. Floyd Banks prepared the source of radioactive zinc. Dr. Livingood kindly furnished information on the assignment of cobalt activities in advance of publication. I am indebted to Professors L. N. Ridenour and G. P. Harnwell for stimulus and advice throughout.

SEPTEMBER 1 AND 15, 1942 PHYSICAL REVIEW. VOLUME 62

Short Range Alpha-Particles from Fluorine Bombarded with Protons

R. A. BECKER,* W. A. FOWLER, AND C. C. LAURITSEN
California Institute of Technology, Pasadena, California

(Received April 17, 1942)

The ranges of the alpha-particles proceeding from the 334-, 867-, 927-, 1220-, and 1363-kev resonances in the bombardment of fluorine with protons were measured. The Q's of those particles obtained at 334, 867, 927, and 1363 kev were found to be identical, and have the value 1.81 ± 0.04 Mev. The Q of the low energy alpha-particles obtained at the 1220-kev resonance was found to be 1.93 ± 0.07 Mev. The two values thus yield an energy separation of 0.12 ± 0.08 Mev for the two corresponding states of O^{16}. In addition it was shown that at least one of the two resonances which are in the neighborhood of 900 kev must yield short range alpha-particles whose angular distribution is not spherically symmetric.

I. INTRODUCTION

THE history and theory of the fluorine plus proton reactions have been discussed rather completely in a recent paper.[1] Consequently only a brief outline will be presented here.

The bombardment of fluorine by high energy protons has been found to give rise to several reactions, the particular mode depending on the angular momenta and energies of the impinging particles. Gamma-radiation in these reactions has, for the most part, been shown to consist of but a single strong line near 6 Mev, exhibiting well-defined resonances. The most accurate measurement of this energy was that made by Lauritsen, Lauritsen, and Fowler.[2] These authors quoted it as 6.2 ± 0.1 Mev. Dee, Curran, and Strothers,[3] and Lauritsen, Fowler, and Lauritsen[4] have shown this energy to be independent of bombarding voltage, demonstrating that but a single state is involved in the emission of this radiation. The reaction now accepted as the origin of this gamma-ray is:

$$F^{19}+H^1\rightarrow{}^{\gamma}Ne^{20}\rightarrow{}^{\gamma}O^{16}+He^4+Q_1 \qquad (1)$$
$${}^{\gamma}O^{16}\rightarrow O^{16}+\gamma,$$

in which the superscript γ refers in the case of the Ne^{20} nucleus to a particular set of excited

* Now at National Bureau of Standards, Washington, D. C.

[1] J. F. Streib, W. A. Fowler, and C. C. Lauritsen, Phys. Rev. **59**, 253 (1941).

[2] T. Lauritsen, C. C. Lauritsen, and W. A. Fowler, Phys. Rev. **59**, 241 (1941).

[3] P. I. Dee, S. C. Curran, and J. E. Strothers, Nature **143**, 759 (1939).

[4] T. Lauritsen, W. A. Fowler, and C. C. Lauritsen, Phys. Rev. **56**, 858A (1939).

states, and in the case of O^{16} to a single excited level. The associated short range alpha-particles were found by McLean, Becker, Fowler, and Lauritsen,[5] and by Burcham and Smith.[6] The value of Q_1 was shown to be approximately 1.75 Mev. Burcham and Devons,[7] employing a magnetic resolution method, found the value of Q_1 to be unchanged at each of the three gamma-ray resonances, 0.33, 0.66, and 0.87 Mev, thus further demonstrating Eqs. (1) to be the correct mechanism.

An alternative mode of the reaction is the emission of long range alpha-particles:

$$F^{19}+H^1\rightarrow{}^{\alpha}Ne^{20}\rightarrow O^{16}+He^4+Q_0, \qquad (2)$$

in which the compound nucleus splits up to form O^{16} in its ground state. In this case the superscript α refers to that set of states of the Ne^{20} nucleus involved in the production of long range alpha-particles. These particles were found by Burcham and Devons to show distinct resonances, superposed on a rising background. Burcham and Smith[8] found the value of Q_0 to be 7.95 Mev. This is in agreement with the sum of Q_1 and the energy of the gamma-ray.

Still another mode of reaction has been pointed out by the work of Halpern and Crane,[9] and of Fowler and Lauritsen.[10] Upon bombarding a CaF_2 target with high energy protons, pairs of electrons were found to emanate directly from the target. Their energies were found by the latter workers to be approximately 5.9 Mev. Fowler and Lauritsen found definite resonances associated with this pair emission. They offered tentatively the following reaction to explain the presence of the pairs:

$$F^{19}+H^1\rightarrow{}^{\pi}Ne^{20}\rightarrow{}^{\pi}O^{16}+He^4+Q_2 \qquad (3)$$
$${}^{\pi}O^{16}\rightarrow O^{16}+e^+ +e^-.$$

The superscript π pertains, in the case of the Ne^{20} nucleus, to a particular group of excited states. Applied to O^{16} it designates a single excited state a distance above the ground level just equal to the total energy of a pair.

Streib, Fowler, and Lauritsen[1] have since shown that pair resonances definitely coincide in at least one case, that at 1350 kev, with a long range alpha-particle resonance, and perhaps in one other at 850 kev. These experimenters found other resonances for pair emission, definitely non-coincident with long range alpha-particle resonances, at 1140 and 1220 kev, with some indication of pairs in the region from 600 to 800 kev. Accepting Eqs. (3) as the explanation of the non-coincident pairs they suggested, in order to explain those pairs coinciding with long range alpha-particles, the reaction:

$$F^{19}+H^1\rightarrow{}^{\alpha}{}^{\pi}Ne^{20}\begin{cases}\rightarrow O^{16}+He^4+Q_0\\ \rightarrow{}^{\pi}O^{16}+He^4+Q_2\end{cases} \qquad (4)$$
$${}^{\pi}O^{16}\rightarrow O^{16}+e^+ +e^-,$$

in which the particular group of excited states of Ne^{20} here involved is permitted by selection rules to decay and form O^{16} in its ground level with the emission of a long range alpha-particle, or alternatively to emit but a low energy alpha-particle. In the latter case the π state of O^{16} is reached, and subsequently decays accompanied by the emission of an electron pair.

In Fig. 1 are presented the excitation functions of the long range alpha-particles, the gamma-radiation, and the electron pairs detected in the fluorine reaction. The curves are from the data of Streib, Fowler, and Lauritsen.[1]

It was the purpose of the present experiment to make a more precise measurement of Q_1, the energy of the short range alpha-particles preceding the emission of gamma-radiation. It was proposed, too, to carry the investigation of these particles to some of the higher resonances. In addition it was hoped to detect the short range alpha-particles associated with the pair resonances, and to measure their energies. Evidence for the existence of these particles is reported, and verifies the suggestion that the pairs emanate from the O^{16} nucleus.

II. EXPERIMENTAL PROCEDURE

The source of high potential employed in these experiments was the electrostatic generator pre-

[5] W. B. McLean, R. A. Becker, W. A. Fowler, and C. C. Lauritsen, Phys. Rev. **55**, 796 (1939).
[6] W. E. Burcham and C. L. Smith, Nature **143**, 795 (1939).
[7] W. E. Burcham and S. Devons, Proc. Roy. Soc. **173**, 555 (1939).
[8] W. E. Burcham and C. L. Smith, Proc. Roy. Soc. **168**, 176 (1938).
[9] J. Halpern and H. R. Crane, Phys. Rev. **55**, 260 (1939).
[10] W. A. Fowler and C. C. Lauritsen, Phys. Rev. **56**, 840 (1939).

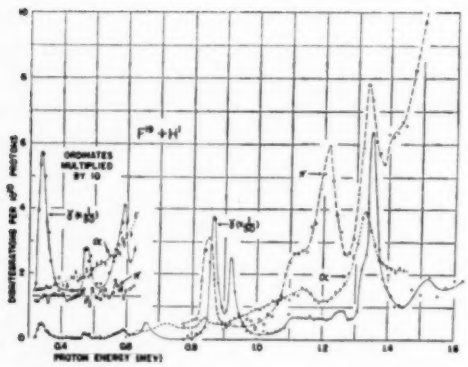

FIG. 1. Excitation curves for the long range alpha-particles, gamma-rays and pairs, from the reaction $F^{19}+H^1$. The ordinates for the gamma-ray curve are reduced to 1/50 of their actual values (after Streib, Fowler, and Lauritsen).

viously described by Lauritsen, Lauritsen, and Fowler.[2] This apparatus, of vertical construction, is capable of operation at a maximum voltage of about 1.7 Mev, with a fluctuation of less than 20 kev. With this generator it is possible to obtain magnetically resolved proton currents of as high as two microamperes at tube pressures of the order of 5×10^{-5} mm Hg.

Throughout the major part of the present work a rotary voltmeter was used. The voltage was read by means of a galvanometer whose deflection was proportional to the current passing between the stator and ground. The constant of proportionality was determined by taking repeated excitation curves of the fluorine gamma-ray resonances near 900 kev, and using the value 867 kev quoted for the lower of the two resonances by Hafstad, Heydenburg, and Tuve,[11] and 927 kev for the upper resonance, given by Bernet, Herb, and Parkinson.[12] It was felt that of the two resonances the most accurately determined value was that for the lower, at 867 kev. Upwards of a dozen such curves were taken, and voltmeter variations of the order of from one to three percent were occasionally observed.

At the time of the concluding series of experiments in the present investigation, some trouble was encountered with the commutator of the rotary voltmeter. Accordingly an oscilloscope was incorporated into the voltmeter circuit so as to permit continuous observation of the shape of the voltage pulse from the stator, thus offering a constant and accurate check of the constancy of the contact resistance between brush and commutator.

In the case of reactions (1), (3), and (4) the expected short range alpha-particle energy is of the order of 2.0 Mev. This corresponds to a range of a little over 1 cm. Consequently the ranges at 90-degree emission of the scattered protons become, at about 700-kev bombarding energy, comparable to those of the ejected short range alpha-particles.

It is evident that for bombarding energies exceeding 600 or 700 kev the scattered protons would mask the alpha-particles, so that in order to observe the latter at high voltages a deflection method would be necessary. For two particles having the same ratio of e^2/m traversing a magnetic field, the radii of curvature will simply be proportional to the square roots of the two energies. Since e^2/m is the same for a proton as for an alpha-particle the restriction is that in order for two such particles to be resolved by means of a magnetic deflection method their energies must differ. One finds that in the case of the fluorine plus proton reaction the energy of an alpha-particle ejected at an angle of 90 degrees to the bombarding beam is given as:

$$E=\tfrac{4}{5}Q+\tfrac{3}{4}E_1, \qquad (5)$$

where E_1 is the bombarding proton energy. If CaF_2 be used then the maximum energy protons are those scattered from the calcium nuclei. Accordingly one finds that the energy of the protons scattered at 90 degrees from Ca^{40} is just 39/41 of the bombarding energy.

In this case, then, the energy of the scattered proton increases more rapidly with primary energy than does that of the ejected alpha-particle. However, if one assumes, as an approximation, that $Q=2.0$ Mev, one finds that for bombarding energies substantially below about 8 Mev the energy of the alpha-particles is greater than that of the scattered protons, and hence the radius of curvature of the alpha-particles is considerably greater than that for the protons. For this reaction, therefore, the magnetic deflection method may be successfully employed. Above 8 Mev complications arise because of the wide dispersion

[11] L. R.Hafstad, N. P. Heydenburg, and M. A. Tuve, Phys. Rev. **56**, 1078 (1939).
[12] E. J. Bernet, R. G. Herb, and D. B. Parkinson, Phys. Rev. **54**, 398 (1938).

of proton energies which is due to varied target penetration.

Figure 2 shows the target arrangement for the present experiment. The bombarding beam is perpendicular to the plane of the paper. The target was enclosed in a short section of lucite tubing so as to permit observation of the beam striking the target. The beam was collimated by a $\frac{1}{4}$-inch hole in a quartz disk just above the target, the illuminated spot on the target being thus $\frac{1}{4}$ inch in diameter. The target was in most cases a slab of fluorite crystal of area just larger than the illuminated spot, cemented to the end of a carbon rod with a drop of shellac, and was less than $\frac{1}{16}$ inch thick. In some cases, however, CaF_2 powder was moistened with ethyl alcohol and allowed to dry on a carbon block. In both instances the target was inclined 45 degrees to the impinging beam, due correction being made for deviations from this angle.

The disintegration products were allowed to pass through a collimating tube immersed in a magnetic field, and into a cloud chamber C of about 15-cm diameter and 3-cm depth. In Fig. 2 the field is perpendicular to the plane of the paper. There are $\frac{1}{8}$-inch slits at points A and B. The average radius of curvature of the tube is 20.5 cm. The tube was inserted between the pole pieces of an electromagnet the field of which had a saturation value of about 12,000 gauss.

The particles were permitted to enter the cloud chamber C through a window W of low air equivalence. It is clear that there would be a certain amount of spreading of the various groups of particles in the chamber, e.g., at 1 Mev the scattered protons would, for a given field strength, be observable as the edge of a brush FG representing the maximum energy of those scattered, while a corresponding resonance group of short range alpha-particles would be represented by a small fan, the edge of which is designated in the figure as HJ.

Possible fine structure in the alpha-particle groups was made evident by using as the gas in the expansion chamber, helium at a pressure equivalent to half an atmosphere, together with water vapor. The stopping power of the mixture was of the order of one-tenth that of air under standard conditions. In this way not only was the apparent magnitude of the range R ($\sim$1 cm under standard conditions) extended but also since for two groups of similar particles of energy difference ΔE the range difference ΔR is related to the stopping power σ as:

$$a\sigma\Delta R=\Delta E \tag{6}$$

it is apparent that the resolving power, in energy, increases as the stopping power decreases. In Eq. (6) a is a constant such that $a\sigma$ is the energy loss per cm, in a given substance, of a particle having an energy E. In this paper the term "stopping power" referred to a substance will be the rate of energy loss of a particle in that material, divided by the rate in air.

The thin window W through which the disintegration products passed into the chamber, consisted of a "Newskin" or lacquer foil of about 2-mm air equivalence supported by a small perforated grid. The hole space of this grid comprised about 60 percent of the total area. It was found that during the whole period of six months of operation the films made of Newskin did not deteriorate.

III. RESULTS

The stopping power of the chamber and air equivalence of the foil were deduced from the ranges observed at 600 kev for the reaction:

$$Li^6+H^1\rightarrow He^3+He^4+Q, \tag{7}$$

in which the Q given by Perlow[13] as 3.945 ± 0.06 Mev was used. In the calibration a thick metallic lithium target was bombarded with 600-kev protons. The target arrangement was the same as that employed in the fluorine case. Before being inserted into the target holder, the lithium was

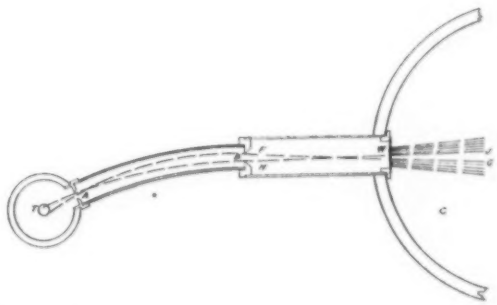

FIG. 2. Target arrangement showing the separation of the alpha-particle group HJ from the scattered protons FG.

[13] Gilbert J. Perlow, Phys. Rev. 58, 218 (1940).

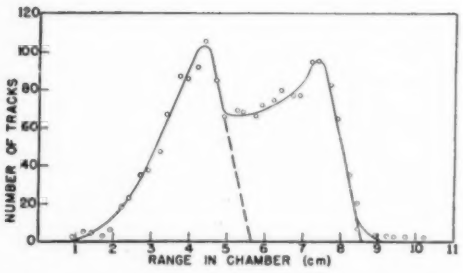

FIG. 3. Alpha-particle groups resulting from the bombardment of a thick lithium target with 600-kev protons.

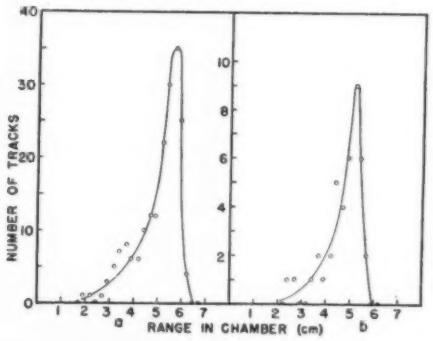

FIG. 4. Alpha-particles observed when bombarding a thick fluorine target with (a) 364-kev protons, and (b) 390-kev protons. In both cases σ had the value 0.105.

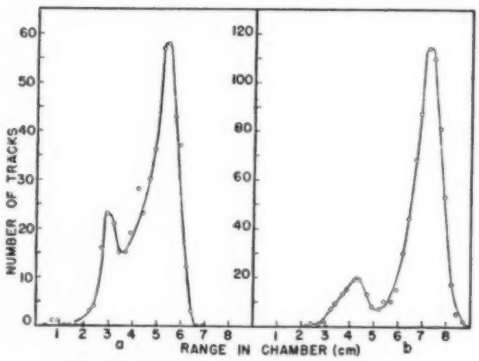

FIG. 5. Alpha-particles found when bombarding a thick fluorine target with 910-kev protons. (a) $\sigma=0.145$, (b) $\sigma=0.105$.

carefully scraped so that a fresh surface might be exposed to the beam. In all interpretations of alpha-particle range data obtained in the present work the range-energy curve of Holloway and Livingston[14] was used. Similarly all computations involving the range-energy relation for protons were made on the basis of the Cornell Curve Revised, drawn from the data of Parkinson, Herb, Bellamy, and Hudson.[15]

In obtaining the lithium data the scattered protons were separated from the alpha-particles by a field of about 10,000 gauss. The results are plotted in Fig. 3 as numbers of tracks *versus* apparent range in the cloud chamber. The curve represents the data selected from about 1200 stereoscopic pictures. The gas in the chamber was 50 cm of the mixture, helium plus water vapor. In the figure the extrapolated range of the He^3 particles may be taken as 8.55 cm, while that of the He^4 group is 5.63 cm. These values remain to be corrected for foil thickness and reduced stopping power of the chamber.

In computing the mean ranges of the He^3 and He^4 particles, the range exponent n is useful. This was obtained as a function of energy from the data of Holloway and Livingston. The value of n for a helium nucleus of mass 3 is identical with that for a He^4 nucleus having $\frac{4}{3}$ the energy of the former. In the present arrangement only those particles emitted at angles of from 89 to 91 degrees to the bombarding beam were observed. Bethe's[16] condition for "good geometry" was well satisfied for the lithium case.

Employing the methods of Bethe and determining the mean ranges by successive approximations from the extrapolated ranges, one finds the air equivalence of the foil for 2-Mev alpha-particles to be 2.5 mm air, and the stopping power of the chamber to be 0.145 when a 50-cm mixture of helium and water vapor was employed. The stopping power of the chamber when filled with a mixture (35 cm) of helium and water vapor was found by comparing the apparent mean ranges in the chamber of the alpha-particles at 1237 kev, with chamber pressures of 35 cm and 50 cm of the helium-water vapor mixture. The observed mean ranges in the two cases were 9.0 cm and 6.5 cm, respectively. If 0.145 is accepted as the stopping power in the latter case this yields 0.105 as the stopping power of the chamber gas at the more reduced pressure.

In order to have an accurate means of computing the Q's for the fluorine alpha-particles account must be taken of target penetration, and for this the stopping power of CaF_2 must be

[14] M. G. Holloway and M. S. Livingston, Phys. Rev. **54**, 18 (1938).
[15] D. B. Parkinson, R. G. Herb, J. C. Bellamy, and C. M. Hudson, Phys. Rev. **52**, 75 (1937).
[16] M. S. Livingston and H. A. Bethe, Rev. Mod. Phys. **9**, 277 (1937).

known. Since this has never been measured a close approximation to it was estimated by a consideration of Mano's[17] measurements. The atomic stopping powers are there given as functions of particle velocity for A ($Z=18$), O ($Z=8$), Ne ($Z=10$) and Al ($Z=13$). Since the stopping power σ is linearly proportional to the atomic number one may assume:

$$\sigma(CaF_2)=\sigma(\tfrac{1}{2}O_2)+\sigma(Ne)+\tfrac{7}{5}\sigma(A)-\tfrac{2}{5}\sigma(Al). \quad (8)$$

Figures 4a and b show the alpha-particle groups obtained by bombarding at energies of 364 and 390 kev, respectively. Presumably these alpha-particles were due to the 334-kev resonance for the gamma-rays. The apparent mean ranges were taken to be 5.7 and 5.2 cm, in the chamber. In each case a mixture of helium and water vapor was used at a pressure of 35 cm Hg. Figure 4a comprises 141 tracks, while the curve of part b of this figure is deduced from 20 tracks.

Figure 5a depicts the structure observed at 910-kev bombardment. The peak represents the alpha-particles emitted at the 867-kev gamma-resonance. The small peak will be considered later, in the theoretical discussion. The pressure in the expanded chamber was in this case 50 cm Hg. The data represent 219 tracks, obtained from about a thousand pictures. Figure 5b shows the data obtained at the same bombarding energy, but with only 35-cm pressure in the chamber. This was taken at a later date than that for the data shown in part (a) of the figure. It comprises 387 tracks, obtained from some 500 photographs.

The result of bombardment at 987 kev is represented in Fig. 6. The alpha-particles emanating from both the 867- and 927-kev levels are clearly resolved. A great deal of work was done at this voltage, 594 tracks being measured from a total of about 2300 pictures. As a result, statistical variations are considerably suppressed.

Figures 7a and b depict the alpha-particles obtained under bombardment by 1389- and 1414-kev protons, respectively. The particles emitted were from the 1363-kev resonance. The curve in part (a) of the figure represents a total of 107

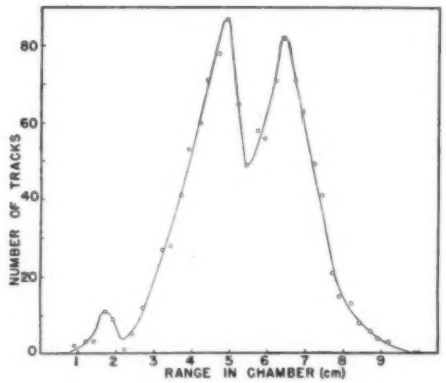

FIG. 6. Two groups of alpha-particles observed as a result of the bombardment of a thick fluorine target with 987-kev protons.

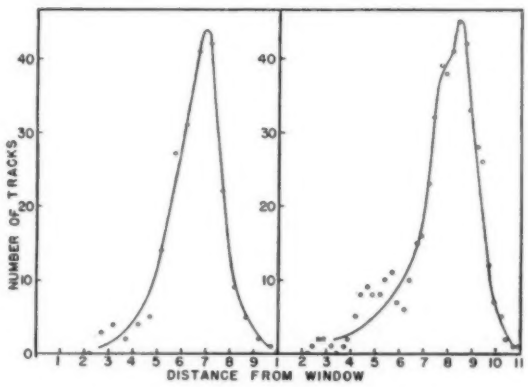

FIG. 7. Alpha-particles found when bombarding a thick fluorine target with (a) 1389-kev protons, and (b) 1414-kev protons. Here $\sigma=0.145$ and 0.105, respectively.

[17] G. Mano, J. de phys. et rad. **5**, 628 (1934).

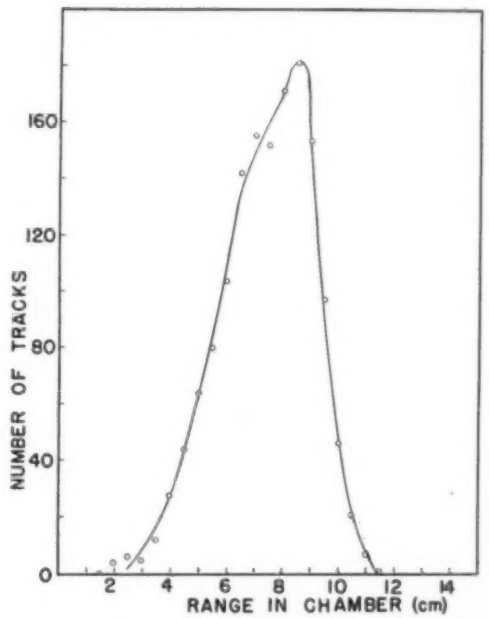

FIG. 8. Alpha-particles observed as a result of the bombardment of a thick fluorine target with 1274-kev protons.

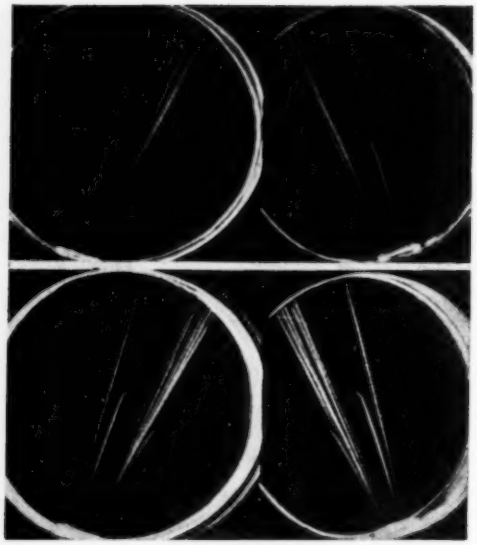

FIG. 9. (Above.) Stereoscopic views of two short range alpha-particles observed at 987-kev bombarding voltage. The longer range particle has suffered a 90-degree collision with a helium nucleus in the chamber.

FIG. 10. (Below.) Stereoscopic views of a long and a short range alpha-particle observed at 1414-kev bombarding voltage.

tracks, and was deduced from about 250 photographs. The curve in part (b) comprises 251 tracks obtained from some 500 pictures.

In Fig. 8 is given the curve obtained at a bombarding energy of 1274 kev, just above the prominent resonance for pair emission at 1220 kev. A great deal of work was done at this bombarding energy, some 3000 photographs having been taken, yielding 737 acceptable tracks.

Figure 9 is a photograph taken at 987 kev. The two alpha-particle tracks are seen to be well separated from the edge of the proton brush. The shorter of the two emanates from a lower point in the target, and presumably arises at the 867-kev resonance. The longer track, originating at the 927-kev resonance, has a right-angled fork near the end of the range, at which point the alpha-particle suffered a collision with a helium nucleus in the chamber. The 90-degree character of the encounter confirms the hypothesis that the disintegration particles are helium nuclei. The only alternative is that the recoil nucleus is a proton, and the initial track a proton scattered by the grid. The heaviness of the track, however, seems to preclude this.

Since the end of the range was greatly magnified in the chamber due to the low stopping power there, much detail for this portion of the tracks was observed. The majority of the alpha-particle tracks observed possessed the spurious curvature exhibited by the short track in Fig. 10. The theory for this type of behavior in a cloud chamber has been developed by E. J. Williams.[18] The track was obtained during 1414-kev bombardment, and was emitted at the 1363-kev gamma-ray threshold of fluorine. In the same photograph is found a long range alpha-particle, which was emitted in a transition to the ground state of O^{16}. As is evident from Fig. 1 there is a resonance maximum for the higher energy particles in this region. It is noticeable, in the pic-

[18] E. J. Williams, Phys. Rev. **58**, 292 (1940).

TABLE I. Summary of data.

Stopping power of chamber	Resonance energy kev	Bombarding energy kev	Apparent mean range cm	ΔR_H cm of air	ΔR_α cm of air	True mean range cm of air	Energy of alpha-particles Mev	Q Mev	No. of tracks
0.105	334	390	5.2	0.10	0.093	0.889	1.69	1.79	20
0.105	334	364	5.7	0.055	0.051	0.899	1.71	1.82	141
0.105	334	368	5.7	0.06	0.056	0.904	1.72	1.83	54
0.145	867	910	5.25	0.15	0.132	1.138	2.12	1.83	219
0.105	867	910	7.2	0.15	0.132	1.138	2.12	1.83	387
0.145	867	936	4.65	0.24	0.211	1.131	2.11	1.81	305
0.105	867	987	4.7	0.435	0.381	1.125	2.10	1.80	594
0.105	927	987	6.6	0.22	0.192	1.135	2.12	1.77	
0.145	1363	1389	6.95	0.12	0.104	1.355	2.475	1.81	107
0.105	1363	1414	8.45	0.235	0.204	1.341	2.455	1.78	251
0.105	1220	1274	8.5	0.23	0.201	1.343	2.46	1.93	737

ture, that the deflection is less for the longer range particle.

The computed Q values for the reaction at various bombarding energies are presented in Table I. Corrections were necessary, and are mentioned below in the sample calculation.

In the table the column headed ΔR_H is the equivalent depth of the target, in cm of air, which the protons must have penetrated before their energies had decreased to the value of the resonance energy. Similarly, the column headed ΔR_α is the equivalent thickness of target material, in cm of air, which the alpha-particles must have traversed in getting out of the target, from the point at which the reaction took place.

As a sample calculation of Q one may take the example of Fig. 4a. The apparent mean range was taken to be 5.7 cm. In this case the bombarding energy was 364 kev, corresponding to a proton range in air at 15°C and 760 mm Hg of 0.415 cm. When the proton energy has decreased to 334 kev the midpoint of the resonance is reached. Since the range of 334-kev protons is 0.36 cm one finds a penetration ΔR_H of the target equivalent to 0.055 cm of air at the above-mentioned conditions of temperature and pressure.

Now the average velocity of the proton in traversing this thickness of target material is 0.8×10^9 cm/sec. The energy of the emitted particle is about 1.7 Mev, and it has a velocity of 0.87×10^9 cm/sec. From Eq. (8) the stopping powers of CaF_2 for particles of these velocities are 3.875 and 3.935, respectively. There is an additional correction, to the extent that the angle of the target was 48.5 degrees. The alpha-particles were compelled to traverse but 0.92 of the geometrical distance through which the protons must have passed in order to reach the given depth in the target. Therefore the increment of range ΔR_α of the alpha-particles, in the target, was $(0.92\times3.935\times\Delta R_H)/3.875$, or 0.051 cm. Furthermore, since the air equivalence of the window was taken to be 0.25 cm we have the true mean range R to be $5.7\times0.105+0.25+0.051=0.899$ cm, whence the energy of the emitted particle was 1.71 Mev. Using the methods of Bethe one finds Q to be 1.80 Mev. A slight correction due to the fact that the alpha-particles were observed at 88 degrees to the original beam rather than at 90 degrees subtracts about 10 kev from the Q value. The corrected Q, then, is 1.79 Mev.

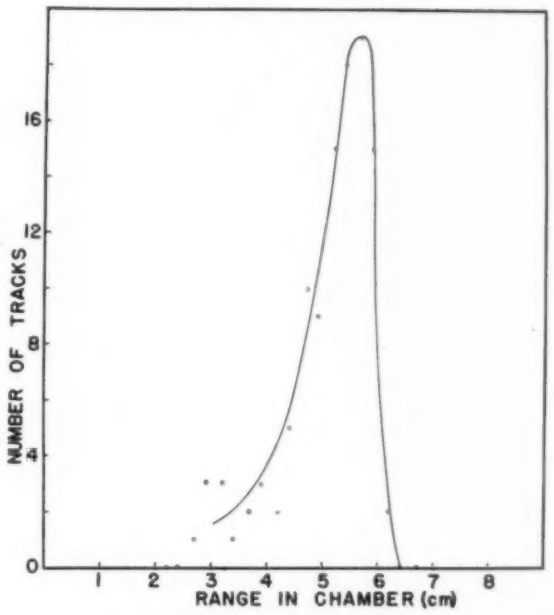

FIG. 11. Alpha-particles found as a result of the bombardment of a thick fluorine target with 368-kev protons.

It is to be emphasized here that the absolute values for Q obtained are dependent only on the slope of the stopping power curve for CaF_2, and are independent of the absolute values of the ordinates. A similar statement can be made for the use, in the computations, of the range-energy relations for both alpha-particles and protons, since the contribution due to proton penetration is just proportional to the difference between two ranges, and in the case of the alpha-particles the curve is standardized by comparing with alpha-particles of known energy which is of the same order as that of the particles measured.

In order to have an additional check on the correctness of the above values for Q a run just above the 334-kev resonance was made after a lapse of about three months. The observations are summarized graphically in Fig. 11, which represents the distribution of 54 tracks. At this later time the null reading voltmeter was employed. The bombarding energy in this case was 368 kev. The apparent mean range was taken as 5.7 cm, yielding a value of 1.83 Mev for Q, in very good agreement with the preceding measurements.

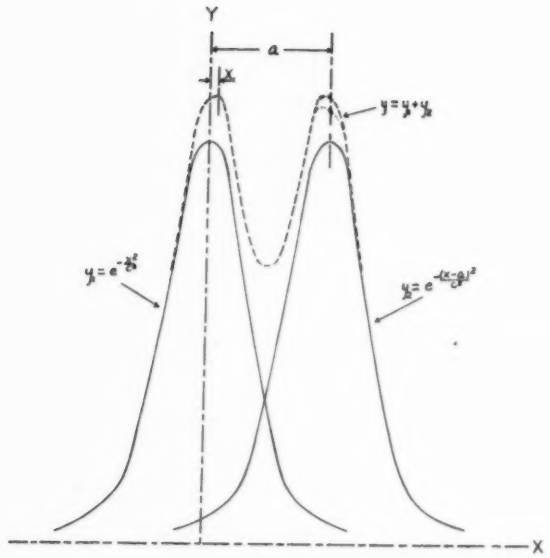

FIG. 12. Sketch showing the shift of two Gaussian peaks due to their proximity to each other.

In computing the results for the bombardment at 987 kev, allowance was made for the shift of the two maxima due to their proximity to one another. Figure 12 shows a sketch idealizing the conditions of the problem at this voltage. Two Gaussian peaks, each of half-width b, are depicted with a true separation a. Because of the proximity of the two peaks the observed separation will be some quantity $a-2x_1$, where $x_1 \ll a$. Let

$$y_1=\exp(-x^2/c^2) \quad \text{and} \quad y_2=\exp(-(x-a)^2/c^2).$$

The positions of the two maxima will be determined by setting

$$dy/dx=0 \qquad \text{where} \qquad y=y_1+y_2.$$

Assuming a good approximation to the observed curve to be when $a=b$ one finds an apparent shift of 20 percent in the separation. When this is taken into consideration it is clear from Table I that within a possible error of 30 kev the two resonances exhibited in Fig. 6 possess identical values for Q.

That the two resonance groups in this case are resolved is due to the fact that alpha-particles originating at the lower resonance must come out from a deeper layer in the target. This is indicated in Fig. 13 which shows a proton beam of 987-kev energy incident on a thick target of CaF_2. At a certain depth in the target the protons will, on the average, have lost 60 kev, which reduces their average energies to 927 kev. At this point many of them will react with fluorine nuclei, and those alpha-particles from this reaction which are emitted at 88 degrees to the original beam are observed in the chamber. Those protons which do not react at this level will penetrate further into the target until they reach that depth of the target at which they will, on the average, have their energies reduced to 867 kev. At this point many will react, as at the higher level, with the fluorine, save that the alpha-particles from the lower level will, in addition to possessing a smaller contribution from the incident proton energy, have to pass through an increased target thickness in order to be observed in the chamber.

It is worthy of note that because the expected alpha-particle ranges are very close to those used in calibrating the apparatus the error in calculated Q's, arising from errors in σ and the air equivalence of the foil, will be a small quantity of the second order.

IV. THEORETICAL DISCUSSION

The small peak on the low energy sides of Figs. 5 and 6 cannot be attributed to a gamma-resonance since the nearest lower gamma-ray resonance is at 660 kev. Consequently the short range alpha-particles from this resonance could not have emerged from the target for either of these bombarding energies. This group cannot be due, therefore, to a resonance of the 6.2-Mev radiation of $F^{19}+H^1$.

It is of importance to notice the difference in the relative height of the two peaks in Fig. 6 from that in the corresponding part of Fig. 1. Because of the comparatively long lifetime (about 10^{-15} second) of the 6.2-Mev state of oxygen it is to be expected that the coupling between the initial and final states of motion of the particles involved will be completely lost, and that consequently the yield of the gamma-radiation should show spherical symmetry. It has recently been demonstrated experimentally by Van Allen and Smith[19] that the fluorine gamma-radiation at three bombarding voltages—370, 900, and 1000 kev—possesses a spherically symmetric angular

[19] J. A. Van Allen and N. M. Smith, Phys. Rev. **59**, 501 (1941).

distribution. This is not necessarily true for the short range alpha-particles preceding this emission, which in general would have an angular distribution deviating from spherical symmetry. Spherical symmetry would be observed if the captured particle possesses zero angular momentum, if the compound nucleus possesses zero angular momentum, or if the emitted particle possesses zero angular momentum, or lastly, for any combination of these three cases.

It is clear that since the relative intensity of the 867- and 927-kev peaks is different for the alpha-particles from that for the gamma-rays, one or both of those two groups of alpha-particles must show an angular distribution different from that of spherical symmetry. This is to be looked for in future distribution measurements of the short range alpha-particles.

Figure 6 furnishes, in addition, an accurate check for the separation of the 867- and 927-kev resonances if one begins by assuming the Q values for the two states to be identical. For example, if one takes for the lower threshold, the value 862 kev, the final Q value for the alpha-particles of this resonance would be 1.84 Mev, or 40 kev greater than the magnitude obtained when using the slightly greater value for the resonance energy. We thus see that the computed Q is very sensitive to the precise value for the resonance voltage. Since the Q for the 927-kev resonance was found to be 1.78 Mev, it might be reasonable to suppose that the separation 927–867 should actually be 4 or 5 kev less than the 60 kev it is at present assumed to be.

The shape of the 1363-kev resonance alpha-particle yield seems to be somewhat different from that of the gamma-radiation shown in Fig. 1. In Fig. 7a and b the back sides of the peaks seem relatively more pronounced than for the gamma-rays. This seems to indicate that the relative intensity at 90-degree emission for the alpha-particles from the 1335- and 1363-kev resonances is somewhat different from the integrated relative intensity which is shown by the gamma-ray peaks.

The Q value for the alpha-particles preceding gamma-ray emission is 1.81 ± 0.04 Mev. The probable error is but 0.01 Mev. However, owing to a possible systematic discrepancy the error is quoted as being 0.04 Mev. In Fig. 1 it is noticed that the ordinates for the pair emission curve should be multiplied by 1/50. This at once rules out the possibility of observing the alpha-particles from the 850-kev resonance for pair emission, since these would be entirely obliterated by the alpha-particles emitted from the 867-kev gamma-ray resonance. The small peak on the low energy side in Figs. 5 and 6 cannot be attributed to this unless the pair alpha-particles possess energies less than those of the particles leading to the 6.2-Mev state of O^{16}. This seems to be very unlikely. Similarly the alpha-particles emitted at the 1350-kev pair resonance would be obliterated by those proceeding from the 1363-kev state.

The only remaining possibility seemed to be to bombard just above the very broad pair maximum, the center of which is located at 1220 kev. The peculiar shape of this peak seems to preclude the possibility that it is due to only a single resonance level, but suggests that it is due to a superposition of several closely spaced resonances.

It is to be mentioned further that this shape should be observed at all angles of emission of the pairs since one expects that owing to the long lifetime of the pair state of O^{16} the emitted electrons should show spherical symmetry. If the peak does actually represent a multiplicity of levels this shape is not necessarily to be expected for the alpha-particles, in which the relative yields may vary somewhat as the angle of emission is changed, the amount of variation depending upon the values of angular momentum involved.

It should be noticed by referring again to Fig. 1

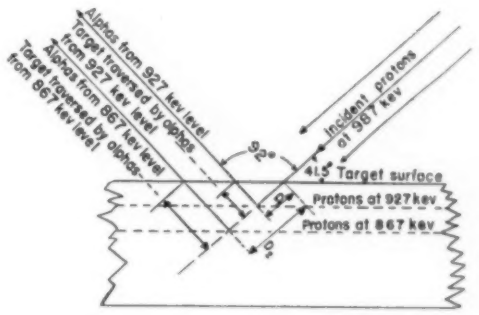

FIG. 13. Resolution of two groups of particles by means of varied target penetration. D_1 is penetration of protons in losing 60 kev; D_2 is penetration of protons in losing 120 kev.

that there seems to be a measurable background of gamma-radiation in the vicinity of 1200-kev bombarding energy. That this did not appear to smear out the emitted short range alpha-particles may indicate that this gamma-radiation is not that emitted by the 6.2-Mev state of O^{16}. It is suggested that this background may be low energy radiation arising from a non-capture excitation of fluorine, similar to that which is known to exist in the Li^7+H^1 reaction at bombarding energies near 800 kev.

Choosing 8.5 cm as the apparent mean range in Fig. 8 for the pair resonant alpha-particles one obtains a Q value of 1.93 ± 0.07 Mev, given in Table I, for the bombarding energy of 1274 kev. The error is somewhat larger in this case, first because the value could be determined at but one voltage, and secondly because the variation in angular distribution, if the peak be complex, might conceivably shift the position of the maximum somewhat. It was thought that a quoted error of 70 kev would be a reasonable one.

It should be mentioned at this point that the existence of a group of alpha-particles at this bombarding voltage, and whose Q value is greater than that of those groups preceding gamma-ray emission, offers the needed evidence that the pairs are given off from O^{16} rather than from Ne^{20}. Until this point had been reached the statement that the electrons were emitted in the decay of a state of O^{16} had been but an assumption. Further evidence is indicated by the somewhat similar structure of the alpha-particle group to that of the pair peak shown in Fig. 1.

The above results indicate a separation for the two states of O^{16} to be about 0.12 ± 0.1 Mev. Although just on the limit of error it is indicated that the pair emitting state is lower than the gamma-ray emitting state. Had the former been higher than the latter, low energy gamma-rays in a transition to the 6.2-Mev gamma-ray state would have been emitted rather than the pairs. Accepting 6.2 ± 0.1 Mev as the energy of the gamma-ray emitting state of O^{16}, one finds the energy of that state giving rise to electron pairs to be 6.1 ± 0.1 Mev. Tomlinson[20] has recently measured the energy of the pairs directly by means of a magnetic spectrograph. The value quoted for the energy was 6.0 ± 0.2 Mev, a result in fair agreement with that quoted in the present work.

An explanation of the small peak in Figs. 5 and 6 could be the existence of a pair peak at about 750 kev. Some evidence for this was obtained in the excitation curves of Streib, Fowler, and Lauritsen. It was not conclusive, however, and was not indicated in Fig. 1.

Other means for measuring the energy of the pair emitting state of O^{16} seem necessary in order to determine more accurately the separation of this from the 6.2-Mev state. Because of the difficulties mentioned above in determining this quantity indirectly by measurement of the associated alpha-particle energy it seems more promising to attempt another determination directly of the pair energy itself. It seems of value, also, to measure the angular distributions of the alpha-particle groups proceeding from the higher energy resonances, and to compare them with the relative intensities here observed at 90-degree emission.

Thanks are due Dr. J. F. Streib for the use of Fig. 1, and also for the preparation of Fig. 2.

[20] E. P. Tomlinson, Phys. Rev. **60**, 159A (1942).

Electric Quadrupole Moments of Light and Heavy Nuclei

SHERRERD B. WELLES
Sloane Physics Laboratory, Yale University, New Haven, Connecticut
(Received June 22, 1942)

Under the assumption that the asymmetrical nuclear charge distribution is due to a single proton, a general expression for the electric quadrupole moment as a function of nuclear spin is obtained. Using the plausible restriction for heavy nuclei that all allowed pairs of values of the orbital angular momentum of the proton and of the core occur with equal probability, we get as a result that the quadrupole moment is negative and that the value increases negatively as the nuclear spin increases. The calculation for light nuclei, taking into account the effect of all particles by using the Hartree model, shows that the addition of a proton to a nucleus, whose Q was originally zero, produces a negative quadrupole moment.

INTRODUCTION

THE existence of a nuclear electric quadrupole moment indicates a deviation from a spherically symmetrical average charge distribution within the nucleus. A positive value indicates a distribution extended along the axis of the nuclear spin (cigar-shaped nucleus) and a negative value implies a flattening toward the plane normal to this axis (watch-shaped nucleus).

With the exception of deuterium, the quadrupole moment has been measured only for nuclei of odd atomic weight. The regularities among the magnetic moments for these and other additional odd nuclei indicate very strongly that the resultant spin of the nuclear particles apart from the orbital angular momentum is $\frac{1}{2}$, i.e., $S=\frac{1}{2}$. Also to a first approximation the magnetic moment is due largely to the odd particle.[1] The question arises as to whether the quadrupole moment might be due to this odd particle. In other words we consider the nucleus, apart from the odd particle, to consist of a charge distribution which is spherically symmetrical and that the departure from this symmetry for the whole nucleus is caused by the odd particle. This means we must consider the odd particle as a proton.

If l is the orbital angular momentum of a single proton and if m is the z component of l, then the quadrupole moment is positive if $l(l+1)$ is greater than $3m^2$, otherwise it is negative. If the orbital angular momentum is directed along the z axis then the quadrupole moment is negative, but there are several orientations of l for which it is positive. The problem is therefore one of determining the effective orientation of the orbital angular momentum of the single proton.

As far as they have been observed, the large quadrupole moments are all positive and are found in the region of the periodic table between atomic numbers sixty and eighty, reaching a maximum at atomic number seventy-one.[1c] And in addition the magnitudes of nine of the moments are too large to be reasonably explained by the asymmetrical charge distribution of one proton. The deviation could be explained by the alpha-particle model. The problem of the energetically favorable packing of spherical alphas has been discussed by Wefelmeier,[1d] who has shown that the most elongated framework of alphas is to be expected in the neighborhood of atomic number 71. In addition Fano[2] has indicated briefly that the angular momentum of a single proton in a p state might well be oriented along the long axis of an elongated nucleus, thus contributing a small negative effect to an already large positive moment due to the alphas.

Of the nine nuclei with observed quadrupole moments that are small enough to be due to a single proton, three are negative, the rest positive. For these nine we can assume a symmetrical core and consider the effect of the single proton. In the first section a general expression for the quadrupole moment as a function of the

[1] (a) Th. Schmidt, Zeits. f. Physik **106**, 358 (1937); (b) H. Margenau and E. Wigner, Phys. Rev. **58**, 103 (1940); (c) D. R. Inglis, Phys. Rev. **60**, 837 (1941); (d) W. Wefelmeier, Naturwiss. **25**, 525 (1937); Zeits. f. Physik **107**, 332 (1937).

[2] See discussion of U. Fano, Naturwiss. **25**, 602 (1937), who has shown that it is at least plausible that the orbital angular momentum should be oriented along the long axis of an elongated nucleus, i.e., $m=l$.

total nuclear spin is derived. By use of a plausible assumption concerning the probability of allowed pairs of values of the orbital angular momentum of the proton and of the core, the expression is found to lead to the result that the quadrupole moment is negative and its value increases negatively as the spin increases. In the second section we shall calculate the quadrupole moment of light nuclei, using the Hartree model.

QUADRUPOLE MOMENTS OF HEAVY NUCLEI

Let us consider the wave function of the ground state of nuclei of odd atomic weight. We limit our discussion to odd nuclei as H^2 is the only even nucleus whose electric quadrupole moment has been measured. If a spin-independent symmetric Hamiltonian is used, then the normal states are doublets, $S=\frac{1}{2}$, and the total orbital angular momentum can assume the values $L_1=J-\frac{1}{2}$ and $L_2=J+\frac{1}{2}$, where J is the total angular momentum of the nucleus. If M is the z component of J, we are interested in the component $M=J$ in the calculation of the quadrupole moment. The total wave function with definite values of J and M can be written as the sum of two functions

$$\Psi(J, M)=a_1\psi(L_1, S, J, M)+a_2\psi(L_2, S, J, M),$$

where

$$|a_1|^2+|a_2|^2=1 \quad \text{and} \quad M=J.$$

Expanding each $\psi(L)$ in terms of functions which have sharp values of m_L and m_S, we have

$$\psi(L_1)=\Phi(L_1, m_L=L_1, m_S=\tfrac{1}{2})\equiv\Phi_+(L_1),$$

$$\psi(L_2)=-\frac{1}{(2J+2)^{\frac{1}{2}}}\Phi(L_2, m_L=L_2-1, m_S=\tfrac{1}{2})$$

$$+\left(\frac{2J+1}{2J+2}\right)^{\frac{1}{2}}\Phi(L_2, m_L=L_2, m_S=-\tfrac{1}{2}),$$

$$\equiv-\frac{1}{(2J+2)^{\frac{1}{2}}}\Phi_+(L_2)+\left(\frac{2J+1}{2J+2}\right)^{\frac{1}{2}}\Phi_-(L_2).$$

If we define $Q=\sum_\pi(3z^2-r^2)$, an operator which acts only on the coordinates of the protons, then the quadrupole moment is

$$\int\Psi^*(J, M=J)Q\Psi(J, M=J)d\tau=|a_1|^2Q_{1,1,+}$$

$$+|a_2|^2\left(\frac{1}{2J+2}Q_{2,2,+}+\frac{2J+1}{2J+2}Q_{2,2,-}\right)$$

$$-\frac{2}{(2J+2)^{\frac{1}{2}}}a_1^*a_2Q_{1,2,+},$$

where

$$Q_{1,1,+}\equiv\int\Phi_+^*(L_1)Q\Phi_+(L_1)d\tau$$

and similarly for the other Q's. In obtaining this equation we have used the fact that Q is Hermitian and also that $\int\Phi_+^*Q\Phi_-d\tau=0$ because of the orthogonality of the spin functions.

We express each $\Phi(L, m_L, m_S)$ in terms of wave functions $\phi(l_\pi, l_\nu, L, m_L)$, where l_π and l_ν are, respectively, the total orbital angular momenta of the protons alone and the neutrons alone.

$$\Phi(L, m_L)=\sum_{l_\pi, l_\nu}C_{(l_\pi, l_\nu, L, m_L)}\phi(l_\pi, l_\nu, L, m_L),$$

where $\Sigma|C|^2=1$, and $|C_{(l_\pi, l_\nu, L, m_L)}|^2$ is the probability that the orbital angular momentum of the protons equals l_π, and that of the neutrons equals l_ν. The only condition on a particular pair of values of l_π and l_ν is that their vector sum is equal to L.

We can expand the wave function for a particular pair of l_π and l_ν in terms of wave functions, each of which has definite z components of l_π and l_ν.[3]

$$\phi(l_\pi, l_\nu, L, m_L)=\sum_{m_\pi, m_\nu}\Theta_{(l_\pi, l_\nu, m_\pi, m_\nu)}$$

$$\times(l_\pi, l_\nu, m_\pi, m_\nu|l_\pi, l_\nu, L, m_L).$$

Since $m_\pi+m_\nu=m_L$, this summation is really a single one. The coefficients have been worked out only as far as $l_\pi=2$ if $l_\pi<l_\nu$, or $l_\nu=2$ if $l_\nu<l_\pi$. Each Θ can be expressed as the product of a function involving the coordinates of the protons

[3] E. U. Condon and G. H. Shortley, *Theory of Atomic Spectra* (Cambridge University Press, 1935), pp. 76–77.

TABLE I. Values of the integral $I=\int\phi^*(l_\pi', l_\nu', L, m_L)Q\phi(l_\pi, l_\nu, L, m_L)d\tau$.

	$L=M_L=0$		$L=M_L=1$			$L=M_L=2$			$L=M_L=3$			$L=M_L=4$			$L=M_L=5$		
	$l_\pi l_\nu$	D	$l_\pi l_\nu$	D	X	$l_\pi l_\nu$	D	X	$l_\pi l_\nu$	D	X	$l_\pi l_\nu$	D	X	$l_\pi l_\nu$	D	X
	00	0	01	0	0.28	02	0	0.48	03	0	0.59	04	0	0.64	05	0	0.68
	11	0	10	−0.40		11	−0.40	.14	12	−0.40	.26	13	−0.40	?	14	−0.40	?
	22	0	11	.20		20	− .56		21	− .56	.08	22	− .56	.16	23	− .56	?
	33	0	12	− .04	.29	12	.40	.34	30	− .67		31	− .67	.05	32	− .67	.11
	44	0	21	− .20		21	− .28		13	.50	?	40	− .73		41	− .73	.04
			22	.20		13	− .12	?	22	− .14	.23	14	.56	?	50	− .77	
			23	− .057	?	22	.12	.22	31	− .50		23	− .06	?	15	.60	?
			32	− .16		31	− .46		14	− .16	?	32	− .40	.16	24	0	?
						23	.33	?	23	.26	?	41	− .62		33	?	?
						32	− .12		32	− .21	.15	15	− .20	?	42	− .55	.11
						24	− .16	?	41	− .59		24	.34	?	51	− .69	
						42	− .41		24	.36	?	42	− .49	.11	25	.38	?
									42	− .36		51	− .68		52	− .53	.05
												25	.36	?	61	− .74	
												52	− .51		26	.36	?
															62	− .61	
															27	− .33	?
															72	− .71	
Value of Q for single free proton	0			−0.40			−0.56			−0.67			−0.73			−0.77	
Average of D's	0			−0.057			−0.14			−0.19			−0.27			−0.34	
Number of D's	∞			8			12			13			15			18	
Average of D's / Q for s.f.p.				14%			25%			28%			37%			44%	
$\bar{D}_{2,2}$ *	0			0			−0.098			−0.16			−0.25			−0.32	

* $\bar{D}_{2,2}=\dfrac{(L_2-1)(L_2+3/2)}{L_2(L_2+1/2)}\bar{D}_{2,2,--}$.

times a function containing only neutron coordinates:

$$\Theta(l_\pi, l_\nu, m_\pi, m_\nu)=\theta(l_\pi, m_\pi)\Omega(l_\nu, m_\nu).$$

It can easily be proved that

$$\int\Omega^*(l_\nu', m_\nu')\Omega(l_\nu, m_\nu)d\tau=\delta(l_\nu', l_\nu)\delta(m_\nu', m_\nu).$$

The magnetic moment of an odd nucleus seems to be due largely to the single odd particle.[1] One immediately wonders whether the quadrupole moment can be understood on the basis of this simple picture also. We will therefore assume in this part of our analysis that the nucleus consists of a core in which the charge distribution is spherically symmetric, and outside is a single proton. The motion of this proton is strongly affected by the other particles, including the other protons, but the latter protons do not contribute to the quadrupole moment. Hence these core protons will act like neutrons in the calculation of Q and l_ν will be the total orbital angular momentum of the core. For the single proton we shall use the normalized associated Legendre function for $\theta(l_\pi, m_\pi)$ to express the angular dependence. Then

$$\int\theta^*(l_\pi', m_\pi')Q\theta(l_\pi, m_\pi)d\tau=\delta(m_\pi', m_\pi)\left\{\delta(l_\pi', l_\pi)2\left[\frac{l_\pi(l_\pi+1)-3m_\pi^2}{(2l_\pi+3)(2l_\pi-1)}\right]\right.$$

$$+\delta(l_\pi', l_\pi+2)\frac{3}{2l_\pi+3}\left[\frac{(l_\pi+m_\pi+2)(l_\pi+m_\pi+1)(l_\pi-m_\pi+2)(l_\pi-m_\pi+1)}{(2l_\pi+1)(2l_\pi+5)}\right]^{\frac{1}{2}}$$

$$\left.+\delta(l_\pi', l_\pi-2)\frac{3}{2l_\pi-1}\left[\frac{(l_\pi+m_\pi)(l_\pi+m_\pi-1)(l_\pi-m_\pi)(l_\pi-m_\pi-1)}{(2l_\pi-3)(2l_\pi+1)}\right]^{\frac{1}{2}}\right\}\langle r^2\rangle_{Av}$$

as can be shown by the use of the recurrence relation for different orders of the associated Legendre function.[4] An expression for the average value of the square of the radius vector will be given later.

Now it readily follows that

$$\int \phi^*(l_\pi', l_\nu', L, m_L) Q \phi(l_\pi, l_\nu, L, m_L) d\tau$$
$$= \delta(l_\nu', l_\nu) \sum (l_\pi', l_\nu', m_\pi', m_\nu' | l_\pi', l_\nu', L, m_L)$$
$$\times (l_\pi, l_\nu, m_\pi, m_\nu | l_\pi, l_\nu, L, m_L)$$
$$\times \int \theta^*(l_\pi', m_\pi') Q \theta(l_\pi, m_\pi) d\tau.$$

The values of the integral on the left-hand side of this equation in units of r^2 have been listed in Table I for $m_L = L$. The values of the integral for $m_L = L-1$ have not been tabulated since they are equal to $(L-3)/L$ times the corresponding integral for $m_L = L$. This general relation is apparent after the integrals have been evaluated for the two cases. The column headed D (direct) gives the sum of the $\delta(l_\pi', l_\pi)$ terms and the column headed X (cross term) gives the sum of the $\delta(l_\pi', l_\pi+2)$ terms coming from $\int \theta^*(l_\pi') Q \theta(l_\pi) d\tau$. As the function $(l_\pi' = 3)$ combines with the function $(l_\pi = 1)$ to give the same value as $(l_\pi' = 1)$ combining with $(l_\pi = 3)$ in the $\delta(l_\pi', l_\pi - 2)$ term, we can multiply the latter by 2 and consider only $l_\pi' > l_\pi$ in the summation below. So we obtain

$$\int \Phi^*(L, m_L) Q \Phi(L, m_L) d\tau = \sum |C(l_\pi, l_\nu)|^2 D$$
$$+ 2 \sum C^*(l_\pi+2, l_\nu) C(l_\pi, l_\nu) X,$$

where the first sum is taken over all pairs of l_π and l_ν that can give L, and the second sum is taken likewise with the additional restriction that $l_\pi+2$ and l_ν can also give L. So

$$\frac{1}{2J+2} Q_{2,2,+} + \frac{2J+1}{2J+2} Q_{2,2,-}$$
$$= \sum |C(l_\pi, l_\nu)|^2 \left\{ \frac{1}{2J+2} D_{2,2,+} + \frac{2J+1}{2J+2} D_{2,2,-} \right\}$$
$$+ 2 \sum C^*(l_\pi+2, l_\nu) C(l_\pi, l_\nu)$$
$$\times \left\{ \frac{1}{2J+2} X_{2,2,+} + \frac{2J+1}{2J+2} X_{2,2,-} \right\}.$$

[4] See, for example, reference 3, Eq. 4^3, 2.

On writing $D_{2,2}$ for the first { } term and $X_{2,2}$ for the second { } term, the last equation reads

$$\frac{1}{2J+2} Q_{2,2,+} + \frac{2J+1}{2J+2} Q_{2,2,-} = \sum |C(l_\pi, l_\nu)|^2 D_{2,2}$$
$$+ 2 \sum C^*(l_\pi+2, l_\nu) C(l_\pi, l_\nu) X_{2,2}.$$

By use of the relation mentioned above, i.e.,

$$D_{2,2,+} = \frac{L_2 - 3}{L_2} D_{2,2,-}$$

the value of $D_{2,2}$ is found to be

$$D_{2,2} = \frac{(L_2-1)(L_2+\frac{3}{2})}{L_2(L_2+\frac{1}{2})} D_{2,2,-}$$

and this can be computed from Table I. An exactly similar relation exists between $X_{2,2}$ and $X_{2,2,-}$.

If the product of three Hermitian functions $H(n_1, q^{\frac{1}{2}}x) H(n_2, q^{\frac{1}{2}}y) H(n_3, q^{\frac{1}{2}}z)$ is used as the radial part of the single proton wave function, it can readily be shown that the average value of r^2 is $(N+\frac{1}{2})/q$ where $N = n_1+n_2+n_3+1$, and with the further relation $N = 2n-l-1$ where n is the principal quantum number and l the azimuthal quantum number.[5] The relation for r^2 holds not only for $l_\pi' = l_\pi$, $n' = n$ but also for $l_\pi' = l_\pi+2$, $n' = n+1$, i.e., corresponding to the same N. For the light elements, the single proton is in the $2p$ shell and $N = 2$, while for the heavy elements at the end of the periodic table, $N = 5$.[6] As a value for $1/q$ we choose 4.2×10^{-26} cm^2 which has been used in calculations of the binding energy of Li^6,[7] and we will multiply this value by a scale factor equal to the square of the ratio of the nuclear radius of the element in question to the nuclear radius of Li^6, i.e., by (atomic weight/6)$^{\frac{2}{3}}$.

Since the X terms in any column of the tables, i.e., for a particular value of L, are all of the same sign, and since the C's are of both signs, the net effect of summing over the distribution of pairs of values of l_π and l_ν is probably small for these X terms. A similar argument may be applied to the terms involved in $Q_{1,2,+}$. So the

[5] See, for example, H. A. Bethe and R. F. Bacher, Rev. Mod. Phys. **8**, 172 (1936), Eq. (187e).

[6] H. Margenau, Phys. Rev. **46**, 613 (1934).

[7] H. Margenau and K. G. Carroll, Phys. Rev. **54**, 705 (1938).

main contribution for heavy nuclei is likely to come from

$$|a_1|^2 \sum C(l_\tau, l_\nu)^2 D_{1,1,+} + |a_2|^2 \sum C(l_\tau, l_\nu)^2 D_{2,2}.$$

Case I. J=1/2

There should be no appreciable quadrupole moment due to the single proton. Cf. N^{13} and N^{15}, both of which have a nuclear spin of $\frac{1}{2}$ and have one proton lacking from a full $2p$ shell. Casimir[8] has shown that there should be no quadrupole moment for those nuclei that have $J=0$ or $\frac{1}{2}$. Experimental evidence on this point is absent for the quadrupole moment is calculated from the departures of the atomic hyperfine structure from the Landé interval rule. Hence for $J=\frac{1}{2}$, each energy level is split into only two levels and therefore no departures from the interval rule could be computed.

Case II. J=3/2

In this case and the following ones some assumption about the probabilities of the different pairs of values of l_τ and l_ν must be made. For simplicity one might assume that all allowable pairs occurred with equal probability, i.e., $|C(l_\tau, l_\nu)|^2 = \text{constant}$ for all $\mathbf{l}_\tau + \mathbf{l}_\nu = \mathbf{L}$. The average of the D terms must then be used and

$$Q = [|a_1|^2(-0.057) + |a_2|^2(-0.098)]r^2 = -0.057(1+0.72|a_2|^2)\langle r^2\rangle_{Av}$$

for the number of terms computed. It is worthwhile to note that as more D terms are taken the average approaches more nearly the value of the quadrupole moment of a free proton with $l_\tau = L$ and $m_\tau = m_L$. This is indicated at the bottom of the tables.

If one arranges in order of increasing energy, the energy levels of a particle in a potential hole with finite walls, one gets the levels $1s$, $2p$, $3d$, $2s$; $4f$, $3p$, $5g$, $4d$, $6h$, $3s$.[6] The last shell is filled with the 92nd proton, and the $4f$ shell starts to be filled with the 21st proton. While the exact ordering of the levels for this simple picture has little meaning for heavy elements, it does indicate that the values of l_τ may range from 0 to 5 in a random fashion, and our assumption of $|C(l_\tau, l_\nu)|^2 = \text{constant}$ gains a little more plausibility.

[8] H. B. G. Casimir, Physica **2**, 719 (1935).

Similarly under the previous assumptions we find for

$$J=5/2, \quad Q=-0.14(1+0.14|a_2|^2)\langle r^2\rangle_{Av},$$
$$J=7/2, \quad Q=-0.19(1+0.31|a_2|^2)\langle r^2\rangle_{Av},$$
$$J=9/2, \quad Q=-0.27(1+0.2|a_2|^2)\langle r^2\rangle_{Av}.$$

So we see that no matter what the value of a_2, the value of Q increases negatively as J increases.

The only observed quadrupole moments of heavy nuclei which are negative are those of $_{29}Cu^{63} = -0.1$, $_{29}Cu^{65} = -0.1$, and $_{83}Bi^{209} = -0.4 \times 10^{-24}$ cm^2.[9] For both isotopes of copper $J=\frac{3}{2}$, and the magnetic moments[10] indicate that a_2 is probably small. For the Bi nucleus $J=9/2$, a_2 is probably large. So we obtain from the single particle picture a value of

$$Q=-0.05(1+0.72|a_2|^2)\times 10^{-24} \text{ cm}^2 \text{ for Cu}$$

and

$$Q=-0.33(1+0.2|a_2|^2)\times 10^{-24} \text{ cm}^2 \text{ for Bi.}$$

These results indicate that for these three nuclei the quadrupole moment may well be due to a single proton outside of a symmetrically charged spherical core.

The statement of Inglis[1] that "a single proton moving in any state but an s state has a quadrupole moment which is negative" of course applies only to a proton with $m=l>0$,[2]

$$Q=\frac{2[l(l+1)-3m^2]}{(2l+3)(2l-1)}=-\frac{2l}{2l+3}.$$

When $l(l+1)>3m^2$ this is no longer true. The combination of the different states with $m_\tau < l_\tau$ with the neutron functions gives rise to many positive terms, as seen in Table I. On the "average," however, these are more than offset by the negative terms.

The three odd nuclei discussed above are the only ones which have negative Q; all the rest have positive values. In these cases the quadrupole moment must be due to the cooperation of more than one proton outside the spherical core or to a different kind of coupling than that corresponding to our assumption. Among the heavy

[9] H. Schüler and Th. Schmidt, Zeits. f. Physik **111**, 165 (1938); **99**, 717 (1936).

[10] See reference 1(c) Fig. 3. A curve through the upper points would give the Schmidt curve $L_1 = J - \frac{1}{2}$, the bottom points would give $L_2 = J + \frac{1}{2}$.

TABLE II. Values of the quadrupole moments of light nuclei and the quantities used in their calculation.

Element	$25Q/\langle r^2\rangle_{Av}$	C_1	C_2	C_3	$\frac{\langle r^2\rangle_{Av}}{25}\times 10^{26}$ cm^2	Q in units of 10^{-26} cm^2
Li^7	$-(C_1^2+10C_2^2)$	0.681	0.732		0.467	−2.7
N^{13}	0					0
Be^7	$-(8\sqrt{5}\,C_1C_2+7C_1^2)$	0.681	0.732		0.467	−5.7
C^{13}	0					0
Li^8	$(5C_1^2-C_2^2)$	0.785	0.619		0.511	1.4
B^{12}	$-6\sqrt{15}\,C_1C_2$	0.785	0.619		0.670	−7.6
Be^9	$(-8\sqrt{5}\,C_1C_2-7C_2^2+7C_3^2)$	0.731	−0.344	−0.589	0.553	3.4
C^{11}	$-(-8\sqrt{5}\,C_1C_2-7C_2^2+7C_3^2)$	0.731	−0.344	−0.589	0.632	−3.9
B^9	$-6\sqrt{3}\,C_2C_3$	0.731	−0.344	−0.589	0.553	−1.2
B^{11}	$6\sqrt{3}\,C_2C_3$	0.731	−0.344	−0.589	0.632	1.3
N^{13}, N^{15}	0					0

nuclei, moreover, the magnitude of Q is much too large to be caused by a single proton.

QUADRUPOLE MOMENTS OF LIGHT NUCLEI

Some confirmation of the results of the foregoing section as well as further insight into the problem may be gained by calculating the quadrupole moments of light nuclei on the basis of the Hartree model. Feenberg and Wigner[11] have determined the ground state terms in this model and Rose and Bethe[12] have determined the nuclear spin, thus the a's and C's are known. The ground state of each odd nucleus is a P state and for Li^7, Be^7, Be^9, B^{11}, C^{11} the nuclear spin is $J=\frac{3}{2}$, hence $|a_1|^2=1$ and $|a_2|^2=0$. For N^{13}, N^{15}, C^{13}, O^{15} the nuclear spin is $J=\frac{1}{2}$ hence $|a_1|^2=0$ and $|a_2|^2=1$. In the case of N^{13} and N^{15} we have one p proton lacking from a complete shell which would have zero Q. But a hole acts like a proton with a negative charge in determining Q. Hence we can apply our previous result, since $J=\frac{1}{2}$, the quadrupole moment must be zero.

The wave functions for one to five identical p particles have been listed below. These are used in the wave functions of the odd nuclei, which have also been included here in order to show the correct phases which are of importance in obtaining the proper sign for the cross terms. In addition the wave functions for the two even nuclei Li^8 and B^{12}, whose ground state is a P state, have been included. All the other even nuclei have as a ground state an S state and hence will have no quadrupole moment, as can be readily shown.

In order that C_3 for B^9 and B^{11} will have the same sign, it is necessary to use for B^{11} the negative of the $P^1(^2D_\nu\,^2D_\pi)$ function used for B^9. This change of signs, when we pass from a nucleus of n_1 protons and n_2 neutrons to one of $6-n_1$ protons and $6-n_2$ neutrons, occurs only when $l_\pi+l_\nu-L$ is odd. The values of the C's for B^9, B^{11}, Be^9, and C^{11} are the same because of the model used, in which the interaction between protons is equal to the interaction between neutrons, and because of the results of the theory of holes.[13] The C's are not very sensitive to the values of the force constants.[14] From the above considerations it follows, for example, that B^9 and B^{11} will have Q's approximately equal in magnitude but opposite in signs. Similarly for Be^9 and C^{11}.

Using the values of Q calculated for the different light nuclei, we see that the substitution of a proton for a neutron makes Q more negative (exception B^{12}). There is no apparent relation for odd proton, even neutron nuclei as two are negative, two are zero, and one is positive. Also for odd neutron, even proton nuclei, two are negative, one is zero, and one is positive. Most interesting is the case of the addition of a proton to a nucleus whose Q was originally zero. This addition results in a negative Q until the p shell is lacking two protons, then the addition has no effect. This confirms the results of the previous section, that a single proton added to a nucleus with spherically symmetric charge distribution should produce a negative quadrupole moment.

The presence of a large cross term in the cal-

[11] E. Feenberg and E. Wigner, Phys. Rev. **51**, 95 (1937).
[12] M. E. Rose and H. A. Bethe, Phys. Rev. **51**, 205 (1937).
[13] See reference 11, Eq. (11).
[14] See reference 12, Note 12.

culated value of Q for light nuclei in many cases might at first glance suggest that we are not justified in neglecting the effect of cross terms in the previous treatment. But the fault lies rather in the Hartree model. The ground state wave function consists of the sum of only two or three "parent" functions and it is well known that this yields a value of the binding energy which is too small. As more functions are used, the agreement becomes better. This would introduce more cross terms for Q which will, as we have indicated above, probably give a small net contribution.

The author is happy to express his thanks and appreciation to Professor Henry Margenau for suggesting this work and for his helpful interest in its progress.

APPENDIX I

Wave functions for:

One p particle

$P^1 = -a$
$P^0 = b$
$P^{-1} = c.$

Two p particles

$D^2 = aa$
$D^1 = -(ba+ab)/2^{\frac{1}{2}}$
$D^0 = (-ca+2bb-ac)/6^{\frac{1}{2}}$
$D^{-1} = (cb+bc)/2^{\frac{1}{2}}$
$D^{-2} = cc$
$P^1 = (-ab+ba)/2^{\frac{1}{2}}$
$P^0 = (-ac+ca)/2^{\frac{1}{2}}$
$P^{-1} = (bc-cb)/2^{\frac{1}{2}}$
$S^0 = -(ca+bb+ac)/3^{\frac{1}{2}}.$

Three p particles

$D^2 = aab$
$D^1 = (-abb+aac)/2^{\frac{1}{2}}$
$D^0 = -(acb+2abc+bac)/6^{\frac{1}{2}}$
$D^{-1} = (-acc+bbc)/2^{\frac{1}{2}}$
$D^{-2} = bcc$
$P^1 = -(abb+aac)/2^{\frac{1}{2}}$
$P^0 = (-acb+bac)/2^{\frac{1}{2}}$
$P^{-1} = -(acc+bbc)/2^{\frac{1}{2}}.$

Four p particles

$D^2 = aabb$
$D^1 = (aacb+aabc)/2^{\frac{1}{2}}$
$D^0 = (-bacb+2aacc-abbc)/6^{\frac{1}{2}}$
$D^{-1} = -(bacc+abcc)/2^{\frac{1}{2}}$
$D^{-2} = bbcc$
$P^1 = (-aacb+aabc)/2^{\frac{1}{2}}$
$P^0 = (bacb-abbc)/2^{\frac{1}{2}}$
$P^{-1} = (bacc-abcc)/2^{\frac{1}{2}}$
$S^0 = -(bacb+aacc+abbc)/3^{\frac{1}{2}}.$

Five p particles

$P^1 = aabbc$
$P^0 = aabcc$
$P^{-1} = -abbcc.$

APPENDIX II

Wave functions for:

Li^7 (2 neutrons, 1 proton) and N^{13} (4 neutrons, 5 protons).

$$C_1(^1D_\nu\,{}^2P_\pi)+C_2(^1S_\nu\,{}^2P_\pi),$$

where

$$P^1(^1D_\nu\,{}^2P_\pi)=\{D_\nu{}^0P_\pi{}^1-3^{\frac{1}{2}}D_\nu{}^1P_\pi{}^0+6^{\frac{1}{2}}D_\nu{}^2P_\pi{}^{-1}\}/10^{\frac{1}{2}}$$

and

$$P^1(^1S_\nu\,{}^2P_\pi)=S_\nu{}^0P_\pi{}^1.$$

For Be^8 (2 protons, 1 neutron) and C^{13} (4 protons, 5 neutrons) the subscripts ν and π are interchanged. $C_1=0.681$, $C_2=0.732$.

Li^8 (3 neutrons, 1 proton).

$$C_1(^2P_\nu\,{}^2P_\pi)+C_2(^2D_\nu\,{}^2P_\pi),$$

where

$$P^1(^2P_\nu\,{}^2P_\pi)=\{P_\nu{}^0P_\pi{}^1-P_\nu{}^1P_\pi{}^0\}/2^{\frac{1}{2}}$$

and

$$P^1(^2D_\nu\,{}^2P_\pi)=\{D_\nu{}^0P_\pi{}^1-3^{\frac{1}{2}}D_\nu{}^1P_\pi{}^0+6^{\frac{1}{2}}D_\nu{}^2P_\pi{}^{-1}\}/10^{\frac{1}{2}}.$$

For B^8 (3 protons, 1 neutron) the subscripts are interchanged. For N^{12} (3 neutrons, 5 protons) the negative of the $P^1(^2P_\nu\,{}^2P_\pi)$ must be used, and for B^{12} (3 protons, 5 neutrons) the subscripts in the N^{12} functions are interchanged. $C_1=0.785$, $C_2=0.619$.

B^9 (2 neutrons, 3 protons).

$$C_1(^1S_\nu\,{}^2P_\pi)+C_2(^1D_\nu\,{}^2P_\pi)+C_3(^1D_\nu\,{}^2P_\pi),$$

where

$$P^1(^1S_\nu\,{}^2P_\pi)=S_\nu{}^0P_\pi{}^1,$$
$$P^1(^1D_\nu\,{}^2P_\pi)=\{D_\nu{}^0P_\pi{}^1-3^{\frac{1}{2}}D_\nu{}^1P_\pi{}^0+6^{\frac{1}{2}}D_\nu{}^2P_\pi{}^{-1}\}/10^{\frac{1}{2}},$$
$$P^1(^1D_\nu\,{}^2D_\pi)=\{-2^{\frac{1}{2}}D_\nu{}^{-1}D_\pi{}^2+3^{\frac{1}{2}}D_\nu{}^0D_\pi{}^1 - 3^{\frac{1}{2}}D_\nu{}^1D_\pi{}^0+2^{\frac{1}{2}}D_\nu{}^2D_\pi{}^{-1}\}/10^{\frac{1}{2}}.$$

For Be^9 (2 protons, 3 neutrons) the subscripts are interchanged. For B^{11} (4 neutrons, 3 protons) the negative of $P^1(^1D_\nu\,{}^2D_\pi)$ must be used and for C^{11} (4 protons, 3 neutrons) the subscripts in the B^{11} functions are interchanged. $C_1=0.731$, $C_2=-0.344$, $C_3=-0.589$.

Cloud-Chamber Study of Collision Electrons in Equilibrium with Mesons

LEO SEREN
University of Chicago, Chicago, Illinois

(Received May 27, 1942)

A 30-cm counter-controlled Wilson cloud chamber contained a tungsten plate of 3.81-cm thickness. A block of lead either 2.54 or 7.62 cm placed above the cloud chamber enabled a distinction to be made between mesons and electron showers. 601 meson tracks were observed (no magnetic field), 497 of which traversed the tungsten plate. From these, the percentage of fast collision electrons in equilibrium with mesons in tungsten and lead was found to be 10.5 percent and 8 percent, respectively, in good agreement with the theories of Bhabha, and Tamm and Belenky. 143 collision electrons with energy range from 13 kev to 175 kev were produced by meson tracks in the gas and indicated a $1/E^2$ differential spectrum. Some interesting individual events associated with mesons are described.

I. RELATION BETWEEN SOFT AND HARD COMPONENT AT SEA LEVEL

IT is now generally believed that the soft component of cosmic rays at sea level consists of electrons, and that the bulk of these electrons arise from the mesons, or penetrating component of cosmic rays. Electrons arise from mesons by three different processes. (1) Mesons create collision electrons[1] by elastic Coulomb field encounters with atomic electrons. (2) Mesons which pass very close to atomic nuclei radiate quanta. The quanta can give rise to electrons by materialization. (3) It is believed that the radioactive decay of the meson liberates an electron and a neutrino. Energetic electrons arising from all three of these processes give rise to cascade progeny. These electrons make up the soft component, which is in equilibrium with the meson component at sea level.

Previous investigators have measured the amount of soft component in equilibrium with the hard component by means of Geiger-Müller counters. But results published in the literature are widely divergent and depend on the conditions of the individual experiment. A consistent picture seems to be that 30–43 percent of cosmic radiation at sea level in free air is soft component.[2] But when the measurements are made under 6 cm Pb, or under $\approx$30 m H_2O equivalent of soil, the decay electrons and progeny are all absorbed, leaving $\approx$10 percent due to collision electrons.[3]

The following factors affect the results of counter experiments. The thickness of the counter walls is very critical because of the large proportion of slow electrons in cosmic rays. By using counters with very thin walls, Danforth and Lipman[4] have shown that the number of cosmic rays between 5×10^6 ev and 10^7 ev is $\frac{1}{8}$ of the total intensity above 10^7 ev. The presence of a roof over the apparatus increases the soft component, and nearby walls can cause side showers which can trip the counters without penetrating the absorber. The geometrical arrangement of the counters affects the experiment strongly since the hard component decreases much more rapidly with zenith angle than does the soft component.[5] Furthermore, a Geiger counter will always count as one particle, two particles which simultaneously fall within its cross-sectional area. So it is easy to see why almost every different counter experiment gives

[1] Collision electrons are sometimes called "knock-ons" or "delta-rays."

[2] W. M. Nielsen and K. Z. Morgan, Phys. Rev. **54**, 245 (1938); K. Greisen, Phys. Rev. **61**, 212 (1942).

[3] P. Auger (Comptes rendus **206**, 346 (1938)) reports that under 1 m H_2O equivalent plus 6 cm Pb, and also 30 m H_2O equivalent soil, 9 percent of soft component is in equilibrium with the penetrating component.

[4] W. E. Danforth and M. R. Lipman, J. Frank. Inst. **217**, 73 (1934). The twofold coincidence set used required particles to penetrate a thickness of only 0.36 gram/cm^2 to be recorded. Setting the lower limit of cosmic-ray energies at 5×10^6 ev excludes practically all electrons from natural radioactivity.

[5] The soft component is more strongly scattered in the atmosphere, hence decreases less rapidly with zenith angle. Beneath 30 meters of soil, Auger and Grivet (Rev. Mod. Phys. **11**, 232 (1939)) found that the soft component diminished only $\approx$20 percent between 0° and 60° zenith angle, while the hard component diminished $\approx$65 percent for the same angles.

a different value for the amount of soft component in equilibrium with the hard component.

The present experiment attempts to simplify the picture by studying electrons produced by mesons by only the first of the above-listed three processes, namely, collision electrons. A Wilson cloud chamber is used to detect the meson and the collision electrons. The cloud chamber enables positive identification of all the collision electrons accompanying the meson in the chamber, and is not subject to the uncertainties of Geiger counter experiments listed above.

In this experiment electrons arising from bremsstrahlung quanta were unimportant in number and those from radioactive decay were not observed. Bhabha[6] has shown from theoretical considerations that the amount of soft component produced by bremsstrahlung quanta is negligible compared to that produced by collision electrons, if the mesons have mass $\geqslant 100$ electrons masses. All the mesons observed here traversed the chamber, hence could not have decayed. A discussion of the amount of soft component arising from decay electrons has been given by Rossi and Greisen.[7]

In this paper the terms "penetrating component" and "mesons" are used synonymously. However, it is possible that as much as 5 percent of the penetrating component may consist of protons.

II. EXPERIMENTAL APPARATUS

The apparatus consisted of a Wilson cloud chamber whose expansions were controlled by a threefold Geiger counter-coincidence system, as shown in Fig. 1. Between the upper two counters and the cloud chamber was a block of lead. This was 7.62 cm thick for most of the expansions, but was reduced to 2.54 cm for others. The upper two counters were glass walled with a copper cylinder, while the small counter was made of brass. All counters were filled with ethyl alcohol and argon gas in the conventional way. The cross-sectional area of the upper counters was 22.8×4.13 cm^2 while that of the small brass counter was 10×0.795 cm^2.

The cloud chamber was 30 cm in diameter, of which a vertical strip 10 cm wide $\times$ 30 cm high was visible. The depth of the illuminated region was 4 cm. A horizontal brass box was built into the front of the chamber similar to the arrangement used by Code.[8] The interior of the brass box was accessible without dismantling the chamber. Contained in the box were 6 bars of tungsten and the brass-walled Geiger counter. The six bars had a total thickness of 3.81 cm. Because of the high density of tungsten (19.3 grams/cm^3), a particle which traverses 3.81 cm suffers an ionization loss equal to that from 6.8 cm of Pb. The cloud chamber was filled with undiluted ethyl alcohol and pure argon gas to a total pressure of 995 mm Hg. The diaphragm and expansion valve were similar to that used by Jones and Hughes.[9] A new expansion ratio backstop plate was built. This plate was adjusted by three screws so that it could control distortions as well as the expansion ratio.

The photographic system consisted of a 35-mm commercial camera and three plane mirrors for

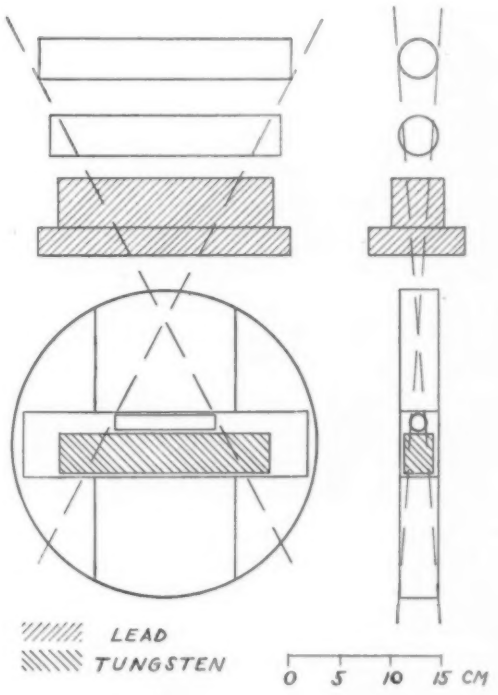

FIG. 1. Arrangement of cloud chamber and triple-coincidence system, showing the lead block above the chamber and the tungsten plate in the chamber.

[6] H. J. Bhabha, Proc. Roy. Soc. London **A164**, 257 (1938).
[7] Bruno Rossi and Kenneth Greisen, Phys. Rev. **61**, 121 (1942).
[8] F. Leslie Code, Phys. Rev. **59**, 229 (1941).
[9] Haydn Jones and Donald Hughes, Rev. Sci. Inst. **11**, 79 (1940).

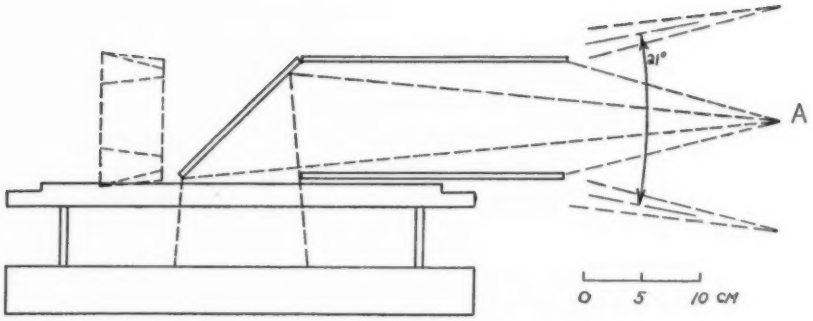

FIG. 2. Stereo-optical diagram, showing cloud chamber, 45° mirror, and two parallel mirrors, enabling a single lens at A to take three pictures.

taking stereo pictures. The lens was a Zeiss f: 2.8 and 50-mm focal length. Figure 2 shows the optical system, which was designed to enable the cloud chamber to operate between the pole pieces of the cosmic-ray magnet at the University of Chicago. During this experiment, however, it was not possible to operate the magnet. The camera looks into the mirror placed at 45° to the plane of the chamber and takes a direct picture. The two plane mirrors parallel to the plane of the chamber enable the camera to view the chamber at an angle of $10\frac{1}{2}°$ on either side of the direct picture. Any two of the three pictures can be used for stereo comparison. When the film is projected on a plane surface, three images appear. For points on the outer two images, their separation is proportional to the distances normal to the plane of the chamber. A calibration was made by photographing the cloud chamber with fine threads on its front and back surface. Thus stereo distances could easily be measured upon projection on a plane surface, without the use of a stereo-calibrator.

The illumination of the cloud chamber was obtained with the use of medium bi-post street lamps. Nine such lamps were mounted on units consisting of street lamp, spherical mirror, and double convex lens. Both the mirror and lens were of short focus, so that the optical system gathered approximately 2.5 out of a possible 4π steradians of luminous flux. The street lamps were of clear glass and the filament was shaped into a slender helix of diameter 0.32 cm and length 3.81 cm. These dimensions were proportional to those of the cross section of the chamber, so that an enlarged image of the filament filled the entire chamber. The image was focused beyond the chamber, so that while passing through the chamber, the light was convergent and out of focus. The beams from nine such units provided a solid bank of illumination for the cloud chamber. The convergent character of the beams was essential in keeping light off the background.

The street lamps were rated at 6000 lumens, drawing 6.6 amperes at 49 volts under normal operation. In this experiment, the lamps were flashed at 77 volts, since banks of three lamps were connected in series across 230 volts, a.c. For each picture the current was left on for $\frac{1}{3}$ second. The make contact was established by ordinary $\frac{3}{16}''$ tungsten contact points, but break was established by a cut-out relay. This relay was actuated by a thyraton, controlled by an electronic time delay circuit.

III. COLLISION ELECTRONS IN EQUILIBRIUM WITH MESONS IN TUNGSTEN

These data result from 497 pictures in which a meson traverses the tungsten plate. That the primary particle was a meson (or other heavy particle) is certain because electrons below 10^{10} ev would not penetrate 3.81 cm of tungsten. In addition, the mesons had to penetrate either 7.62 or 2.54 cm of Pb above the cloud chamber. Above the apparatus was only a thin roof. The electrons which accompany mesons emerging from the bottom of the tungsten plate give a true picture of equilibrium conditions within the tungsten. The results in Table I give the number of fast and slow electrons accompanying the mesons out of the tungsten. Electrons whose tracks were straight were classed as fast electrons. Since their tracks showed no scattering

TABLE I. No. of collision electrons N accompanying 497 mesons emerging from 3.81 cm of tungsten.

	N fast ($E>1$ Mev)	N slow ($E<1$ Mev)	N total (N fast $+N$ slow)	N slow heavy particles (short dense tracks)
	52	22	74	3
Percent of mesons traversing tungsten	52/497 = 10.5%	22/497 = 4.4%	74/497 = 14.9%	3/497 = 0.6%

TABLE II. Collision electron showers accompanying 497 mesons emerging from 3.81 cm of tungsten.

No. of showers	Particles per shower
Fast electron showers ($E>1$ Mev)	
3	2
1	3
2	5
Slow electron showers ($E<1$ Mev)	
3	2

in the gas, their kinetic energy was above 1 Mev. Electrons whose tracks did show scattering in the gas were classed as slow electrons of kinetic energy <1 Mev. A few short, dense tracks were observed, which must have been caused by heavy particles.

Most of the electrons which accompanied the mesons occurred singly, but cases of showers of collision electrons occurred also. The results are listed in Table II.

Some of the slow electrons probably arose from radioactive contamination. Hence the data presented on slow collision electrons are not as accurate as those for the fast collision electrons.

Collision electrons were also created in the lead block (either 2.54 or 7.62 cm thick) above the cloud chamber, and in the glass ring at the top of the chamber. These data are not as accurate as those for the collision electrons arising from the tungsten plate because the lead block was 4.45 cm above the top of the cloud chamber, and the glass ring (2 grams/cm^2) was not thick enough to allow equilibrium. In spite of these inaccuracies these data do give a good idea of the number of collision electrons arising in such cases, and are presented in Table III.

The collision electrons from the lead had to pass through the glass ring, which set a lower limit to the energy of the fast electrons. Electrons which showed no scattering in the gas had $E>1$ Mev in the chamber. But 4.3 Mev was necessary to penetrate the glass ring, or a total kinetic energy >5.3 Mev when emerging from the lead. Again the data on slow electrons are subject to inaccuracies due to the presence of such electrons from radioactive contamination.

Table III gives the results of 601 pictures in which mesons traversed the lead and glass ring. This number is larger by 104 than the number of mesons which traversed both the lead and the tungsten, because (a) some of the mesons traversed the top half of the chamber at such an angle as to pass out of view below the tungsten and (b) some of the mesons stopped in the tungsten. Showers of electrons sometimes tripped the threefold coincidence system, but they were easily distinguished from the mesons, and were not counted. Figures 3, 4, and 5 show typical collision electrons arising from the tungsten or lead.

From theoretical considerations, the number of collision electrons which accompany mesons as they traverse different substances has been calculated by two different authors. Tamm and Belenky[10] give the results in the form of an

[10] Ig. Tamm and S. Belenky, J. Phys. Acad. Sci. U.S.S.R. 1, 177 (1939).

TABLE III. No. of collision electrons N accompanying 601 mesons traversing the lead block and upper glass ring of cloud chamber.

Lead			Glass			
N fast ($E>5.3$ Mev)	N slow ($4.3<E<5.3$ Mev)	N total (N fast$+$ N slow)	N fast ($E>1$ Mev)	N slow ($E<1$ Mev)	N total (N fast$+$ N slow)	
48	10	58	13	3	16	
48/601 = 8%	10/601 = 1.7%	58/601 = 9.7%	13/601 = 2.2%	3/601 = 0.5%	16/601 = 2.7%	Percent of mesons traversing lead or glass

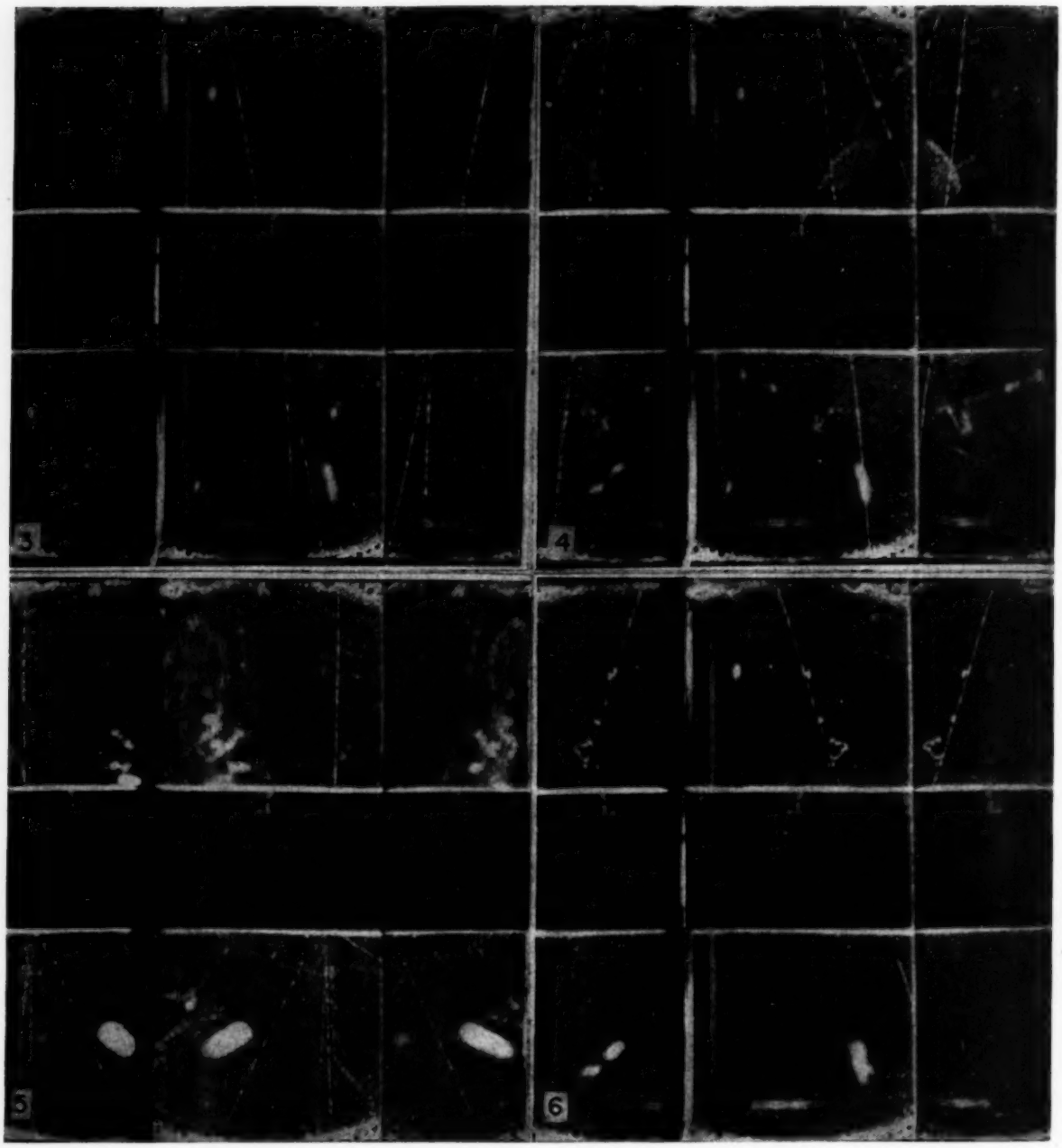

FIGS. 3–6.

FIG. 3. A meson penetrates 3.81 cm of tungsten and is accompanied by a collision electron. The central picture corresponds to a direct view while the two outer pictures are used for stereo comparison.

FIG. 4. A collision electron arising in the lead block above the cloud chamber accompanies the meson. The electron is stopped, but the meson penetrates the tungsten without multiplication.

FIG. 5. An electron shower of 5 particles accompanies the meson traversing the tungsten.

FIG. 6. Low energy collision electrons produced in the gas. Three such electrons arise from the meson track in the top half of the chamber.

integral spectrum $N(E)$, of the mean number of electrons of energy greater than E which accompany mesons in air and Pb. Bhabha's[6] results give two points of the integral spectrum, namely, $N(E_c)$ the number of electrons of energy greater than the critical energy, and $N<(E_c)$ the number

TABLE IV. Theoretical and experimental values of the percent of electrons $N(E)$ of energy greater than E which accompany mesons in lead.

Theory			Experiment	
Bhabha	Tamm and Belenky	Tamm and Belenky		
$E_0=10^{10}$ ev $\mu=100m$	$E_0=10^{10}$ ev $\mu=100m$	$E_0=1.7\times10^{9}$ ev $\mu=160m$	Tungsten	Lead
E_c for Pb, 10 Mev $N(E_c)=9.0\%$	E_c for Pb, 10 Mev $N(E_c)=5.3\%$	E_c for Pb, 10 Mev $N(E_c)=2.3\%$		
	$E=5.3$ Mev $N(E)=8.1\%$	$E=5.3$ Mev $N(E)=4.0\%$		$E=5.3$ Mev $N(E)=8.0\%$
	$E=4.3$ Mev $N(E)=9.7\%$	$E=4.3$ Mev $N(E)=5.0\%$		$E=4.3$ Mev $N(E)=9.7\%$
	$E=1.3$ Mev $N(E)=18.8\%$	$E=1.3$ Mev $N(E)=11.0\%$		
			$E=1$ Mev $N(E)=10.5\%$	
$N(E)=19.0\%$ Total			$N(E)=14.9\%$ Total	

of electrons of energy less than the critical energy, the sum of these two giving N total. The results are given for air or water, and lead.

The interaction between mesons and atomic electrons of matter is due mostly to Coulomb forces. But when a meson passes very close to an electron, as happens in the production of high energy collision electrons, the spin of the meson becomes all important.[11] From other experiments in cosmic rays spin 1 seems unlikely for the meson, and spin 0 and spin ½ give essentially the same collision cross sections. So, in this sense, the integral spectrum of collision electrons may be said to be spin independent.

Tamm and Belenky have shown that the shape of the integral spectrum $N(E)$ is rather insensitive to variations of mass and energy of the generating mesons. They have calculated $N(E)$ for two kinds of primary mesons. (a) $\mu=100m$ and $E_0=10^{10}$ ev; (b) $\mu=160m$ and $E_0=1.7\times10^{9}$ ev (μ=mass of meson; m=mass of electron; E_0=energy of generating meson) and find that the curves differ by only a few percent. Hence the integral spectra $N(E)$ are applicable to sea level mesons, whose spectrum has a maximum at $\approx1.5\times10^{9}$ ev. Tamm and Belenky further show that the customary neglect of ionization losses for electrons of greater than critical energy reduces up to 50 percent the number of electrons in the vicinity of the critical energy.

The integral spectrum $N(E)$ of collision electrons decreases monotonically with increasing energy E, and decreases faster for lead than for air. The production of collision electrons is proportional to the density of electrons, hence is proportional to Z. But the cascade absorption of high energy collision electrons introduces a factor $1/Z^2$, so that the number of high energy collision electrons in different elements falls off roughly as $1/Z$.

The experimental and theoretical values of the percentage of electrons accompanying mesons in lead are given in Table IV. Since the atomic number of tungsten (74) is not far different from that of lead (82), the experimental values for tungsten may be compared with the theoretical values for lead. The experimental values from the glass ring cannot be compared with the theory since the glass ring was not thick enough to allow equilibrium. The energy and mass of the mesons used in the theoretical calculations are given in the table.

In view of the scarcity of theoretical and experimental values of $N(E)$, a comparison is

[11] The cross section for production of high energy collision electrons by mesons is given for spin 0, ½, and 1 by B. Rossi and K. Greisen, Rev. Mod. Phys. **13**, 244 (1941).

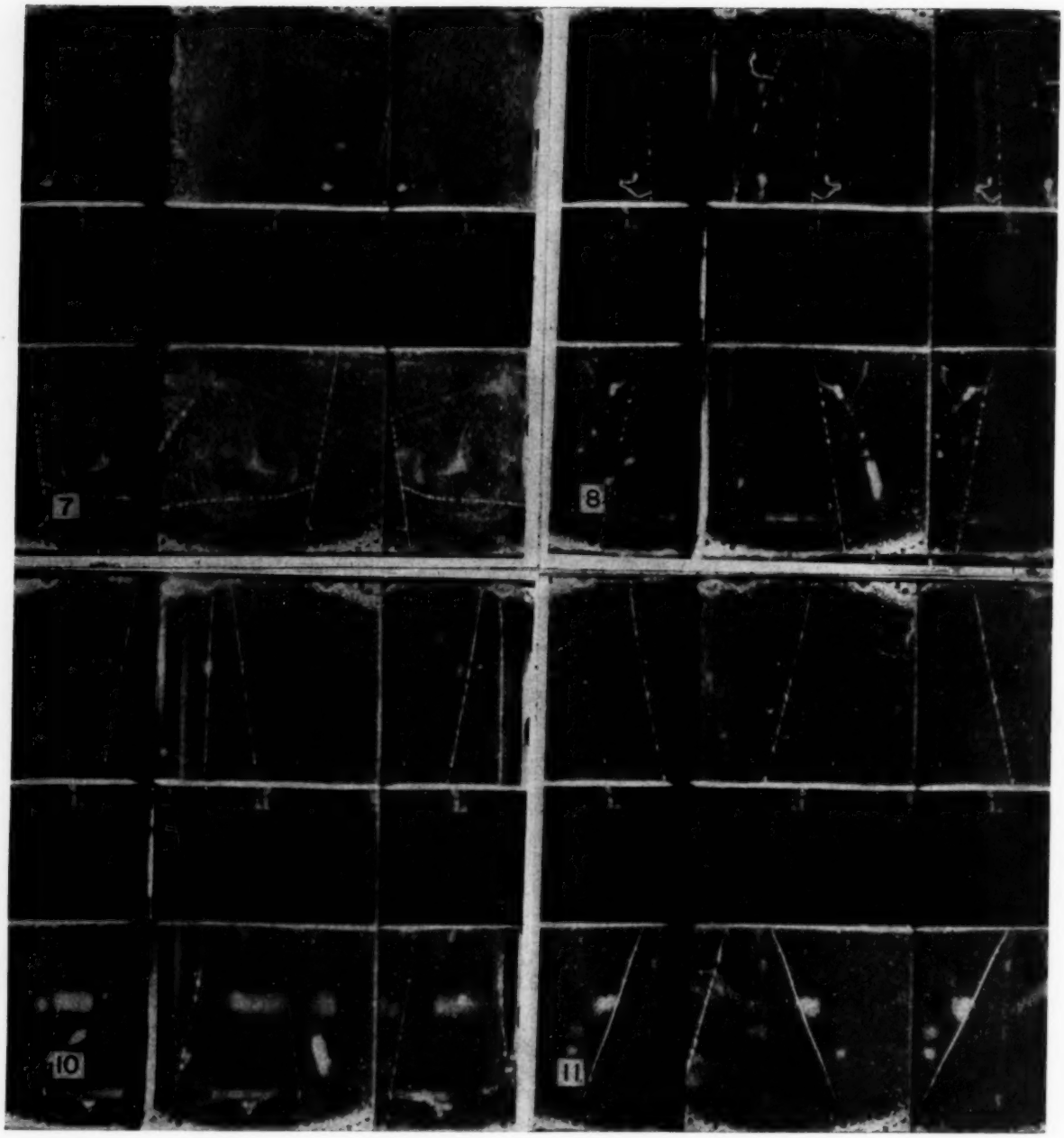

FIGS. 7–8, 10–11.

FIG. 7. Two collision electrons arise from the meson track in the bottom half of the chamber. One electron passes out of view.

FIG. 8. Three collision electrons from a single meson. The meson produces a collision electron in the gas near the top of the tungsten plate, and penetrates the tungsten with a small deflection due to scattering. A collision electron also arises from the lead above the chamber and gives rise to a secondary collision electron in the gas near the top of the photograph.

FIG. 10. Shower of two mesons arising from the 7.62 cm Pb above the chamber penetrates the tungsten without multiplication. One of the tracks is slightly blurred in the botton half of the chamber due to motion of the gas.

FIG. 11. Possible nuclear disintegration arising in the tungsten. The penetrating particle shows very small scattering (2°) in the 3.81-cm tungsten plate. The heavily ionizing particle appears to arise in the center of the tungsten, and gives rise to two low energy collision electrons in the gas. These can be seen best in the right-hand picture.

made by interpolation. Recall that $N(E)$ is a decreasing function of E. The experimental data from tungsten are smaller than all of the interpolated theoretical values, but do not differ much from that of Tamm and Belenky for E_0 1.7×10^9 ev. The experimental data from lead agree very well with Tamm and Belenky for E_0 10^{10} ev. These values are greater than Tamm and Belenky for E_0 1.7×10^9 ev but are only slightly smaller than interpolated values of Bhabha.

Bhabha[6] has calculated also the probabilities of mesons being accompanied by shower electrons of energy greater than critical energy. Experimental values obtained from Table II are compared with Bhabha's values in Table V.

The agreement is rather close considering the small number of showers observed. A more detailed study of collision electron showers has been made by Lovell.[12]

IV. LOW ENERGY COLLISION ELECTRONS PRODUCED IN THE GAS OF THE CLOUD CHAMBER

One hundred and forty-three collision electrons were observed arising in the gas of the cloud chamber. These had ranges in the gas from 2 mm (the smallest discernable) to 130 mm. Figures 6, 7, and 8 show typical collision electrons produced. The cloud chamber was filled with ethyl alcohol, C_2H_5OH (vapor pressure at room temperature 45 mm Hg) plus 950 mm Hg of argon to make a total pressure of 995 mm Hg. To a good approximation, the gas can be considered entirely argon, having a density of 2.33×10^{-3} g/cm³. The 143 collision electrons were produced by 601 mesons which traversed the chamber for an average path length of 17.11 cm in the gas. Thus the total meson path length was 103.82 meters, corresponding to a thickness of 24.2 grams/cm² of argon.

The range in cm of the collision electrons multiplied by the density of the gas gives the range in grams/cm² of argon. From natural radioactivity, the range of beta-rays in grams/cm² of aluminum *versus* energy is well known.[13] Since aluminum lies close to argon in the periodic table, the experimental beta-ray curves can be used to determine the energies of the collision electrons. The values deduced for low energy collision electrons may be high by a factor not exceeding 1.5 because the true scattered length of track measured in the cloud chamber is longer than the equivalent aluminum range.

TABLE V. Probabilities of mesons in lead being accompanied by showers of electrons.

No. of electrons in shower	2	3	4	5
Bhabha's values	0.014	—	0.0057	0.0038
Experimental values	0.006	0.002	—	0.0040

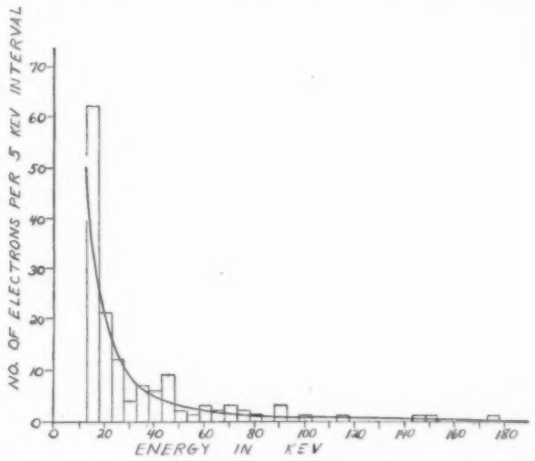

FIG. 9. Collision electrons produced in the gas of the cloud chamber by 103.82 meters of meson track. The blocks represent experimental points, and the solid curve the Rutherford formula.

In this manner the energies of one hundred forty-three collision electrons were tabulated. The energy spectrum pictured in Fig. 9 was then made by means of a block diagram, the height of each block being proportional to the number of collision electrons having energies in a given 5-kev spread. The solid curve in Fig. 9 is the theoretical value of the number of collision electrons given by the Rutherford formula (discussed below). The agreement between theory and experiment is quite good, both as to the shape of the spectrum and the total number of electrons in the spectrum. At the lowest energy interval, an additional number of electrons is observed, due to Auger electrons arising from krypton impurities of the argon gas.[14]

[12] A. C. B. Lovell, Proc. Roy. Soc. **A172**, 568 (1939).

[13] Franco Rasetti, *Elements of Nuclear Physics* (Prentice-Hall, New York, 1936).

[14] The K-absorption limit for krypton is 14.3 kev, giving an Auger electron range of ≈2 mm in the cloud chamber. The K limit for argon is 3.2 kev, giving only a blob in the meson track. A rough check of the number

The Rutherford formula was developed to explain ionization losses of radioactive particles. But for low energy transfers it applies equally well to cosmic rays. Such low energy transfers are not dependent on the spin of the meson.[15] The probability that a meson will produce a collision electron in the energy range E, $E+dE$ in traversing a thickness of matter dx grams/cm^2 is given by the Rutherford formula:

$$P(E)dEdx=\frac{2\pi n(Z)r_0^2\,dE}{m(A)\beta^2\quad E^2}dx.$$

$\beta=v/c$ velocity of mesotron; m=mass of electron in ev/c^2; r_0=classical electron radius, e^2/mc^2; n=Avogadro's no. For sea level mesons, β may be set equal to unity to a good approximation. The differential spectrum for low energy collision electrons falls off as $1/E^2$ and is indicated by the block diagram of Fig. 9.

Integration of the Rutherford formula gives the total number of collision electrons in the gas:

$$N(E)=\int_{13\text{ kev}}^{200\text{ Mev}}P(E)dE.$$

The lower limit is 13 kev since this is the lowest energy collision electron which can be detected. The integral is practically independent of its upper limit, so long as it is large compared to the lower limit.[16] On setting dx equal to 24.2 grams/cm^2 of argon, integration gives $N=124$ collision electrons. Counting the number of collision electrons in the blocks of the energy spectrum, and substituting the theoretical value for the lowest energy interval, one gets 115. Thus the comparison with the theory is quite good considering the small number of particles observed.

The result of the energy spectrum may be interpreted as follows. In passing through light elements, fast mesons (or electrons) create approximately $120/(24.2)=5$ collision electrons of energy greater than 13 kev per gram/cm^2. Low energy electrons from cosmic rays are more numerous than is generally believed, and play an important part in counter experiments.

V. INTERESTING INDIVIDUAL EVENTS ASSOCIATED WITH MESONS

Pictures obtained show one meson shower, one possible nuclear disintegration, and a number of slow mesons which are stopped in the tungsten.

Out of 591 pictures, 10 show 2 mesons traversing the tungsten in the center of the chamber. Nine of these have mesons which do not show space or time association, hence are not related. (Space association refers to the tracks diverging from some point above the cloud chamber. Time association refers to the age of the tracks. Two sharp tracks cannot be separated by more than 5×10^{-2} sec.) One picture shows two mesons of apparently the same age traversing the tungsten, yet, from the fact that they converge toward a point *below* the cloud chamber, these mesons cannot be related.

The probability for a second meson to accompany the counter controlled expansion of the cloud chamber is easily calculated. The meson flux at sea level has been given as 0.64 per cm^2 per minute per unit solid angle.[17] The cloud chamber had a cross section of $10\times4=40$ cm^2. To penetrate the tungsten, the mesons had to travel at least 20 cm in the chamber, giving a solid angle of $40/400=0.1$. The sensitive time of the cloud chamber being of the order 3×10^{-1} sec. (because of the low sweep field), the probability of a meson traversing for a random expansion was $\approx1.3\times10^{-2}$. This shows that for 600 controlled expansions, 8 should have two meson tracks. This number is of the same order as the number (10) actually observed.

---

of electrons in the 13–18 kev interval was made as follows. The number of blobs due to K ionization of argon was found to be ≈60 per meter of track, or 6000 for the total track. Krypton comprises ≈1 percent of argon. Furthermore, K ionization of krypton is only $\frac{1}{2}$ as frequent as argon, because krypton has twice as many electrons. Thus the total number of electrons from K ionization of krypton should be $\frac{1}{2}$ of 1 percent of 6000, or 30. From the 13–18 kev interval of the spectrum it will be seen that the observed number exceeds that given by the Rutherford formula by approximately 30.

[15] See pp. 243 and 244 of reference 11.

[16] The energy E which a collision electron of mass m receives from a meson of mass is determined from classical mechanics

$$E=\frac{2(mc^2)p^2\cos^2\theta}{[mc+(p^2+\mu^2c^2)^{\frac{1}{2}}]^2-p^2\cos^2\theta},$$

where p is the momentum of the meson and θ the angle between the meson and electron track. Setting $\cos\theta$ equal to unity gives $E_{\max}$. For $p=1.5\times10^9$ ev/c, $\mu=10^8$ ev/c^2, $m=5\times10^5$ ev/c^2, the formula gives $E_{\max}=200$ Mev.

[17] See page 571 of reference 12.

Figure 10 shows two mesons of the same age diverging from a point in the 7.62 cm of lead above the chamber and traversing the tungsten. This event is interpreted as a true meson shower. Showers of penetrating particles at sea level have been obtained by counter experiments,[18] but cloud-chamber evidence is quite rare. Janossy[19] has obtained a photograph of 3 mesons penetrating 2 cm of Pb in the cloud chamber without multiplication. At higher altitudes three pictures of meson showers have been reported.[20] Such meson showers may give information on the production of mesons.

Figure 11 may represent a nuclear disintegration. A penetrating particle traverses the tungsten with no appreciable scattering. From the center of its path in the tungsten a heavily ionizing particle emerges, after having itself traversed 1.9 cm of tungsten. The heavily ionizing particle is not appreciably scattered in the gas, and emits two small collision electrons of range ≈ 1 mm. (These can be seen best in the right-hand view.) Near the bottom of the chamber, the heavily ionizing particle passes into the back velvet.

The heavily ionizing particle cannot be an electron. An electron which ionized so heavily would have a low velocity ($\beta < 0.3$); it would be greatly scattered and could have a range of only ≈ 1 cm in the chamber. If the heavily ionizing particle is a proton, it must have an energy of 150 Mev to penetrate 1.9-cm tungsten. If it is a meson, it must have 64 Mev to penetrate the 1.9 cm of tungsten.

The primary particle of Fig. 11 has an energy $\approx 10^9$–10^{10} ev which is deduced from its small scattering (2°) in the 3.81 cm of tungsten. Williams'[21] theory of the scattering of cosmic-ray particles gives a mean scattering angle $\bar{\alpha} = 2.2 \times 10^9$ ev degrees for 3.81 cm of tungsten.

It is unlikely that the heavily ionizing particle is produced by an elastic collision for then the primary would show a greater change in direction, having given up so much of its energy in the process.

The small collision electrons arising from the heavily ionizing particle seem to indicate that the particle is traveling slowly in the gas ($\beta \approx 0.1$). Only a proton could have a range as great as the observed range (10.4 cm in the chamber before passing into the background velvet) with a velocity as low as $\beta = 0.1$.

For most nuclear disintegrations that have been observed, the energy per particle is below 100 Mev and the total energy of all charged particles is less than 200 Mev per disintegration. The single heavily ionizing particle observed here has by itself 150 Mev which seems rather high for a nuclear disintegration. If the heavily ionizing particle is a meson, it has at present no theoretical explanation.

Nuclear disintegrations arising in cloud chambers have been reported by several observers in the past. From 9188 exposures taken at 4300 meters, Anderson[22] reports 6 definite nuclear disintegrations, 5 occurring in a 0.35-cm lead plate and one occurring in the gas of the chamber. The energies of the heavily ionizing particles, where measureable by curvature, were below 50 Mev. From 20,500 counter controlled photographs at sea level, Brode and Starr[23] observed 10 definite nuclear disintegrations arising from the walls or metal plates inserted in the cloud chamber. Several other cloud-chamber nuclear disintegrations have been reported.[24] A great number of nuclear disintegrations have been observed in photographic emulsions.[25]

In regard to the number of slow mesons at sea level, the data can be analyzed in the following way. Of the 601 mesons observed, 71 traversed the top of the chamber diagonally so as to pass out of view in the bottom half. For

[18] L. Janossy, private communication to the University of Chicago; G. Wataghin *et. al.*, Phys. Rev. **57**, 61, 339 (1940); P. Auger and J. Daudin, Phys. Rev. **61**, 549 (1942).
[19] L. Janossy *et al.*, Nature **148**, 660 (1941).
[20] D. J. Hughes, Phys. Rev. **60**, 414 (1941); W. M. Powell, Phys. Rev. **60**, 413 (1941); E. O. Wollan, Phys. Rev. **60**, 532 (1941).
[21] E. J. Williams, Proc. Roy. Soc. **169**, 531 (1939).
[22] C. D. Anderson and S. H. Neddermeyer, Phys. Rev. **50**, 263 (1936).
[23] R. B. Brode and M. A. Starr, Phys. Rev. **53**, 3 (1938).
[24] P. Auger and P. Ehrenfest, J. de phys. et rad. **8**, 204 (1937); J. Crussard and L. Leprince-Ringuet, J. de phys. et rad. **8**, 213 (1937); P. Kunze, Zeits. f. Physik **83**, 1 (1933); S. Nishida, Proc. Phys. Math. Soc. Japan **19**, 818 (1937). W. M. Powell (Phys. Rev. **61**, 670 (1942)) gives an interesting report of 156 stars obtained from 19,000 expansions at 4300 meters. The stars arise from the argon gas and from five 1-cm Pb plates.
[25] A bibliography of work on nuclear disintegration can be obtained from M. Shapiro, Rev. Mod. Phys. **13**, 58 (1941).

these 71 mesons, it cannot be ascertained whether or not they penetrated the tungsten plate. Of the remaining 530 pictures, 131 were taken with 2.54 cm of Pb above the chamber and 399 were taken with 7.62 cm of Pb above the chamber. Six and 27 of these, respectively, were stopped in the 3.81 cm of tungsten, equivalent to 6.8 cm of Pb. The use of the momentum *vs.* range curves of Rossi and Greisen[26] then gives the following results for sea level mesons: $33/530=6.2$ percent of the penetrating component with momentum between 1 and 3×10^8 ev/c. This is in good agreement with the meson spectrum obtained at sea level by Hughes.[27]

The author deeply appreciates the assistance of Dean A. H. Compton, who has made possible this work. Professor Auger has been of great value in interpreting the experimental results. Messrs. O'Donnel and Kahlberg of the machine shops were of great help in building the apparatus.

[26] See page 249 of reference 11.

[27] D. J. Hughes, Phys. Rev. **57**, 592 (1940).

SEPTEMBER 1 AND 15, 1942 PHYSICAL REVIEW VOLUME 62

A Precision Determination of h/e by Means of the Short Wave-Length Limit of the Continuous X-Ray Spectrum at 20 kv

WOLFGANG K. H. PANOFSKY, ALEX E. S. GREEN, AND JESSE W. M. DUMOND
Norman Bridge Laboratory of Physics, California Institute of Technology, Pasadena, California

(Received April 7, 1942)

A redetermination of h/e by the method of the short wave-length limit of the continuous x-ray spectrum was undertaken in order to obtain further evidence as to the discrepancy among the determinations of atomic constants. The accuracy of the experiment is improved by (1) large primary x-ray intensity, (2) the use of a high resolving power double crystal spectrometer, (3) reduction in background and improvement in the sharpness of the limit by the use of balanced filters, (4) improved accuracy in voltage measurements, and (5) cleaning the target in vacuum. The sources of error both in the measurements and the interpretation of the data are discussed. Our result is $h/e=(1.3786\pm0.0002)\times10^{-17}$ erg sec./e.s.u. This value is found to be in fair, though not complete, agreement with measurements of other atomic constants.

I. THE PRESENT STATE OF OUR KNOWLEDGE OF THE VALUE OF h/e

EVER since absolute x-ray wave-length measurements and the revision of the value of the viscosity of air caused the accepted value of the electronic charge to be raised from the original Millikan value to the neighborhood of 4.8×10^{-10} e.s.u., there appeared a new discrepancy among the values of the natural constants.[1] This discrepancy arises from the fact that values of h/e derived from methods permitting a direct measurement of this quantity failed to agree satisfactorily with the "indirect" value of h/e, i.e., the value derived from other measurements of functions of the atomic constants e, m, and h. The present state of this discrepancy has been thoroughly discussed by Birge,[2,3] Dunnington,[4] Kirchner,[5] and DuMond.[6,7]

The methods for a direct measurement of h/e available at the present time, are: (1) the determination of the short wave-length limit of the continuous x-ray spectrum; (2) the photoelectric effect; (3) the determination of excitation and ionization potentials; (4) the determination of the excitation voltages of x-ray series as compared to the corresponding absorption edges; (5) measurement of the radiation constant c_2. Of these methods at present the first stands out

[1] R. T. Birge, Phys. Rev. **48**, 918 (1935).

[2,3] R. T. Birge, *Reports on Progress in Physics*, London Physical Society (in print); R. T. Birge, Rev. Mod. Phys. **13**, 233 (1941).

[4] F. G. Dunnington, Rev. Mod. Phys. **11**, 65 (1939).

[5] Kirchner, "Die Atomaren Konstanten e, m, und h." Ergeb. d. exakten Naturwiss. (1939).

[6,7] J. W. M. DuMond, Phys. Rev. **56**, 153 (1939); J. W. M. DuMond Phys. Rev. **58**, 457 (1940).

in accuracy above the others and therefore it is the deviation of these measurements from the indirect value which causes most concern. For convenience the values of h/e as obtained by previous investigators are tabulated here:

1.3800—Ohlin[8] (corrected for cathode work function by Birge[9])
1.3775—Schwarz and Bearden[10] (mean value of Cu and W values)
1.3775—Schaitberger (re-computed by DuMond[7])
1.3765—DuMond and Bollman[11] (re-computed by DuMond[7])
1.3759—Feder[12] (re-computed by DuMond[7])
1.3754—Kirkpatrick and Ross[13] (re-computed by DuMond[7])
1.3749—Duane, Palmer, and Yeh[14] (re-computed by DuMond[7]).

As compared to these results Birge[3] computes as the most probable *indirect* value

$$h/e=(1.3793_3\pm 0.0002_3)\times 10^{-17} \text{ erg sec./e.s.u.}$$

It is seen from the above table that the only measurement in substantial agreement with the indirect value is the measurement of Ohlin. All the other measurements lie from 0.15 percent to 0.3 percent lower than the indirect value.

II. THE ISOCHROMAT METHOD

In the present experiment, as in the past ones listed above, the method of isochromats was used in locating the short wave-length limit. This method consists ideally in monochromatizing an x-ray beam and measuring the intensity in the monochromatic beam as a function of the voltage applied to the x-ray tube. The resulting curve is called an isochromat. In practice these ideal conditions can of course not be realized owing to the fact that (a) the "monochromatization" will actually consist of the production of an x-ray beam whose wave-length distribution has a sharp peak at a particular wave-length with the intensity decaying asymptotically on either side, and (b) since an electron beam perfectly homogeneous as to energy cannot be produced. The effect of these two deviations from an ideal isochromat condition is the same: both causes make an actually observed isochromat appear as a weighted superposition of ideal isochromats with voltage coordinates slightly shifted; if the wave-length of an ideal isochromat is changed by an amount $\Delta\lambda$, this change will cause the isochromat to shift along the voltage axis by an amount given by $\Delta V=-hce^{-1}\lambda^{-2}\Delta\lambda$. Let us analyze mathematically the effect of such a deviation from ideal conditions.

Let $y=f(z)$ be the equation of an ideal isochromat where z stands for the variable proportional to the x-ray tube voltage and y for the variable proportional to the x-ray intensity in the monochromatic beam. Let $F(z)$ be the experimentally observed function. Let us choose $z=0$ to be the short wave-length limit of the ideal isochromat; i.e., let $f(z)=0$ for $z\leqslant 0$. $F(z)$ is then formed by a weighted superposition of functions $f(z)$ whose independent variable differs by an amount x from the independent variable of the observed isochromat. The weights given to these various ideal components will then be a function of x only. Let this function be $g(x)$. We then have

$$F(z)=\int_{x=-\infty}^{x=z} g(x)f(z-x)dx, \qquad (1)$$

the upper limit being $x=z$ since $f(z-x)=0$ for $x\geqslant z$. This equation theoretically permits solution for the function $f(z)$, provided the functions $F(z)$ and $g(x)$ are known for all values of their argument. Practically such a reversion is, however, not possible since the functions $F(z)$ and $g(x)$ are not known for large values of the variable. We must, however, remember that a solution for the complete ideal isochromat $f(z)$ is not necessary, but that only a location of the point at which the argument of $f(z)$ is zero is necessary. The location of this point can be effected as follows: let us examine the second derivative of

[8] Per Ohlin, Dissertation, Uppsala (1941); Per Ohlin, "Meddelande Fran Fysika Institutionen," Uppsala 12–12–1939.
[9] Private communication.
[10] Bearden and Schwarz, Bull. Am. Phys. Soc., May 1–3 (1941).
[11] J. DuMond and V. L. Bollman, Phys. Rev. **51**, 400 (1937).
[12] H. Feder, Ann. d. Physik [5] **1**, 497 (1929).
[13] P. Kirkpatrick and P. A. Ross, Phys. Rev. **45**, 454 (1934).
[14] Duane, Palmer, and Yeh, J. Opt. Soc. Am. **5**, 376 (1921).

the observed isochromat. From Eq. (1):

$$F''(z)=g(z)f'(0)+\int_{-\infty}^{z} g(x)f''(z-x)dx$$
$$=g(z)f'(0)+\int_{0}^{\infty} g(z-u)f''(u)du. \quad (2)$$

Let us now assume that the ideal isochromat can be composed of straight line sections, i.e., let

$$f'(x)=a_i, \quad x_{i-1}<x<x_i, \quad i=1\cdots\infty. \quad (3)^*$$

Equation (2) then reduces to

$$F''(z)=g(z)f'(0)+\sum_{i=1}^{\infty} g(z-x_i)(a_{i+1}-a_i). \quad (4)$$

This equation shows that $F''(z)$ is composed of two terms, namely (a) the term $g(z)f'(0)$ representing the influence of the intercept at the origin of the ideal isochromat on the curvature of the real isochromat, and (b) the term

$$\sum_{i=1}^{\infty} g(z-x_i)(a_{i+1}-a_i)$$

which represents the influence of the breaks in slope at the points x_i on the curvature of the observed isochromat. In the case in which the term (b) is negligible we see therefore that the second derivative of the observed isochromat will reach a maximum at the same point at which $g(x)$ reaches a maximum; if therefore our voltage and wave-lengths are measured to the peak of their distribution curves, then *the second derivative* or "bending" (and hence approximately the curvature) of the observed isochromat will reach a maximum at the short wave-length limit of the ideal isochromat corresponding to these voltages. In discussing our actual results we shall approximately compute the term (b) and we shall show that it is negligible. For purposes of locating the threshold of the continuous spectrum it is therefore sufficient to determine the point of maximum bending of a physical isochromat.

It follows from the above analysis that a location of the threshold by extending the straight line portion of the isochromat onto the voltage axis is not permissible; in fact it can be shown that the choice of the point whence to project the tangent onto the axis can arbitrarily modify the value of the intercept. The use of the point of maximum bending for the location of the "true" intercept was first suggested by DuMond and Bollman.[11]

III. EXPERIMENTAL ARRANGEMENTS

(1) The X-Ray Tube

The precision attainable in this experiment is principally limited by the intensity available near the short wave-length limit; it was lack of sufficient primary intensity which forced former investigators[11] to decrease the resolving power of the monochromator to a serious extent. In this experiment our primary x-ray intensity was derived from the Watters Memorial x-ray tube and power supply, whose construction is described elsewhere.[15] In these experiments the tube current was maintained at 100 ma; this corresponds to an intensity five times larger than that in former experiments at this voltage.

(a) *Discussion of Target Deposits*

A serious problem in the performance of this experiment is the question of target deposits. A very thin layer of low atomic number material on the x-ray tube target will produce an appreciable energy loss of the electrons impinging on the target; owing to the low x-ray production efficiency in low atomic number materials the x-rays produced in such layers might easily escape observation. Low atomic number materials deposited on the target would therefore tend to cause an apparent shift in the observed isochromat toward higher voltages and therefore an apparent higher value of h/e. Preliminary experiments definitely established both the production of deposits on the target probably partly derived from the filament and partly derived from the

* The assumption involved in Eq. (3) does not involve any significant restriction. It has been found by all earlier observers that an isochromat is generally composed of portions of practically constant slope, joined by short portions of the curve of sharp curvature, the so-called "knees." The assumption made in Eq. (3) is therefore in agreement with experiment. Part of the purpose of this analysis is to investigate the influence of these knees on the location of the threshold. Note that the spectra discussed here are "thick" target spectra. The x-radiation from a "thick" target has components originating at varying depths within the target. A thick target spectrum is therefore essentially a superposition of thin target spectra corresponding to varying electron energies.

[15] J. DuMond and J. P. Youtz, Rev. Sci. Inst. **8**, 291 (1937).

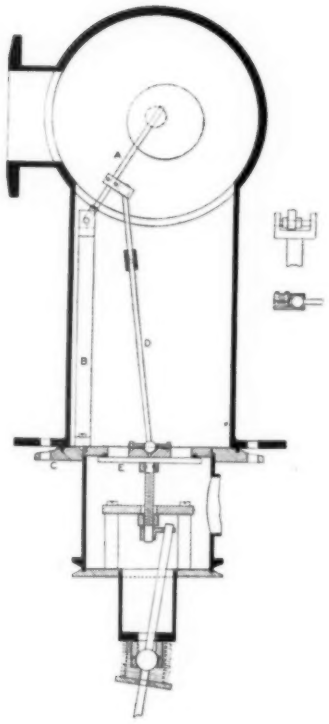

FIG. 1. Transverse cross section of x-ray tube looking at face of target from cathode end showing mechanism by which the target can be cleaned in vacuum. A steel wire brush is mounted on the arm A and is driven through the sylphon valve at the bottom. The target is outlined in one particular position (solid circle) and the path of the center of the target when gyrating is indicated (dotted circle).

electron beam; the latter deposits probably contain carbon as their principal component. In order to eliminate or at least retard the formation of these deposits the pumping system of the x-ray tube was redesigned to avoid diffusion of oil vapor into the x-ray tube and also to permit higher pumping speed.

(*b*) *Vacuum Target Cleaning Device*

Despite these measures the formation of deposits still proved a serious obstacle to the reliability of our measurements. As a solution to this problem a device was therefore installed in the x-ray tube to permit cleaning the target in vacuum (Fig. 1). An arm A is mounted on an upright post attached to the stationary plate C of a sylphon valve at the bottom of the x-ray tube. This arm is driven through an adjustable rod D from the moveable plate E of the valve. This rod has two $\frac{1}{2}''$ balls silver-soldered into its ends which engage cups in the moveable plate E and the arm A, respectively. Figure 1 shows both the outline of the target and the path (dotted line) described by its center as it is gyrated by means of the mechanism designed by DuMond and Youtz. The arm carries a brush facing the target; this brush is made of piano wire sections soldered into a brass ring. Cleaning of the target is effected by closing the valve as shown; the levers are so adjusted that the brush is now located between the cathode and anode just in front of the filament. The target is then gyrated; the brush will then clean exactly that area which the electron beam strikes during regular operation of the tube. The target is made of copper with a thin layer of gold deposited on its surface by an amalgamation process. A small area in the center of the target is silverplated for the production of the silver K lines for calibration purposes.

In order to obtain the Ag $K\alpha$ calibration lines the (ordinarily eccentric) target can be centered by external means to cause the electron beam to strike the silverplated center.

(*c*) *Effect of Internal Target Cleaning*

The effect of this device on the readings is shown in Fig. 2. Curve A on this figure is an isochromat obtained after operating the tube for a long time; curve B is an isochromat observed under identical conditions as curve A excepting for the fact that the "scratching" device was operated every two or three points. It is seen that in this extreme case a shift of nearly 1 percent is observed in the abscissa of each point, corresponding to an equal fractional change in the value of h/e. It is also seen that at least with the detection sensitivity used here, the radiation from the carbon is not observed.

The bearing of the existence of this effect on the former work on this subject is naturally difficult to infer. In particular the rate of formation of deposits of this nature is of course widely different in various investigations. In particular in regard to the work of Ohlin[8] the question of target deposits deserves serious consideration. At the voltages used in Ohlin's experiment a few molecular layers of low atomic number materials deposited on the target are sufficient to cause an error of several parts in ten thousand; Ohlin's apparatus is evacuated by means of an oil pump

without the use of a refrigerating trap; the presence of organic vapors in the tube is therefore not unlikely.

(*d*) *Discussion of the Effect of the Pressure in the X-Ray Tube*

Another question which we might discuss here is that of the error introduced into an h/e determination by the presence of secondary electrons in the electron beam which have been released from the cathode by positive ion impact. Ohlin[8] describes an effect of pressure in the x-ray tube on the shape and position of his observed isochromats. Ohlin shows that in his experiment the sharpness of the short wave-length limit intercept is materially decreased as the pressure in the x-ray tube is increased; in his experimental curves this "blurring" is also accompanied by a very large rise in intensity. Ohlin tentatively ascribed this effect to the x-rays produced by the secondary electrons in the electron beam; these electrons will, of course, have larger energies than the thermionic electrons from the filament. Ohlin tried to measure the positive ion current in the tube directly and found it much too small to account for the observed effect. It seems therefore unlikely to ascribe the observed effect to the cause mentioned. In particular owing to the small energy of such secondaries[16] their influence on the value of h/e as measured at higher voltages ought to be entirely negligible. A possible explanation of the phenomena observed by Ohlin might be the fact that Ohlin used a vacuum curved crystal spectrometer in his investigation; the vacuum in the spectrometer was common to the x-ray tube. The x-ray beam is monochromatized by reflecting it off a curved crystal and then passing it through a narrow slit. Any scattering in front of this slit (e.g., by residual air in the poor vacuum case) would materially decrease the resolving power of this method of monochromatization; this decreased resolving power would both cause a blurring of the limit and also the greatly increased intensity, which Ohlin actually observed.

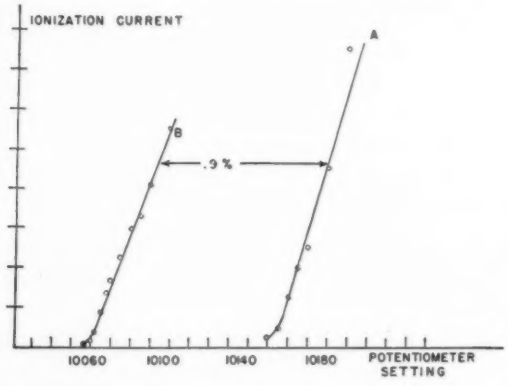

FIG. 2. Two isochromats showing the effect of the internal target cleaner. Curve *A* is observed with a highly contaminated target while curve *B* is observed with the target cleaner in operation.

[16] L. Linford, Phys. Rev. **47**, 279 (1938); Hill, Buechner, Clark, and Fisk, Phys. Rev. **55**, 463 (1939).

(2) The High Voltage D. C. Power Supply

The power supply used in this experiment remains practically as originally described.[15] Since these experiments were performed at relatively low voltages only half of the voltage doubling circuit described in the earlier paper is used. The power supply is designed for maximum stability of x-ray tube voltage. Nevertheless, principally owing to instability in filament emission, considerable voltage fluctuations remain. In order to smooth out these remaining fluctuations a voltage regulator of the degenerative type was designed to operate in the high voltage line. This regulator was built in the summer of 1939 and has been in satisfactory operation since then. It is of a similar design to the circuit recently published by Parratt and Trischka.[17] The circuit of the regulator is shown in Fig. 3. Qualitatively it operates as follows: the voltage divider R_1-R_0 divides the voltage across the x-ray tube in the ratio 1 : 400; any changes in this voltage are amplified by a 3-stage d.c. coupled voltage amplifier of approximately 200,000 total gain. This amplifier feeds the amplified voltage fluctuation back into the line in reverse phase. It can be seen by a simple analysis that any incoming voltage fluctuations will be reduced in the ratio 1 : 500 approximately, provided that the magnitude of the incoming fluctuations does not exceed the allowable operating range of the power stage (3 6L6 tubes operated in parallel). The resistor R_8 protects the device against overload since at

[17] L. G. Parratt and J. W. Trischka, Rev. Sci. Inst. **13**, 17 (1942).

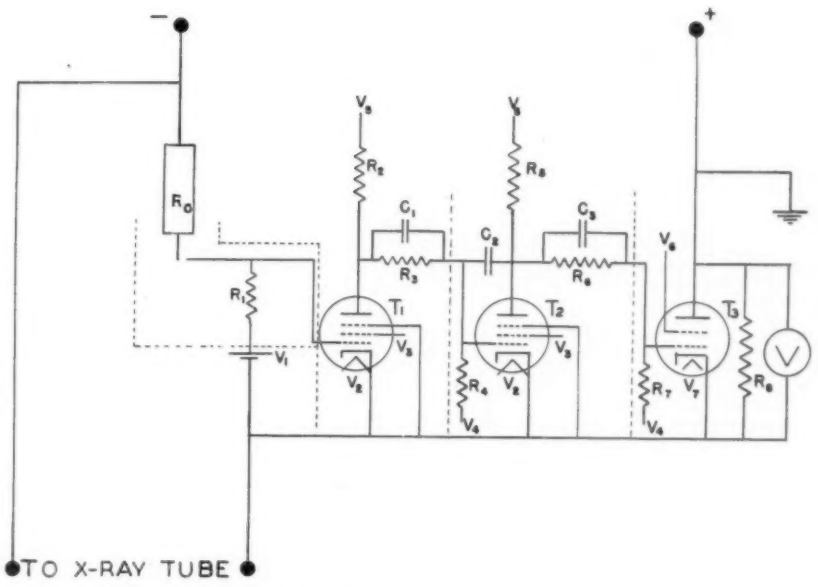

FIG. 3. Diagram of electronic voltage stabilizer: T_1, T_2—1852; T_3—3 6L6G in parallel; V_1—0–180 v variable bias voltage (battery); V_2—6 v (storage battery); V_3—45 v (battery); V_4—−90 v (battery); V_5—360 v (battery); V_6—250 v (regulated power supply); V_7—6.3 v (transformer); R_0—400×10⁶ (Type MVR); R_1, R_5—1 meg; R_2, R_3, R_4, R_6, R_7—0.5 meg; R_8—7500, 100 watt; C_1, C_3—1000 $\mu\mu f$; C_2—adjust for best performance.

100-ma load current the drop across the power-stage cannot exceed 750 volts. The condenser C_2 was found to be necessary to suppress phase shift oscillations. Constant voltage is maintained by adjusting the variable bias battery V_1 to the required value; as long as the applied voltage is held (by external manual control of the generator field) so that the drop across the regulator does not vary more than 100 volts, the output voltage was found at an operating voltage of 20 kv to be constant to ± 1 part in 50,000 for long periods of time.

(3) The Filament Supply

The 30-ampere, 5-volt filament of the x-ray tube is supplied by a set of large storage batteries constantly charged by a set of generators driven by a motor at ground potential through an insulating belt. Owing to the large internal impedance of the high voltage supply it is necessary to adjust the filament current within very close limits; also all sliding contacts in the filament circuit must be avoided in order to assure stability. The current was therefore controlled by means of a monel tubing mercury rhoestat: A vertical tube of monel 0.008″ in wall thickness is jacketed with an oil bath and placed in series with the x-ray tube filament; the mercury can be raised and lowered inside this tube by means of a tubulated flask connected to the lower end of the tube through Koroseal tubing. This arrangement permits a total resistance variation of about 0.1 Ω.

(4) The Monochromator

(a) *The Spectrometer*

Monochromatization was effected by means of the two-crystal spectrometer described by DuMond and Marlow.[18] Two calcite crystals were cleaved out of a single block and were mounted and aligned according to the optical method of DuMond and Hoyt.[19] The crystals remained entirely untreated; i.e., they were neither ground nor etched. A rocking curve in the parallel position of the spectrometer showed a full width at half maximum of 10.5″ at 20 kv; this corresponds to a width of about 11 volts.

[18] J. DuMond and D. Marlow, Rev. Sci. Inst. **8**, 112 (1937).
[19] J. DuMond and A. Hoyt, Phys. Rev. **36**, 1702 (1930).

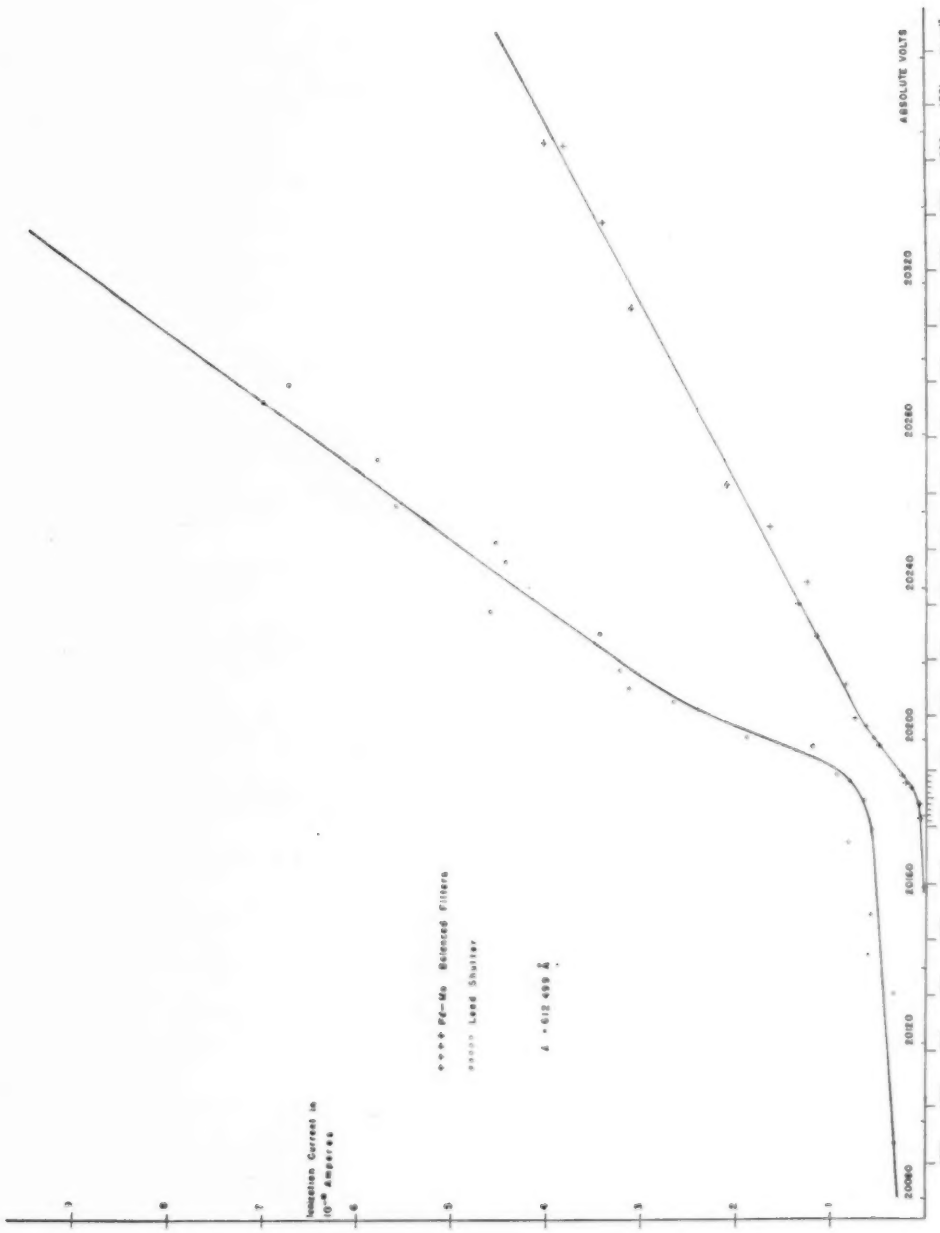

FIG. 4. Isochromats observed at $\lambda = 612.499$A. The upper curve is observed using a lead shutter for obtaining difference readings; the lower curve is obtained by the use of a set of Pd-Mo balanced filter. The corrected x-ray tube voltage is absolute volts and the computed h/e values are plotted on the abscissa.

(*b*) *Calibration of the Spectrometer*

For reasons described below, it was not feasible to choose a monochromatization wave-length at the peak of some well-known spectral line. It was therefore necessary to standardize the spectrometer at a well-known wave-length chosen near to the desired wave-length and then to compute the actual wave-length from the small angular shift (about 30′) of the crystals away from the standard position. The wave-length chosen for reference was the Ag $K\alpha_1$ line whose wave-length has been carefully investigated by numerous workers.[20] In our computation we adopted the value of Elg[21] (λ Ag $K\alpha_1 = 558.231$ X.U.);* the wave-length chosen for monochromatization was $\lambda = 612.499$A.

(*c*) *The Ion Chamber and Ion Current Amplifier*

The x-ray intensity was measured by means of a methyl bromide filled ionization chamber and a Western Electric electrometer tube No. D96475, operated in the Barth[22] circuit as described by Penick.[23] The circuit is operated with a 5×10^{11} ohm grid shunt; its over-all sensitivity is 4×10^{-17} amp./mm.

(*d*) *The Use of Balanced Filters*

A considerable number of lead stops and conduits were used in order to reduce scattering. These stops were located by means of a careful photographic survey of the position of the beam and the scattered radiation. In particular it was found necessary to place a stop directly after the second crystal in order to block tangential non-coherently scattered radiation from the crystal face.

As was mentioned above, an isochromat as actually observed will deviate to a considerable extent from the ideal shape partly owing to the effect of imperfect monochromatization. This imperfection is partly caused by the finite width of the crystal diffraction pattern and partly by incoherent scattering in the monochromator. The incoherent scattering causes a non-monochromatized x-ray leakage through the monochromator. Since the scattering is dependent on the x-ray wave-length, it will contribute to the isochromat a strongly voltage dependent background. Both these causes will contribute a "tail" to the isochromat of only slow convergence; it is the presence of this tail or "fillet" which caused difficulty in the interpretation of the results of former investigators. In this work it was attempted to effect a further reduction of this fillet by the use of a set of Ross[24] balanced filters. As is well known, a Ross filter consists of a set of two foils of different atomic number; the effective thicknesses of the foils (adjusted by inclination to the x-ray beam) is such that the absorption of the two foils is identical both at wave-lengths shorter than the K-absorption edge of the heavier material and at wave-lengths longer than at the K edge of the lighter material. In practice these two conditions cannot be precisely fulfilled simultaneously with two homogeneous foils.

Let us now assume that the pass band of the spectrometer is located just on the short wave-length side of the K edge of the lighter material constituting the balanced filter (see Appendix). Let us assume that the filters are perfectly balanced on the long wave-length side but not on the short wave-length side. Now consider the change in intensity as one filter is substituted for the other in the x-ray beam. Let us assume that the voltage is close to the short wave-length

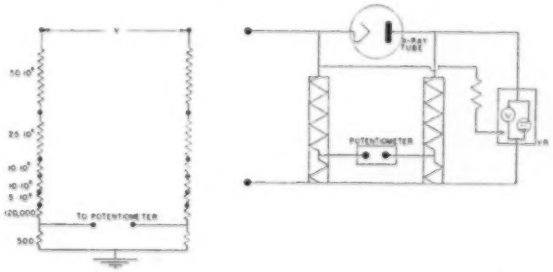

FIG. 5. Diagram of voltage dividers and connections.

[20] Kellstrom, Zeits. f. Physik **41**, 516 (1927); C. D. Cooksey and D. Cooksey, Phys. Rev. **36**, 85 (1930); J. A. Bearden, Phys. Rev. **43**, 92 (1933); V. Zeipel, Arkiv f. Mat. Astr. och Fysik **25A**, No. 8 (1935); G. Berger, as quoted by Ingelstam; Ingelstam, Nova Acta Reg. Soc. Scien. Ups. [4] **10**, No. 5 (1936); S. Elg, Zeits. f. Physik **106**, 315 (1937).

[21] S. Elg, reference 20.

* The wave-length is expressed on the Siegbahn scale of wave-lengths in which the effective grating space of calcite in the first order of reflection is taken as 3029.04 X.U. at 18°C. Wave-lengths expressed in these units must be multiplied by $\lambda g/\lambda s = 1.00203_4$ in order to be reduced to absolute c.g.s. units.

[22] Barth, Zeits. f. Physik **87**, 399 (1934).

[23] D. B. Penick, Rev. Sci. Inst. **6**, 115 (1935).

[24] P. A. Ross, J. Opt. Soc. Am. and Rev. Sci. Inst. **16**, 433 (1928).

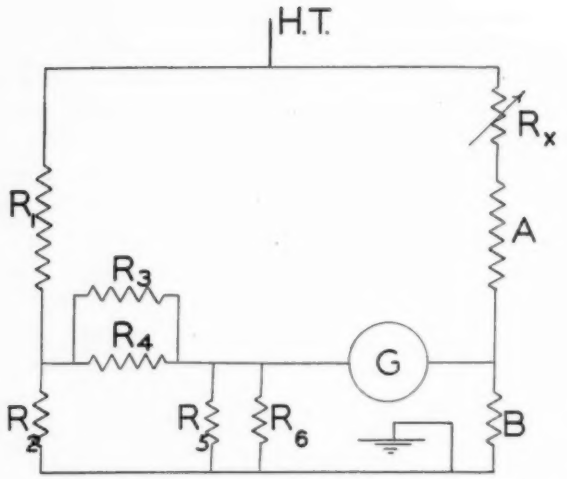

FIG. 6. Bridge circuit for a precision determination of the resistance ratio A/B. The nominal values of the resistances are:
R_1—10^6 ohms R_3—10^6 ohms R_5—5000 ohms
R_2—100 ohms R_4—50,000 ohms R_6—5000 ohms
R_x—0–10^6 ohms (variable).
The ratio R_1/R_2 is known to a high degree of precision.

limit. Since there is no primary intensity at wave-lengths shorter than the limit, the slight unbalance of the filters on the short wave-length side will not contribute any change in intensity. The entire intensity shift must therefore derive from the wave-length band contained between the short wave-length limit and the K edge of the lighter metal of the filter pair. The action of the balanced filter set is therefore to "clip off" the pass band of the spectrometer a small wave-length interval (the length of the interval will depend on the angular setting of the crystals) beyond the center of the pass band on the long wave-length side. The "fillet" from imperfect monochromatization will therefore be materially reduced. The background from incoherent scattering will also be largely eliminated.† The overall intensity is decreased by a factor of about 2.5 if the thickness of the filters is correctly chosen. Figure 4 shows two isochromats observed in one case using a set of balanced filters (Mo−Pd) and in the other case simply a lead shutter; the spectrometer is set at a wave-length differing by about 6 X.U. from the Mo K edge. The effective suppression of the "tail" and background is evident from the figure.

† See Appendix.

IV. VOLTAGE MEASUREMENT

(1) Description of the Devices used for Voltage Measurement

The voltage applied to the x-ray tube was measured by means of a voltage divider and potentiometer arrangement as shown in Fig. 5. The divider consists of two $100\times10^6 : 500\Omega$ resistance ratios immersed in oil. Their construction is described in an earlier paper.[15] It will be noted that the two resistance ratios measure very unequal voltages; hence in order to have the potentiometer actually measure a voltage proportional to the total x-ray tube voltage, it is essential that the two ratios be equal, to a sufficiently high precision. It can be shown that for the ratios used here the error due to this cause cannot exceed 1.6×10^{-5}. It can also be shown that to an accuracy of 1 in 10^5 the dividing ratio of the divider which has the larger part of the x-ray tube voltage across it can be used in the computation. The problem of voltage measurement therefore reduces essentially to establishing an accurate ratio of order 1 : 200,000. By the method of calibration shown below, it became evident that the stability of the high resistance unit was not too satisfactory; the ratio would change by several parts in 10,000 during a day's run. In order to avoid introducing error into the final result due to this cause it was decided to adopt a method of calibration which was sufficiently rapid so the voltage divider ratio could be checked in a few minutes during a run.

(2) Voltmeter Calibration

Through the kind cooperation of Dr. Frank Wenner of the Bureau of Standards we had available two high quality manganin resistance boxes, made by Otto Wolff, Berlin. One of these contains 10 sections of 100,000Ω each and the other one contains 10 sections of 1000Ω each. None of the sections differs by more than 3×10^{-4} from their mean value. Dr. Wenner suggested a method by which these resistance standards could be used to build up an accurately known resistance ratio of nominal value 1 : 10^4; we shall briefly describe the method here. Let

R_s = resistance of the 10^6 box with its units series connected,

R_p = resistance of the 10^6 box with its units parallel connected,

r_s = resistance of the 10^4 box with its units series connected,

r_p = resistance of the 10^4 box with its units parallel connected.

It can then be shown[25] that

$$R_s/r_p=(10^4R_p/r_s)\{1+0(\delta^2)\},$$

where δ is the deviation of the resistance sections from their mean. Hence to an accuracy of 10^{-7} we have that

$$R_s/r_p=10^4R_p/r_s.$$

Since $R_p/r_s\sim 1$ we can measure this ratio to very high precision in a Wheatstone bridge by using a method of interchanges of R_p and r_s. It was thus possible to measure R_p/r_s to a precision of better than one part in 10^6. Great care was taken to eliminate errors due to contact resistances and crossleakages. After having thus established an accurate 10^4 ratio, these resistances ($R_s=R_1$; $r_p=R_2$) were connected with other manganin standards as shown in Fig. 6. The nominal value of the resistances R_3, R_4, R_5, and R_6 are $10^6\Omega$, 50,000Ω, 5000Ω, and 5000Ω, respectively. These values were determined to an accuracy of 1 in 10^6 in terms of sections of the 10^6 or $10^4\Omega$ boxes, by using in all cases an interchange method on an equal arm bridge. The bridge circuit shown in Fig. 6 was then balanced by adjusting the resistance R_x. The equation of balance is

$$\frac{A+B+R_x}{B}=\frac{R_1+\rho_1}{\rho_1}\cdot\frac{\rho_3+\rho_2}{\rho_3},$$

where

$$\rho_2=R_3R_4/(R_3+R_4),$$

$$\rho_3=R_5R_6/(R_5+R_6),$$

$$\rho_1=R_2(\rho_2+\rho_3)/(R_2+\rho_2+\rho_3).$$

Owing to the fact that the power dissipation of the 10^6 ohm box is limited to 100 watts (the $10^6\Omega$ box consists of 40 coils through each of which oil is circulated by Bakelite tubes extending into the coils), this measurement could not be made at a voltage in excess of 10 kv. It was shown by direct measurement of the temperature coefficient of the $10^6\Omega$ unit that heating errors would amount to less than 2 in 10^5. Since the voltage divider ratio $(A+B)/B$ is needed at 20 kv, an independent measurement of the load coefficient of the voltage divider was made. This was done by determining each half of the $100\times10^6:500$ ratio (i.e., two $50\times10^6:500$ ratios) at voltages from 3 kv to 10 kv. A bridge similar to the one shown in Fig. 6 was used. Since a 20-kv load across the entire divider is equivalent to a 10-kv load across each half, the load coefficient can safely be inferred from such a measurement, in particular since it is small. The load coefficient was determined to cause a correction of -1.0×10^{-4} to the voltage ratio as observed directly at 10 kv.

A complete calibration of the divider was made between every 2 or 3 points on the isochromats shown in Fig. 4; the effect of the drift in divider ratio on the precision of the results can therefore be considered as eliminated.

(3) Ripple Measurement

The ripple was measured by placing an oscilloscope in series with a 0.2-μf condenser directly across the x-ray tube. The oscilloscope was calibrated by placing the terminals of a 150∼ oscillator across the x-ray tube terminals and observing the oscilloscope deflection. The measured ripple voltage is 6 volts peak to peak. This ripple volt-

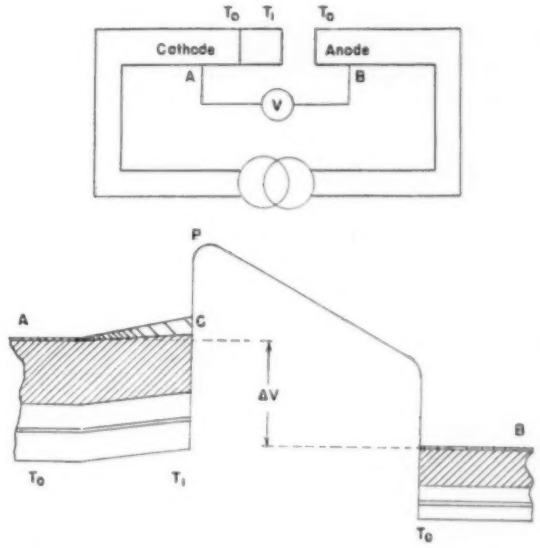

FIG. 7. Schematic diagram of the x-ray tube circuit and the corresponding energy bands of the electrons. T_0 represents room temperature while T_1 is the cathode temperature. ΔV is the voltage measured by a voltmeter attached to A and B.

[25] Wenner, J. Res. Nat. Bur. Stand. **25**, 229 (1940) RP 1323.

age will constitute an additional component of the "smearing" function $g(x)$; it will not, however, give rise to a correction to the voltage scale.

V. INTERPRETATION OF RESULTS

(1) The Measurements

Our final isochromats are shown in Fig. 4. On the axis of abscissa are plotted values of absolute voltage and values of h/e based on the auxiliary constants: $c=2.9977_6\times10^{10}$ cm/sec.; $d_1=3.02904\times10^{-8}$ Siegbahn cm; $\lambda_\varrho/\lambda_s=1.00203$; $pq=1.00034$. The points on the graph have been corrected for (1) the individual calibrations of the divider, (2) ½ the P.D. across the x-ray tube filament, (3) the cathode work function. We estimate the point of maximum curvature of both graphs to be at

$$h/e=1.3786\times10^{-17} \text{ erg sec./e.s.u.}$$

(2) The Work Function Correction

The corrections applied to the voltage scale have been discussed in a former paper.[11] It might be added, however, that Ohlin[8] claims that the work function correction does not rest upon a sound basis. This justifies discussing this correction again in some detail. Let Fig. 7 represent the schematic diagram of the x-ray tube circuit and the corresponding energy level diagram. A potentiometer measurement such as we have used for measuring the voltage will measure the difference in energy of the edge of the Fermi distribution of A and B, respectively. An electron in passing from A to P will have acquired the following energies: (1) Energy AC, owing to change in levels caused by Kelvin P.D., (2) energy CP, thermionic work function; (3) decrease in work function due to external field; (4) thermal energy of the electron corresponding to its electron temperature. It is these terms plus the energy $e\Delta V$ which are available for conversion into radiation at the anode. These four terms are the same energy terms which account for the so-called *calorimetric* work function; i.e., the work function measured by observing the extra heat input into a cathode, required to keep it at constant temperature when emission current is drawn. Such determinations are numerous;[26] all of them give results agreeing within a few tenths of a volt with the *thermionic* work function. Probably the most direct proof for the necessity of the work function correction is offered by the early work of Richardson and Cooke.[27] In their experiments Richardson and Cooke measured the heat input into the anode as a function of anode voltage and found that if this power be extrapolated to zero external voltage, a power input approximately corresponding to the work function remained. The precision of these experments is insufficient to distinguish between the calorimetric and thermionic work functions. We believe therefore that the cathode work function correction must be applied.

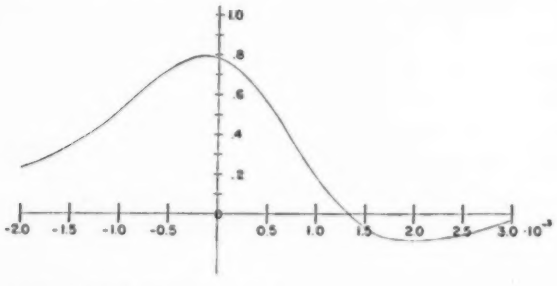

FIG. 8. Plot of the function

$$\frac{1}{1+(2/1.3\times10^{-3})^2}-\frac{1}{2}\left\{\frac{1}{1+[(x-1.5\times10^{-3})/1.3\times10^{-3}]^2}\right\}$$

indicating the shift in the point of maximum bending introduced by a change in slope at $x=1.5\times10^{-3}$ equal to one-half of the slope of the isochromat at the origin. The abscissa is expressed as fractional voltage.

(3) Discussion of Errors

Because of the lack of a generally accepted procedure for obtaining an error estimate we shall here adopt the following procedure:

(1) In cases where effective "limits" of error are available (such as in the case of N.B.S. certificates of standard cells, etc.) we shall divide these limits by 3.5‡ to obtain the "probable" error; (2) in cases were a "probable" error can be estimated (such as in the case of the interpretation of a set of scattered data), we shall combine its value directly with the values obtained from (a).

[26] Richardson and Cooke, Phil. Mag. **20**, 173 (1910); **21**, 404 (1911); **25**, 624 (1913); **26**, 472 (1913); Lester, Phil. Mag. **31**, 197 (1916); Wilson, Proc. Nat. Acad. Sci. **3**, 426 (1917); Phys. Rev. **24**, 666 (1924); Davisson and Germer, Phys. Rev. **20**, 300 (1922); **24**, 666 (1924); Michel and Spanner, Zeits. f. Physik **35**, 395 (1928); Dushman, Rowe, Ewald, and Kidner, Phys. Rev. **25**, 338 (1925).

[27] Richardson and Cooke, Phil. Mag. **20**, 173 (1910); **21**, 404 (1911).

‡ On the basis of a Gaussian distribution the probability of an error greater than 3.5 times the probable error is 1 percent approximately.

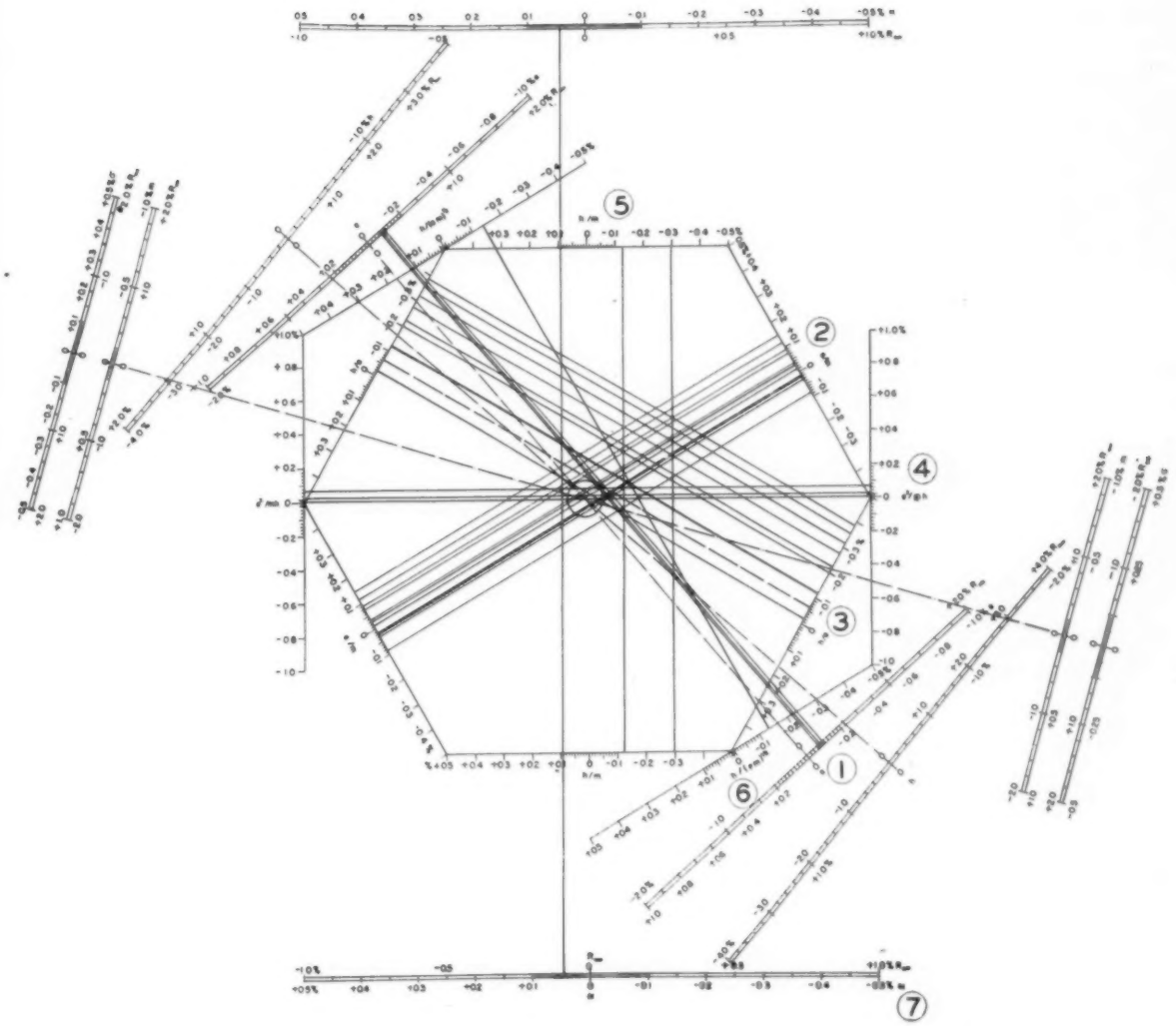

FIG. 9. Isometric consistency chart of the atomic constants. The values plotted are shown in the adjacent table (Table II).

(a). *Interpretation of Isochromat*

The probable error in locating the point of maximum curvature is estimated as 10^{-4}. The question of the validity of the maximum curvature method was checked quantitatively as follows: The term

$$\sum_{i=1}^{\infty} g(z-x_i)(a_{i+1}-a_i)$$

in Eq. (4) was computed directly. We used for $a_{i+1}-a_i$ the break in slope observed in the isochromats of Fig. 4, and assumed $g(z)$ to have the form

$$g(z)=\frac{C}{1+(z^2/a^2)}. \tag{5}$$

The width a at half maximum was assumed to be composed of the terms: (1) The half-width of the 2-crystal spectrometer "window curve," $a_1=5\times10^{-4}$ (expressed as fractional width); (2) the ripple voltage spread, $a_2=1.5\times10^{-4}$; (3) the spread caused by "vertical divergence" of the x-ray beam in the spectrometer, $a_3=5\times10^{-4}$; (4) the spread caused by the potential drop across the filament, $a_4=1.5\times10^{-4}$. If we make the conservative assumption that these widths be additive, we obtain

$$a=13\times10^{-4}.$$

If, with the use of these parameters, $F''(z)$ is plotted (Fig. 8), a curve is obtained whose max-

TABLE II. Isometric consistency chart of the atomic constants.

The consistency of determinations of seven functions of the atomic constants e, h, and m by various methods is compared in Fig. 9 graphically by the method of DuMond. The origin of the chart is arbitrarily chosen as $e_0=4.80650\times10^{-10}$ e.s.u. $m_0=9.11780\times10^{-28}$ gram. $h_0=6.63428\times10^{-27}$ erg-sec. $e_0/m_0=1.75850\times10^{7}$ e.m.u./gram. $h_0/e_0=1.38028\times10^{-17}$ e.s.u. $h_0/m_0=7.27621$ c.g.s.u. $e_0^2/h_0m_0=3.81921\times10^{24}$ e.s.u. $h_0/(e_0m_0)^{\frac{1}{2}}=1.00216\times10^{-3}$ e.s.u. $R_\infty=109737$ cm^{-1}. $\alpha_0=7.29870\times10^{-3}$.

The measurements are based on the following set of auxiliary constants: $c=2.99776\times10^{10}$ cm/sec. $F=96514$ absolute coulomb/physical gram-equivalent. $p=1.00048$. $q=0.99986$. $pq=1.00034$. $\lambda g/\lambda s=1.00203$.

The values plotted are, reading in all cases from the highest to the lowest values:

(1) e	4.8030×10^{-10}	Söderman, Nature **135**, 67 (1935);
	4.8026	Bearden, Phys. Rev. **37**, 1210 (1931); **47**, 883 (1935); **48**, 385 (1935);
	4.8021	Bäcklin, Zeits. f. Physik **93**, 450 (1935).
(2) e/m	1.76110×10^{7}	Perry and Chaffee, Phys. Rev. **36**, 904 (1930);
	1.76048	Houston and Chu, Phys. Rev. **51**, 446 (1937); **55**, 423 (1939); **55**, 175 (1939);
	1.76006	Bearden, Phys. Rev. **54**, 698 (1938);
	1.75982	Dunnington, Phys. Rev. **52**, 475 (1937);
	1.75914	C. Robinson, Phys. Rev. **55**, 423A (1939);
	1.75913	Drinkwater, Richardson, and Williams, Proc. Roy. Soc. **A174**, 104 (1940);
	1.75900	Kirchner, Ann. d. Physik [5] **8**, 975 (1931); [5] **12**, 503 (1932);
	1.75870	Goedicke, Ann. d. Physik [5] **36**, 47 (1939);
	1.75820	Shaw, Phys. Rev. **54**, 193 (1938);
	1.75815	Shane and Spedding, Phys. Rev. **47**, 33 (1935);
	1.75797	R. C. Williams, Phys. Rev. **54**, 558 (1938);
	1.75700	Kinsler and Houston, Phys. Rev. **45**, 104 (1934).
(3) h/e	1.3800×10^{-17}	Ohlin, Dissertation, Uppsala (1941); Arkiv For Mat. Astr. och Fysik **27B**, No. 10 (1940).
	1.3793	(Dotted line) indirect value, Birge;
	1.3786	This research;
	1.3775	Schwarz and Bearden, Bull. Am. Phys. Soc. May 1–3, (1941);
	1.3775	Schaitberger, Ann. d. Physik [5] **24**, 84 (1935);
	1.3765	DuMond and Bollman, Phys. Rev. **51**, 400 (1937);
	1.3759	Feder, Ann. d. Physik **51**, 497 (1929);
	1.3754	Kirkpatrick and Ross, Phys. Rev. **45**, 454 (1934);
	1.3749	Duane, Palmer, and Yeh, J. Opt. Soc. Am. **5**, 376 (1921).
(4) e^2/mh	3.8219×10^{24}	Robinson, Phil. Mag. **22**, 1129 (1936);
	3.8203	Robinson and Clews, Proc. Roy. Soc. **A176**, 28 (1940);
	3.8194	Kretschmar, Phys. Rev. **43**, 417 (1933).
(5) h/m	7.255	Ross and Kirkpatrick, Phys. Rev. **45**, 223 (1934);
	7.267	Gnan, Ann. d. Physik [5] **20**, 361 (1934).
(6) $h/(em)^{\frac{1}{2}}$	1.00079	von Friesen, Proc. Roy. Soc. **A160**, 424 (1937); Dissertation Uppsala (1936).
(7) α	7.3019×10^{-4}	Christy and Keller, Phys. Rev. **58**, 658 (1940).

The values of e are those calculated by Birge,[3] but corrected to correspond to the value of the Faraday given above.

The values of e/m are those calculated by Birge (Phys. Rev. **60**, 766 (1941)).

The values of h/e are those re-calculated by DuMond,[7] excepting for the value of Ohlin, which is corrected for the cathode work function by Birge (private communication).

The values of h/m are as corrected by Kirchner.[5]

The values of e^2/mh of Robinson were corrected here for the changes in auxiliary constants.

The value of e^2/mh of Kretschmar was corrected by Kretschmar.

imum is displaced by 1×10^{-4} from $z=0$. Considering the highly conservative estimate of the a parameter in Eq. (5) we can put 10^{-4} as a *limit* of error due to this cause.

(*b*). *Wave-Length Measurement*

The error in wave-length measurement is composed of the following terms: (1) Uncertainty in the Ag $K\alpha_1$ line wave-length 2×10^{-5} (P.E.); (2) uncertainty in $\lambda g/\lambda s$ 6×10^{-5} (P.E.); (3) uncertainty in location of Ag $K\alpha_1$ line 3×10^{-5} (P.E.); (4) accuracy of angular setting of spectrometer 7×10^{-5} (limit); (5) stability of crystal position during runs 8×10^{-5} (limit) (by direct measurement). This gives 8×10^{-5} for the probable error of wave-length measurement.**

(*c*). *Voltage Measurement*

The uncertainty in voltage measurement is composed of the following terms: (1) uncertainty in standard cell voltage 1×10^{-4} (limit); (2) uncertainty in potentiometer calibration 2×10^{-4} (limit); (3) uncertainty in calibration of auxiliary standards 1×10^{-4} (limit); (4) uncertainty in calibration of voltage divider 1×10^{-4} (limit); (5) uncertainty[3] in pq 3×10^{-5} (P.E.). This gives 8×10^{-5} as the probable error of voltage measurement.

(*d*). *Combination of Errors*

If we take the error in c^2 to be 3×10^{-5} (P.E.) (Birge[3]) and combine these estimates we obtain 1.6×10^{-4} for our total probable error. Our result therefore becomes $h/e=(1.3786\pm.0002)\times10^{-17}$ erg sec./e.s.u.

(4) Comparison of the Result with other Determinations

This result is shown in relation to other determinations of the atomic constants on the DuMond consistency chart,[6] Fig. 9. Our measurement is shown by the heavy lines in the h/e group of measurements while Birge's "indirect" value is shown as the dotted line.

Our value lies 0.07 percent lower than the indirect value but considerably higher than other "direct" determinations other than the work of Ohlin.[8] It is of course difficult to attribute causes to these differences which are considerably beyond the probable error in all cases. We might mention however that it has been found in the case of the experiment of DuMond and Bollman,[11] considerable error might have been introduced by failing to consider the temperature coefficient of the voltage divider used by them. A

** The probable errors are combined by geometrical addition.

recalibration of the 14,000 : 1 resistance ratio used by them by an improved bridge method revealed that a change of several tenths of a percent toward higher ratios (higher h/e) would occur if the dividers were loaded up to 20 kv. We can of course see no particular reason for a disagreement with other experiments excepting for the fact that these experiments described here were executed under conditions of higher resolving power of monochromatization of the x-ray beam and the careful elimination of other sources of error already described above, many of which precautions were not mentioned as taken by the other observers.

ACKNOWLEDGMENTS

In the performance of this experiment we have received generous help from many sources. In the first part of this work, notably in the construction and tests of the voltage divider a great deal of the work was performed by Dr. Howland H. Bailey. We are also greatly indebted to Dr. Frank Wenner for the kind loan of resistance standards and his advice concerning precision electrical measurements. The set of balanced filters used in this experiment was kindly loaned to us by Professor Paul Kirkpatrick of Stanford University.

The funds for this investigation were derived partially from the gift of Dr. Leon L. Watters of New York City for research work in x-rays and atomic structure known as the Watters Memorial Research Funds. We are grateful for this opportunity to express our sincere appreciation for this gift.

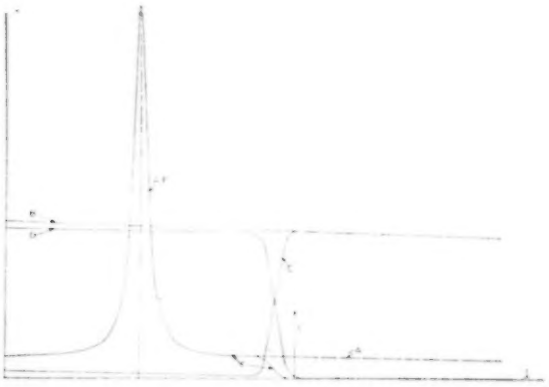

FIG. 10. Graphical representation of the action of balanced filters in conjunction with the 2-crystal spectrometer in "clipping" one wing of the monochromator pass band. Curve A represents the pass band of the 2-crystal monochromator alone. B is the transmission curve of Pd in this region; C is the transmission curve of Mo. D represents the differential transmission of the two filters; i.e., $D=B-C$. E is the wave-length at which the filters are balanced. F is the final pass band of the "compound monochromator." The width of the spectrometer window curve, the slope of the absorption edge, and the separation between them are drawn to the scale as used in this experiment. The curve A has been lifted bodily upward by the addition of a constant so as greatly to exaggerate the height of its wings in order to make visible the clipping effect.

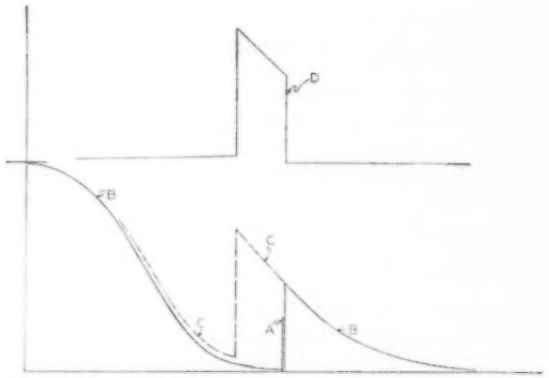

FIG. 11. The curves of Fig. 10 drawn on a small enough scale such as to show the Pd edge also. Note in particular the imperfect balance at short wave-length.

APPENDIX

Discussion of the Use of Balanced Filters in the Improvement of the Sharpness of the Isochromat Intercept

In the main body of this paper we discussed briefly the "clipping action" produced by the use of a set of balanced filters in conjunction with a two-crystal spectrometer. We shall now discuss this process in somewhat more detail, first as to the operation required in the actual use of the method, and second as to its theory.

(1) The pass band of the two-crystal spectrometer is adjusted so that its center falls a few X.U. on the *long* wave-length side of the K edge of the lighter of the two metals constituting the filter.

(2) The obliquity of the filters to the x-ray beam is adjusted until no difference in ionization is detectable when one filter is substituted for the other. During this process the x-ray tube is operated at a voltage about 10 kv above the voltage corresponding to the limit at the wave-length of the monochromator pass band. This assures that the filters have the same absorption on the long wave-length side of the region embraced by their K-absorption discontinuities.

(3) The pass band of the two-crystal spectrometer is moved until its center lies at a wave-length about 6 X.U. *shorter* than the K-edge wave-length of the lighter of the two metals. The peak of the pass band is now in that spectral region *between* the K edges of the two filters where

their absorptions are widely different. It is much closer to the softer of the two edges, however.

(4) Readings for plotting the isochromat are now obtained by taking differences between ionization readings observed through the heavier foil and readings observed through the lighter foil. The difference in ionization thus observed is between two to three times smaller than the total ionization observed without the use of filters.

Let curve A in Fig. 10 and also in Fig. 11 represent the transmission curve of the two-crystal spectrometer; the shape of this curve represents the combined effect of ideal crystal diffraction pattern width, crystal imperfection, incoherent scattering, and vertical divergence of the x-ray beam passing through the monochromator. As the accelerating voltage is varied in exploring an isochromat, this curve is "folded" with the ideal spectral distribution of the x-ray beam. The resultant curve will not exhibit a sharply defined break at the short wave-length limit but it will have a very wide region of changing curvature, owing to the wings or approaches of the monochromator pass band. The width of this region renders the exact location of the short wave-length limit difficult.

Let curve C represent the fractional transmission [approximately equal to $\exp(-ad\lambda^3 \sec\theta)$ save for absorption discontinuities; d = thickness of filter, θ = obliquity to x-ray beam] of the lighter metallic foil (Mo in this work) and curve B the transmission curve of the heavier foil (Pd). In steps (1) and (2) of the procedure outlined above the filters are adjusted so that the transmission difference curve ($D=B-C$), averaged over the pass band located at E, will vanish. Owing to the slight difference in absorption jump ratio of Pd and Mo this adjustment will give rise to non-zero values of the difference curve on the short wave-length side of the K edge of the heavier filter (see curve D in Fig. 11). It is this difference curve D which, when multiplied point by point with the original pass band A will give the actual transmission curve (F; Fig. 10, 11) of the "compound monochromator." It will be observed that the long wave-length wing of the transmission curve is now almost completely suppressed. This transmission curve F, if folded into the ideal spectral distribution, will give rise to the actually observed isochromats, in which the quantum limit is now much more sharply defined. It will be noted that the imperfect balance of the two filters at short wave-lengths bears no influence on the resultant curve, since there is no spectral intensity there.

It might be noted that this system of monochromatization does not increase the number of readings necessary in obtaining an isochromat, since even without using balanced filters the ionization readings must be obtained relative to the background by means of lead shutter difference readings.

It is important to call attention to the fact that without this balanced filter refinement the steeply rising spectral intensity of the continuous spectrum as one passes from the limit towards longer wave-lengths, is available to "shine through" the rather slowly decaying foot or approach of the spectrometer pass band on its long wave-length side. This approach has a law of decay similar to the inverse square of the wave-length difference from the peak of the pass band. On the other hand, the law of increase of the continuous spectrum is more or less linear for a great distance relative to the width of the pass band. Thus the intensity transmitted at any particular wave-length will vary at large distance from the peak as the inverse first power of the distance from the peak; the integrated or total intensity would therefore be logarithmically divergent, provided that the continuous spectrum would continue to rise linearly indefinitely. Notwithstanding the fact that the latter condition is not fulfilled in practice, this divergence indicates that a dangerously strong emphasis falls on the shapes of the continuous spectrum and of the spectrometer pass band at *large distances* from the peak of the one and the limit of the other. It was to avoid this danger that we have here adopted the balanced filter technique for clipping off most of the long wave-length approach of the spectrometer pass band.

The use of balanced filters with the two-crystal monochromator has also another very important purifying effect already alluded to. The crystal monochromator alone permits a considerable amount of non-monochromatized radiation to enter the ionization chamber by the mechanism of incoherent scattering from the crystal faces as well as air scattering and scattering from lead stops and other obstacles. All wave-lengths present in the primary x-ray beam can contribute to this intensity. Compared to the weak monochromatized intensity when settings are close to the short wave-length limit this general scattered radiation can become very considerable in intensity. Furthermore as the voltage is varied to explore the isochromat, this scattering does not remain constant but varies rather rapidly with voltage and hence there is superposed upon the true isochromat a background which is neither level nor linear and which contributes still more to the difficulty of accurately locating the quantum limit. The balanced filter method, since it in effect "clips off" or suppresses the effect of all wave-lengths of the spectrum on the soft side of the region between the two K edges of the filters, therefore effectively eliminates the background of incoherent scattering.

Beta-Ray Spectra of Arsenic, Rubidium, and Krypton*

G. L. WEIL**
Pupin Physics Laboratories, Columbia University, New York, New York
(Received June 22, 1942)

Cloud-chamber measurements are described in which the β-rays emitted by the radioactive nuclei As^{76} ($T=27$ hours), $Kr^{88,\geq 90}$ ($T=3$ hours), and the latter's decay product, $Rb^{88,\geq 90}$ ($T=18$ minutes), were investigated. The krypton and rubidium activities were separated from uranium fission products. The observed upper energy limit of the disintegration electrons from As^{76} is 2.71 Mev. The complexity of the spectrum is apparent from the observed momentum distribution. A Fermi plot yields an extrapolated end point of 2.78 Mev. A K-U plot analyzes into components with extrapolated end points of 0.97 Mev and 3.32 Mev. The decay of As^{76} was followed and found to have a half-life of 26.8 hours. The β-rays from the active rubidium have an observed upper energy limit at 5.1 Mev. Although a Fermi plot analyzes into two components with extrapolated end points at 2.5 Mev and 5.0 Mev, a K-U plot indicates a single group with extrapolated end point at 5.8 Mev. The possible instability of the rubidium decay product, a strontium isotope, is discussed. A measurement of the half-life of the rubidium activity yields $T=17.5$ minutes. The measurement and K-U analysis of the complex spectrum due to krypton and rubidium disintegrations yields an extrapolated upper energy limit of 2.5 Mev for the β-rays emitted by $Kr^{88,\geq 90}$. A plot of the Sargent points indicates that all of the β-transitions involved in the above measurements are of the "forbidden" type.

INTRODUCTION

THIS paper is a report on some cloud-chamber investigations of the disintegration electrons from As^{76} and certain rubidium and krypton activities separated from uranium fission products. Preliminary communications[1] of some of the results have already been published. The arsenic measurements were performed in collaboration with Dr. W. H. Barkas.

Although the beta-ray spectrum of As^{76} had been previously investigated,[2] because of the complexity of the spectrum and disagreement as to the relative populations of the two energy groups, it seemed worthwhile to repeat the measurement with a larger total number of tracks in the spectrum and higher resolution.

Arsenic ($Z=33$) has a single stable isotope with mass number 75. The radioactive isotope As^{76} can be produced by the following nuclear reactions: $As(d, p)$, $As(n, \gamma)$, $Br(n, \alpha)$, $Ge(p, n)$, and $Se(d, \alpha)$. It has a half-life of about 27 hours with emission of negative electrons corresponding to the transition

$$As^{76} \rightarrow Se^{76} + \beta^-.$$

A relatively small number of positrons are also emitted[3] which arise from the transition

$$As^{76} \rightarrow Ge^{76} + \beta^+.$$

The isotopes of rubidium found in nature have the mass numbers 85 and 87. The latter is observed to be naturally β^--active with a period of the order of 10^{10} years. On irradiating rubidium with slow neutrons two β^--activities are observed[4] with half-lives of about 18 days and 18 minutes. These activities are attributed to the isotopes Rb^{86} and Rb^{88}, which would be expected to be formed by $Rb(n, \gamma)$ reactions. However, from these observations it is impossible to assign the two activities to the specific isotopes. Recently[5] the 18-day Rb activity has been produced by a $Sr(d, \alpha)$ reaction, thus identifying this period with Rb^{86}, and, consequently, the 18-minute period with Rb^{88}.

An 18-minute rubidium activity was also identified among the fission products of uranium,[6] and later shown to be the decay product of an active krypton having a period of about 3 hours.[7]

---

* Submitted in partial fulfillment of the requirements for the degree of Doctor of Philosophy in the Faculty of Pure Science, Columbia University, New York, New York. Publication assisted by the Ernest Kempton Adams Fund for Physical Research of Columbia University.

** Now at the Metallurgical Laboratory, University of Chicago, Chicago, Illinois.

[1] G. L. Weil and W. H. Barkas, Phys. Rev. **56**, 485 (1939); G. L. Weil, Phys. Rev. **60**, 167A (1941).

[2] M. V. Brown and A. C. G. Mitchell, Phys. Rev. **50**, 593 (1936); Harteck, Knauer, and Shaeffer, Zeits. f. Physik **109**, 153 (1938).

[3] W. Schaeffer and P. Harteck, Zeits. f. Physik **113**, 287 (1939).

[4] A. H. Snell, Phys. Rev. **52**, 1007 (1937).

[5] Helmholz, Pecher, and Stout, Phys. Rev. **59**, 902 (1941).

[6] O. Hahn and F. Strassmann, Naturwiss. **27**, 529 (1939).

[7] Heyn, Aten, and Bakker, Nature **143**, 516 (1939); A. Langsdorf, Jr., Phys. Rev. **56**, 205 (1939); G. N. Glasoe and J. Steigman, Phys. Rev. **58**, 1 (1940).

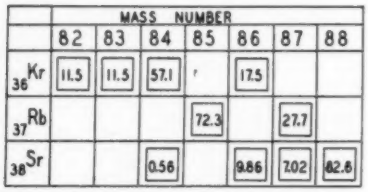

FIG. 1. The stable isotopes of Kr (mass numbers 78 and 80 omitted), Rb, and Sr, with percent abundance.

From the mass numbers of the stable nuclei in the neighborhood of rubidium (Fig. 1), it is clear, if one neglects the possibility of isomers, which will be done here and in following discussions, that the fission 18-minute activity cannot be due to Rb^{86}, since Kr^{86} is stable. Glasoe and Steigman[7] have shown that the decay product of this rubidium activity either is stable, or is unstable with a half-life less than five minutes or greater than a year. Furthermore, they separated a 14.5-minute rubidium activity from the uranium fission products which is assigned to Rb^{89} on the basis of its decaying into a known 55-day strontium.[8] Thus, the 18-minute activity must be attributed to $Rb^{88,\geq 90}$, and because of the similarity between it and the slow neutron induced activity, it has been tentatively assigned to Rb^{88}.

Krypton ($Z=36$) has the stable isotopes with mass numbers 78, 80, 82, 83, 84, and 86. The 175-minute krypton separated from uranium fission products cannot be produced by the usual nuclear reactions. It is genetically related to the 18-minute rubidium discussed above,

$$Kr^{88} \xrightarrow{175\ \text{min.}} Rb^{88} \xrightarrow{18\ \text{min.}} Sr^{88}\ (\text{Stable})$$

and accordingly must be given the same mass number as that tentatively assigned to its decay product, namely, Kr^{88}. Another interpretation is also possible, namely,

$$Kr^{\geq 90} \rightarrow Rb^{\geq 90} \rightarrow Sr^{\geq 90}.$$

In this case the Sr might very well be radioactive.

APPARATUS

Cloud Chamber

The cloud chamber used for the measurements was 6″ in diameter and $\frac{3}{4}$″ deep. The floor of the chamber consisted of a brass plate covered with black velvet and sealed by means of a rubber diaphragm. The expansion was produced mechanically through the action of a compressed spring and rotating cam. An intermediate expansion was used in order to clear the chamber more effectively before the main expansion. As source of vapor a 50-50 ethyl alcohol and water mixture was used. Before all runs the chamber was flushed and filled with hydrogen.

Magnetic Field

The chamber was situated in a magnetic field produced by a pair of Helmholtz coils. The mean diameter of the coils was 16″, and the mean separation of the pair 8″. Each half of the Helmholtz pair was made up of four separate coils each wound with 500 turns of No. 10 B and S copper wire and connected in series. Spaces between the coils allowed for air cooling.

The uniformity of the magnetic field in the region of the cloud chamber was investigated with a flip coil (1 cm^2 effective area) and ballistic galvanometer. It was found that the field intensity perpendicular to the plane of the chamber was constant to within ± 2.5 percent over the sensitive volume of the chamber. By calibrating the flip coil and galvanometer in the known field of a standard solenoid, the constant of the Helmholtz coils was found to be 42.7 gauss per ampere. With a 240-volt d.c. supply, the maximum field obtainable was 1200 gauss. In order to avoid overheating of the coils, the field was applied two seconds before an expansion and removed immediately afterward. The field current was monitored during a run with an ammeter which was calibrated and checked from time to time with a standard resistance, Weston cell, and potentiometer. During a run the field was maintained constant to ± 1 percent.

Illumination

Illumination was provided by condenser discharges in air at low pressure. Two discharge tubes were used, each about 4″ long and made of 4-mm I.D. capillary Pyrex tubing with 60-mil tungsten seal-ins at each end. They were roughly evacuated and each connected across a bank of thirty condensers,[9] each of 1-μf capacity, con-

[8] L. A. DuBridge and J. Marshall, Phys. Rev. **57**, 348A (1939).

[9] The author is indebted to the Bell Telephone Laboratories, New York, New York, for the loan of these condensers.

nected in parallel. The condensers were charged to about 2500 volts, and the discharges through the capillary tubes were initiated by ionization produced by ignition coils. The capillary tubes had a useful life of about 3000 discharges, after which time their light producing efficiency became too low, due to discoloration and minute cracks on the inner wall, to enable photographing of beta-tracks. The light from these sources was collimated by means of slits and cylindrical lenses. The depth of the illuminated region of the cloud chamber was about $\frac{3}{8}''$.

Camera

Photographs were taken with a single camera mounted directly above the chamber with the lens axis perpendicular to the plane of the chamber. The camera was equipped with a Kern f : 1.8, 45-mm focal length lens, which was used at full aperture. The distortion of the lens was found to be negligible. 200 feet of 35-mm film in the camera could be moved one frame at a time by means of a ratchet and toothed wheel operated by a plunger and solenoid.

Timing

The various operations of a cycle were timed by means of switches operated by cams mounted on the same shaft as the cam controlling the expansion of the chamber. A complete cycle was performed in 15 seconds.

Source Holders

The glass top of the chamber had a 1″ hole near its periphery through which the arsenic and rubidium sources were introduced. The sources were held in a light wire frame attached to a brass plug which fitted in the hole. By using a rubber gasket seal the plug and source could be inserted and the cloud chamber operated within a few minutes afterward. Once inside the chamber the source could be rotated about an eccentric axis so that it was "seen" by the camera.

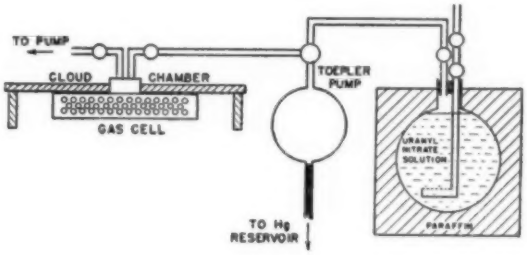

FIG. 2. Diagram illustrating method of extracting active Kr from irradiated uranyl nitrate solution, and of introducing it into gas cell.

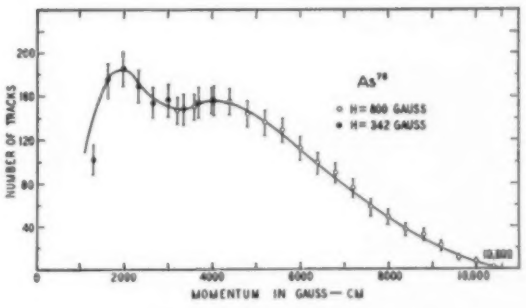

FIG. 3. The momentum distribution of the electrons from As^{76} ($T = 26.8$ hours). The complexity of the spectrum is indicated by the resolution of the two peaks. The length of a vertical line through a point is the uncertainty estimated by taking the square root of the number of observed tracks corresponding to the point.

For the measurements of the krypton disintegrations a thin-windowed gas cell was introduced inside the cloud chamber. This cell was a rectangular brass box $4'' \times 1'' \times \frac{5}{8}''$ with $\frac{1}{16}''$ walls. One of the faces, $4'' \times \frac{5}{8}''$, consisted of an aluminum foil (12.4 mg/cm²) held between two $\frac{1}{32}''$ brass plates drilled out with $\frac{1}{8}''$ holes to form a grill. The hole area amounted to 62 percent of the total area of that face. The aluminum foil was sealed between the plates with a rubber gasket. The cell could be evacuated and filled with the active krypton by means of $\frac{1}{8}''$ copper tubing connecting to the interior of the cell and brought out through a hole in the glass top of the chamber. In order to reduce back-scattering of the β-particles, the inside walls of the cell were coated with a 2 mm thick layer of Aquadag. It was found that the presence of the cell in the cloud chamber produced no noticeable effect beyond two or three millimeters from the front face.

METHOD OF TRACK MEASUREMENT

For measuring the tracks the film was replaced in the camera and reprojected to full size on to a screen. The radii of curvature of the tracks were then compared with arcs of known radii drawn on white cardboard in steps of 0.5 cm from 2 to 26 cm. In the region of small curvatures the error in matching a track was of the order of 10 percent.

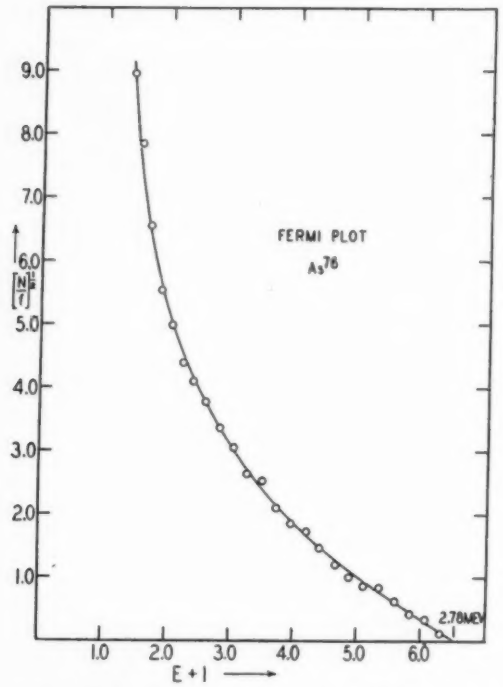

FIG. 4. Fermi plot of As^{76} data shown in Fig. 3. The total electron energy, $E+1$, is given in mc^2 units.

In the matter of selection of tracks the following rules and criteria were adhered to: (1) the track must originate at the source; (2) the track must not be visibly scattered within the first 10 cm of its length; (3) at least 10 cm of track length must be measurable; (4) the tangent to the track at its point of origin must lie within a certain fixed angle, that angle being determined by two lines drawn from the two edges of the source such that the distance along each line from the source to the periphery of the chamber was exactly 10 cm. The last two criteria made certain that the solid angle remained constant for particles in different momentum intervals.

The error introduced in the momentum by neglecting the vertical component was at the most 0.5 percent due to the small depth of the illuminated region and the minimum track length measured.

PREPARATION OF SOURCES

Arsenic

The preparation and separation[10] of the active isotope was as follows. The radioactive isotope As^{76} was produced by the $As(n, \gamma)$ reaction using slow neutrons. The arsenic was irradiated in the form of a saturated aqueous solution of cacodylic acid. The solution was contained in a boron-free glass flask imbedded in a paraffin block. For the neutron irradiations three different types of sources were used; (1) about 750 millicuries (Rn+Be); (2) D−D source;[11] (3) $Be(p, n)$ reaction in the cyclotron. After irradiation the active arsenic, present as ions in the solution, was precipitated as a sulphide by passing H_2S through the solution. Previously the solution had been slightly acidified and a few milligrams of $AsCl_3$ added as a carrier. The precipitate was then dried, pressed between two pieces of filter paper, and inserted in the source holder. The total surface density of a source averaged about 29 mg/cm².

Rubidium

The preparation of the rubidium sources was as follows. A saturated aqueous solution of uranyl nitrate was irradiated for several hours with neutrons, which had been slowed down in paraffin, from the cyclotron. After irradiation the solution was set aside for 3 hours to allow short period gaseous products to decay. After this period, air was bubbled through the solution and, together with the active krypton it had accumulated, collected by water displacement in a brass vessel. An aluminum foil, of surface density 3.5

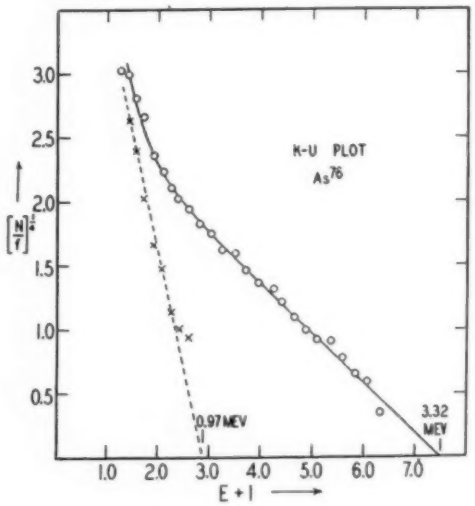

FIG. 5. K-U plot of As^{76} data shown in Fig. 3.

[10] L. Szilard and T. A. Chalmers, Nature **134**, 462 (1934).

[11] The author is indebted to Dr. W. H. Zinn for the use of his D–D neutron source.

mg/cm², was supported inside the vessel, insulated from it, and maintained at a negative potential of about 1200 volts with respect to the container. This foil collected the positively charged recoil rubidium ions produced in the gas by the krypton disintegrations. After collecting for 45 minutes the foil was removed and placed in the source holder.

Krypton

The active krypton was collected in the gas cell in the following manner. The boron-free glass flask containing the uranyl nitrate solution was sealed with a rubber stopper through which a tube led to a sintered glass disk at the bottom of the solution. Another tube through the stopper connected to the air space above the solution. Both these tubes were equipped with stopcocks. After evacuating the space above the liquid the solution was irradiated for several hours with neutrons from the cyclotron. After irradiation the short period gaseous products were allowed to decay for three hours. The flask was then connected to the gas cell through a Toepler pump, this system having previously been evacuated. The arrangement is shown in Fig. 2. After passing a few cubic centimeters of air through the solution, the air, together with the active krypton picked up, was pumped into the gas cell. This process was repeated twice. The pressure in the cell amounted to about 5 cm of Hg.

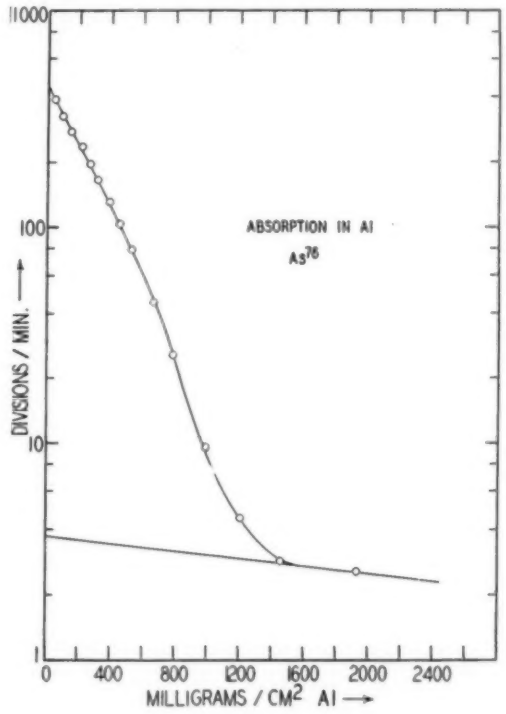

FIG. 6. Absorption in Al of β-rays from As^{76}. Measurements were made using a high pressure ionization chamber and string electrometer. The maximum range of 1.48 g/cm² corresponds, according to Feather's formula ($R=0.543\,E-0.160$), to an energy of 3.0 Mev.

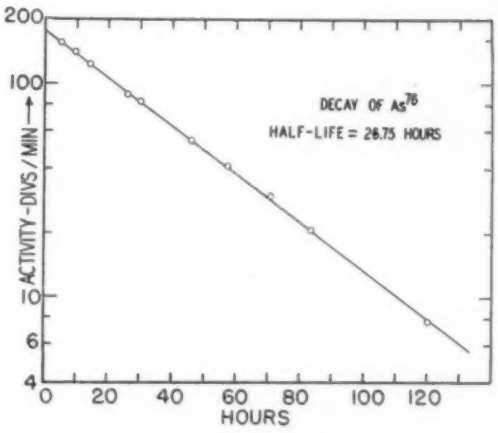

FIG. 7. The decay of As^{76}.

Since the half-life of the krypton is 3 hours, and that of the rubidium 18 minutes, the electrons observed in the cloud chamber resulted from the disintegrations of both types of nuclei. In order to be sure that the ratios of the two activities would be the same for different runs, the track photography was always started 10 minutes after the gas cell had been filled.

RESULTS

Arsenic

The observed momentum distribution of the disintegration electrons from As^{76} is shown in Fig. 3. Runs were taken at two magnetic field strengths of 342 and 800 gauss. The purpose of this procedure was to bring the low and the high momentum parts of the spectrum into the region of easily measured curvatures. The data obtained at the two field strengths overlapped sufficiently to allow correlation of the two sets of observations. The spectrum represents the results of the measurement of 2650 tracks plotted in intervals of 400 $H\rho$.

From Fig. 3 one obtains the upper limit of the β-rays from As^{76} at $H\rho=10{,}600\pm500$ gauss-cm, corresponding to an energy of 2.71 ± 0.14 Mev.

The complexity of the spectrum is readily seen from the presence of the two maxima at $H\rho = 2500$ and $H\rho = 4000$. The average energy of the electrons is found to be 0.94 Mev.

Fermi and K-U plots[12] of the data are shown in Figs. 4 and 5. The upper energy region of the observed spectrum can be fitted by a Fermi distribution, which, upon extrapolation, yields an end point of 2.78 Mev. The K-U plot can be analyzed into two components having extrapolated end points of 0.97 and 3.32 Mev. In agreement with other similar measurements a 20 percent difference is found between observed and K-U extrapolated end points. On the basis of the K-U analysis, the low energy component contains about 20 percent of the total number of tracks in the spectrum.

An absorption measurement in aluminum of the β-rays from As^{76} yielded a range of 1.48 g/cm^2, corresponding to an energy of 3.0 Mev as determined by Feather's range-energy formula.[13] Figure 6 shows the absorption curve obtained.

The decay of As^{76} was followed for over five half-lives (Fig. 7) and found to have a single period of $T = 26.75 \pm 0.15$ hours. By assuming the existence of the two groups suggested by the K-U analysis, the partial disintegration constants were computed. These values, taken with the K-U extrapolated energies and also with the latter reduced by 20 percent, are plotted on a Sargent[14] diagram (Fig. 8). Both transitions are of the "forbidden" type.

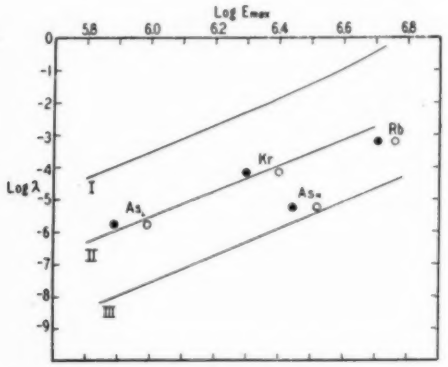

FIG. 8. Sargent diagram. The open circles represent points corresponding to K-U extrapolated energy limits, the filled circles to K-U end points decreased by 20 percent. As$_H$ and As$_L$ represent, respectively, the high and low energy groups of As^{76}.

[12] Kurie, Richardson, and Paxton, Phys. Rev. **48**, 167 (1935).

[13] N. Feather, Proc. Camb. Phil. Soc. **34**, 599 (1938).

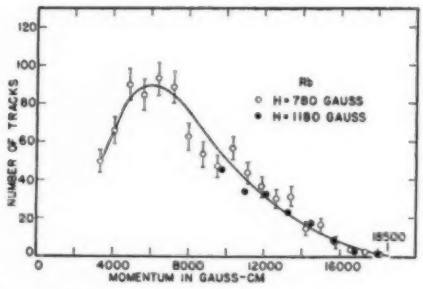

FIG. 9. Momentum distribution of β-rays from Rb ($T = 17.5$ minutes) separated from uranium fission products.

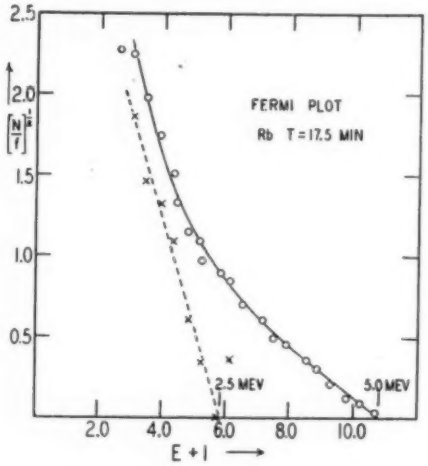

FIG. 10. Fermi plot of Rb data shown in Fig. 9.

Rubidium

The observed distribution in momentum of the β-particles from the 18-minute rubidium separated from uranium fission products is shown in Fig. 9. A total of 1360 tracks was measured at magnetic field strengths of 780 and 1180 gauss. The observed upper limit at $H\rho = 18{,}500 \pm 500$ gauss-cm corresponds to an energy of 5.06 ± 0.15 Mev. The mean energy of electrons is found to be 1.8 Mev.

A Fermi plot of the data is given in Fig. 10. It is possible to analyze the observed spectrum into two components having the shapes of Fermi "allowed" distributions. The extrapolated end points are 2.5 Mev and 5.0 Mev. A K-U plot of the data (Fig. 11) indicates a single distribution with extrapolated end point of 5.8 Mev.

[14] B. W. Sargent, Proc. Roy. Soc. **139**, 659 (1933).

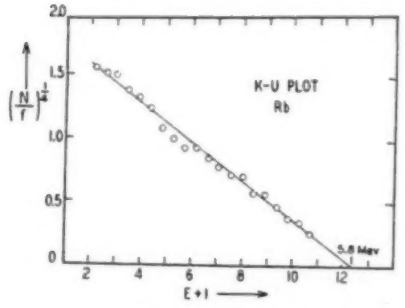

FIG. 11. K-U plot of Rb data shown in Fig. 9.

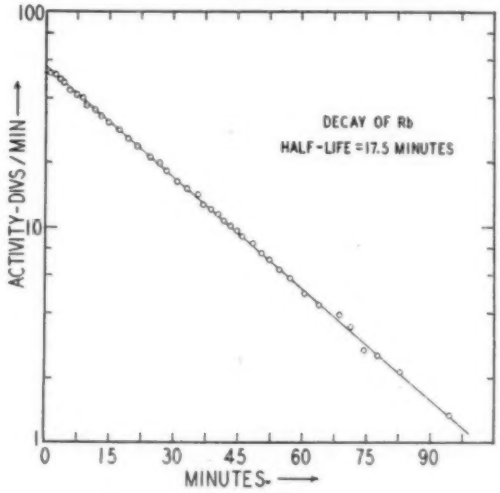

FIG. 12. Decay of Rb activity.

The decay of the rubidium activity was followed for over 5 half-lives (Fig. 12) and found to have a half-life $T=17.5\pm0.5$ minutes.

Krypton

As previously mentioned, the electrons observed from the gas cell are due to both krypton ($T=175$ minutes) and rubidium ($T=18$ minutes) disintegrations. Figure 13 gives the observed momentum distribution of the Kr+Rb β-particles, representing the measurement of 900 tracks at a magnetic field strength of 700 gauss. The end point at $H\rho=18{,}000$ agrees closely with that obtained for the rubidium disintegration electrons, indicating that the upper energy region of the composite spectrum is due to the rubidium disintegrations.

A K-U plot of the complex Kr+Rb spectrum (Fig. 14) can be analyzed into two components. The extrapolated end point of the high energy group occurs at 5.8 Mev, in agreement with that obtained for the 18-minute rubidium, while the low energy group, due to krypton, has an extrapolated end point of 2.5 Mev.

The Sargent points (Fig. 8) for the rubidium and krypton activities indicate that both transitions are "forbidden."

DISCUSSION OF RESULTS

Arsenic

The observed momentum distribution of the electrons from As^{76} is undoubtedly distorted slightly in the low energy region due to scattering in the source itself.[15] The result of this distortion will be to lower the ratio of the population of the high to that of the low energy group.

A comparison of the present results with those reported by other investigators is given in Table I. In all cases the measurements were made with a Wilson cloud chamber. It is seen that the agreement as to the observed upper energy limit is very good. Although in the other investigations the complexity of the spectrum was apparent only in the K-U analysis, in the present results the observed spectrum clearly indicates the presence of at least two groups. The results reported here also confirm the relative populations of the two energy groups as found by Harteck (*et al.*). The K-U extrapolated end point of the low energy group is found to be about 10 percent lower than that found by the other authors.

From the existence of the two energy groups of electrons emitted by As^{76} one would also expect the emission of a γ-radiation with an energy

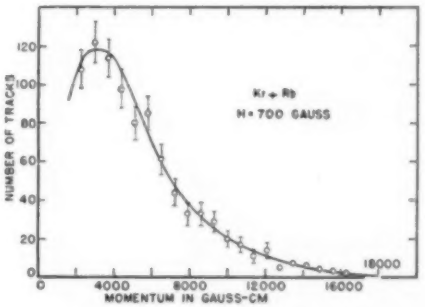

FIG. 13. Momentum distribution of β-rays from Kr ($T=175$ minutes) and Rb ($T=17.5$ minutes). Since the Kr, separated from uranium fission products, decays into the shorter-lived Rb, disintegration electrons from both isotopes are present in the observed spectrum.

[15] A. W. Tyler, Phys. Rev. **56**, 125 (1939); J. L. Lawson, Phys. Rev. **56**, 131 (1939).

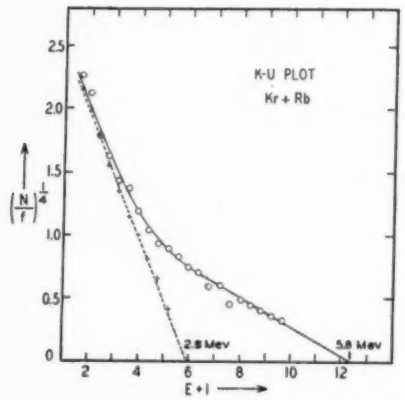

FIG. 14. K-U plot of (Kr+Rb) data shown in Fig. 13. The agreement of the extrapolated end point of the high energy group with that found for Rb alone (Fig. 11) identifies the low energy group as due to Kr disintegrations.

equal to the energy difference of the two end points. Harteck (*et al.*) observed 5 electron-positron pairs with an average energy of 2.16 Mev, which value is in substantial agreement with the difference of the K-U extrapolated upper limits. They also found two pairs with an average energy equal to 3.15 Mev, suggesting the existence of another low energy electron group. Measurements[16] of β and γ coincidences also suggest the presence of this third component in the As^{76} β-spectrum. At present the available information is not of sufficient accuracy to allow more than speculation as to the energy level system of Se^{76}.

It should be mentioned that the upper limit of the low energy group of a complex spectrum, as determined by a K-U analysis, has rather large uncertainty limits. The K-U method of analysis is, to a large extent, arbitrary, and the only justification for its use is the fact that the present theory of β-decay is unable to give precise information as to the shape of β-spectra resulting from various types of "forbidden" transitions.

Rubidium

Because of the fact that a "thin" source was used for the measurement of the β-particles emitted by rubidium ($T=18$ min.), one would expect little distortion of the observed spectrum resulting from scattering within the source.

The analysis of the observed distribution into two components having the shapes of Fermi "allowed" distributions is doubtful because of the statistical errors of the observations. It is still quite possible that we have a single group with a K-U distribution. However, if one assumes the analysis to be correct, the two energy groups might either be due to transitions from rubidium to two strontium energy levels, or, on the other hand, to a rubidium disintegration followed by a very short-lived strontium disintegration. On the basis of the latter hypothesis, the 18-minute rubidium activity must be attributed to $Rb^{\geq 90}$. Furthermore, attributing the high energy component to the short-lived strontium, one would expect, for an "allowed" transition, a strontium activity with a half-life of the order of 2 sec.

Glasoe and Steigman measured the absorption of the β-particles in aluminum, and found a maximum range equivalent, by Feather's formula, to 4.6 Mev. This value is in reasonable agreement with the present observed upper limit of 5.1 Mev. From their absorption curve it appears that about 1 percent of the total ionization with no absorbing material is accounted for by γ-radiation. This would indicate that the rubidium spectrum is complex.

Krypton

It is of interest to note that in this measurement, where the existence of two energy groups of electrons, namely Kr and Rb disintegrations, is to be expected, the K-U plot does analyze into two components. This perhaps justifies to some extent the practice of interpreting K-U plots as indicating simple or complex spectra, particularly so, since in Fig. 10 there is not much indication of complexity.

Since the krypton isotope responsible for the

TABLE I. Comparison of As^{76} results.

	No. of tracks measured	Observed upper energy limit (Mev)	Average energy (Mev)	K-U extrapolated end points (Mev)	Intensity ratio—high to low energy groups
Brown and Mitchell (reference 2)	150	2.81	0.62	3, 4, 1.09	0.8
Harteck (*et al.*) (reference 2)	1750	2.81	1.3	3, 2, 1.1	3.7
Sagane (*et al.*)[a]	1515			2.75, 1.31	4.9
Weil	2650	2.71	0.94	3.3, 0.97	3.5

[16] F. Norling, Zeits. f. Physik **111**, 158 (1938); Mitchell, Langer, and McDaniel, Phys. Rev. **57**, 1107 (1940).

[a] Sagane, Kojima, Miyamoto, and Ikawa, Proc. Phys. Math. Soc. Japan **21**, 660 (1939).

175-minute activity must have the same mass number as the rubidium nucleus with 18-minute half-life, we must assume the radioactive krypton isotope to be $Kr^{\geq 90}$ if the rubidium activity should be due to $Rb^{\geq 90}$.

ACKNOWLEDGMENTS

The author wishes to express his sincere thanks to Dean G. B. Pegram and Professor J. R. Dunning for their continued interest and helpful advice. The author also takes pleasure in acknowledging his indebtedness to Dr. W. H. Barkas, who collaborated in the measurements on arsenic; to Dr. G. N. Glasoe and Dr. J. Steigman for many helpful suggestions in connection with the preparation of the radioactive sources; and to Mr. H. Glassford for his able assistance during the course of the experiments.

SEPTEMBER 1 AND 15, 1942 PHYSICAL REVIEW VOLUME 62

Ionization of Argon and Neon by Electron Impact

D. P. STEVENSON* AND J. A. HIPPLE
Westinghouse Electric and Manufacturing Company, Research Laboratories, East Pittsburgh, Pennsylvania
(Received June 25, 1942)

The "ionization efficiency curve" for singly charged argon is found to have at least one inflection of the type first observed by E. O. Lawrence for mercury. The relative probabilities of forming singly and doubly charged argon and neon are tabulated. Careful examination of the initial portions of the "ionization efficiency curves" for singly charged neon and argon and doubly charged argon shows the "tails" to be largely characteristic of the ionization cross section and not purely caused by spread in electron energy as often has been assumed.

THE ionization efficiency curves of the rare gases, particularly argon, are very commonly used to calibrate electron acceleration voltage scales in mass spectroscopic studies. Despite this, the form of these curves has not been extensively studied. The most complete reports on the ionization of the rare gases by electron impact are in the important papers of P. T. Smith[1] and W. Bleakney.[2] The former studied the total ionization cross sections of helium, neon, and argon as a function of the impacting electron energy. Bleakney determined the relative probability of forming singly and multiply charged ions.

In the course of checking the behavior of our 180° mass spectrometer tube we have obtained considerable data on the ionization efficiency curves of argon II (A^+), argon III (A^{++}) and neon II (Ne^+), for electrons of less than 250-volt energy. Since our data, which we believe to be more reliable for reasons given below, differ in significant detail from the previous work, we are reporting them here.

The instrument used in this research will be described in detail elsewhere, hence only pertinent details are recorded. The 180° mass spectrometer tube (16-cm radius) with the wide slits in use has a resolving power of about 1 in 150. The tube and accessories are mounted in the cavity of a water cooled spherical solenoid. A magnetic field strength of ~1000 oersteds was used. The electrons were supplied by an oxide coated, platinum cathode. The electron accelerating voltage is controlled by a wire wound potentiometer and the apparent voltage measured with calibrated voltmeter which can be read with an accuracy of ±0.1 percent. The linear variation of the positive ion current with the pressure and the current in the electron beam showed that only primary processes were observed. The total electron emission ranged from 10 to 18μ amp. while the beam itself carried from 0.5 to 4μ amp.

In Fig. 1 we show the ionization efficiency curves of the ions A^+, A^{++}, Ne^+, and Ne^{++} for electrons of less than 225-electron volt energy. The broken lines show Bleakney's results. Al-

* Westinghouse Research Fellow. Now at Shell Oil Company, Emeryville, California.
[1] P. T. Smith, Phys. Rev. **36**, 1293 (1930).
[2] W. Bleakney, Phys. Rev. **36**, 1303 (1930).

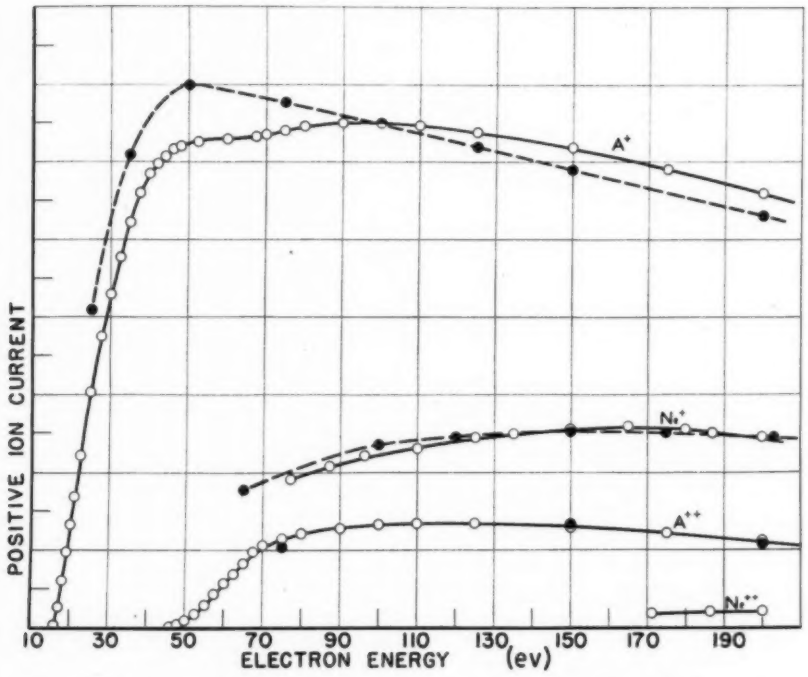

FIG. 1. The ionization efficiency curves for A^+, A^{++}, Ne^+, and Ne^{++}. Solid curves and open circles—this research. Broken curves and solid circles from reference 2 of text. The voltage scale was corrected by taking the "initial break" of the A^+ curve at 15.7 ev. The ordinates are arbitrary and different for argon and neon.

though our data for the ions Ne^+ and A^{++} are in reasonably good agreement with the earlier work, it will be noted that for $V^- > 100$ our curve for A^+ decreases more slowly than Bleakney's. Furthermore, Bleakney's curve for A^+ shows a relatively sharp maximum in the region ours shows a well-defined shoulder preceding a very flat maximum. In many respects this "peculiarity" of the ionization efficiency curve of A^+ is similar to the phenomena observed in mercury vapor.[3] Smith[1] observed the inflection in the argon ionization cross section curve at ~ 50 volts, but attributed it to the onset of the reaction giving A^{++}. The reason Bleakney did not observe the phenomenon probably lies in the lower sensitivity of his mass spectrometer and his use of a tungsten filament as an electron source. The much greater spread in energy of the electrons from the very hot tungsten source smears out the finer details. Even the energy spread in electrons from an oxide coated filament causes detail to be lost. This may be seen from comparison of our results on the initial portions of the ionization efficiency curve of mercury, Fig. 2, with the results of Nottingham's extremely careful study of this atom (see refer-

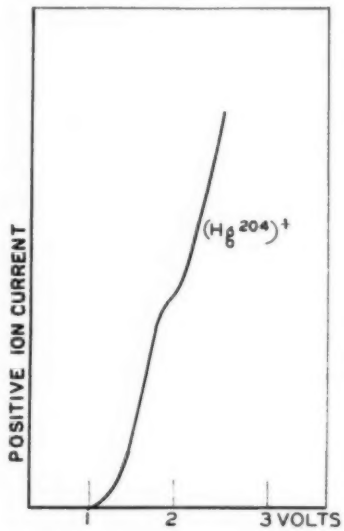

FIG. 2. The initial portion of the ionization efficiency curve for $(Hg^{204})^+$. The voltage scale is uncorrected, the ordinate arbitrary.

[3] a. E. O. Lawrence, Phys. Rev. **28**, 947 (1926); b. M. Bell, Phys. Rev. **55**, 201 (1939); c. W. B. Nottingham, Phys. Rev. **55**, 203 (1939).

ence 3c, Fig. 13). A careful study of argon, employing the precautions Nottingham observed, would probably reveal interesting details that our instrument is not capable of showing.

Because of their possible value for comparison with theoretical calculations we have recorded in Table I the ratios of the currents of doubly charged ions to singly charged ions for argon and neon at some round values of the impacting electron energy. The precision of the measurements, as indicated by the reproducibility, is at worst 2 percent.

Knowledge of the manner in which the ionization probability goes to zero when the electron energy approaches the ionization potential is important if ionization efficiency curves are to be used to determine critical potentials. Early workers assumed the deviations from linearity at low electron energies to be due to the spread in the electron energies.[1] Thus to obtain critical potentials the linear portion of the ionization efficiency curve was extrapolated to zero current. Tate, Smith, and Vaughan[4] in determining the ionization potential of nitrogen assumed that the ionization probability goes to zero with a finite slope but discarded the assumption of a linear dependence of the probability on electron energy. In their work on acetylene,[4] however, linear extrapolations were used to fix appearance potentials.

The approximations necessary to make quantum mechanical calculations of the ionization cross sections possible break down so badly near the critical potentials that the theory is unable to discuss the form of the initial portions of the curve. If the "tails" are primarily due to a spread of the electron energies, one would expect very close similarity to exist between the initial portions of the curves for singly charged argon and neon. The initial portions of the ionization efficiency curves of A^+ and Ne^+ are shown in Fig. 3. The ordinates for the two curves were so chosen that the linear portions are parallel. It will be noted that the tail of the curve for A^+ is considerably broader than that for Ne^+. The difference between the extrapolated linear intercepts is $5.4_7 \pm 0.1$ ev compared with the difference between the spectroscopically determined ionization potentials, 5.78 volts. These observations can be interpreted only as indicating that the curved tails are to a large extent a characteristic of the ionization process. The slope of the curve for double ionization of argon continues to increase for about 10 ev after the ion A^{++} first appears. This is to be compared to the 1- to $2\frac{1}{2}$-volt region in which the slope of the curves for A^+ and Ne^+ increases.

If one draws a smooth curve through the observed points and extrapolates to zero current assuming an essentially zero initial slope, the differences between the intercepts are $(Ne^+)_0 - (A^+)_0$

TABLE I. Ratio of currents of doubly and singly charged ions.

Electron energy V^- volts	Argon $(i++/i+)$[a]		Neon $(i++/i+)$[a]	
50	0.014	(0.021)[b]		
60	0.090			
70	0.167	(0.138)		
80	0.186			
90	0.197			
100	0.204	(0.208)		(0.034)[c]
125	0.210			
150	0.208	(0.223)		(0.081)
175	0.204		0.074	
200	0.199	(0.210)	0.082	(0.114)
225	0.193			

[a] These are ratios of currents. The relative ionization probabilities are obtained by dividing the tabulated quantities by 2.
[b] Bleakney, reference 2 of text. These values were obtained from measurements made on a photographic enlargement of Fig. 6 of reference 2. From Fig. 3 of Tate, Smith, and Vaughan [Phys. Rev. **48**, 525 (1935)] one finds for $V^-=100$ volts $A^{++}/A^+=0.216$.
[c] Figure 3 of reference 2.

[4] J. T. Tate, Z. T. Smith, and A. L. Vaughan, Phys. Rev. **48**, 525 (1935).

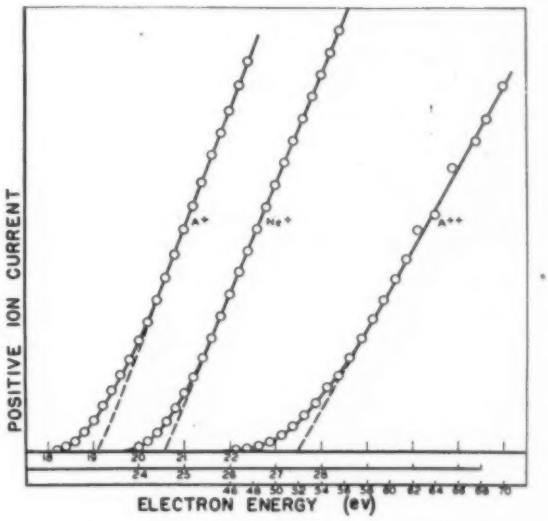

FIG. 3. The initial portions of the ionization efficiency curves for A^+, Ne^+, and A^{++}. Ordinate arbitrary and different for each curve. Note that voltage scale for A^{++} is $\frac{1}{2}$ that for A^+ and Ne^+, and that to save space the curves have been subjected to horizontal translation.

$=5.6_5\pm0.15$ ev and $(A^{++})_0-(A^+)_0=28.0\pm0.5$ ev. These differences agree with the spectroscopic values[5] within the experimental uncertainty of our results. These results seem to provide real justification for determining differences between appearance potentials from the initial breaks of curves obtained under similar conditions of sensitivity.[6] This procedure clearly reduces uncertainties due to contact potentials and the spread in the electron energy by cancellation. The close check between the electron impact and spectroscopic results indicates that the difference in the sharpness of onset of ionization introduces no error as great as that inherent in the mass spectroscopic measurements themselves.

APPENDIX I

We assume that the probability of the reaction

$$X+\epsilon^-\rightarrow X^++2\epsilon^-$$

is given by the expressions,

$$\rho(V^-)=0 \qquad V^-\leqslant I^s=\text{ionization potential of } X, \quad (1)$$

$$\rho(V^-)=(V^--I^s) \qquad V^-\geqslant I^s, \quad (2)$$

where $\rho(V^-)$ is the probability of the ionization of X by an electron of energy V^-. Furthermore, we assume that the energy of the electrons in the bombarding beam is

$$V^-=V_a+\epsilon$$

where V_a=applied potential and ϵ=thermal energy, and that the distribution in ϵ is Maxwellian, i.e.,

$$n(\epsilon)=KN^-(1/kT)^{\frac{1}{2}}\epsilon^{\frac{1}{2}}e^{-\epsilon/kT}$$

where T=characteristic absolute temperature, N^-=total current in beam. Then the positive ion current as a function of the electron energy, for the parameter $\beta\geqslant 0$, is

$$I^+(V_a)\propto\frac{2}{\sqrt{\pi}}\left[\tfrac{2}{3}\beta^{\frac{3}{2}}e^{-\beta}+\frac{\sqrt{\pi}}{2}(\tfrac{3}{2}-\beta)\{1-\Phi(\sqrt{\beta})\}\right] \quad (3)$$

$$\beta=(I^s-V_a)/kT$$

$$\Phi(\sqrt{\beta})=\frac{2}{\sqrt{\pi}}\int_0^{\sqrt{\beta}}\exp(-u^2)\,du,$$

TABLE II. Test of Eq. (5).

Molecule	ion	$I^+(\beta=\frac{3}{2})\div$slope
Neon	Ne^+	$0.24_3\pm0.01$
Argon	A^+	$0.33_4\pm0.01$
Argon	A^{++}	$1.5_2\pm0.1$
Ethane	$C_2H_6^+$	$0.20_6\pm0.01$
Propane	$C_3H_8^+$	$0.24_1\pm0.01$
n-butane	$C_4H_{10}^+$	$0.28_6\pm0.01$
i-butane	$C_4H_{10}^+$	$0.29_4\pm0.01$
Propylene	$C_3H_6^+$	$0.30_2\pm0.01$
iso-butylene	$C_4H_8^+$	$0.24_7\pm0.01$
Equation (5)	—	0.465

[5] R. F. Bacher and S. Goudsmit, *Atomic Energy States* (McGraw-Hill, New York, 1932). I^s(A I)=15.69 volts. I^s(A II)=27.72 volts. I^s(Ne I)=21.47 volts.

[6] L. G. Smith, Phys. Rev. **51**, 263 (1937) and reference 4.

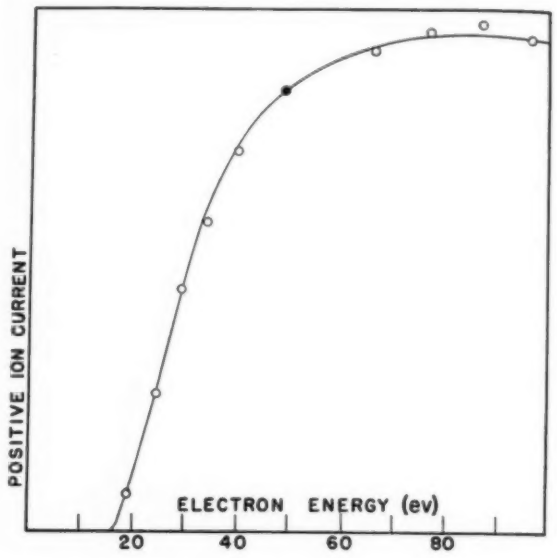

FIG. 4. The curve shows the ionization efficiency curve for N_2^+ determined by Hagstrum and Tate (reference 8). The open circles are from this research. The closed circle indicates the point at which the two curves were arbitrarily made to fit.

while for $\beta\leqslant 0$

$$I^+(V_a)\propto(\tfrac{3}{2}-\beta). \quad (4)$$

The constant of proportionality is the same for Eqs. (3) and (4), thus for $\beta=\frac{3}{2}$ the positive ion current should be

$$\left[I^+(V^-)=C\cdot\frac{2}{\sqrt{\pi}}\left(\frac{3}{2}\right)^{\frac{1}{2}}e^{-\frac{1}{2}}\right]=0.465\ C, \quad (5)$$

where C is the proportionality constant or the slope of the linear portion of the ionization efficiency curve. In Table II we record the observed value of the ratio of I^+ (at linear intercept) to slope for a number of atoms and molecules.

Since the form of the energy distribution of the electrons is well established,[7] the failure of Eq. (5) to agree with the experiments indicates that Eq. (2) is without justification.

APPENDIX II

As a check on the reliability of the ionization efficiency curves of Fig. 1 as plotted from data taken with our instrument, our curve for N_2^+ was compared with that reported by Hagstrum and Tate;[8] Fig. 4 shows the very satisfactory agreement of these curves and tends to promote confidence that the inflection in the A^+ curve is real. Another favorable factor is the excellent agreement obtained for the ethane spectrum taken with this instrument and the crossed-field instrument at Princeton.[9]

[7] K. T. Compton and I. Langmuir, Rev. Mod. Phys. **2**, 123 (1930).

[8] H. D. Hagstrum and J. T. Tate, Phys. Rev. **59**, 354 (1941).

[9] D. P. Stevenson and J. A. Hipple, J. Am. Chem. Soc. (to be published).

The Influence of an "Uneven" Anisotropy on the Path of Light Rays

PHILIPP FRANK
Harvard University, Cambridge, Massachusetts

(Received June 19, 1942)

The refractive index of a medium may be $\mu(\mathbf{r}, \mathbf{s}) = \mu_0(\mathbf{r}) + \mu_1(\mathbf{r}, \mathbf{s})$ the vector $\mathbf{r}$ denoting the coordinates of a point and the unit vector $\mathbf{s}$ the direction of the light ray, while μ_1 may be any function of $\mathbf{s}$. The deflection of a ray pencil $\mathbf{s} = \mathbf{s}(\mathbf{r})$ by the anisotropy μ_1 is defined by the "curvature vector $\mathbf{k}$ of the deflected rays relative to the rays in the isotropic medium μ_0." We find $\mathbf{k} = \mathbf{s} \times \text{curl } \mathbf{A}(\mathbf{r}, \mathbf{s})$, $\mathbf{s}$ being $\mathbf{s}(\mathbf{r})$ and $\mathbf{A} = \mu_1 \mathbf{s} + \text{grad}_{\mathbf{s}}\, \mu_1 - \mathbf{s}(\mathbf{s}\, \text{grad}_{\mathbf{s}}\, \mu_1)$, $\text{grad}_{\mathbf{s}}$ which implies differentiation with respect to the components of $\mathbf{s}$. The simplest case, notwithstanding the anisotropy of crystals, is $\mu_1 = \mathbf{s}\mathbf{g}(\mathbf{r})$, $\mathbf{g}$ being an arbitrary function of $\mathbf{r}$. This case covers, for example, the deflection of light rays by the motion of the medium. We have only to put $\mathbf{g} = -(1/c^2)\mu_0^2 \mathbf{w}(\mathbf{r})$. Here μ_0 is the refractive index and $\mathbf{w}$ the velocity distribution in the medium. A second example is the deflection of electron rays in an electromagnetic field. We have to put $\mathbf{g} = (\epsilon/c)\mathbf{a}(\mathbf{r})$. Here $\mathbf{a}$ is the vector potential of the field.

IF the refractive index of a medium is dependent upon the direction of the light ray we speak of an "anisotropy" of the medium. The refractive index μ at a certain point may be an arbitrary function of the rectangular coordinates x, y, z and of the direction of the light ray

$$\mu = \mu(\mathbf{r}, \mathbf{s}). \tag{1}$$

The vector $\mathbf{r}$ has the components x, y, z and the vector $\mathbf{s}$ the components $\cos\alpha$, $\cos\beta$, $\cos\gamma$, α, β, γ being the angles between the light ray and the axes. If

$$\mu(\mathbf{r}, -\mathbf{s}) = \mu(\mathbf{r}, \mathbf{s}) \tag{2}$$

the anisotropy may be called an "even" one. All crystals have an even anisotropy. If for a certain medium Eq. (2) does not hold we speak of an "uneven" anisotropy.

Examples of "uneven" anisotropy are provided by the path of light rays through moving bodies or the path of electrons through an electromagnetic field. The formulae we are going to develop will embrace in one mathematical pattern all these problems.

According to Fermat's principle the path of a light ray gives to the integral

$$T = \int \mu(\mathbf{r}, \mathbf{s}) ds \tag{3}$$

a minimum value. In this formula ds is the length of a curve element. The differential equations of the light rays are then evidently the Lagrange differential equations of the variation problem of Eq. (3).

If the medium were isotropic, μ would only depend on $\mathbf{r}$ and the Lagrange equations could be expressed by the simple vector equation

$$d\mathbf{p}/ds = \text{grad } \mu(\mathbf{r}), \tag{4}$$

$$\mathbf{p} = \mu(\mathbf{r})\mathbf{s}. \tag{5}$$

If μ is dependent also on $\mathbf{s}$, the differential equation of the light rays keeps its simple form (4). However, the connection between $\mathbf{p}$ and μ is no longer given by the simple Eq. (5) but by[1]

$$\mathbf{p} = \mu(\mathbf{r}, \mathbf{s})\mathbf{s} + \mathbf{Q}(\mathbf{r}, \mathbf{s}). \tag{6}$$

To express $\mathbf{Q}$ in a simple way we introduce the vector $\text{grad}_{\mathbf{s}}\, \mu$. Its components are the partial derivatives of μ with respect to the three components of $\mathbf{s}$. It has to be distinguished from grad μ, the components of which are the derivatives with respect to x, y, z. Then[1]

$$\mathbf{Q} = \text{grad}_{\mathbf{s}}\, \mu - \mathbf{s}(\mathbf{s}\, \text{grad}_{\mathbf{s}}\, \mu), \tag{7}$$

$$\mathbf{Q}\mathbf{s} = 0, \tag{8}$$

$\mathbf{Q}$ is perpendicular to $\mathbf{s}$.

$\mathbf{s} = \mathbf{s}(\mathbf{r})$ may be a "bundle" of rays; through every point $\mathbf{r}$ passes just one ray of this bundle. $\mathbf{s} = \mathbf{s}(\mathbf{r})$ is called an "orthotomic bundle" if by substituting $\mathbf{s} = \mathbf{s}(\mathbf{r})$ into (6) we obtain a vector field $\mathbf{p}(\mathbf{r})$ that is met normally by the ∞' "wave surfaces" of the bundle $\mathbf{s}(\mathbf{r})$. There is a simple

[1] P. Frank, Zeits. f. Physik **80**, 4 (1933).

condition which a bundle of curves $\mathbf{s}$ has to meet in order to be an "orthotomic bundle" of light rays in a medium with the refractive index $\mu(\mathbf{r}, \mathbf{s})$.

$\mathbf{s}(\mathbf{r})$ has to satisfy the equation

$$\text{curl } \mathbf{p}(\mathbf{r}) \times \mathbf{s}(\mathbf{r}) = 0 \tag{9}$$

if we denote by $\mathbf{a} \times \mathbf{b}$ the vector product of the vectors $\mathbf{a}$ and $\mathbf{b}$.

The length of $\mathbf{p}$ is, by the way, the ratio c/w, c meaning the vacuum speed of light and w the speed of the normal displacement of the wave surface.

The formulae (6), (7), (9) enable us to solve the problem of the deflection of light rays by an uneven anisotropy of the medium.

We start considering the path of light rays in an isotropic medium with the refractive index $\mu_0(\mathbf{r})$. We call this path the "undisturbed" path. Then we alter the medium in such a way that an anisotropy is produced. The refractive index is now

$$\mu(\mathbf{r}, \mathbf{s}) = \mu_0(\mathbf{r}) + \mu_1(\mathbf{r}, \mathbf{s}). \tag{10}$$

We obtain a new path of the rays: the "disturbed" path. If we substitute μ from (10) into (6) and (7), we obtain:

$$\mathbf{p} = \mu_0(\mathbf{r})\mathbf{s} + \mathbf{A}(\mathbf{r}, \mathbf{s}), \tag{11}$$

$$\mathbf{A} = \mu_1(\mathbf{r}, \mathbf{s})\mathbf{s} + \text{grad}_{\mathbf{s}}\, \mu_1 - \mathbf{s}(\mathbf{s}\, \text{grad}_{\mathbf{s}}\, \mu_1). \tag{12}$$

If the medium is isotropic we have

$$\mu = \mu_0(\mathbf{r}), \quad \mathbf{p} = \mu_0(\mathbf{r})\mathbf{s}. \tag{13}$$

If $\mathbf{s}(\mathbf{r})$ is an arbitrary bundle of curves the left-hand term of (9) is not necessarily equal to zero. However, it is a measure for the departure of the bundle of curves $\mathbf{s}$ from the light rays in the medium with the refractive index $\mu(\mathbf{r}, \mathbf{s})$. If we put

$$\mathbf{k} = \text{curl } \mathbf{p}(\mathbf{r}) \times \mathbf{s}(\mathbf{r}) \tag{14}$$

the vector $\mathbf{k}$ may be called the "relative curvature of the bundle of curves $\mathbf{s}$ with respect to the light rays in the medium with the refractive index μ". This is a generalization of what is called in the elementary mathematics the "curvature of a curve."

Starting from these remarks it will be easy to give a concise formula for the departure of the "disturbed" light rays from the "undisturbed" ones, or in other words for the deflection of the light rays produced by the anisotropy. We take as a measure of this departure the relative curvature $\mathbf{k}_0$ of the light rays in the medium with the refractive index $\mu(\mathbf{r}, \mathbf{s})$ with respect to the light rays in the medium with the refractive index $\mu_0(\mathbf{r})$.

If $\mathbf{s}(\mathbf{r})$ is a bundle of light rays in the anisotropic medium with the refractive index $\mu(\mathbf{r}, \mathbf{s})$ we conclude from (14) and (13)

$$\mathbf{k}_0 = \text{curl } \mu_0(\mathbf{r})\mathbf{s} \times \mathbf{s}(\mathbf{r}). \tag{15}$$

Then we conclude from (9) and (11)

$$\text{curl } \mu_0 \mathbf{s} \times \mathbf{s} + \text{curl } \mathbf{A} \times \mathbf{s} = 0 \tag{16}$$

and therefore from (15) and (16)

$$\mathbf{k}_0(\mathbf{r}) = \mathbf{s} \times \text{curl } \mathbf{A}. \tag{17}$$

If we replace in (12) $\mathbf{s}$ by a specific bundle $\mathbf{s}(\mathbf{r})$, $\mathbf{A}(\mathbf{r}, \mathbf{s})$ becomes a function of merely $\mathbf{r}$.

We are now going to discuss a simple case of "uneven" anisotropy which is of particular importance in the application of our formulae to problems of physics.

We assume a medium with a particular refractive index $\mu(\mathbf{r}, \mathbf{s})$ of the form (10), for which $\mathbf{s}$ cancels in the right-hand term of (12). Then $\mathbf{A}$ becomes a function of $\mathbf{r}$ only.

$$\mathbf{A}(\mathbf{r}, \mathbf{s}) = \mathbf{g}(\mathbf{r}). \tag{12a}$$

Multiplying (12) by $\mathbf{s}$ we obtain

$$\mu_1(\mathbf{r}, \mathbf{s}) = \mathbf{g}(\mathbf{r})\mathbf{s}, \quad \mu = \mu_0(\mathbf{r}) + \mathbf{g}(\mathbf{r})\mathbf{s}. \tag{18}$$

Then the refractive index μ becomes a linear function of $\mathbf{s}$. This is the simplest case of "uneven" anisotropy. μ can be expressed by means of *one* vector field $\mathbf{g}(\mathbf{r})$ which describes the characteristic optical properties of our medium. The deflection produced by this anisotropy is then after (17), (18);

$$\mathbf{k}_0(\mathbf{r}) = \mathbf{s}(\mathbf{r}) \times \text{curl } \mathbf{g}(\mathbf{r}). \tag{19}$$

APPLICATIONS

We examine as a first example the anisotropy produced by stationary motion in an isotropic medium. The distribution of velocity in the medium may be given by the vector field $\mathbf{w}(\mathbf{r})$. We denote the speed of light in vacuum by c and in our medium, when at rest, by $v_0(\mathbf{r})$, the

velocity by the vector $\mathbf{v}_0$. The velocity of light in the medium, when at motion, may be $\mathbf{v}$. We assume that the velocity $\mathbf{w}$ of the medium is such that we have

$$\mathbf{v}=\mathbf{v}_0+\mathbf{w}, \quad \mathbf{v}=v\mathbf{s}. \tag{20}$$

If we denote by $\mu_0(\mathbf{r})$ the refractive index of the medium, when at rest, and by μ, when at motion, we obtain:

$$\mu_0(\mathbf{r})=c/v_0, \quad \mu=c/v. \tag{21}$$

If we assume that the velocities of the medium are small relative to the velocity of light we get as the first approximation

$$\mu(\mathbf{r}, \mathbf{s})=\mu_0(\mathbf{r})-(1/c)\mu_0^2\mathbf{s}\mathbf{w}. \tag{22}$$

This is a special case of the uneven anisotropy described by (18).

$$\begin{gathered}\mu_1(\mathbf{r}, \mathbf{s})=-(1/c^2)\mu_0^2(\mathbf{r})\mathbf{s}\mathbf{w}(\mathbf{r}),\\ \mathbf{g}=-(1/c^2)\mu_0^2(\mathbf{r})\mathbf{w}(\mathbf{r}).\end{gathered} \tag{23}$$

Then we obtain by substituting $\mathbf{g}$ from (23) into (19):

$$\mathbf{k}_0=(1/c^2)\ \text{curl}\ (\mu_0^2\mathbf{w})\times\mathbf{s}. \tag{24}$$

This formula gives us the deflection of light rays $\mathbf{s}$ which is produced by a velocity distribution $\mathbf{w}(\mathbf{r})$ in an isotropic medium with the refractive index μ_0. Equation (24) gives us immediately the classical results of Stokes and Fresnel concerning the optical phenomena in moving bodies.

A second example is the influence of wind upon the quickest path of an airplane. If there is no wind the quickest path is, of course, the straight line. If there is a distribution $\mathbf{w}(\mathbf{r})$ of wind velocity in the region the plane has to pass there is a deviation from the rectilinear path. The straight line is no longer the "shortest." As for the mathematical formulation this problem is identical with the problem of the path of light rays in a moving medium. If we assume that the wind speed w is small relative to the speed v_0 impressed on the plane by the power of its motor we can apply directly (24). If we take into account (21) and the constancy of v_0 we conclude from (24):

$$\mathbf{k}_0=(1/v_0^2)\ \text{curl}\ \mathbf{w}\times\mathbf{s}. \tag{25}$$

In this equation $v_0\mathbf{k}_0$ is the "curvature" in the ordinary sense of this word. It is obvious that the straight path remains the best to pursue if there are no whirls in the wind distribution.

As a third example we examine the "electron rays," the path of an electron with the charge ϵ through an electromagnetic field which is given by the scalar potential $\phi(\mathbf{r})$ and the vector potential $\mathbf{a}(\mathbf{r})$. We denote by m the mass of the electron, by c the speed of light in the vacuum, and by E the initial energy of the electron. According to K. Schwarzschild's *Minimum Principle of Electrodynamics* the electron rays are geometrically light rays in a medium with the refractive index.[2]

$$\mu(\mathbf{r}, \mathbf{s})=[2m(E-\epsilon\phi(\mathbf{r})]^{\frac{1}{2}}+(\epsilon/c)\mathbf{a}\mathbf{s}. \tag{26}$$

This is obviously a special case of (18) with

$$\mu_0(\mathbf{r})=[2m(E-\epsilon\phi)]^{\frac{1}{2}}, \quad \mathbf{g}(\mathbf{r})=(\epsilon/c)\mathbf{a}. \tag{27}$$

By substituting $\mathbf{g}$ from (27) into (19) we obtain:

$$\mathbf{k}_0=(\epsilon/c)\mathbf{s}\times\text{curl}\ \mathbf{a}. \tag{28}$$

If we denote the intensity of the magnetic field by $\mathbf{h}$, we have

$$\text{curl}\ \mathbf{a}=\mathbf{h} \tag{29}$$

and therefore

$$\mathbf{k}_0=(\epsilon/c)\mathbf{s}\times\mathbf{h}. \tag{30}$$

We see from (27) that the rays traverse the electric field like an isotropic medium. The influence of the magnetic field is the influence of an anisotropy characterized by the vector $(\epsilon/c)\mathbf{a}$. The vector $\mathbf{k}_0$ in (30) means therefore the deflection of the electron rays produced by the magnetic force. $\mathbf{k}_0$ is the "relative curvature" of the electron rays in the electromagnetic field with respect to the path of the rays in the purely electric field. Equation (30) is, of course, a form of the law of Biot-Savart or of the "Lorentz force." The speed of the electron does not occur in this form of the law. It gives exactly the "relative curvature" produced by the magnetic field.

---

[2] Frank-Mises, *Differentialgleichungen der Mechanik und Physik* (1935), Vol. 2, Chap. 1, p. 3 (61); W. Glaser, Zeits. f. Physik **80**, 451 ff (1933).

A Theory of the Initial Avalanche in the Breakdown of a Discharge Counter in Helium

SANBORN C. BROWN
Massachusetts Institute of Technology, Cambridge, Massachusetts
(Received July 9, 1942)

On the basis of the discussion on Townsend's criterion for breakdown, definite hypotheses are arrived at as to the behavior of both the positive ions and the photons in the initial avalanche in the breakdown between coaxial cylinders in helium. Calculations of the shape of the field through which the avalanche passes show that to a good approximation the field is proportional to $1/r$ up to a point where the space charge effect of the positive ions in the avalanche starts to modify the field, and thereafter the field through which the avalanche travels can be considered constant. The functional form of the photon effect leads to the assumption that two types of photons are operative, which can be identified with the resonance radiation of He I and He II. Theoretically derived graphical methods for predicting breakdown voltages are given. Comparison between theoretical and experimental threshold curves leads to good agreement for all cylindrical geometries from that usually employed in Geiger-Müller counters up to the limiting case of parallel plates.

A NUMBER of attempts have been made to explain the observed breakdown characteristics of discharge counters, but all of these have dealt only with the special geometrical conditions of the Geiger-Müller counter.[1] The following discussion treats the breakdown characteristics between coaxial cylinders in general up to the limiting case of parallel plates. It deals only with the first avalanche, that is the group of ions and electrons formed by the initial charged particle, and does not treat the action of the succeeding avalanches which build up the space charge which finally quenches the discharge. The experimental data, and therefore the entire discussion, have been carried out only for helium gas contaminated with mercury vapor.

The Townsend criterion for breakdown of a self-maintaining discharge states that

$$\gamma n = 1. \qquad (1)$$

γ is the number of electrons liberated at the cathode per ionization in the gas and n is the number of ion pairs formed in the initial discharge. The investigation proceeded in the following manner. First, experimental curves of the threshold voltage for cylinders of various different radii were obtained. Second, the mathematical forms for n and γ were sought which would fit the experimental threshold curves and would be useful in predicting threshold voltages in terms of the counters. Third, a reasonable physical interpretation was given for these theoretical functions.

[1] S. Werner, Zeits. f. Physik 90, 384 (1934).

EXPERIMENTAL

The experimental curves of threshold voltage as a function of pd are shown in Fig. 1. The

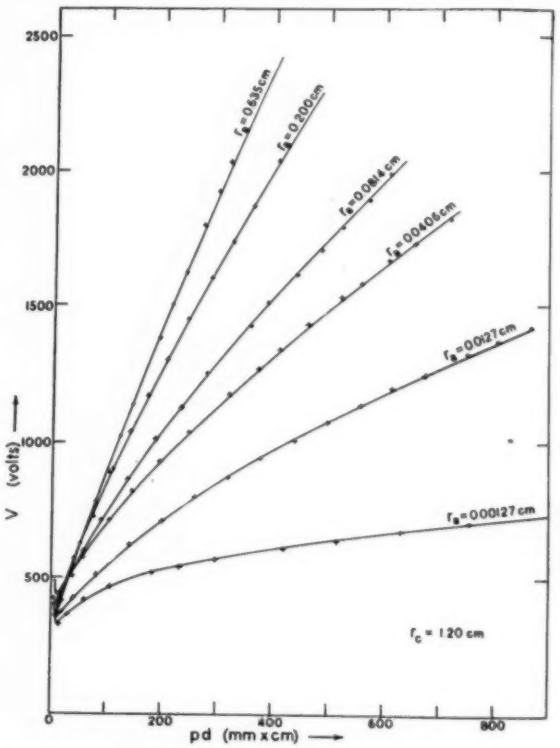

FIG. 1. Threshold voltage for discharge counters of varying anode radius and constant cathode radius for helium contaminated with mercury vapor.

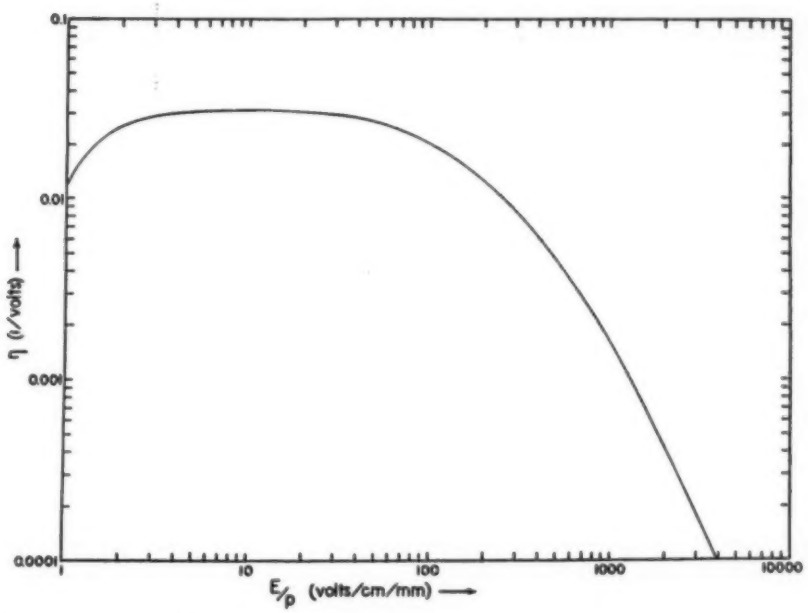

FIG. 2. The ionization per volt as a function of E/p calculated from Engel and Steenbeck's data for helium (contaminated with mercury vapor).

pressure p is measured in mm of mercury. d is the width of the gap between the cathode and the anode and is, therefore, $r_c - r_a$ where r_c and r_a are the radii of the cathode and anode, respectively. The threshold voltage is taken to be that potential for which all pulses from the counting tube due to an external source of radiation are of the same size. This is a sharply defined point and one which marks the lower edge of the discharge counter region in which a self-maintaining discharge occurs in the counter. The gas used was ordinary tank helium and the pressure was measured by means of a mercury manometer. The gas was, therefore, neither of high purity nor free from mercury vapor.

APPLICATION OF THE TOWNSEND THEORY

The Townsend theory tells us in Eq. (1) that to support a self-maintaining discharge, the voltage between the electrodes must be of sufficient magnitude so that the ionization by collision of an entering charged particle is large enough to create enough ion-pairs in the avalanche in order that the photons created in the initial avalanche strike the cathode surface, and produce at least one electron to keep the discharge going.

If α, the first Townsend coefficient, is the number of ion pairs formed per centimeter of path of the initiating electron as it travels through the field E, it is well known that α/p is a function of E/p where p is the pressure in millimeters of mercury. The form of this function has been measured experimentally many times. It seems more significant, however, from a theoretical point of view, to discuss the problem in terms of a coefficient η, the ionization per volt.[2] η itself is a function of E/p and is related to α through the equation $\eta = \alpha/E$. The relation between η and E/p, calculated from Engel and Steenbeck's[3] curve of α/p as a function of E/p, is shown in Fig. 2. The data of Engel and Steenbeck apply to parallel plates and to helium contaminated with mercury vapor corresponding to that used in the present investigation. The reason for not using pure He is the practical one that counters do not work as satisfactorily with the pure gas. A logical explanation of this can be found in the fact that pure rare gas atoms have high lying metastable levels which have a long enough lifetime to introduce spurious counts in the counter. Even small admixtures of mercury vapor, whose ionization potential is lower than

[2] M. J. Druyvesteyn and F. M. Penning, Rev. Mod. Phys. **12**, 87 (1940).

[3] A. Engel and M. Steenbeck, *Elektrische Gasenladungen* (Julius Springer, 1932), p. 105.

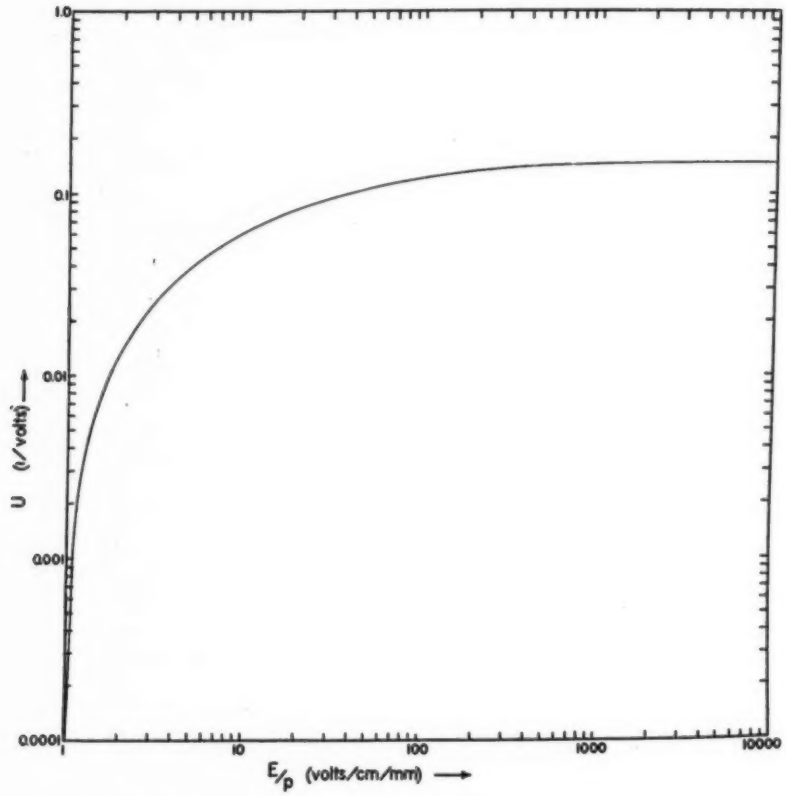

FIG. 3. The function u defined in Eq. (4) is shown plotted against E/p.

the metastable levels in He, will prevent the long life of the metastable states by the ionization of the Hg atoms, and thus prevent the spurious counts which make the pure gas counters unsatisfactory.

One may determine the total number of ion pairs formed in a discharge from the relation that $dn=-\alpha n dr$ and therefore

$$n=\exp\int_{r_c}^{r_a}\alpha dr. \tag{2}$$

For cylindrical geometry α depends on r and the straightforward method of computing n for a particular case would be to plot a curve of α as a function of r for values of the field E computed from the equation

$$E=2q/r,$$

where

$$2q=V/\ln\frac{r_c}{r_a} \tag{3}$$

and V is plotted in Fig. 1. The curve of α as a function of r could be graphically integrated to determine n.

This is a very tedious procedure, and to avoid it the following method was introduced. Since $E=2q/r$ we may write

$$\int -\alpha dr=2q\int(\alpha/E^2)dE.$$

Actually we would prefer this expression in terms of η and E/p and we therefore have

$$\int -\alpha dr=2q\int\frac{\eta p}{E}d(E/p).$$

We may therefore define a function u such that

$$u=\int_0^{E/p}\frac{\eta p}{E}d(E/p) \tag{4}$$

and we may rewrite Eq. (2) in the form

$$n=\exp\left[2q(u_a-u_c)\right], \tag{5}$$

where u_a refers to the value of u at the anode and u_c its value at the cathode. The usefulness

of this function u comes from the fact that it is a function of E/p alone for a particular gas and can therefore be computed once and for all for this gas. No further integrations need be made in determining n for any cylindrical geometry as long as Eq. (3) holds. Figure 3 shows the form of u, computed from Engel and Steenbeck's data, plotted as a function of E/p.

FORM OF THE INITIAL AVALANCHE

The electric field between two charged coaxial cylinders is proportional to $1/r$. In general if an electron enters the counter at r_c it will first travel in a part of the field which is so low that no ionization by collision takes place. The part of the field in which no ionization takes place will be called the 0 region. In this work we have considered that the 0 region extends to the point where $E/p=1$, E being measured in volts per centimeter and p in millimeters of mercury. For values of E/p greater than 1, ionization by collision takes place, giving rise to the formation of an avalanche. The space in which this occurs is designated as the A region. If one considers that the field remains proportional to $1/r$ from $E/p=1$ up to the E/p at the anode, the total number of ions formed in the avalanche becomes entirely unreasonable, especially for the case of high pressures. It seems therefore necessary to postulate a third region, let us call it S, in which the space charge of the avalanche modifies the electric field in such a way as to limit its size.

This modification is due to the positive ions left behind the avalanche and which, because of their larger mass, are practically stationary compared to the electrons. Their field would be difficult to calculate directly without knowing how much an avalanche spreads as it advances, but it is certainly proportional to their number n. By introducing an empirical constant B, we have

$$E=(2q/r)-Bn. \tag{6}$$

A comparison with the experimental threshold curves leads to the value $B=10^{-10}$ volt/cm $\times$ions. Because of the fact that the space charge correction contains n, which is an exponential function, the correction has no effect on E until a certain critical value of r and it then has a very large effect.

Equations (5) and (6) can be combined only if the space charge field is small compared to that at the center wire, that is, in the A region. In the S region the effect of the distribution of space charge is too important to allow the simple approximation of Eq. (6). There must be a delicate balance in the S region, the field tending to increase as $1/r$, but on the other hand any increase in field increases the ionization, hence increasing the space charge which decreases the field. It is therefore evident that the field cannot change much, and the simplest assumption is that it remains constant, the ionization being just sufficient to prevent any further increase. This is supported by the agreement with the experimental data.

The shape of the field modified by the space charge of the avalanche computed up to the S region by Eq. (6) and considered constant from r_s, the edge of the space charge region, to r_a is shown in Fig. 4.

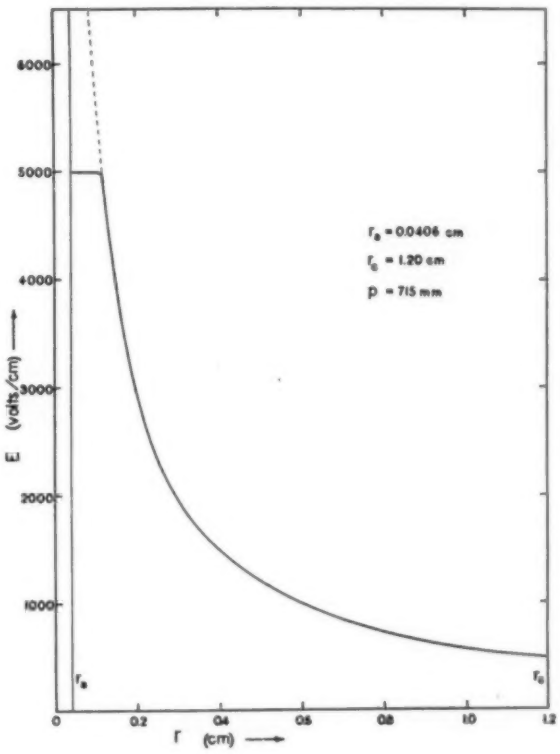

FIG. 4. The solid line shows the field of an avalanche modified by space charge. The dotted line shows how the field would have continued had not space charge had an effect.

TOTAL NUMBER OF ION PAIRS FORMED IN INITIAL AVALANCHE

The total number of ion pairs formed in the initial avalanche in the A region is given directly by Eq. (5).

$$n_a = \exp\left[2q(u_a - u_c)\right].$$

The boundary of the S region is defined, somewhat arbitrarily, by

$$\frac{d}{dr}\left(\frac{2q}{r} - Bn\right) = 0.$$

Since $dn = -\alpha n dr$

$$2q/r^2 = Bn\alpha. \tag{7}$$

Using the fact that $E = 2q/r$ and $\alpha = E\eta$ we have

$$r_s = 1/Bn_s\eta_s, \tag{8}$$

where n_s is the number of ions reaching r_s. By solving Eq. (8) by trial and error we can determine r_s, since the number of ion pairs formed from r_c to r_s is given by

$$n_s = \exp\left[2q(u_s - u_c)\right]. \tag{9}$$

The total number of ions in the avalanche formed when space charge has an effect is the number formed from r_c to r_s given in Eq. (9), plus the number formed in the constant field from r_s to r_a. The number of ions in the S region is

$$n_a - n_s = n_s \exp\left[\alpha_s(r_s - r_a)\right]. \tag{10}$$

By combining Eqs. (9) and (10) and putting it in terms of the variables we have been using in our calculations, the total number of ion pairs formed in the initial avalanche when space charge comes into the equation is given by

$$n_a = \exp\left[2q(u_a - u_c) + 2q\eta_a(1 - r_a/r_s)\right]. \tag{11}$$

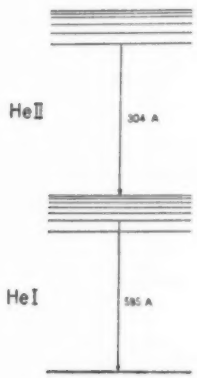

FIG. 5. Schematic energy level diagram of the helium atom.

FORM OF THE PHOTOELECTRIC EFFECT

Having determined a satisfactory form for n we now return to our fundamental assumption, the validity of Eq. (1). We must now look for a functional form of γ which will be equal to $1/n$ at breakdown for all cylindrical geometries. If we assume that the secondary electrons are liberated from the cathode through the action of photons, we may set γ equal to the number of photons produced in the gas per ionization, less those absorbed on the way to the cathode, times their photoelectric efficiency. We could designate the corresponding probabilities as ϕ, χ, and ψ. ϕ is then a function of the value of E/p, and therefore of u, in the gas where the ionization occurs as E/p determines the energy of the electronic impacts on the gas atoms. Since three-fourths of the ions are formed in the last two ionization free paths, only the value of E/p at the anode need be considered. χ is a function of the amount of gas which the photon must traverse, which can be represented by pd, the pressure times the distance the photons must travel. ψ depends only on the nature of the photon and of the cathode surface. In general there may be several kinds of photons with different absorption and photoelectric properties, so that γ is in general a sum of terms such as

$$\gamma = \textstyle\sum_i \phi_i\chi_i\psi_i. \tag{12}$$

The experimental data can be represented by using two such terms, which in general would have the form

$$\gamma = \gamma_{\mathrm{I}} + \gamma_{\mathrm{II}} = \exp\left(-\lambda_1 - \mu_1 pd - \kappa_1 u_a\right) + \exp\left(-\lambda_2 - \mu_2 pd - \kappa_2 u_a\right).$$

Actually, fitting the constants to the data shows that some of these constants are negligible, and the form which appears satisfactory is

$$\gamma = \gamma_{\mathrm{I}} + \gamma_{\mathrm{II}} = \exp\left(-\lambda_1 - \mu pd\right) + \exp\left(-\lambda_2 + \kappa u_a\right), \tag{13}$$

where the constants have the following values:

$\lambda_1 = 6$; $\lambda_2 = 64$;
$\mu = 0.25/\mathrm{cm} \times \mathrm{mm\ Hg}$; $\kappa = 400$ volts/effective ionization.

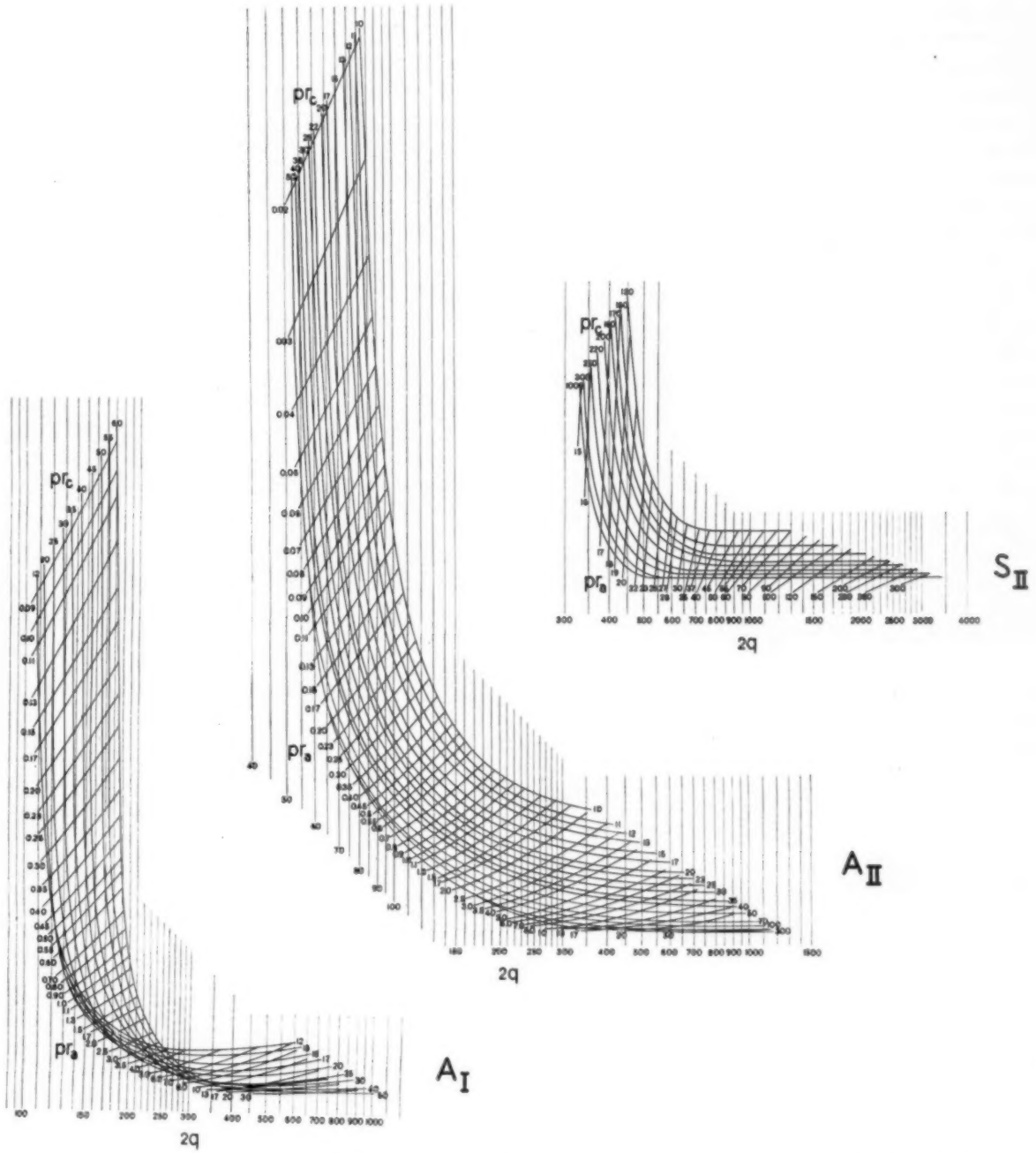

FIG. 6. Theoretical curves for predicting threshold voltages in terms of experimentally observable parameters.

PHYSICAL INTERPRETATION OF THE FORM OF γ

It would appear from the form of Eq. (13) that there are two types of photons involved. The excitation of the first is independent of the energy of impact, but it is strongly absorbed in the gas. The second is more strongly excited by higher energy impacts, but is not absorbed in the gas.

Let us consider for a moment the energy level scheme of the helium atom, a sketch of which is shown in Fig. 5. The most easily excited line in the He I spectrum would be its resonance radiation at 585A. In the process of ionization, the He I spectrum would be fully developed, and therefore the intensity of the lines would be

independent of the mode of excitation and therefore independent of the energy of impact of the electrons in the gas. On the other hand, its outstanding characteristic would be its very high absorption in the helium gas surrounding the discharge, as the photons originating from transitions between excited levels would not be effective photoelectrically. These characteristics are just what is observed in the case of γ_{I}.

The ionization potential of He II is 54 volts. The average voltage drop per ionization in the avalanche in counter discharges lies between 30 and 50 volts. This is the average voltage, of course, so that a fairly large percentage would have energies considerably higher than this. For example, for a mean free path value of 34 volts, 19 percent will go over 57 volts and 14 percent will go over 68 volts. This means that although there is no trouble in exciting He II in the discharge, the spectrum will not be fully developed and therefore the intensity of its lines will depend on its mode of excitation and hence on E/p. On the other hand the 304A resonance radiation of He II would not be expected to be highly absorbed in the normal helium gas of the counter. These are just the characteristics shown by the functional form of γ_{II}.

It seems reasonable, therefore, to adopt the following picture of the photoelectric effects in the initial discharge of a helium counter: In general both the He I and the He II spectrum are excited. Since the resonance radiation of He I is the most copiously produced it will have the dominating effect as long as the pressure in the counter is low enough to allow these photons to reach the cathode. For pressures around 10 mm of Hg, however, the path length in the gas is too long for these photons to reach the cathode, and thereafter the photoelectric effect depends upon the resonance radiation of He II.

THEORETICAL PREDICTION OF THRESHOLD VOLTAGE

Using the breakdown Eq. (1), and the forms of these quantities as given by Eqs. (5), (11), and (13), it would be useful to be able to predict threshold voltages in terms of experimentally convenient parameters. These parameters are p, the pressure of the filling gas; r_a, the radius of the anode; and r_c, the radius of the cathode. From the point of view of ease in algebraic manipulation four distinct cases will be discussed: A_{I} in which the avalanche is formed in a $1/r$ field and the dominating photoelectric effect is due to the interaction of He I photons and the cathode walls, A_{II} in which the avalanche is formed in $1/r$ field and He II photons are effective, S_{I} in which the avalanche is modified by space charge and He I photons are effective, and S_{II} in which the avalanche is modified by space charge and He II photons are effective.

CASE A_{I}

Treating the A_{I} case first, we can write as Eq. (1)

$$n=\gamma^{-1}.$$

By the use of Eqs. (5) and (13) we may write

$$2q(u_a-u_c)=\lambda_1+\mu p(r_c-r_a). \tag{14}$$

Let us write Eq. (3) in the form

$$pr_a=2q/(E_a/p). \tag{15}$$

Equations (14) and (15), together with the plots of Figs. 2 and 3, determine q and η_a in terms of pr_a and pr_c. The breakdown potential follows from q and r_c/r_a by the equation

$$V=2q\ln(r_c/r_a). \tag{16}$$

The equations are best solved graphically. Equation (15) does not contain pr_c and hence determines a family of curves of $1/\eta_a$ against $2q$, each for an assumed value of pr_c. Eliminating pr_a between Eqs. (14) and (15) we obtain

$$\lambda_1+\mu pr_c=2q\left(u_a-u_c+\frac{\mu p}{E_a}\right), \tag{17}$$

and this determines a family of curves of $1/\eta_a$ against $2q$ for assumed values of pr_c. These curves are shown in Fig. 6, plot A_{I}. This plot will allow us to predict threshold voltages for the A_{I} region. We enter the plot with the experimental parameters pr_a and pr_c. The intersection of a pr_a and a pr_c line for a particular case corresponds to a value of $2q$ from which the threshold voltage can be computed by means of Eq. (16).

One of the most noticeable characteristics of this plot is the crossing over of the curves around $2q=250$. This leads to the prediction that at low pressure for a particular cathode radius, large

values of r_a will have lower threshold voltages than smaller values of r_a, whereas for higher pressures the reverse is true, and the lower the value of r_a, the lower the threshold voltage. This phenomenon has been observed by Haines,[4] although the precision of the experimental observations in this present work shown in Fig. 1 does not bring out this point.

CASE A_{II}

To obtain a convenient plot from which to predict threshold voltages in the A_{II} region, we again use Eqs. (5) and (13) to obtain the equation

$$2q(u_a-u_c)=\lambda_2-\kappa u_a. \tag{18}$$

Here again since we know that

$$E_c/p=2q/pr_c$$

and u_c is a function of E_c/p, by assuming values of pr_c we can get a family of curves for different values of pr_c by plotting $1/\eta$ as a function of $2q$.

Equation (15) gives us again a method of determining a family of curves for different values of pr_a. The complete plot is shown in plot A_{II} of Fig. 6. The method for using this plot is exactly the same as was described for the A_I plot.

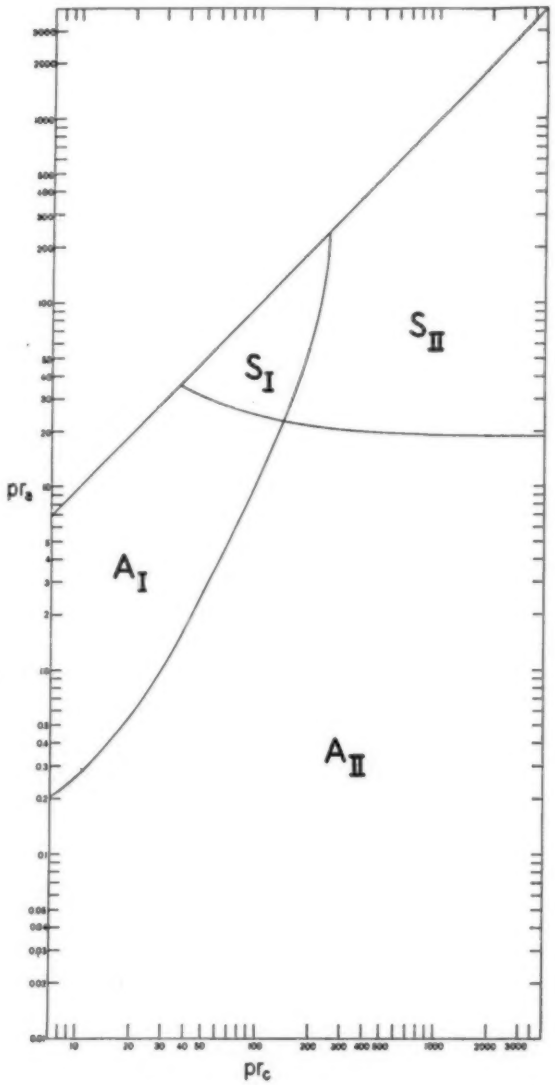

FIG. 7. A theoretical plot showing the regions in which various modes of breakdown take place as a function of experimentally observable parameters.

[4] C. L. Haines, Rev. Sci. Inst. **7**, 411 (1936).

CASE S_{II}

To arrange the equations in a useful form for calculation in the region in which the avalanche is modified by space charge, requires a little more manipulation.

In the S_{II} region we have the expression for n in Eq. (11) and for γ in Eq. (13), so that we may write

$$2q(u_a-u_c)+2q\eta_a\left(1-\frac{r_a}{r_s}\right)=\lambda_2-\kappa u_a, \tag{19}$$

and combining Eqs. (8) and (9), since $u_s=u_a$, we have

$$Br_s\eta_s=\exp\left[2q(u_c-u_a)\right]. \tag{20}$$

Equations (15), (19), and (20) determine q, $\eta_s=\eta_a$, and r_s, in terms of pr_a and pr_c. Eliminating pr_c between Eqs. (19) and (20) we obtain

$$2q\eta_a\left(1-\frac{r_a}{r_s}\right)=\lambda_2-\kappa u_a+\ln\left(Br_s\eta_s\right). \tag{21}$$

Eliminating pr_s between Eqs. (15) and (21) we have

$$2q\eta_a\left(1-\frac{pr_a}{2q}\frac{E_s}{p}\right)=\lambda_2-\kappa u_a+\ln\left(\frac{B\eta_s}{E_{s/p}}\right)+\ln\frac{2q}{p}. \tag{22}$$

The last term in this equation turns out, on calculation, to be negligible, so this equation determines the curve of $1/\eta_a$ against $2q$ for assumed values of pr_a.

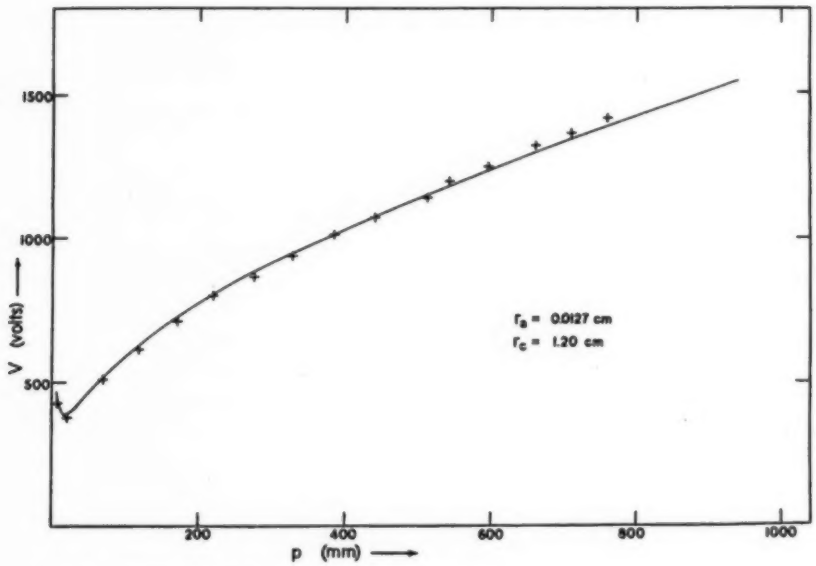

FIG. 8a. Comparison between theoretically predicted threshold voltages (the solid lines) and the experimental points (crosses). A counter falling wholly within the A_{II} region.

Equations (15) and (20) give

$$2q(u_a-u_c)=\ln\left(\frac{E_{a/p}}{B\eta_a}\right)-\ln\left(\frac{2q}{p}\right), \quad (23)$$

and this equation determines the curve of $1/\eta_a$ against $2q$ for assumed values of pr_c. These two families of curves plotted on each other are shown in Fig. 6, plot S_{II}, and can be used to predict threshold voltages in the S_{II} region in the same manner as was described for the curves in the A_I region.

CASE S_I

In the S_I region, Eq. (19) becomes

$$2q(u_a-u_c)+2q\eta_a\left(1-\frac{r_a}{r_s}\right)=\lambda_1+\mu p(r_c-r_a). \quad (24)$$

Unfortunately in this case, it is not possible to eliminate pr_c between Eqs. (20) and (24), as it appears in the latter both implicitly in u_c and explicitly in μpr_c. In other words, since the function u is expressed only graphically in Fig. 3 and not analytically, no plot of the S_I region has been computed similar to those computed for the other three regions shown in Fig. 6. A fuller discussion of the behavior of a counter operating in this region follows later in this paper.

BOUNDARIES OF THE REGIONS

A brief study of the curves in Fig. 6 will show that for the same values of pr_a and pr_c the different plots will predict different values of $2q$ and therefore different values of threshold voltage. Let us consider the boundaries between the different regions separately. At the boundary between the A_I and the A_{II} or the S_I and the S_{II} regions we have a competition between the He I and the He II radiation as to which will be more effective in producing photoelectrons at the cathode. Whichever is able to do so most readily will have the dominating effect, and therefore whichever plot will predict the lower threshold voltage will be the one to use. On the boundary between the A_I and the S_I region or the A_{II} and the S_{II} region, the question is whether or not the avalanche is modified by space charge. The shape of the field modified by the space charge of the avalanche is shown in Fig. 4. From this plot we can see that physical significance can only be attached to any equation involving this region when the field in the space charge region is equal to or less than the field computed without space charge. This amounts to saying that, for example, Eqs. (20) and (21) do not have physical significance for values of $2q$ below the values of $2q$ from Eqs. (15) and (18). Therefore

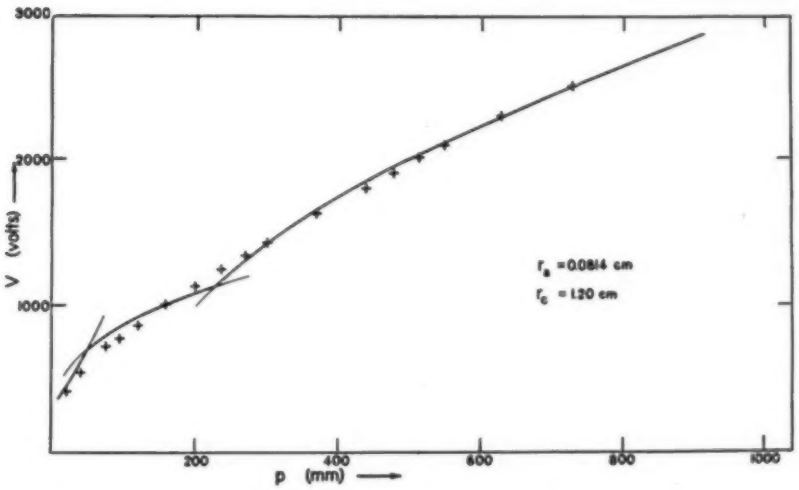

FIG. 8b. A counter starting in the A_I region, passing through the A_{II} region, and ending in the S_{II} region.

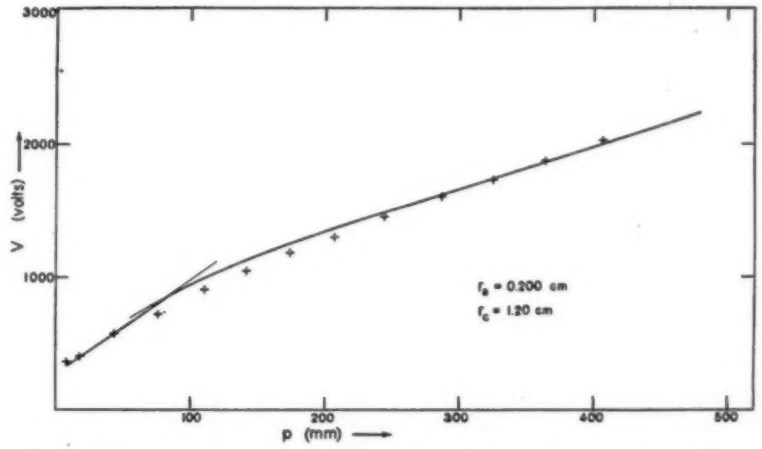

FIG. 8c. A counter passing through the point common to all four regions.

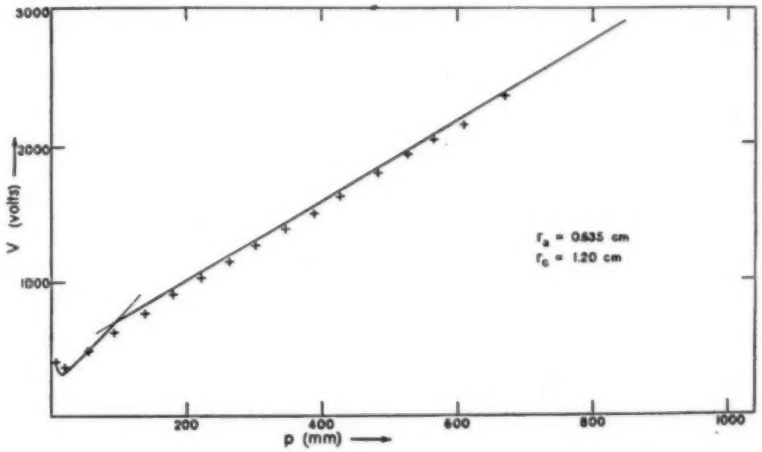

FIG. 8d. A counter starting in the A_I region and ending in the S_{II} region.

the S_{II} plot is only valid when it predicts values of $2q$ and therefore threshold voltages which are equal to or greater than those predicted of the A_{II} plot. This is, of course, what one would expect physically, since it requires more voltage across the electrodes to start a self-maintaining discharge if the field of the avalanche is reduced by space charge than would be the case if space charge were not there.

By knowing the factors which determine the boundaries of the regions in which the different plots are significant, we can compute the boundaries once and for all so that in the actual use of Fig. 6 we can know beforehand which plot we must use.

A plot of the operating regions has been computed and is shown in Fig. 7. One enters this plot with the experimental parameters pr_a and pr_c, and it is immediately evident in what region the counter under these particular conditions is operating. Particular counters, with their fixed values of r_a and r_c, lie in straight lines at 45° on this plot. The upper limiting line drawn on this plot is for the case $r_a=r_c$.

COMPARISON OF THEORY AND EXPERIMENT

The test of any theory is how well it predicts experimentally observed facts. Let us therefore see how well the theoretical curves will fit the experimentally determined values of threshold voltage with changes of pressure for several widely varying cylindrical geometries. This comparison is made in Fig. 8, in which the solid lines are the theoretical curves and the crosses are the experimental points.

Figure 8a is a case in which the counter falls wholly within the A_{II} region, which is generally the case for the so-called Geiger-Müller counters where the center wire is of very small diameter.

Figure 8b is a case in which the counter starts at low pressure in the A_I region, then as the pressure increases, passes through the A_{II} region, and at high pressure operates wholly within the S_{II} region. No attempt has been made to smooth the theoretical curves as they cross from one region into another. As a matter of fact, they are extended beyond the place where they are significant to emphasize the shapes of the separate theoretical curves.

Figure 8c shows the case for the particular counter which passes through the point common to all the regions. It actually operates in only two regions, A_I and S_{II}.

Figure 8d shows the case of a counter which operates at low pressure in the A_I region, and at high pressures, operates in the S_{II} region. Only the theoretical curves for the A_I and S_{II} regions are given, although it should pass through the S_I region. In this particular example in which $r_c/r_a=1.9$, the S_I region covers a range in pressure of about 50 mm of Hg. The curve would fall above the A_I curve and below the S_{II} at the part of the curve shown in the figure as the junction between the A_I and S_{II} curves. It is both because of the fact that the S_I region is so narrow even when the cathode and anode approach each other in radius, and for the fact that the theoretical predictions are sufficiently good by extrapolating the A_I and S_{II} regions that the much more complicated computation of the S_I region has been omitted.

It can be seen from these examples that it is possible to predict, by means of the present theory, threshold voltages over a wide range of cylindrical geometries, knowing only the experimentally measurable parameters r_a, r_a, and p, and that these predicted curves agree well with the experimental determinations.

In conclusion the author wishes to express his sincere appreciation for the constant help and encouragement of Professor W. P. Allis and Professor Robley D. Evans.

Connection Between the Kinematic and Dynamical Theories of X-Ray Diffraction

H. EKSTEIN
University of Kansas City, Kansas City, Missouri

(Received March 5, 1942)

The diffraction of x-rays by very small crystals has been described by Laue's kinematic theory; the case of very large crystals is treated by the dynamical theory of Darwin and Ewald. It is shown here that both theories are deducible from limiting cases of a general integral equation. In a subsequent paper this integral equation will be used to give an approximate solution applying to crystals of intermediate size.

IN his first papers on x-ray diffraction, M. von Laue gives the theory[1] which covers the case of small crystals. This treatment is called the kinematic theory. It supposes that the oscillators in the crystal are only under the influence of the incident (primary) wave and it neglects the interaction between the oscillators. The conclusion is that the diffracted amplitude at a very remote point situated in the direction of a unit vector $\mathbf{s}$, is proportional to

$$\Psi = \int \rho(\mathbf{r}) \exp\left[j(\mathbf{s}k - \mathbf{K}_0)\cdot\mathbf{r}\right] dv, \qquad (1)$$

where $\rho(\mathbf{r})$ is the electronic density, $\mathbf{K}_0$ the wave vector of the incident wave, $k = \nu/c = 1/\lambda$ is the vacuum wave number, and $j = 2\pi i$.

For large crystals, the kinematic theory is no longer valid. The secondary waves emitted by the oscillators cannot be neglected in comparison with the incident wave. P. P. Ewald's dynamical theory takes complete account of these interactions in the infinite crystal. However, we shall here describe a simplified form of the dynamical theory given by von Laue.[2]

In von Laue's formulation of the dynamical theory the electric displacement $\mathbf{d}$ and the magnetic field intensity $\mathbf{h}$ are represented in the form

$$\mathbf{d} = \exp(j\nu t)\exp(-j\mathbf{K}_0\cdot\mathbf{r}) \sum_{m_1 m_2 m_3} \mathbf{D}_{m_1 m_2 m_3} \times \exp(-j\mathbf{A}_{m_1 m_2 m_3}\cdot\mathbf{r}), \qquad (2a)$$

$$\mathbf{h} = \exp(j\nu t)\exp(-j\mathbf{K}_0\cdot\mathbf{r}) \sum_{m_1 m_2 m_3} \mathbf{H}_{m_1 m_2 m_3} \times \exp(-j\mathbf{A}_{m_1 m_2 m_3}\cdot\mathbf{r}). \qquad (2b)$$

Here, the $\mathbf{A}_{m_1 m_2 m_3}$ signify the lattice vectors of the reciprocal lattice. $\mathbf{K}_0$ is a constant (at first arbitrary) vector, $\mathbf{r}$ is the radius vector of position.

Equations (2a) and (2b) state that the field quantities are products of plane wave functions with functions having the periodicity of the crystal lattice. Application of Maxwell's equations to (2a) and (2b) yields a secular equation which determines the allowed values of $\mathbf{K}_0$ and the sets of coefficients $\mathbf{D}_m$ belonging to each value of $\mathbf{K}_0$.

We shall generalize von Laue's theory in such a way that it describes the effect of *any limited object in the field of an incident plane wave.* Fourier integrals instead of Fourier sums must be used for the general case.

Let the incident wave be

$$\mathbf{d}_0 \exp(j\nu t)\exp(-j\mathbf{K}_0\cdot\mathbf{r}),$$

where $|\mathbf{K}_0| = k$. Between the quantities $\mathbf{d}_0$ and $\mathbf{h}_0$ of the primary wave, there exist the relations (from Maxwell's equations)

$$\mathbf{h}_0 \times \mathbf{K}_0 = k\mathbf{d}_0, \qquad (3a)$$

$$\mathbf{d}_0 \times \mathbf{K}_0 = -k\mathbf{h}_0. \qquad (3b)$$

We split the total field intensities $\mathbf{d}_t$ and $\mathbf{h}_t$ into a term representing the primary wave and a second term which represents the radiation diffracted by the object.

$$\mathbf{d}_t = \exp(j\nu t)\left[\mathbf{d}_0 \exp(-j\mathbf{K}_0\cdot\mathbf{r}) + \mathbf{d}\right], \qquad (4a)$$

$$\mathbf{h}_t = \exp(j\nu t)\left[\mathbf{h}_0 \exp(-j\mathbf{K}_0\cdot\mathbf{r}) + \mathbf{h}\right]. \qquad (4b)$$

These equations imply that the field quantities are periodic in time with the frequency ν. The quantities $\mathbf{d}_t$ and $\mathbf{h}_t$ cannot be represented as Fourier integrals, because they include the plane

[1] M. von Laue, Encyklopaedie d. math. Wiss. **5**, 3 (1915).
[2] M. von Laue, Ergeb. d. exakt. Naturwiss. **10**, 133 (1931).

wave functions which do not vanish at infinity. But the additional quantities $\mathbf{d}$ and $\mathbf{h}$ must vanish at infinity. Indeed, they can be considered as representing the radiation of the excited dipoles of the object, and these are known to vanish like e^{-jkr}/r. Therefore, we may represent them as Fourier integrals.

We express the corresponding quantities in the primitive and Fourier space by the same letters, small ones for the primitive space, capital for the Fourier space. $\mathbf{R}$, for instance, is the radius vector and dV the space element of the Fourier space.

$$\mathbf{d}=\exp(j\nu t)\int \mathbf{D}(\mathbf{R})\exp(-j\mathbf{R}\cdot\mathbf{r})dV, \quad (5a)$$

$$\mathbf{h}=\exp(j\nu t)\int \mathbf{H}(\mathbf{R})\exp(-j\mathbf{R}\cdot\mathbf{r})dV. \quad (5b)$$

Integration is extended over the entire Fourier space. In the following, all integrations are extended over the infinite space, if not expressly stated otherwise.

The inversions of (5a) and (5b) are:

$$\mathbf{D}(\mathbf{R})=\exp(-j\nu t)\int \mathbf{d}(\mathbf{r})\exp(j\mathbf{R}\cdot\mathbf{r})dv, \quad (6a)$$

$$\mathbf{H}(\mathbf{R})=\exp(-j\nu t)\int \mathbf{h}(\mathbf{r})\exp(j\mathbf{R}\cdot\mathbf{r})dv. \quad (6b)$$

In order to apply Maxwell's equations, we form

$$\operatorname{curl}\mathbf{h}_t=\exp(j\nu t)\Big(\int \mathbf{H}\times\mathbf{R}\exp(-j\mathbf{R}\cdot\mathbf{r})dV + \mathbf{h}_0\times\mathbf{K}_0\exp(-j\mathbf{K}_0\cdot\mathbf{r})\Big), \quad (7)$$

$$\frac{1}{c}\frac{\partial\mathbf{d}_t}{\partial t}=\exp(j\nu t)\frac{j\nu}{c}\Big(\int \mathbf{D}\exp(-j\mathbf{R}\cdot\mathbf{r})dV + \mathbf{d}_0\exp(-j\mathbf{K}_0\mathbf{r})\Big). \quad (8)$$

According to the third Maxwell equation, (7) and (8) are equal. Therefore:

$$\int(\mathbf{H}\times\mathbf{R}-k\mathbf{D})\exp(-j\mathbf{R}\cdot\mathbf{r})dV + (\mathbf{h}_0\times\mathbf{K}_0-k\mathbf{d}_0)\exp(-j\mathbf{K}_0\cdot\mathbf{r})=0. \quad (9)$$

The second term here vanishes because of the relation (3a). Therefore:

$$\mathbf{H}\times\mathbf{R}=k\mathbf{D}. \quad (10)$$

Let us now consider a function of the dielectric constant ϵ

$$\psi=1-\epsilon^{-1}. \quad (11)$$

As ϵ is variable in space, ψ is also a function of $\mathbf{r}$. The object is finite, and therefore ψ vanishes at infinity and may be represented by a Fourier integral.

Let us note that ψ has a simple physical significance: the dielectric constant is related to the susceptibility μ by the equation

$$\epsilon=1+4\pi\mu. \quad (12)$$

If μ is small compared to unity, as is the case for electromagnetic oscillations in the x-ray range,

$$\psi=4\pi\frac{\mu}{1+4\pi\mu}\approx 4\pi\mu \quad (12a)$$

is proportional to the susceptibility, or in the usual approximation, to the electronic density.[3]

The Fourier representation of ψ is

$$\psi=\int \Psi(\mathbf{R})\exp(-j\mathbf{R}\cdot\mathbf{r})dV \quad (13)$$

and the inversion:

$$\Psi=\int \psi\exp(j\mathbf{r}\cdot\mathbf{R})dv. \quad (13a)$$

According to (4a), (5a), and (11),

$$\frac{\mathbf{d}_t}{\epsilon}=\mathbf{d}_t(1-\psi) =\exp(j\nu t)\Big[(1-\psi)\mathbf{d}_0\exp(-j\mathbf{K}_0\cdot\mathbf{r}) + \int \mathbf{D}\exp(-j\mathbf{R}\cdot\mathbf{r})dV - \psi\int \mathbf{D}\exp(-j\mathbf{R}\cdot\mathbf{r})dV\Big]. \quad (14)$$

The first term can be written in another form. According to (13) we obtain, by substitution of

[3] For the exact relation between susceptibility and electronic density, cf. G. Molière, Ann. d. Physik **35**, 272 (1939).

the variable $(\mathbf{R}+\mathbf{K}_0)$ for $\mathbf{R}$:

$$\psi \exp(-j\mathbf{K}_0\cdot\mathbf{r}) = \int \Psi(\mathbf{R}) \exp[-j\mathbf{r}\cdot(\mathbf{R}+\mathbf{K}_0)]dV = \int \Psi(\mathbf{R}-\mathbf{K}_0) \exp(-j\mathbf{r}\cdot\mathbf{R})dV.$$

The integration limits being infinite, no change in them is necessary by the substitution.

By means of (13), we transform the last term in (14):

$$\psi\int \mathbf{D}\exp(-j\mathbf{R}\cdot\mathbf{r})dV = \int\int \mathbf{D}(\mathbf{R}_1)\exp(-j\mathbf{R}_1\cdot\mathbf{r})\Psi(\mathbf{R}) \times\exp(-j\mathbf{R}\cdot\mathbf{r})dVdV_1,$$

where dV and dV_1 signify the volume elements in the two three-dimensional spaces swept out by $\mathbf{R}$ and $\mathbf{R}_1$, respectively. If we introduce the new variable

$$\mathbf{R}+\mathbf{R}_1=\mathbf{R}_2$$

besides $\mathbf{R}_1$, then

$$\psi\int \mathbf{D}\exp(-j\mathbf{R}\cdot\mathbf{r})dV = \int\int \exp(-j\mathbf{R}_2\cdot\mathbf{r})\Psi(\mathbf{R}_2-\mathbf{R}_1)\mathbf{D}(\mathbf{R}_1)dV_1dV_2 = \int \exp(-j\mathbf{R}\cdot\mathbf{r})dV\int \Psi(\mathbf{R}-\mathbf{R}_1)\mathbf{D}(\mathbf{R}_1)dV_1.$$

For reasons of simplicity, we have suppressed in this last formula the subscript 2 on $\mathbf{R}_2$ which has no importance as $\mathbf{R}$ is an integration variable.

Thus we obtain instead of (14):

$$\frac{\mathbf{d}_t}{\epsilon} = \exp(j\nu t)\Big[\mathbf{d}_0\exp(-j\mathbf{K}_0\cdot\mathbf{r}) - \mathbf{d}_0\int \Psi(\mathbf{R}-\mathbf{K}_0)\exp(-j\mathbf{R}\cdot\mathbf{r})dV + \int \mathbf{D}\exp(-j\mathbf{R}\cdot\mathbf{r})dV - \int dV\exp(-j\mathbf{R}\cdot\mathbf{r})\int \Psi(\mathbf{R}-\mathbf{R}_1)D(\mathbf{R}_1)dV_1\Big]. \quad (15)$$

Let us form

$$\operatorname{curl}\frac{\mathbf{d}_t}{\epsilon} = j\exp(j\nu t)\Big[\mathbf{d}_0\times\mathbf{K}_0\exp(-j\mathbf{K}_0\cdot\mathbf{r}) - \int \mathbf{d}_0\times\mathbf{R}\Psi(\mathbf{R}-\mathbf{K}_0)\exp(-j\mathbf{R}\cdot\mathbf{r})dV + \int \mathbf{D}\times\mathbf{R}\exp(-j\mathbf{R}\cdot\mathbf{r})dV - \int dV\exp(-j\mathbf{R}\cdot\mathbf{r})\int \Psi(\mathbf{R}-\mathbf{R}_1) \times\mathbf{D}(\mathbf{R}_1)\times\mathbf{R}dV_1\Big] \quad (16)$$

and

$$-\frac{1}{c}\frac{\partial \mathbf{d}_t}{\partial t} = -jk\exp(j\nu t)\Big(\mathbf{h}_0\exp(-j\mathbf{K}_0\cdot\mathbf{r}) + \int \mathbf{H}\exp(-j\mathbf{R}\cdot\mathbf{r})dV\Big). \quad (17)$$

According to the fourth Maxwell equation, (16) and (17) are equal. The first terms on the right sides cancel out owing to (3b) and we conclude as above:

$$-k\mathbf{H} = -\Psi(\mathbf{R}-\mathbf{K}_0)\mathbf{d}_0\times\mathbf{R}+\mathbf{D}\times\mathbf{R}+\mathbf{R} \times\int \Psi(\mathbf{R}-\mathbf{R}_1)\mathbf{D}(\mathbf{R}_1)dV_1. \quad (18)$$

In order to eliminate $\mathbf{H}$ by means of (10), we multiply (18) vectorially by $\mathbf{R}$:

$$-k\mathbf{H}\times\mathbf{R} = -k^2\mathbf{D} = -\Psi(\mathbf{R}-\mathbf{K}_0) \cdot(\mathbf{d}_0\times\mathbf{R})\times\mathbf{R}+(\mathbf{D}\times\mathbf{R})\times\mathbf{R} + \int dV_1\{[\mathbf{R}\times\Psi(\mathbf{R}-\mathbf{R}_1)\mathbf{D}(\mathbf{R}_1)]\times\mathbf{R}\}. \quad (19)$$

The triple vector product

$$(\mathbf{R}\times\mathbf{D})\times\mathbf{R}$$

is geometrically the projection of the vector $\mathbf{D}$ on the plane normal to $\mathbf{R}$, multiplied by $\mathbf{R}^2$. Following von Laue we express this fact by the notation

$$(\mathbf{R}\times\mathbf{D})\times\mathbf{R} = \mathbf{R}^2\mathbf{D}_{[\mathbf{R}]}.$$

Thus, (19) becomes:

$$-k^2\mathbf{D}=\mathbf{R}^2\mathbf{d}_{0[\mathbf{R}]}\Psi(\mathbf{R}-\mathbf{K}_0)-\mathbf{R}^2\mathbf{D}$$
$$+\mathbf{R}^2\int\Psi(\mathbf{R}-\mathbf{R}_1)\mathbf{D}(\mathbf{R}_1)_{[\mathbf{R}]}dV_1$$

or finally

$$\mathbf{D}(\mathbf{R})\frac{\mathbf{R}^2-k^2}{\mathbf{R}^2}-\int\Psi(\mathbf{R}-\mathbf{R}_1)\mathbf{D}(\mathbf{R}_1)_{[\mathbf{R}]}dV_1$$
$$=\mathbf{d}_{0[\mathbf{R}]}\Psi(\mathbf{R}-\mathbf{K}_0). \quad (20)$$

This is an inhomogeneous singular integral equation to which the usual theorems on integral equations cannot be applied. Substituting the variable

$$\mathbf{L}=\mathbf{D}\frac{\mathbf{R}^2-k^2}{\mathbf{R}^2}, \quad (21)$$

(20) becomes:

$$\mathbf{L}(\mathbf{R})-\int\Psi(\mathbf{R}-\mathbf{R}_1)\frac{\mathbf{R}_1^2}{\mathbf{R}_1^2-k^2}\mathbf{L}(\mathbf{R}_1)_{[\mathbf{R}]}dV_1$$
$$=\mathbf{d}_{0[\mathbf{R}]}\Psi(\mathbf{R}-\mathbf{K}_0). \quad (22)$$

It appears that the kernel becomes infinite along the sphere $\mathbf{R}^2=k^2$, and this singularity cannot be eliminated by iteration.

This kind of integral equation has been studied by E. Picard[4] who called it integral equation of the third kind. In treating it, Picard leaves a small region neighboring the singularity out of the integration domain, and then lets the area of this region tend to zero. The result depends upon the way in which the limiting process is performed, and the solution is a function of a set of arbitrary parameters which are characteristic for the particular kind of limit. Picard proves that the solution of the equation, considered as the result of a given limiting process, exists, and has in general the same kind of poles as the kernel.

Now, the physical problem demands an unequivocal solution, and we must get, by physical considerations, a supplementary rule which definitely selects a solution. Let us first ask for the cause of the difficulty encountered. We have seen above that $\mathbf{d}$ must be expected to vanish like e^{-jkr}/r, i.e., too slowly to satisfy the ordinary convergence conditions. The theory of Fourier integrals shows[5] that the Fourier transforms of this kind of functions have in general singularities of the character of a real pole. The inversion theorem is applicable only if the integral is defined in some particular way, and not in the Riemann or Lebesgue sense. Evidently, this fact is responsible for the singularities in the integral equation.

We can force the diffraction to vanish sufficiently rapidly at infinity, if we suppose the finite object imbedded in a weakly absorbing medium and not in vacuum as we did. If we then let the absorption of the surrounding medium tend to zero, we can obtain a solution which agrees with the solution looked for, except that it has another behavior at infinity. This is true as long as the diffracting object is limited.

If the dielectric constant ϵ of the imbedding medium has a small negative imaginary part, the length of the wave vector $\mathbf{K}_0$ is no longer equal to k, but also has a small imaginary part. Repeating the calculation with this hypothesis gives again Eq. (20) or (22), with the sole difference that the value of k is now

$$k=(\nu/c)-i\kappa,$$

where κ vanishes in the limit. (We have suppressed a supplementary real part, small as compared to k, because it has no importance for the limiting process.) In this case, the integral in Eq. (22) becomes convergent, and we may expect to obtain a bounded solution $\mathbf{L}$.

Supposing we know the solution, let us calculate the diffracted amplitude $\mathbf{d}$ at a very distant point $\mathbf{r}$. We use polar coordinates R, $\theta_1\Phi$ in the Fourier space so that $\theta=0$ in the direction $\mathbf{r}$. We then have, according to (5a) and (21):

$$\mathbf{d}=\exp(j\nu t)\int_0^\infty\frac{R^4}{R^2-k^2}dR\int_0^{2\pi}d\Phi\int_0^\pi\mathbf{L}$$
$$\times\exp(-jrR\cos\theta)\sin\theta d\theta.$$

For large values of r we will expand the integral over $d\theta$ in decreasing powers of r. Substituting

[4] E. Picard, Ann. Sci. Ecole Normale Sup. **28**, 459 (1911).

[5] S. Bochner, *Vorlesungen ueber Fouriersche Integrale* (Leipzig 1932).

$x=\cos\theta$, we obtain by integration by parts:

$$\int_0^{\pi} \mathbf{L}\exp(-jrR\cos\theta)\sin\theta d\theta$$

$$=\int_{-1}^{+1}\mathbf{L}\exp(-jrRx)dx=\left|\frac{\exp(-jrRx)\mathbf{L}}{-jrR}\right|_{-1}^{+1}$$

$$+\left|\frac{\exp(-jrRx)\mathbf{L}'}{(-jrR)^2}\right|_{-1}^{+1}+\cdots$$

$$+\int\frac{\exp(-jrRx)\mathbf{L}^{(n)}}{(jrR)^{n+1}}dx.$$

Keeping only the first term of this expansion, we have;

$$-\frac{1}{jrR}[\mathbf{L}(0)\exp(-jrR)-\mathbf{L}(\pi)\exp(jrR)].$$

Thus, only those points of the Fourier space which lie on the line pointing to the considered point $\mathbf{r}$, must be taken into account. This result is almost trivial. Indeed, the Fourier analysis means that we consider the diffraction field as a superposition of plane waves, the wave vectors of which are equal to $\mathbf{R}$. Clearly, only those plane waves reach a very remote point which are directed toward it. We now call s the distance of a point on this line from the origin, positive in the direction of the point $\mathbf{r}$. We have

$$\mathbf{d}=\frac{-\exp(j\nu t)}{jr}2\pi\int\frac{|s|s^2}{s^2-k^2}\mathbf{L}(s)\exp(-jsr)ds,$$

where the factor 2π is due to the integration over Φ.

This integral can be evaluated by complex contour integration. Setting $s=x+iy$, we integrate over the contour formed by the real axis and a semicircle of infinite radius which includes the lower half of the complex plane. If r increases, the factor $\exp[-j(x+iy)r]$ tends to zero, so that the integral over the infinite semicircle vanishes. The $\lim \mathbf{d}$ is consequently equal to the sum of the residues. $Im(k)$ is negative and small, so that the contour includes a pole at $s=k$ which is near to the real axis. If we now let $Im(k)$ decrease and r increase, all residues except that at $s=k$ will vanish because of the factor $\exp[-j(x+iy)r]$ and we obtain

$$\lim\mathbf{d}=\frac{2\pi i\exp(j\nu t)2\pi k^3}{2\pi ir}\frac{}{2k}\exp(-jrk)\mathbf{L}(k)$$

$$=\frac{\pi k^2}{r}\mathbf{L}(k)\exp[j(\nu t-rk)]. \quad (23)$$

Thus, the diffracted amplitude at a very remote point $\mathbf{r}$ is proportional to $\mathbf{L}(\mathbf{s}k)$, if $\mathbf{s}$ is a unit vector in the direction $\mathbf{r}$.

We consider now the case of *very small diffracting objects in a vacuum*, or of very weak over-all susceptibility.

The additional field $\mathbf{d}$ is small as compared with $\mathbf{d}_0$. Likewise, as Ψ vanishes everywhere for $\epsilon=1$, it must be small in the case under consideration. We may expect that the integral in the Eq. (22) will be small of second order against the right side which is small only of first order. As a first-order approximation, we will neglect the integral and write:

$$\mathbf{L}(\mathbf{R})=\mathbf{d}_{0[\mathbf{R}]}\Psi(\mathbf{R}-\mathbf{K}_0). \quad (24)$$

The amplitude at a very remote point $\mathbf{r}$ is, according to (23):

$$\mathbf{d}=\frac{\pi k^2}{r}\exp[j(\nu t-rk)]\mathbf{d}_{0[\mathbf{s}k]}\Psi(\mathbf{s}k-\mathbf{K}_0). \quad (25)$$

If the field intensity of the incident wave is *normal* to the plane defined by $\mathbf{r}$ and $\mathbf{K}_0$, then

$$\mathbf{d}_{0[\mathbf{s}k]}=\mathbf{d}_0.$$

If, on the other hand, $\mathbf{d}$ lies *in* the plane, then

$$\mathbf{d}_{0[\mathbf{s}k]}=\mathbf{d}_0\cos 2\theta,$$

where 2θ is the angle between $\mathbf{K}_0$ and $\mathbf{r}$. For a non-polarized primary wave, we obtain the intensity, according to (25)

$$|\mathbf{d}|^2\sim|\mathbf{d}_0|^2\frac{1+\cos^2 2\theta}{2}$$

$$\times\left|\int\psi\exp[j\mathbf{r}(\mathbf{s}k-\mathbf{K}_0)]dv\right|^2. \quad (26)$$

In the case under consideration, (12a), ψ is proportional to the electron density. We thus see that (26) is the formula (1) of the kinematic theory (including the polarization factor), as is to be expected for a first approximation.

Let us next consider the other limiting case, namely that of *an infinite periodic medium*. For this purpose, we shall substitute new variables in Eq. (20). Introducing $\mathbf{R}+\mathbf{K}_0$ instead of $\mathbf{R}$ and $\mathbf{D}(\mathbf{R}-\mathbf{K}_0)$ instead of $\mathbf{D}(\mathbf{R})$, we obtain

$$\mathbf{D}(\mathbf{R})\frac{\mathbf{K}^2-k^2}{\mathbf{K}^2}-\int\Psi(\mathbf{R}-\mathbf{R}_1)\mathbf{D}(\mathbf{R}_1)_{[\mathbf{K}]}dV_1 = \mathbf{d}_{0[\mathbf{K}]}\Psi(\mathbf{R}), \quad (27)$$

where $\mathbf{K}=\mathbf{R}+\mathbf{K}_0$.

If we pass to the case of the infinite crystal, the primary (vacuum) wave vanishes, and with it the right side of Eq. (27). The Fourier integral (13a) degenerates into a Fourier sum. We can express this by saying that Ψ is different from zero only at certain points of the Fourier space $\mathbf{R}=\mathbf{A}_m$. We can write

$$\Psi=\sum_m \Psi_m\delta(\mathbf{R}-\mathbf{A}_m),$$

where the Ψ_m are the Fourier coefficients. $\mathbf{D}$ degenerates into a function of the same type. Thus we obtain:

$$\frac{\mathbf{K}_m^2-k^2}{\mathbf{K}_m^2}\mathbf{D}_m-\sum_q\Psi_{m-q}\mathbf{D}_{q[m]}=0. \quad (28)$$

This is von Laue's fundamental equation for the infinite crystal.

Let us discuss the particular case of the infinite homogeneous medium. According to (11) and (13a), we have

$$\Psi=\int\psi\exp(j\mathbf{R}\cdot\mathbf{r})dv=\frac{\epsilon-1}{\epsilon}\int\exp(j\mathbf{R}\cdot\mathbf{r})dv.$$

Ψ is zero everywhere except at $\mathbf{R}=0$, where it becomes infinite. But the integral of Ψ over the neighborhood of $\mathbf{R}=0$ is finite:

$$\int\Psi dV=\frac{\epsilon-1}{\epsilon}\lim_{a\to\infty}\int\frac{1}{\pi}\frac{\sin 2\pi aX}{X}dX \cdot\int\frac{1}{\pi}\frac{\sin 2\pi aY}{Y}dY\cdot\int\frac{1}{\pi}\frac{\sin 2\pi aZ}{Z}dZ=\frac{\epsilon-1}{\epsilon},$$

where X, Y, Z are the components of $\mathbf{R}$. Thus, we may write:

$$\Psi(\mathbf{R})=\frac{\epsilon-1}{\epsilon}\delta(\mathbf{R}).$$

Inserted in (27), this gives:

$$\mathbf{D}\frac{\mathbf{K}^2-k^2}{\mathbf{K}^2}=\frac{\epsilon-1}{\epsilon}\mathbf{D}. \quad (29)$$

Where $\mathbf{D}$ is different from zero, one concludes from (29):

$$\frac{\mathbf{K}^2-k^2}{\mathbf{K}^2}=\frac{\epsilon-1}{\epsilon}. \quad (30)$$

As the right side of this equation is a constant, it can be satisfied only for $\mathbf{K}=\mathbf{K}_0+\mathbf{R}$ a constant. To make a geometric picture, we draw a sphere, the center of which is the end of the vector $-\mathbf{K}_0$, and the radius of which is $|\mathbf{K}_0|$. On this sphere, $|\mathbf{K}_0+\mathbf{R}|=|\mathbf{K}_0|$ is constant. This sphere is the locus of all points where $\mathbf{D}$ is not zero. From (30) follows:

$$\frac{\mathbf{K}_0^2-k^2}{\mathbf{K}_0^2}=\frac{\epsilon-1}{\epsilon} \quad \text{or} \quad \frac{|\mathbf{K}_0|}{k}=n=\sqrt{\epsilon}. \quad (31)$$

In the case—the only one that is interesting—where the displacement $\mathbf{d}$ is not zero everywhere, $\mathbf{D}$ must become infinite on the sphere in such a way that its integral keeps a finite value.

Let us consider a contribution to the integral

$$\mathbf{d}=\exp(j\nu t)\int\mathbf{D}\exp(-j\mathbf{R}\cdot\mathbf{r})dV,$$

which corresponds to a solid angle $d\Omega$. Let us choose as origin the end of the vector $-\mathbf{K}_0$ and let s be the distance between the origin and a point situated in the cone $d\Omega$. Then we can write

$$\mathbf{d}=\exp(j\nu t)\int\mathbf{F}(\Omega)d\Omega\int\delta(s-|\mathbf{K}_0|)\exp(-jsr)ds,$$

where $\mathbf{F}$ is an arbitrary function. The integral over ds represents a plane wave of wave-length $1/|\mathbf{K}_0|$ and of direction s. We thus obtain, for a

general solution, as we should, a superposition of plane waves with wave-length $1/|\mathbf{K}_0|$ which, according to (31), satisfies the Maxwell relation

$$|\mathbf{K}_0|/k=\sqrt{\epsilon}.$$

Let us note that the quantity $\mathbf{K}_0$ plays another role in the Eqs. (28) and (29) (which relate to an infinitely extended medium) than in the inhomogeneous Eq. (20). In (20), $\mathbf{K}_0$ is equal to k, whereas in (28) and (29), $\mathbf{K}_0$ is a characteristic value, which must assume certain discrete values if there are to be solutions different from zero.

In a subsequent paper, the general Eq. (22) will be used to give an approximate solution of the diffraction problem applicable to crystals of the intermediate size.

This paper was begun at the Mineralogical Laboratory of the Sorbonne, Paris. I wish to express my thanks to Professor Ch. Mauguin for many helpful discussions.

SEPTEMBER 1 AND 15, 1942 PHYSICAL REVIEW VOLUME 62

The Diffraction of X-Rays by Argon in the Liquid, Vapor, and Critical Regions

A. EISENSTEIN AND N. S. GINGRICH
University of Missouri, Columbia, Missouri

(Received June 22, 1942)

The x-ray diffraction pattern of argon has been obtained for 26 different conditions of pressure and temperature ranging from 0.8 atmos. and 84.35°K to 51.1 atmos. and 168°K with a variation in density from 1.401 g/cc to 0.038 g/cc. The intensity in each case is given in electron units. The patterns for argon of high density show sharp maxima while those of low density show much less pronounced maxima or none at all. It is noted that there is considerable small angle scattering in patterns for argon near the saturated vapor curve and at moderate or high pressures and temperatures. Six liquid patterns and one vapor pattern have been analyzed for the atomic distribution. At higher pressure and temperature along the saturated vapor curve, the liquid structure gradually becomes less pronounced, and the structure of liquid and vapor near the critical point are generally similar in nature.

INTRODUCTION

ALTHOUGH x-ray diffraction studies have been made with liquid argon[1–3] at one temperature and with gaseous argon[4] near room temperature, no work has been reported of attempts to obtain a consistent series of diffraction patterns of argon at various pressures and temperatures. The present work was undertaken to obtain these patterns over wide ranges of pressure and temperature, and to determine the atomic distribution curves for some of the more important cases. It is of particular interest to include a study of the region near the critical pressure and temperature because of the many interesting properties found in this region.[5–7]

Ether,[8] isopentane,[9] and nitrogen[10] have been studied for the effect of pressure and temperature on their x-ray diffraction patterns. For ether and isopentane, temperatures and pressures above and below the critical values were used, whereas for nitrogen, studies were made at several pressures all at one temperature considerably above the critical temperature. In all three investigations, emphasis was placed on considerations of the position and shape of the first diffraction peak and detailed study was limited, generally, to scattering angles of less than 15°. Neverthe-

[1] W. H. Keesom and J. de Smedt, Proc. Amst. Akad. **25**, 118 (1922); **26**, 112 (1923).
[2] K. Lark-Horovitz and E. P. Miller, Nature **146**, 459 (1940).
[3] A. Eisenstein and N. S. Gingrich, Phys. Rev. **58**, 307 (1940).
[4] E. O. Wollan, Rev. Mod. Phys. **4**, 205 (1932).
[5] A. L. Clark, Chem. Rev. **23**, 1 (1938).
[6] O. Maass, Chem. Rev. **23**, 17 (1938).
[7] W. H. Barnes, Chem. Rev. **23**, 29 (1938).
[8] R. D. Spangler, Phys. Rev. **46**, 698 (1934).
[9] C. A. Benz and G. W. Stewart, Phys. Rev. **46**, 703 (1934).
[10] G. G. Harvey, Phys. Rev. **46**, 441 (1934).

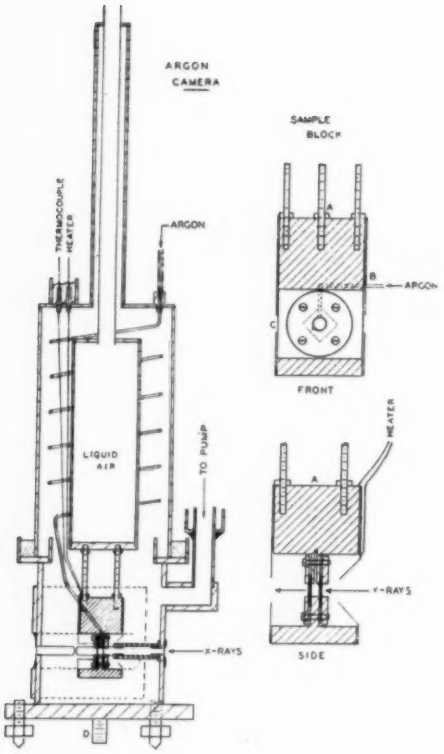

FIG. 1. Showing construction and arrangement of argon cell in vacuum chamber.

less, interesting qualitative and semi-quantitative arguments were based upon the results of these pioneering investigations, adding to our information concerning liquid structure. In the cases of ether and isopentane, for example, it was concluded that the position and intensity of the diffraction peak depended primarily on the density of the fluid and that no abrupt change in the pattern, and hence in the structure of the fluid, took place as the critical pressure or temperature was passed.

By using a somewhat arbitrarily modified form of an equation due to Debye[11] for the scattering of x-rays by gases at densities considerably less than that of the liquid, it was shown[12] that the general form of the ether curves as a function of density could be reproduced reasonably well. It is true, also, that an arbitrarily chosen molecular structure factor for ether had to be used to obtain reasonable agreement between experimental and calculated curves, particularly at small angles of diffraction. Debye's equation also gave reasonably good agreement[10] with experiment in the case of nitrogen as a permanent gas up to 100 atmospheres and it was concluded that the decrease in scattering at small angles is due to the fact that there are a large number of scattering centers within a small space, rather than to any preferred grouping of the molecules.

Although these pioneer efforts have supplied much interesting information, it is highly desirable that some element should be investigated, for which the atomic structure factor is known, and that monochromatic diffraction patterns be obtained to large enough angles to attempt analyses for the atomic distributions according to the method applied to liquids.[13] Perhaps the most nearly ideal substance, considering all factors, is argon. The argon atom is spherically symmetrical, its structure factor is well-known, the optimum thickness for Mo $K\alpha$ radiation is reasonable, its triple point (83.99°K, 0.674 atmos.)[14] critical pressure (47.996 atmos.)[14] and critical temperature (150.66°K)[14] can be conveniently reached, it can be obtained in sufficiently pure form at reasonable cost, and considerable theoretical work has been done on it.[15] Hence, argon has been chosen for the present work.

EXPERIMENTAL METHODS

A full-wave rectifier supplied 25 ma at 38 kv to a grid controlled x-ray tube[16] having a molybdenum target. The operation of this tube continued to be satisfactory over long periods of use, particularly in the matter of target cleanliness. X-rays from this target passed through a thin aluminum window and then were selectively reflected from a rocksalt crystal to produce a well-collimated beam of Mo $K\alpha$ radiation which was directed upon the argon sample.

The argon was contained in a flat sample with beryllium windows, the normal to the sample being set at an angle of 12° 12′ with the beam in a vacuum chamber. The cell was 0.19 cm thick with the entrance beryllium window 0.070 cm

[11] P. Debye, J. Math. and Phys. **4**, 133 (1925).
[12] N. S. Gingrich and B. E. Warren, Phys. Rev. **46**, 248 (1934).
[13] P. Debye and H. Menke, Erg. d. Tech. Rontgenkunde, Volume 2 (1931).
[14] *International Critical Tables* (McGraw-Hill Company, 1926), Vol. 3.
[15] E.g., J. G. Kirkwood and E. Monroe, J. Chem. Phys. **9**, 514 (1941).
[16] A. Eisenstein, Rev. Sci. Inst. **13**, 208 (1942).

thick and the exit beryllium window 0.032 cm thick. The vacuum chamber was a camera (radius 5.08 cm) normally used in photographic work and its essential details are shown in Fig. 1. The x-rays entered the camera through a collimating tube and the diffracted rays passed through a $\frac{1}{4}''$ milled slot covered with thin aluminum foil. The argon cell with ground beryllium windows and indium gaskets was a $\frac{1}{4}''$ hole in a large block of brass fastened to the bottom of a metal Dewar flask and fitted with an electric heater to maintain the temperature constant at whatever temperature was desired. Three copper-constantan thermocouples compared with one calibrated by the Bureau of Standards were fastened to the block at points *A*, *B*, and *C* of Fig. 1, the one at *C* being used both to measure the temperature and to operate the device[17] for maintaining constant temperature. This unit consisted of the thermocouple balanced against a potentiometer and connected to a sensitive galvanometer from whose mirror a V-shaped light beam was reflected on a photo-cell 2.5 meters from the galvanometer. The photo-cell current controlled the fraction of a cycle that a thyratron was conductive and this, in turn, controlled the amount of current in the brass block heater. In all cases, the temperature was maintained constant to better than 0.05° and the actual temperature was known to about 0.1° in all cases except for the lowest temperature, which was known to better than 0.05°.

TABLE I. Positions of peaks.

Pattern	Position of first peak	Position of second peak	Position of third peak	Position of fourth peak	Ratio of intensity of main peak to that at $\sin\theta/\lambda=0.7$
1	0.159	0.287	0.42	0.57	12.5
2	0.158	0.288	0.43	0.57	10.0
3	0.158	0.288	0.43	0.57	10.0
4	0.153	0.277	0.44		8.2
5	0.149	0.28	0.4		7.7
6	0.144	0.34			7.5
7	0.14	0.28			6.4
8	0.135				
9	0.10				
10	0.10				
19	0.125				
22	0.11				
23	0.151	0.28	0.45		
24	0.146	0.28	0.46		
25	0.137	0.25			
26	0.13				

[17] R. M. Zabel and R. R. Hancox, Rev. Sci. Inst. **5**, 28 (1934).

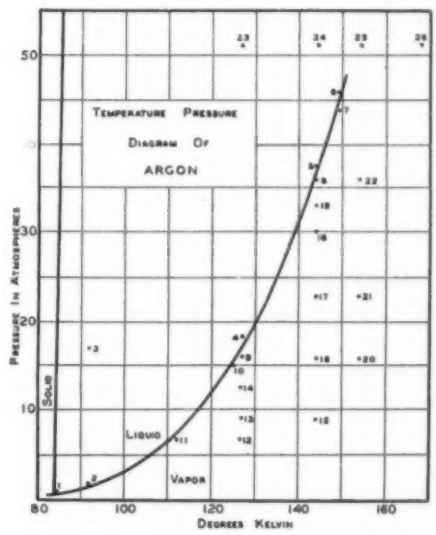

FIG. 2. Pressure-temperature diagram for argon with the conditions for each run indicated by points and identified by numbers. The densities for some of the points are, in g/ml: 1, 1.401; 2, 1.365; 4, 1.100; 5, 0.87; 6, 0.737; 7, 0.330; 8, 0.221; 9, 0.089; 10, 0.079; 11, 0.038. See Fig. 9.

Argon gas was introduced into the cell through small Super-Nickel tubing and through a hole in the brass block.

The cell could be evacuated and then filled with argon gas of 99.6 percent purity after passing through a cooling coil to remove oil and water vapor. The pressure of the argon was measured with a dead-weight gauge for the higher pressures and with a calibrated dial gauge for the very low pressures. These pressures are not known to better than about 0.1 atmosphere, though it is believed that for a given run the pressure remained quite constant.

A Geiger counter supported on the spectrometer arm measured the diffracted x-ray intensity[18] as a function of angle. Collimating slits before the counter made it possible to approach the main beam to within 2° without interference from the main beam. The Geiger counter pulses were amplified by a conventional amplifier, introduced into a scaling circuit which could be used as a scale of 2, 4, 8, or 16, and finally recorded on a Cenco counter.

In practice, the adjustments for the desired temperature and pressure were made a few hours in advance of making a run so that the system would reach equilibrium. Calibration of the zero

[18] A. Eisenstein and N. S. Gingrich, Rev. Sci. Inst. **12**, 582 (1941).

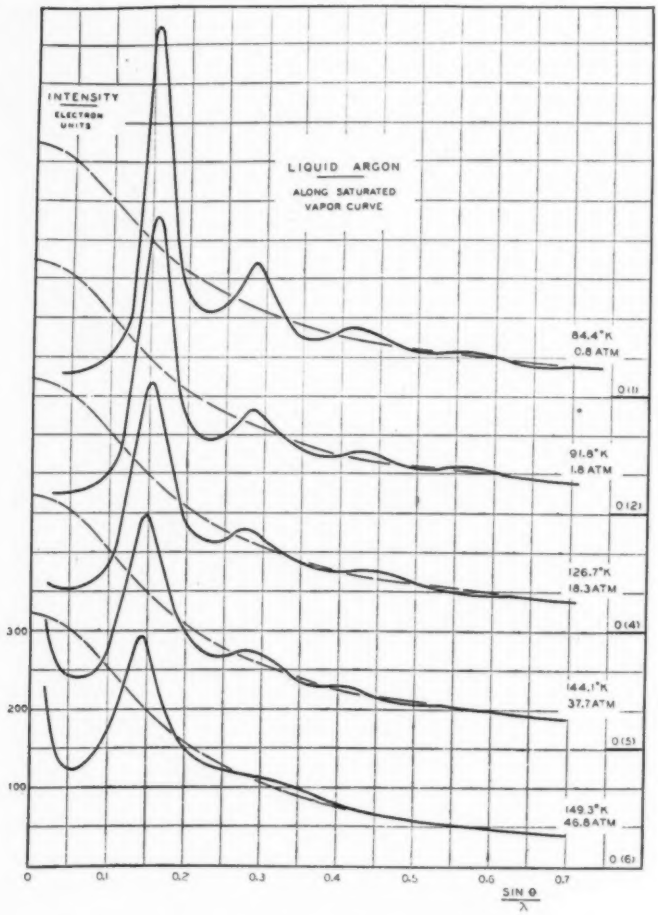

FIG. 3. The intensity patterns for argon liquid, in electron units, as a function of sin θ/λ, for the P-T conditions numbered 1, 2, 4, 5, and 6.

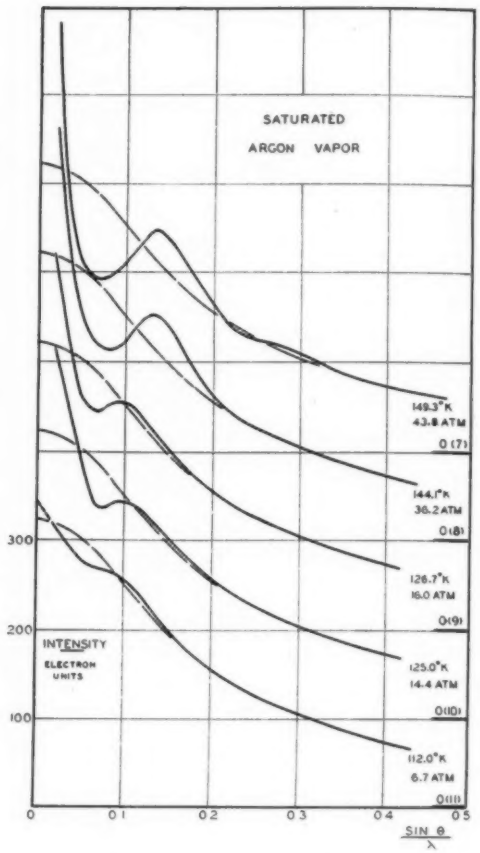

FIG. 4. The intensity patterns for argon vapor in electron units, as a function of sin θ/λ, for the P-T conditions numbered 7, 8, 9, 10, and 11.

angle was made by locating the main peak on each side of zero for all runs in which the main peak was reasonably sharp. As a check on the absolute accuracy of the measurements of the diffraction angles, the argon was replaced by powdered aluminum whose lattice constant, and hence diffraction pattern, is well known. From this work, it is concluded that the angular determinations are correct to within one percent.

EXPERIMENTAL RESULTS

X-ray diffraction patterns of argon were obtained with the argon under 26 different conditions of pressure and temperature. These 26 conditions are shown graphically in Fig. 2, with a number to identify each run. Figures 3 to 8, inclusive, show the diffraction patterns fully corrected for background counting-rate, for absorption, for polarization, and for incoherent radiation. In all cases, the curves are plotted with intensity in electron units and the f^2 curve is shown drawn in as used for later analysis. In Table I the positions of the peaks are listed for these patterns, together with the ratio of intensity at the main peak to that at $\sin/\lambda = 0.7$ for some of the patterns.

Figure 3 shows patterns for liquid argon at points 1, 2, 4, 5, and 6 along the saturated vapor curve. The pattern having the most pronounced peaks is No. 1, taken at 0.8 atmos. and 84.35°K, as near to the triple point as was feasible. The ratio of the intensity at the main peak to that at $\sin\theta/\lambda = 0.7$ was 12.5, the highest ratio of all the cases.

The peaks of pattern No. 2 are all less pronounced than the corresponding peaks of No. 1.

For all pressures and temperatures, Mo $K\alpha$ radiation was used, and, in addition, pattern No. 2 was also taken with Ag $K\alpha$ radiation of wavelength 0.56A. Emphasis was placed on a careful determination of this pattern because of the fact that previous results by different investigators[2,3] in this region were not in full accord. The ratio of the intensity at the main peak to that at sin $\theta/\lambda = 0.7$ was 10.0 in this case.

No. 4 was less sharp than No. 2, No. 5 less sharp than No. 4, and No. 6 less sharp than No. 5. In addition, it is to be noted that as the temperature and pressure are raised, the main peak is shifted to smaller angle, and that scattering at sin θ/λ less than 0.05 becomes increasingly large.

Figure 4 shows the patterns for the pressures and temperatures of Nos. 7, 8, 9, 10, and 11. They are all for argon vapor close to the saturated vapor condition, with Nos. 7, 8, and 9 being close companions to the liquid of Nos. 6, 5, and 4, respectively. At temperatures less than 112°K, the density was so low in the vapor state that sufficient intensity was difficult to obtain with the present cell size. The relation between density and temperature for liquid and vapor along the saturated vapor curve is given in Fig. 9. The deviations of the intensity curves of Nos. 10 and 11 from the f^2 curve at angles greater than sin $\theta/\lambda = 0.1$ are considered to be experimental error since the low counting rates introduced large probable errors. As in the case of the liquid curves, these vapor curves also show marked excess scattering at small angles for the high temperature-high pressure conditions. The main peak increases in prominence as the density of the vapor increases.

Figure 5 shows a group of curves, Nos. 9, 14, 13, and 12, all taken at 126.7°K and at various pressures. The intensity curve of No. 12 is the same as the f^2 curve to within the precision of the present determinations at that low density and volume. The increase in small angle scatter-

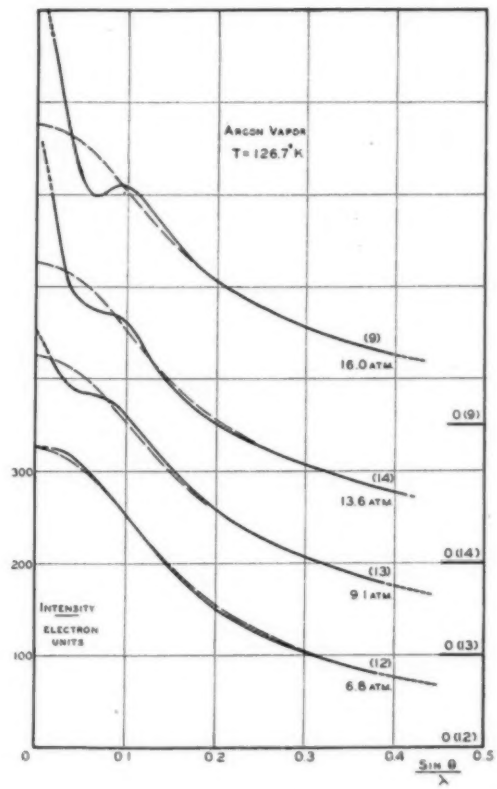

FIG. 5. The intensity patterns for argon vapor in electron units as a function of sin θ/λ, at a constant temperature of 126.7° K for the pressures corresponding to points numbered 9, 14, 13, and 12.

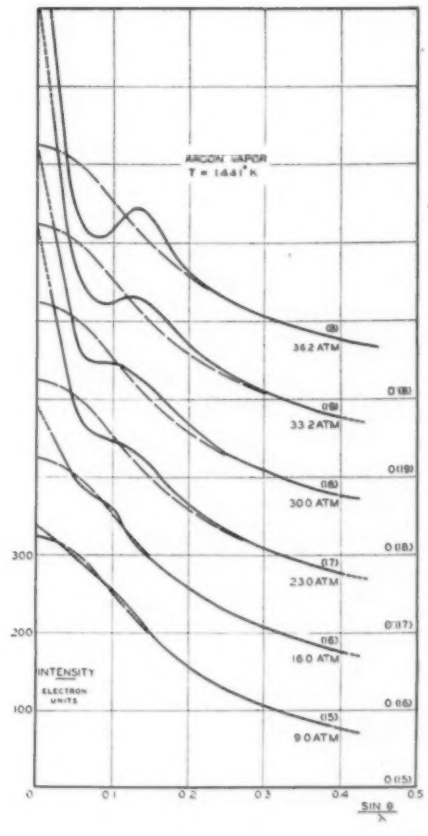

FIG. 6. The intensity patterns for argon vapor in electron units as a function of sin θ/λ, at a constant temperature of 144.1°K for the pressures corresponding to points numbered 8, 19, 18, 17, 16, and 15.

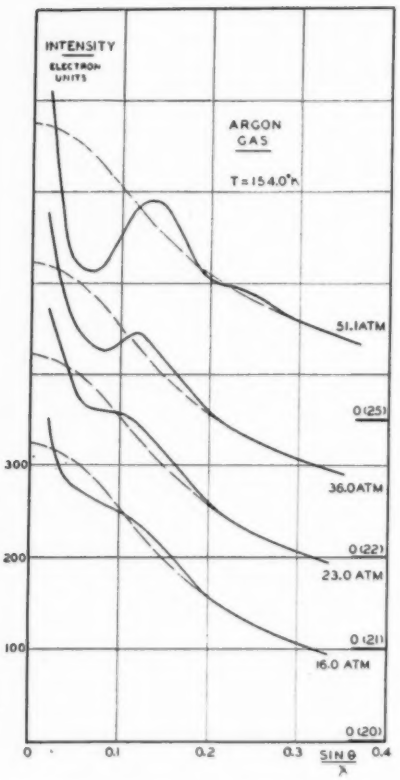

FIG. 7. The intensity patterns for argon gas in electron units as a function of sin θ/λ at a constant temperature of 154.0°K for the pressures corresponding to points numbered 25, 22, 21, and 20.

ing as the vapor approaches saturation is quite evident though the main diffraction peak never becomes very prominent.

Figure 6 shows a group of curves, Nos. 8, 19, 18, 17, 16, and 15 all taken at 144.1°K and at various pressures. No. 15 deviates from the f^2 curve by experimental error, No. 16 deviates significantly at small angles only and this deviation becomes more marked as the vapor approaches saturation in Nos. 17, 18, 19, and 8. These latter curves also show, progressively, the formation of a feeble main peak.

Figure 7 includes the series of curves Nos. 25, 22, 21, and 20 all at 154.0°K and at the various pressures listed. This series is unique in that all were taken at a temperature higher than the critical temperature (150.66°K) and in that one of them, No. 25, was also at a pressure higher than the critical pressure (47.996 atmos.). Considerable small angle scattering appears in all these patterns of a permanent gas, and increase of pressure tends to enhance the sharpness of the pattern, as before.

Figure 8, showing the group of curves, Nos. 23, 24, 25, and 26 illustrates the effect of temperature change at a constant pressure whose value is higher than the critical pressure (47.996 atmos.). Curve No. 23 under a condition far removed from the saturated vapor curve shows little scattering at small angle, No. 24 shows more, and Nos. 25 and 26 show quite a large amount. There is a marked washing-out of the patterns as the temperature is increased, particularly between 144.1°K and 154°K.

Curve No. 3 is the only one not reproduced here. It was quite similar to No. 2 though there was a slight shift in the main peak position, that of No. 3 being at a slightly higher value of sin θ/λ than that of No. 2.

ANALYSIS OF PATTERNS

These intensity curves may be analyzed to obtain atomic distribution curves, by the method outlined elsewhere.[19] An analysis of this kind results in a curve of $4\pi r^2\rho(r)$ as a function

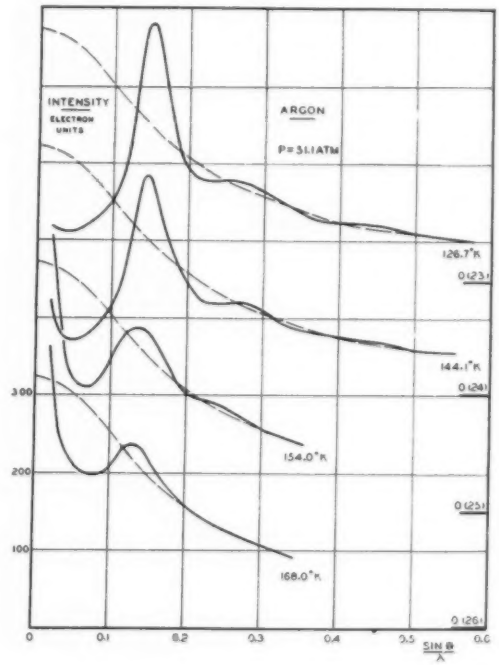

FIG. 8. The intensity patterns for argon in electron units as a function of sin θ/λ at a constant pressure of 51.1 atmos. for the temperatures corresponding to points numbered 23, 24, 25, and 26.

[19] B. E. Warren, J. App. Phys. **8**, 646 (1937).

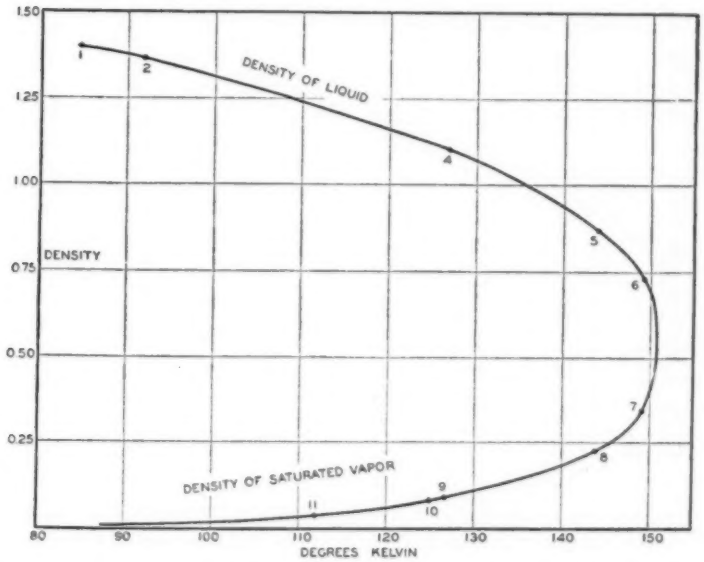

FIG. 9. Showing the density of argon liquid and saturated vapor along the saturated vapor curve as a function of temperature.

of r. The area under this curve between r and $r+dr$ represents the number of atoms at a distance r from any atom in the body of the sample.

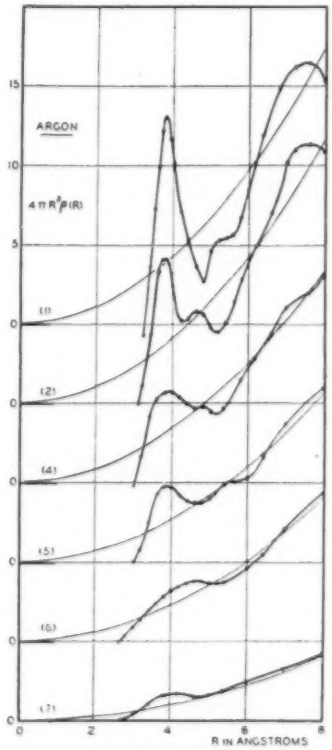

FIG. 10. Showing the atomic distribution curves for argon at several pressures and temperatures along the saturated vapor curve. Curves 1, 2, 4, 5, and 6 are for liquid argon; curve 7 is for argon vapor.

Analyses were carried out for the intensity curves Nos. 1, 2, 4, 5, and 6 for argon in the liquid state and for curve No. 7 for argon vapor, all near the saturated vapor curve (Fig. 9) where the density of argon was known. The result of this work is shown in Fig. 10. Table II gives the values of the positions of the first peaks, the positions of the second peaks or prominences, and the areas under these peaks where this can be obtained with any reasonable degree of reliability. Since none of the peaks is discrete, i.e., isolated, these areas must be somewhat arbitrary, though these data may be considered approximately representative.

Graphical analysis was used in all the work here reported, and points were determined at intervals of 0.1A, 0.2A, 0.4A, 0.6A, or 1.0A in r as seemed necessary. The precision in the location of the various r values cannot be greater than that of the determination of the diffraction angles, or about 1 percent.

DISCUSSION OF RESULTS

In their general aspects, the present experimental results are in accord with the previous work on ether, isopentane, and nitrogen. They show, for example, the same sort of gradual transition in the patterns from that of the liquid to that of the rarified gas with no abrupt change in passing the critical temperature or the critical

pressure. Density is the most important factor in the production of a peak in the intensity curve, though it may not be the only factor.

The first indication that the x-ray diffraction pattern of a substance having a specific volume greater than the critical volume showed a feeble peak was noted by Spangler[8] for ether. In this case, a vestige of a peak persisted as far as a specific volume 10 or 15 percent greater than the critical volume. Stewart and Benz,[9] working with isopentane, noted the persistence of a feeble peak up to specific volumes as much as 90 percent greater than the critical volume. Harvey[10] obtained a peak in the intensity curve for nitrogen as a permanent gas at specific volumes near the critical volume. In the present work, there is a faint indication of interference effects in pattern No. 11 for which the argon had a specific volume roughly 1500 percent greater than the critical volume. The occurrence of slight interference effects at as low a specific volume as this cannot be taken as proof nor as rigorous disproof of the cybotactic view,[20] but the present authors prefer to ascribe its origin simply to a frequently recurring distance in an almost random array of atoms.

Some of the diffraction curves taken with liquid argon, and many of them taken with argon vapor, exhibit considerable intensity at sin θ/λ less than 0.05. This sharp rise in intensity at very small angles appears to be present in the work on ether and isopentane, but in the present work its existence and its magnitude are emphasized by comparison with the rarified gas or f^2 curve. The primary condition for obtaining this effect appears to be that the argon must be near the saturated vapor curve, but this is apparently not the only condition necessary, for no small angle scattering was found at very low pressures and temperatures along this curve. Perhaps the best way to describe the area in which it may be found is to outline a fan shaped area about the saturated vapor curve, beginning, from these results, at a temperature of about 120°K on its vapor side and increasing in width, with the greatest width in the critical region. On the liquid side of the curve, the fan shaped area may be narrower than that for the vapor and it may start at a higher temperature. Figure 4 shows this effect to be pronounced in all the curves taken near the saturated vapor curve, with the exception of No. 11. In Figs. 5, 6, and 7, nearly all the curves show the effect very well. At constant pressure, the curves in Fig. 8 all have some small angle scattering, but those at 154°K and 168°K have a large amount of it. Even in Fig. 3 showing only liquid curves, at least two of the curves have unmistakable small angle scattering. Of all 26 curves, Nos. 7 and 8 have the largest amount of this scattering. The existence of this scattering is taken to indicate large scale density fluctuations in the vapor or in the liquid. Unfortunately, the method of Debye and Menke[13] is not capable of supplying much information from scattering in this region, with the present state of refinements in experimental technique, and hence the more qualitative approach is necessary. The use of Bragg's law, or Ehrenfest's relation,[21] however, enables one to calculate the approximate distances required to produce the scattering as found. A calculation of this sort leads to the conclusion that characteristic distances of about 10A and greater are present. In the vapor, one might visualize the existence of clusters of atoms, some of which could possibly be termed fog droplets. In the liquid, this clustering to give large scale density fluctuations reminds one of the idea of cybotaxis. Super-saturated vapor is known to form very fine fog particles and a calculation of the radii[22] of these droplets can be made for given conditions of pressure, temperature, surface tension, and molecular weight. Possibly a similar effect takes place in saturated, or nearly saturated vapor.

TABLE II. Peak distances and coordination numbers from areas under curves.

Pattern	First peak distance	First coordination number	Second peak distance	Second coordination number
(Crystal)	3.82A	12	5.4A	6
(1)	3.79A	10.2–10.9	5.3A	
(2)	3.79A	6.8– 7.2	4.7	3.2–4.7
(4)	3.8A	5.9– 6.2	4.8	
(5)	3.8A	3.9– 4.6	5.4	
(6)	4.5A	6		
(7)	4.1A	2		

[20] G. W. Stewart, Rev. Mod. Phys. **2**, 116 (1930).

[21] P. Ehrenfest, Proc. Amst. Akad. **17**, 1184 (1915).

[22] E.g., R. Becker and W. Doring, Ann. d. Physik **416**, 719 (1935).

From liquid patterns taken at constant temperature, some information can be obtained regarding the compressibility of liquid argon. For example, the three pairs, 2–3, 4–23, and 5–24, may be compared. It is true that the accuracy of the determination of the main peak positions is about one percent, but the relative position of one main peak with respect to another main peak can be made with higher accuracy. Thus, the peak of No. 3 is at a value of sin θ/λ about 0.0007 greater than that for No. 2, or by about $\frac{1}{2}$ percent. On the questionable assumption that the main peak is the sole agency determining interatomic distances, this would indicate a decrease in specific volume of about 1.5 percent for an increase in pressure from 1.8 atmos. to 17.0 atmos. at 91.8°K. Similarly, one can calculate that in going from 18.3 atmos. to 51.1 atmos. at 126.7°K, a decrease in specific volume of nearly 5 percent takes place, or with an increase from 37.7 atmos. to 51.1 atmos. at 144.1°K, there is a decrease in specific volume of slightly over 6 percent.

The atomic distribution curves of Fig. 10 are of interest since the determination of these curves constitutes an attempt to obtain quantitative data directly from the experimental work. The atomic distribution curve for pattern No. 1 taken at 84.35°K and 0.8 atmos., has its first peak at 3.79A. The area under this peak represents from 10.2 to 10.9 atoms depending upon how the peak is extrapolated to zero on its large r side. These values are to be compared with the crystal values of 3.82A and 12 atoms. They are in good accord with the calculation of Rice[23] who concludes that the first coordination number should be from 10 to 10.5 in the liquid. The second coordination sphere occurs at 5.3A while in the crystal it is 5.4A with six atoms at this distance.

Pattern No. 2 taken at 1.8 atmos. and 91.8°K gave distribution curve No. 2. At 3.79A there are 6.8–7.2 atoms and at 4.7A there are 3.2–4.7 atoms, depending on how the curves are drawn in. The unusual feature here is that with a change of only 7.4° in temperature and 1 atmos. in pressure, there appears a marked decrease in sharpness and area of the first peak and a large shift toward small r of the second peak. Special attention was given to checking the experimental curves of 1 and 2 but no significant difference could be obtained on repetition. It is true that in no other liquid element has the effect of temperature on its pattern been studied as close to the triple point as in this case. The differences between the results of Lark-Horovitz and Miller[2] and those of the present writers[3] can be explained particularly if consideration is given to the experimental conditions in each investigation. In the former case, the argon was cooled by passing liquid air through a hole in the copper block which held the argon, and the argon temperature probably was close to their stated temperature, 89.2°K, whereas in the latter work, liquid argon dripped from the bottom of a Dewar flask into a capillary tube, and no direct measurement of the argon temperature was attempted. It is believed more likely that the temperature in this case may have been a few degrees higher than the reported 90°K. Furthermore, the temperature probably varied by several degrees as fresh liquid air was introduced into the Dewar flask, thus tending to smear out the pattern somewhat.

An interesting comparison was made between distribution curves 1 and 2 by obtaining the areas under these curves up to 6.2A where they cross the $4\pi r^2\rho_0$ curves. For curve 1, the area was 19.7 and for curve 2 it was 19.1 or about 3 percent difference. The difference in density of the argon in these two cases is 2.6 percent.

The first peak of curve 4 is more flat than for curves 1 or 2, its position is 3.8A and it covers an area of about 5.9–6.2. The secondary peak is very small and it occurs at 4.8A. Curve 5 shows a peak at 3.8A which covers an area of about 3.9–4.6. The secondary peak has moved outward to 5.4A. Curve 6 gave an unusual appearing first peak at about 4.5A. No attempt was made to repeat this experimental work, but in any case, it is felt that the curve probably is of some value in illustrating the gradual loss of structure.

Curve 7 shows the result of an analysis of an argon vapor diffraction pattern. It is seen that there is no marked change in the general structure as exhibited by the high temperature-high pressure liquids and by this high temperature-high pressure vapor.

Another effect of some interest is the gradual shift toward small r of the point at which the

[23] O. K. Rice, J. Chem. Phys. **7**, 883 (1939).

distribution curves are zero. These values of r are 3.24A for 1, 3.10A for 2, 3.03A for 4, 3.0A for 5, 2.7A for 6, and 2.6A for 7. This is presumably due to the fact that the more energetic atoms at high temperature approach each other to slightly smaller distances than at the lower temperatures.

ACKNOWLEDGMENTS

This work was generously supported by grants from the American Academy of Arts and Science, from the American Association for the Advancement of Science, from the Elizabeth Thompson Science Fund, and from the University of Missouri Research Council.

SEPTEMBER 1 AND 15, 1942 PHYSICAL REVIEW VOLUME 62

On the $^2\Pi_u \rightarrow {}^2\Pi_g$ Bands of CO_2^+. Part II*

S. MROZOWSKI
Ryerson Physical Laboratory, University of Chicago, Chicago, Illinois

(Received June 12, 1942)

In continuation of the first part of the work containing the rotational analysis of 10 sub-bands belonging to the progression $v''_1=0$ of the $^2\Pi_u \rightarrow {}^2\Pi_g$ band system of CO_2^+, 24 new sub-bands were analyzed. These bands belong to the progressions $v''_1=1$ and $v''_1=2$. It was found that the substate $^2\Pi_{3/2g}$, $v''_1=1$ is split into two levels, the splitting being probably caused by an interaction (resonance) with some other unidentified substate (very probably one of the vibronic substates corresponding to two quanta of bending vibration). A similar splitting was found in the substate $^2\Pi_{3/2u}$, $v'_1=4$. Weaker perturbations, manifested by anomalous B values, Λ-doubling increasing proportionally to about $J^{2.5}$, and shifts of vibrational levels were detected in several other vibrational levels. A selection rule forbidding transitions between vibrational levels showing opposite perturbation shifts in the vibrational energy has been found. The new constants obtained are: $\Delta G''^a{}_1=1241.77$, $\Delta G''^b{}_1=1287.32$, $\Delta G''^b{}_2=1209.55$ (all $^2\Pi_{3/2g}$): $\Delta G''_1=1265.75$, $\Delta G''_2=1256.89$ ($^2\Pi_{1/2g}$); $\Delta G'^a{}_4=1062.50$, $\Delta G'^b{}_5=1055.25$, $\Delta G'_6=1103.97$ ($^2\Pi_{3/2u}$); $\Delta G'_5=1108.50$, $\Delta G'_6=1106.99$ ($^2\Pi_{1/u}$). Further, for $^2\Pi_{3/2g}$, $B''^a{}_1=0.3754$, $B''^b{}_1=0.3814$, $B''_2=0.3769$; for $^2\Pi_{1/g}$, $B''_1=0.3803$, $B''_2=0.3793$; for $^2\Pi_{3/2u}$, $B'^a{}_4=0.3421$, $B'_5=0.3427$, $B'_6=0.3417$; for $^2\Pi_{1/u}$, $B'_5=0.3460$, $B'_6=0.3458$. The values of the constants reported in Part I are corrected and the Λ-doubling for all levels is evaluated. Formulas for unperturbed values of B (both substates $^2\Pi_{3/2}$ and $^2\Pi_{1}$) are: $^2\Pi_g B''_v=B''_0-0.0012v''_1$, $^2\Pi_u B'_v=B'_0-0.0011v'_1$; for unperturbed zero band lines $\nu_{v'v''}=\nu_{00}+1131v'_1-3v'_1(v'_1+1)-1280v''_1+7.25v''_1(v''_1+1)$.

INTRODUCTION

IN the first part of this work published several months ago[1] the rotational analysis of five double bands of the $^2\Pi_u - {}^2\Pi_g$ band system of CO_2^+, belonging to the $v''_1=v''_2=v''_3=0$ progression of the symmetrical vibration (v'_1 varying, $v'_2=v'_3=0$), was reported. It was shown there that the lower state of these bands is the ground state of the CO_2^+ molecule and that the molecule is linear in both $^2\Pi$ states. Both states $^2\Pi$ are inverted. The method of excitation used and the procedure followed in determining wave numbers from the photographs, obtained in the second order of the 30-foot grating spectrograph, were described in Part I. In continuation of this work, the rotational analysis of bands belonging to the $v''_1=1$ and $v''_1=2$ progressions of the symmetrical vibration (v'_1 varying) has now been carried out and is reported below. In contradistinction to the case of the progression $v''_1=0$, this part of the analysis encountered some difficulties caused by specific perturbations occurring in these bands. All bands of the progression $v''_1=0$ show a structure exactly like that of case $a^2\Pi \rightarrow {}^2\Pi$ bands of diatomic molecules, with no measurable Λ-doubling in the $^2\Pi_{3/2u} \rightarrow {}^2\Pi_{3/2g}$ sub-bands and a linear doubling in the $^2\Pi_{1/u} \rightarrow {}^2\Pi_{1/g}$ sub-bands. Only a slight deviation in the $\Delta G'$ values was observed, which pointed to a vibrational perturbation of the levels $v'_1=3$ and (still more) of $v'_1=4$ of $^2\Pi_{3/2u}$. But for the vibrational state $v''_1=1$ the sublevel $^2\Pi_{3/2g}$ is very strongly perturbed: in fact it must be in almost exact resonance with some other unknown level

* Assistance in the preparation of materials was furnished by the personnel of Works Progress Administration Official Project No. 30538.

[1] S. Mrozowski, Phys. Rev. **60**, 730 (1941).

(probably one of the vibronic levels corresponding to two quanta of the bending vibration of the same state $^2\Pi_g$), and is split into two levels denoted in this work by 1^a and 1^b. A very strong Λ-doubling increasing faster than proportionally to J^2, and a positive value of the rotational constant D''_1 in both levels 1^a and 1^b accompany this interaction. A similar splitting of a sublevel $^2\Pi_{3/2}$ is found in the excited state $^2\Pi_u$ for $v'_1=4$; and anomalous Λ-doublings appear in the levels $v''_1=2$ of $^2\Pi_{3/2g}$ and $^2\Pi_{\frac{1}{2}g}$, and in $v'_1=4^a$, 5, 6, and 7 of $^2\Pi_{3/2u}$. Although all bands show the same simple rotational structure as for case a $^2\Pi\rightarrow{}^2\Pi$ bands of diatomic molecules, the vibrational analysis has been made difficult by a peculiar selection rule for the a and b perturbed levels (see below). The proper classification of bands could be obtained only by way of the rotational analyses, and since the B values for different vibrational states differ very little, a high accuracy in the determination of wave numbers was indispensable.

Results

The $v''_1=0$ progression of bands. Corrections to Part I

A critical reconsideration of the data reported in Part I, especially of the values of weighted averages of $\Delta_2F''_0$ for the lower values of the rotational quantum number J, and the application of more exact graphical methods, resulted in a slight change of the constants reported in Part I. The new values are the following:

$$\begin{aligned} {}^2\Pi_{3/2g}:\ & B''_0=0.3797\pm0.0001 \\ & D''_0=-(1.5\pm0.2)10^{-7}. \\ {}^2\Pi_{\frac{1}{2}g}:\ & B''_0=0.3815\pm0.0001 \\ & D''_0=-(1.6\pm0.2)10^{-7} \\ & p''_0=+0.0047\pm0.0010. \end{aligned}$$

For the new B''_0 values, the difference between the $^2\Pi_{\frac{1}{2}}$ and $^2\Pi_{3/2}$ values is in excellent agreement with the results of Bueso-Sanllehi[2] and is exactly equal to the value predicted by the theory of Hill and Van Vleck.[3] On the other hand, both D''_0 values are this time a little greater than the value -1.3×10^{-7} expected on the basis of the formula[4] $D=-4B^3/\nu_1^2$. The new value of the

[2] F. Bueso-Sanllehi, Phys. Rev. **60**, 556 (1941).
[3] Cf. R. S. Mulliken, Rev. Mod. Phys. **2**, 113 (1930).
[4] W. H. Schaffer, unpublished work, showed the applicability of this formula to triatomic linear molecules.

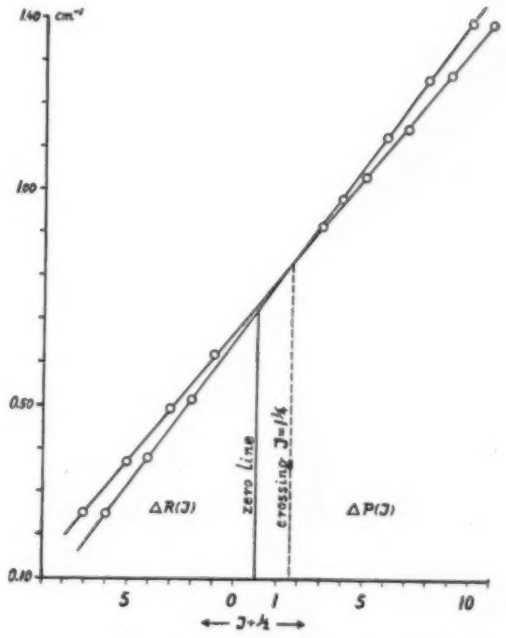

FIG. 1. Illustrating for the case of the sub-band $(1,0)^2\Pi_{\frac{1}{2}u}\rightarrow{}^2\Pi_{\frac{1}{2}g}$ the determination of p''_0 from the crossing point of two straight lines corresponding to the alternate first differences in P and R branches.

Λ-doubling constant [the Λ-doubling of a term $T(J)$ is $\pm\frac{1}{2}p(J+\frac{1}{2})$ and not $\pm p(J+\frac{1}{2})$ as erroneously given in Part I] has been obtained as an average of values determined in many different ways. Since all the differences $p'-p''$ are obtained with high accuracy from the graphs of the first differences in P and R branches (from the angle under which two straight lines cross, see Fig. 1) a fairly exact knowledge of at least one p is very important. All other p's are then found by the use of the differences $p'-p''$ and their absolute values are obtained with almost the same accuracy as that of the original p. The methods applied for determination of p''_0 were: (1) a value a little higher than before is obtained for p''_0 from the corrected averages of $\Delta_2F''_0$; (2) a value for p''_1 has been determined from the average Δ_2F_1'''s (state $v''_1=1$, $^2\Pi_{\frac{1}{2}g}$ see Table III) and then the value of p''_0 was found by using various differences $p'_{v'}-p''_1$ and $p'_{v'}-p''_0$; (3) the first differences in the P and R branches are linear functions of J, and the two straight lines obtained for alternate distances $\Delta P(J)=P(J+1)-P(J)$ cross at $J_{cr}=p''/(p'-p'')$ (see Fig. 1). With the values $p'-p''$ and J_{cr} obtained from the graph, an approximate value

TABLE I. Sub-bands $^2\Pi_{3/2a} \rightarrow {}^2\Pi_{3/2g}$.

$J-\frac{1}{2}$	(0,1ᵃ) $\nu_0=27290.80$ Unres. Q branch $\nu=27290.65$ R	P	(1,1ᵃ) $\nu_0=28417.6$ R	P	(4ᵉ,1ᵃ) $\nu_0=31722.9$ R	P	(5,1ᵃ) $\nu_0=32835.65$ R	P	$^2\Pi_{3/2g}(v_1''=1^a)$ Δ_2F_1''a Aver.	1st diff.
1	27292.28	missing							4.50	
2	92.98	27288.82							5.97	1.47
3	93.56	87.88							7.51	1.54
4	94.01	87.04							9.00	1.49
5	94.45	86.05							10.48	1.48
6	94.80	85.01							11.98	1.50
7	95.14	83.98			31726.67 h			32828.90	13.50	1.52
8	95.37	82.82			31726.67 e		32839.85 h	27.70	14.98	1.48
9		81.65			31726.67 a	31713.14	32839.85 e	26.30	16.42	1.44
10 h		80.38	28422.59 h		31726.67 d	11.81	32839.85 a	24.95	18.00	1.58
11 e	95.79	79.15	28422.59 e		31726.67	10.25	32839.85 d	23.40	19.50	1.50
12 a	95.79	77.74	28422.59 a		26.47	08.68		21.87	21.05	1.55
13 d	95.79	76.36	28422.59 d	28403.00	26.09	07.00	39.42	20.27	22.50	1.45
14	95.63	74.83	22.30	01.43	25.76	05.32	39.12	18.60	24.05	1.55
15	95.63	73.42	22.30	28399.95	25.44	03.64	38.85	16.90	25.55	1.50
16	95.37	71.70	22.05	98.30	25.05	01.80	38.39	15.04	26.10	1.55
17	95.37	70.22	21.88	96.75	24.44	31699.90	37.95	13.27	28.57	1.47
18	94.80	68.37	21.35	94.90	23.91	97.89	37.34	11.27	30.09	1.52
19	94.65	66.79	21.12	93.26	23.31	95.98	36.81	09.37	31.54	1.45
20	94.01	64.80	20.52	91.27	22.55	93.82	35.97	07.20	33.10	1.56
21	93.78	63.11	20.19	89.58	21.76	91.67	35.37	05.20	34.58	1.48
22	92.98	60.93	19.32	87.32	20.99	89.48	34.35	02.87	36.13	1.55
23	92.66	59.25	18.90	85.53	20.17	87.22	33.50	00.74	37.60	1.47
24	91.66	56.84	17.94	83.12	19.06	84.93	32.44	32798.15	39.16	1.56
25	91.30	55.09	17.44	81.30	17.96	82.46	31.58	95.94	40.62	1.46
26	90.12	52.52	16.21	78.60	16.94	79.99	30.28	93.28	42.19	1.57
27	89.70	50.70	15.69	76.70	15.83	77.41	29.23	90.91	43.63	1.44
28	88.30	47.93	14.24		14.53	74.80	27.78	88.02	45.20	1.57
29	87.88	46.08	13.75		13.14		26.70	85.59	46.68	1.48
30	86.26	43.12	12.00				24.95	82.56	48.24	1.56
31	85.78	41.21	11.46				23.75	79.97	49.70	1.46
32	83.98	38.01					21.87	76.72	51.27	1.57
33	83.44	36.02					20.67	74.12	52.73	1.46
34	81.40	32.70					18.57	70.61	54.32	1.59
35	80.84	30.70					17.28	67.95	55.79	1.47
36	78.60	27.04						64.35	57.39	1.60
37	78.02	25.05							58.81	1.42
38	75.55	21.21							60.42	1.61
39	74.90	19.20							61.82	1.40
40	72.21	15.13							63.46	1.64
41	71.50	13.08							64.84	1.38
42	68.63	08.76							66.52	1.68
43	68.00	06.70							67.88	1.36
44	64.80	02.11							69.58	1.70
45	64.17	00.10							70.88	1.30
46	60.73	27195.29							72.68	1.80
47	60.06	93.33							73.95	1.27
48	56.38	88.05							75.78	1.83
49	55.74	86.11								
50	51.82	80.60								
51	51.14									

of p'' is calculated. This procedure has been applied to all bands of the progression $v''_1=0$ to get p''_0 directly, and to all bands of the progression $v''_1=1$ to get p''_1 and then to determine p''_0 by using the differences $p'-p''$. The bands ending on level $v''_1=2$ were not used since the level $v''_1=2$ shows an anomalous nonlinear Λ-doubling. All values obtained for p''_0 by these different methods lie within the range $0.004-0.006$ and the final value given above has been adopted after critical examination of all these data.

The $v''_1=1$ progression of bands

As already mentioned in the introduction, the sublevel $^2\Pi_{3/2g}$ is split into two levels, here denoted 1^a and 1^b, and therefore instead of two we have three progressions of sub-bands. The wave numbers of the lines and the average $\Delta_2F''_1$ values are presented for these in Tables I, II, and III. Asterisks marking blended lines are omitted, since there are many weak lines present on the plates and it is often very difficult to decide if an anomalous intensity of a line is caused by a real blend, a coincidence with a weak but sharp Rowland ghost, or with an unsharp Lyman ghost. The number of cases where blends have been definitely established by the analysis as belonging to lines of different bands or by the strongly anomalous intensity is relatively much smaller, and the marking only of these cases with asterisks would be far from representing the real situation. Naturally in taking averages of Δ_2F's and evaluation of all

TABLE II. Sub-bands $^2\Pi_{3/2u} \rightarrow {}^2\Pi_{3/2g}$.

$J-\frac{1}{2}$	(0,1[b]) $\nu_0=27245.25$ R	P	(2,1[b]) $\nu_0=29494.70$ R	P	(3,1[b]) $\nu_0=30614.75$ R	P	(4[b],1[b]) $\nu_0=31734.90$ R	P	$^2\Pi_{3/2g}(v_1''=1^b)$ $\Delta_2F_1''b$ Aver.	1st diff.
4				29490.80					7.62	
5		27240.20		89.71		30609.69		31729.77	9.15	1.53
6	27248.82	39.10		88.61		08.59		28.65	10.68	1.53
7	49.03	37.89		87.37	30618.40 h	07.32	31738.41 h	27.34	12.21	1.53
8	49.16 h	36.61	29498.51 h	86.08	30618.40 e	06.03	31738.41 e	26.15	13.73	1.52
9	49.16 e	35.27	29498.51 e	84.72	30618.40 a	04.66	31738.41 a	24.70	15.25	1.52
10	49.16 a	33.89	29498.51 a	83.29	30618.40 d	03.28	31738.41 d	23.29	16.76	1.51
11	49.16 d	32.43	d	81.82		01.76		21.73	18.28	1.52
12	49.03	30.93	98.22	80.20		00.18	38.10	20.17	19.81	1.53
13	48.82	29.33	98.00	78.52	17.81	30598.45	37.79	18.50	21.34	1.53
14	48.55	27.67	97.68	76.86	17.47	96.77	37.45	16.76	22.86	1.52
15	48.21	25.92	97.24	75.08	17.00	94.99	37.01	14.95	24.38	1.52
16	47.93	24.14	96.78	73.24	16.56	93.16	36.53	13.16	25.92	1.54
17	47.38	22.30	96.24	71.27	15.99	91.08	35.94	11.08	27.44	1.52
18	46.94	20.41	95.71	69.33	15.37	89.15	35.37	09.12	29.00	1.56
19	46.24	18.38	94.93	67.20	14.62	86.95	34.61	06.97	30.52	1.52
20	45.65	16.35	94.26	65.14	13.92	84.88	33.88	04.86	32.08	1.56
21	44.84	14.15	93.30	62.83	12.97	82.56	32.95	02.53	33.56	1.48
22	44.15	12.10	92.53	60.67	12.15	80.37	32.10	00.35	35.11	1.55
23	43.12	09.69	91.41	58.15	11.03	77.87	30.99	31697.90	36.61	1.50
24	42.39	07.54	90.50	55.90	10.12	75.54	30.06	95.54	38.18	1.57
25	41.21	04.91	89.22	53.22	08.79	72.85	28.75	92.81	36.69	1.51
26	40.35	02.70	88.25	50.82	07.79	70.42	27.73	90.37	41.25	1.56
27	39.02	27199.92	86.77	47.97	06.24	67.54	26.19	87.55	42.74	1.49
28	38.01	97.66	85.71	45.52	05.16	65.06	25.09	85.00	44.30	1.56
29	36.52	94.65	84.09	42.47	03.43	62.00	23.32	81.94	45.79	1.49
30	35.48	92.25	82.85	39.88	02.27	59.41	22.26	79.38	47.37	1.58
31	33.74	89.12	81.01	36.63	00.33	56.10	20.25	76.08	48.85	1.48
32	32.70	86.60	79.72	34.01	30599.00	53.40	19.06	73.38	50.44	1.59
33	30.70	83.29	77.64	30.57	96.77		16.76		51.89	1.45
34	29.49		76.33	27.83	95.55		15.48			
35	27.30				93.16					
36	26.12				91.77					
37	23.69									
38	22.49									
39	19.81									
40	18.54									

constants the points corresponding to lines of anomalous intensity or unsymmetrical structure have been treated as less reliable.

The molecular constants obtained from $\Delta_2F''_1$ for the ground state of CO_2^+ with one quantum of symmetrical vibration $v''_1=1$ are the following:

$^2\Pi_{3/2g}$ substate a: $B''_1=0.3754\pm0.0002$
$D''_1=+(6.3\pm0.5)10^{-7}$,
$F''_1<0$.

$^2\Pi_{3/2g}$ substate b: $B''_1=0.3814\pm0.0002$
$D''_1=+(2.2\pm0.4)10^{-7}$,
$F''_1\neq0$.

$^2\Pi_{1/2g}$ $B''_1=0.3803\pm0.0001$
$D''_1=-(1.5\pm0.2)10^{-7}$
$p''_1=+0.0050\pm0.0002$.

The last constant has been obtained by assuming p''_0 to have exactly the value $+0.0047$ given in a preceding section and by the comparison of differences $p'_n-p''_1$ with $p'_n-p''_0$ (all these differences are given at the end of this paper). The limits of errors for p'' and p' here and in all subsequent parts of this work refer to uncertainties relative to p''_0; the much greater uncertainty of the absolute value of p''_0 will not be included in these figures. The substate $v'_1=1$ of $^2\Pi_{1/2g}$ shows no evidence of any perturbation. Both substates a and b of $^2\Pi_{3/2g}$ are very anomalous: both have positive and relatively large D values, while the Λ-doublings have opposite signs in the a and b states and increase faster than proportionally to J^2. Since the exponent varies slightly with J it was decided not to try to represent the Λ-doubling by a simple formula but to give the dependence of Λ-doubling on J in the form of a graph. The curves 1^a and 1^b in Fig. 4 are directly obtained from the second differences in the P and R branches, since the levels $v'_1=0$, 1, 2, 3, and 4^b of $^2\Pi_{3/2u}$ show no observable Λ-doubling. Having obtained the Λ-doubling in the 1^a, $^2\Pi_{3/2g}$ substate, we determine the Λ-doublings in $v'_1=4^a$ and 5 of $^2\Pi_{3/2u}$ from the bands $(4^a, 1^a)$ and $(5, 1^a)$. The Λ-doubling of $^2\Pi_{3/2u}$, 4^a is almost equal to that of the $^2\Pi_{3/2g}$, 1^a substate and that of $^2\Pi_{3/2u}$, 5 amounts to a little more than a half of this.

The splitting of the state $^2\Pi_{3/2g}$, 1 into two substates must be caused by a very strong interaction with some other vibrational state of the $^2\Pi_{3/2g}$ or of the $^2\Pi_{1/2g}$ electronic state, since it is practically certain that no other electronic

TABLE III. Sub-bands $^2\Pi_{1/2u} \rightarrow {}^2\Pi_{1/2g}$.

$J-\frac{1}{2}$	(0,1) $\nu_0=27202.65$ R	P	(1,1) $\nu_0=28328.65$ R	P	(2,1) $\nu_0=29449.55$ R	P	(3,1) $\nu_0=30565.55$ R	P	(4,1) $\nu_0=31677.35$ R	P	(5,1) $\nu_0=32785.82$ R	P	$^2\Pi_{1/2g}(v''=1)$ Δ_2F_1'' Aver.	1st diff.
1		27201.49						30563.48						
2		00.64						62.64						
3		27199.76						61.60		31673.28				
4		98.78						60.55		72.33		32780.86		
5		97.77					30569.35	59.41	31680.92	71.17	32789.32	79.62		
6		96.68					30569.35	58.26	31680.92	70.00	32789.32	78.44	12.20	
7		95.53			29453.60		69.55 h	56.97	81.21 h	68.71	89.69 h	77.16	13.70	1.50
8		94.29			29453.60 h		69.55 e	55.72	81.21 e	67.42	89.69 e	75.93	15.20	1.50
9	27207.18	93.11	28333.01 h		53.68 e		69.55 a	54.23	81.21 a	66.00	89.69 a	74.47	16.70	1.50
10	27207.18 h	91.77	28333.01 e		53.68 a	29438.50	69.55 d	52.90	81.21 d	64.56	89.69 d	73.10	18.22	1.52
11	27207.18 e	90.40	28333.01 a		53.68 d	37.07	69.35	51.31	80.92	62.98	89.32	71.42	19.74	1.52
12	27207.18 a	88.98	28333.01 d	28314.79	53.60	35.52	69.35	49.84	80.92	61.45	89.32	69.92	21.28	1.54
13	27207.18 d	87.48		13.33	53.60	34.01	68.93	48.11	80.51	59.70	88.79	68.14	22.82	1.54
14	06.97	85.92	32.75	11.70	53.22	32.35	68.75	46.47	80.31	58.06	88.60	66.50	24.33	1.51
15	06.82	84.36	32.50	10.14	53.00	30.57	68.24	44.65	79.78	56.16	88.02	64.51	25.85	1.52
16	06.49	82.66	32.15	08.40	52.64	28.92	67.92	42.88	79.38	54.38	87.72	62.77	27.37	1.52
17	06.27	80.97	31.82	06.69	52.31	27.21	67.33	40.88	78.70	52.38	86.90	60.65	28.90	1.53
18	05.82	79.17	31.42	04.77	51.79	25.28	66.86	39.02	78.22	50.50	86.49	58.82	30.42	1.52
19	05.46	77.36	30.90	02.97	51.30	23.42	66.10	36.87	77.41	48.31	85.55	56.56	31.92	1.50
20	04.91	75.42	30.33	00.96	50.66	21.39	65.52	—Cu—	76.81	46.30	85.05	54.59	33.46	1.54
21	04.42	73.52	29.75	28299.04	50.13	19.38	64.59	32.63	75.85	43.95	83.90	52.17	34.97	1.51
22	03.75	71.46	29.02	96.90	49.28	17.20	63.90	30.52	75.12	41.84	83.27	50.06	36.47	1.50
23	03.14	69.45	28.40	94.86	48.59	15.13	62.89	28.12	73.98	39.33	81.98	47.50	38.01	1.54
24	02.37	67.28	27.57	92.58	47.64	12.80	62.00	25.87	73.17	37.10	81.28	45.27	39.54	1.53
25	01.64	65.14	26.81	90.41	46.84	10.53	60.85	23.32	71.88	34.47	79.78	42.50	41.05	1.51
26	00.74	62.83	25.83		45.73	08.08	59.93	20.98	70.93	32.11	78.94	40.18	42.56	1.51
27	27199.92	60.59	24.99		44.85	05.80	58.62	18.24	69.48	29.33	77.34	37.29	44.09	1.53
28	98.87	58.19			43.52	03.10	57.54	15.80	68.44	26.84	76.39	34.83	45.59	1.50
29	97.86	55.83			42.60	00.79	56.07	12.98	66.84	23.90	74.59	31.76	47.13	1.54
30	96.79	53.29			41.24	29398.04	54.91	10.38	65.69	21.33	73.54	29.26	48.62	1.49
31	95.76	50.83			40.05	95.47	53.34	07.38	63.94	18.27	71.69	25.97	50.17	1.55
32	94.47	48.18			38.64	92.63	52.00	04.70	62.64	15.51	70.52	23.35	51.66	1.49
33	93.33	45.60			37.30	89.93	50.22	01.58	60.77	12.28	68.37	19.95	53.20	1.54
34	91.91	42.83			35.65	87.00	48.81	30498.76	59.36	09.47	67.05	17.27	54.70	1.50
35	90.65	40.11			34.31		46.88	95.48	57.32	06.10	64.71	13.65	56.20	1.50
36	89.13	37.23			32.55		45.39	92.54	55.78	03.17	63.35	10.81	57.72	1.52
37	87.78	34.46					43.38	89.14	53.60	31599.59	60.93	07.06	59.26	1.54
38		31.40					41.74	86.07	51.95	96.53	59.47	04.12	60.76	1.50
39		28.51					39.53	82.55	49.58	92.85	56.83	00.19	62.30	1.54
40		25.36					37.77	79.33	47.87	89.68	55.27	32697.20	63.78	1.48
41		22.33					—Cu—	75.69	45.30	85.83	52.49	93.08	65.33	1.55
42		19.08					33.50	72.39	43.47	82.57	50.73	89.96	66.80	1.47
43		15.92					31.12	68.56	40.80	78.55		85.79	68.34	1.54
44		12.58					29.10	65.11	38.86	75.20		82.49	69.84	1.50
45		09.35					26.40	61.10	36.05	71.00		78.01	71.37	1.53
46		05.79					24.28	57.62	33.93	67.52		74.61	72.88	1.51
47		02.49					21.56	53.52	30.96	63.16		70.09	74.40	1.52
48		27098.86					19.31	49.92	28.77	59.53		66.61	75.92	1.52
49		95.36					16.47		25.66	55.04		61.88	77.41	1.49
50		91.66							23.37	51.36		58.31	78.92	1.51
51		88.02								47.64			80.50	1.58
52		84.23								42.87				
53		80.47								38.13				
54		76.43												

state is very close to the ground state. The smaller values of the constants D''_1 and F''_1 and of the Λ-doubling for the substate 1^b indicate that this substate is the less anomalous one and probably contains more of the character of the $v''_1=1$, $^2\Pi_{3/2g}$ substate than the other one (1^a). Nevertheless both interacting substates are certainly in a very close resonance; in fact, for the unperturbed $^2\Pi_{1/2g}$ substates $v''_1=0$ and 1, we obtain $\Delta G''_1=1265.75$ cm^{-1} which is only slightly more (1.2 cm^{-1}) than the average of $\Delta G''_1$ for the 1^a and 1^b substates. In Fig. 2 a level scheme is presented which shows the bands observed in the double progression $v''_1=1$, $^2\Pi_{3/2g}$ and the substates involved. The perturbations of the positions of the levels are drawn on a greatly exaggerated scale in order to make the relations more evident; the shifts Δ from the unperturbed positions are given in cm^{-1} on the right-hand side of the drawing. For the states $v''_1=1^a$ and 1^b, $^2\Pi_{3/2g}$ the Δ's were obtained by assuming the $\Delta G''_1$ value to be equal to 1265.75, in other words by assuming the $^2\Pi_g$ doublet separation to be independent of the vibrational quantum number. (This, of course, may not be quite correct. If, for example, actually the $^2\Pi_g$ separation decreases with increase in vibrational number, $\Delta G''_1$ would be greater than 1265.75, and the calculated Δ's would be more asymmetrical than in Fig. 1.) The Δ's for the excited state $^2\Pi_{3/2u}$ were calculated by assuming for the unperturbed positions of the levels the values obtained from the vibrational formula given at the end of this paper. The values of the vibrational constants

were chosen so as to make the Δ for the levels $v'_1=6$ and 7 ($^2\Pi_{3/2u}$) very small, as seems to be required by consideration of the dependence of the B' values on v'_1 (cf. Fig. 5). On the right-hand side of Fig. 2 is also given the magnitude of the Λ-doubling in cm^{-1} for the arbitrarily chosen sample level, $J=37\frac{1}{2}$. Astonishingly enough, positive perturbations of position ($\Delta>0$) are in the case of $^2\Pi_{3/2u}$ not accompanied by a positive Λ-doubling, as they are for $^2\Pi_{3/2g}$. Just the absence of a Λ-doubling was the reason for no anomalous behavior of the bands (3, 0) and (4, 0) [this last band will now be denoted (4^b, 0)] was observed in the case of the $v''_1=0$ progression described in Part I, although the values of the $\Delta G''$s pointed toward the existence of a perturbation.

All the transitions observed are represented in Fig. 2 by arrows, the thickness of the lines giving an idea about their relative intensities. Besides the transitions investigated and included in Tables I and II, two more arrows were inserted, including one corresponding to the band (1, 1^b) which has been observed, but which lines have not been measured, since they are extremely weak and barely visible among other stronger lines. The inclusion of this band would not increase the accuracy of the average values of $\Delta_2F''_1$. The position of the band edge was determined and found to agree very well with the predicted value. The second transition included in Fig. 1 is the band (6, 1^a) which was not observed in this work, but has been identified as the band λ2945 observed by Fox, Duffendack, and Barker[5] and by Smyth (Smyth's b_7 band).[6] The operation of a special selection rule can be inferred from Fig. 2: transitions with observable intensity occur between moderately or strongly perturbed levels only if the positions of both upper and lower level are shifted in the same direction. By denoting the levels with positive Δ's as type b, with negative Δ's as type a, this selection rule can be expressed in the following way: only the transitions $a\rightarrow a$ and $b\rightarrow b$ are strongly allowed. It is very astonishing that transitions from the moderately perturbed levels ($v'_1=2$, 3, and 5) to the other sublevel $v''_1=1$, $^2\Pi_{3/2g}$ do not occur at least weakly. This point, however, was carefully checked and no traces of any weak band edges were detected at the predicted positions. Unperturbed or very weakly perturbed levels are simultaneously of both type a and b. Since only one double level (i.e., a and b) in $^2\Pi_{3/2u}$ and one in $^2\Pi_{3/2g}$ were observed it is impossible to say at present if the direction of the shift solely determines the type of the level. The preliminary analysis shows that the level $v''_1=5$ of $^2\Pi_g$ (both substates) is very strongly perturbed, and it will probably be possible to study further the operation of the selection rule in that case. In general the relations are not completely clear, since a weak band edge corresponding to the transition (4^b, 2), $^2\Pi_{3/2u}\rightarrow{}^2\Pi_{3/2g}$ is observed, and no traces of a corresponding edge for the transition (4^a, 2) could be detected, although according to the rule only the latter should be present (see the next paragraph below: the substate $v''_1=2$, $^2\Pi_{3/2g}$ is perturbed downwards and has a negative Λ-doubling, hence should be of type a). On the other hand Fox, Duffendack, and Barker,[5] and Smyth[6] reported a quite strong band λ3280.5 (g_7)

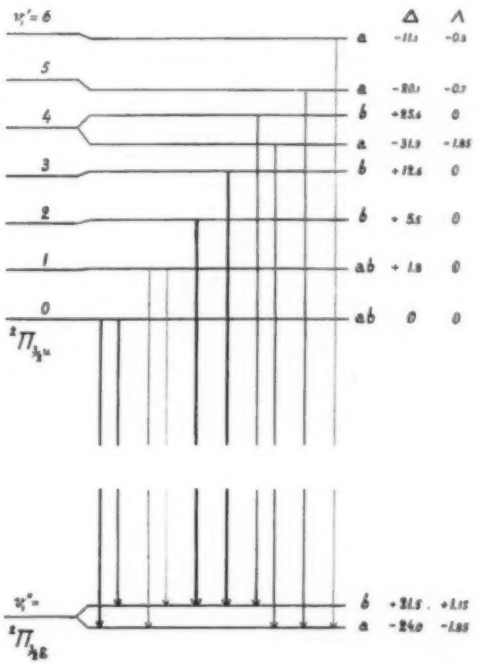

FIG. 2. Graphical presentation of transitions observed in the progression $v''_1=1$ for the sub-bands $^2\Pi_{3/2u}\rightarrow{}^2\Pi_{3/2g}$. Δ represents the shift (in cm^{-1}) from the calculated position of the level, caused by perturbation. Λ is the Λ-doubling for the level $J=37\frac{1}{2}$.

[5] G. W. Fox, O. J. Duffendack, and E. F. Barker, Proc. Nat. Acad. **13**, 320 (1927).
[6] H. D. Smyth, Phys. Rev. **38**, 2000 (1931).

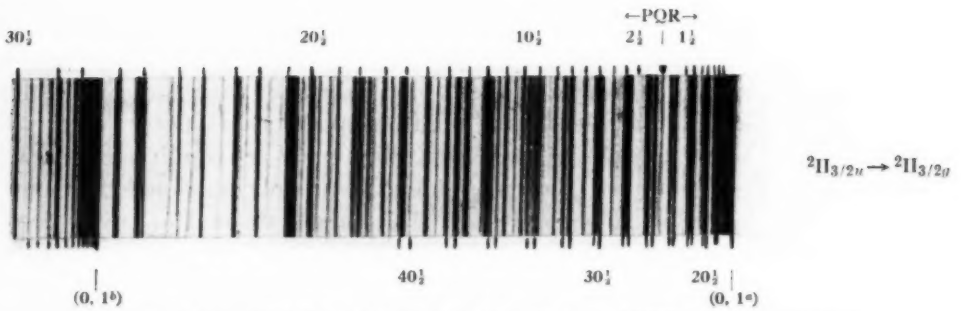

FIG. 3. Enlargement of a photograph of the sub-band λ3662 with the quantum numbers of lines given.

which exactly fits into the scheme as the missing $(4^a, 2)$ band. Further, the identification of the level 4^a, $^2\Pi_{3/2u}$ could be considered as doubtful, since the rotational analysis of only one band originating from this state was obtained. But a band edge at λ3032 has been detected that is exactly at the position where the sub-band $(4^a, 0)$ is expected. Since the lines of this band are very weak, approximately as weak as the lines of the sub-band $(4^b, 0)$, but are overlapped by the stronger sub-band $(4, 0)$ $^2\Pi_{\frac{1}{2}u} \rightarrow {}^2\Pi_{\frac{1}{2}g}$, no rotational analysis has been tried in this case.

The two sub-bands $(0, 1^a)$ λ3662.5 and $(0, 1^b)$ λ3668.8 form the greater part of the so-called double band λ3660, which was studied in detail with high resolution by Schmid.[7] The

[7] R. Schmid, Zeits. f. Physik **84**, 732 (1933).

TABLE IV. Sub-bands $^2\Pi_{3/2u} \rightarrow {}^2\Pi_{3/2g}$.

$J-\frac{1}{2}$	(0,2) $\nu_0=26035.67$ R	P	(1,2) $\nu_0=27162.45$ R	P	(2,2) $\nu_0=28285.20$ R	P	(5,2) $\nu_0=31580.50$ R	P	(6,2) $\nu_0=32684.55$ R	P	$^2\Pi_{3/2g}(v_1''=2)$ Δ_2F_2'' Aver.	1st diff.
2		26033.66								32681.66		
3		32.76								80.68		
4		31.80								79.62		
5		30.80				28280.28				78.43		
6		29.71				79.09		31574.39		77.23		
7		28.62				78.09	h	73.31	h	75.91		
8		27.43		27154.38		76.76	31584.26 e	71.94	32688.06 e	74.61	15.06	
9		26.23	h	53.00	28289.44 h	75.61	31584.26 a	70.66	32688.06 a	73.20	16.55	1.49
10	26040.25 h	24.91	27166.90 e	51.79	28289.44 e	74.14	31584.26 d	69.26	32688.06 d	71.68	18.07	1.52
11	26040.25 e	23.60	27166.90 a	50.32	28289.44 a	72.88		67.74		70.09	19.58	1.51
12	26040.25 a	22.17	27166.90 d	48.91	28289.44 d	71.43		66.20		68.48	21.10	1.52
13	26040.25 d	20.75		47.30		69.92	83.79	64.55	87.52	66.73	22.60	1.50
14	40.12	19.21	66.70	45.83		68.29	83.46	62.89	87.26	65.02	24.12	1.52
15	40.00	17.67	66.49	44.27	88.91	66.73	83.03	61.09	86.83	63.19	25.64	1.52
16	39.72	16.01	66.24	42.58	88.58	65.00	82.57	59.28	86.39	61.24	27.14	1.50
17	39.45	14.36	65.89	40.88	88.23	63.27	82.11	57.35	85.79	59.25	28.63	1.49
18	39.08	12.59	65.46	39.07	87.78	61.44	81.48	55.44	85.21	57.20	30.13	1.50
19	38.69	10.83	65.07	37.23	87.30	59.58	80.75	53.37	84.52	55.10	31.64	1.51
20	38.20	08.93	64.49	35.34	86.71	57.58	80.08	51.36	83.75	52.91	33.14	1.50
21	37.73	07.08	64.02	33.40	86.14	55.66	79.21	49.12	82.85	50.61	34.65	1.51
22	37.11	05.08	63.33	31.39	85.41	53.56	78.42	46.90	82.05	48.28	36.16	1.51
23	36.53	03.10	62.79	29.35	84.74	51.49	77.42	44.54	81.04	45.89	37.67	1.51
24	35.78	00.97		27.14	83.89	49.25	76.50	42.27	80.04	43.38	39.16	1.49
25	35.11	25998.88		25.03	83.10	47.08	75.30	39.70	78.88	40.90	40.67	1.51
26	34.23	96.64		22.70	82.13	44.71	74.39	37.40	77.72	38.19	42.19	1.52
27	33.45	94.47		20.45	81.23	42.43	72.97	34.59	76.44	35.57	43.69	1.50
28	32.44	92.08		18.00	80.06	39.91	71.94	32.10	75.21	32.83	45.21	1.52
29	31.58	89.81			79.09	37.53	70.38	29.22	73.80	29.90	46.71	1.50
30	30.46	87.28			77.82	34.81	69.16	26.65	72.38	27.08	48.22	1.51
31	29.51	84.93			76.76	32.36	67.52		70.84	24.18	49.72	1.50
32	28.24	82.24			75.29	29.62	66.16		69.25	21.07	51.22	1.50
33	27.19	79.82			74.14	27.02	64.14		67.55	18.01	52.72	1.50
34	25.79	77.01			72.54	24.10			65.77	14.88	54.23	1.51
35	24.64	74.48			71.28	21.38			63.98	11.57	55.73	1.50
36	23.09	71.55			69.54	18.33			62.12	08.25	57.23	1.50
37	21.86	68.91			68.14	15.54			60.17	04.90	58.72	1.49
38	20.16	65.84			66.28	12.33			58.17	01.43	60.22	1.50
39	18.85	63.12			64.77	09.47			56.08	32598.06	61.70	1.48
40	17.03	59.91			62.79	06.06					63.24	1.54
41	15.62	57.11			61.20	03.12					64.72	1.48
42	13.65	53.78			59.04	28199.56					66.22	1.50
43	12.17	50.85			57.42							
44	10.04	47.43			55.08							
45	08.53				—							
46	06.22				50.84							
47	04.57				—							
48	02.14				46.33							
49	00.43											

TABLE V. Sub-bands $^2\Pi_{\frac{1}{2}u} \rightarrow {}^2\Pi_{\frac{1}{2}g}$.

$J-\frac{1}{2}$	(0,2) $\nu_0=25945.78$ R	P	(1,2) $\nu_0=27071.75$ R	P	(2,2) $\nu_0=28192.65$ R	P	(5,2) $\nu_0=31528.95$ R	P	(6,2) $\nu_0=32635.95$ R	P	$^2\Pi_{1/2g}(v_1''=2)$ Δ_2F_2'' Aver.	1st diff.
3								31526.05		32633.06		
4	25948.77	25942.00						25.08		32.02		
5		40.96		27066.92				24.10		31.02		
6	49.55	39.92		65.80			31532.66	22.88	32639.62	29.90		
7		38.75		64.66			31532.66	21.73	32639.62	28.71	12.15	
8		37.58		63.47		28184.31	32.90 h	20.42	39.84 h	27.37	13.65	1.50
9		36.36	27076.32 h	62.21	28196.97 h	83.06	32.90 e	19.17	39.84 e	26.15	15.15	1.50
10	50.51 h	35.10	27076.32 e	60.92	28196.97 e	81.69	32.90 a	17.73	39.84 a	24.60	16.65	1.50
11	50.51 e	33.72	27076.32 a	59.56	28196.97 a	80.33	32.90 d	16.37	39.84 d	23.30	18.17	1.52
12	50.51 a	32.28	27076.32 d	58.12	28196.97 d	78.83	32.66	14.75	39.62	21.62	19.70	1.53
13	50.51 d	30.84	27076.32	56.62		77.36	32.66	13.24	39.62	20.18	21.22	1.52
14	50.34	29.33	76.08	55.08	96.67	75.74	32.27	11.50	38.97	18.38	22.75	1.53
15	50.22	27.79	75.90	53.52	96.49	74.12	32.09	09.90	38.97	16.81	24.25	1.50
16	49.99	26.15	75.63	51.77	96.12	72.40	31.50	07.97	38.19	14.88	25.78	1.53
17	49.74	24.50	75.34	50.12	95.80	70.68	31.16	06.29	38.19	13.22	27.29	1.51
18	49.36	22.70	74.90	48.30	95.34	68.81	30.51	04.19	37.31	11.07	28.82	1.53
19	49.00	20.98	74.52	46.52	94.90	66.97	30.05	02.34	36.96	09.30	30.34	1.52
20	48.54	19.06	73.97	44.56	94.29	64.97	29.22	00.16	36.02	06.96	31.86	1.52
21	48.07	17.18	73.47	42.67	93.74	63.06	28.65	31498.21	35.57	05.06	33.37	1.51
22	47.49	15.16	72.79	40.61	92.98	60.94	27.60	95.86	34.37	02.62	34.88	1.51
23	46.92	13.22	72.18	38.65	92.34	58.89	26.99	93.79	33.96	00.70	36.37	1.49
24	46.20	11.10	71.39	36.42	91.48	56.62	25.82	91.31	32.62	32598.06	37.90	1.53
25	45.52	09.00	70.68	34.27	90.71	54.44	25.08	89.05	32.02	96.01	39.40	1.50
26	44.68	06.79	69.76	31.98	89.71	52.07	23.73	86.48	30.52	93.19	40.94	1.54
27	43.89	04.60	68.89	29.73	88.81	49.77	22.88	84.18	29.90	90.98	42.43	1.49
28	42.96	02.28	67.90	27.32	87.74	47.28	21.43	81.32	28.16	88.04	43.97	1.54
29	42.00	25899.92	66.92	24.99	86.68	44.87	20.42	78.88	27.37	85.80	45.46	1.49
30	40.96	97.52	65.80	22.45	85.50	42.26	18.81	75.96	25.56	82.69	46.98	1.52
31	39.90	95.08	64.66	19.95	84.31	39.71	17.73	73.44	24.60	80.32	48.48	1.50
32	38.75	92.55	63.47	17.27	82.98	36.96	15.94	70.32	22.63	77.02	50.00	1.52
33	37.58	89.94	62.21	14.66	81.69	34.34	14.75	67.76	21.62	74.52	51.50	1.50
34	36.36	87.35	60.92	11.99	80.26	31.42	12.81	64.48	19.41	71.09	53.04	1.54
35	35.03	84.63	59.56	09.16	78.83	28.64	11.58	61.73	18.38	68.55	54.54	1.50
36	33.78	81.95	58.12	06.33	77.29	25.68	09.38	58.25	15.98	64.90	56.08	1.54
37	32.28	79.06	56.62	03.44	75.74	22.76	07.97	55.44	14.88	62.30	57.55	1.47
38					74.12	19.68	05.70	51.84	12.37		59.11	1.56
39					72.40	16.62	04.19	48.93	11.07		60.57	1.46
40					70.68	13.45	01.80	45.14	08.25		62.14	1.57
41						10.27	00.16	42.12	06.96		63.60	1.46
42						06.92	31497.60	38.14	04.23		65.17	1.57
43						03.61	95.86	35.12	02.65		66.64	1.47
44						00.22	93.20	30.96			68.15	1.51
45							91.31	27.83				
46							88.49					
47							86.48					
48							83.66					
49							81.32					

new photographs show that Schmid's sub-band λ3661.5 is non-existent, and that the sub-band λ3670.2 is formed by an irregular grouping of lines which definitely do not belong to our system. The real structure of the two sub-bands λ3662.5 and λ3668.8 was not recognized by Schmid, because of the lower resolution available to him. The extremely great Λ-doubling in the level 1^a is the cause of the misleading apparent doublet structure in the lines of the sub-band λ3662.5 (see Fig. 3). Schmid investigated the Zeeman effect in the CO_2^+ bands and found that, in the entire region 3000–4000A, only the double band λ3660 shows noticeable effects. This is in excellent agreement with the classification given above, since for all bands ending on one of the two levels 1^a and 1^b strong Zeeman shifts are expected. The absence of an influence of the magnetic field on all the unperturbed $^2\Pi_u \rightarrow {}^2\Pi_g$ bands is to be explained by an approximate equality of the Zeeman shifts of energy levels in the upper and lower states, together with the selection rules for the magnetic quantum numbers.[8] If, however, one of the states is perturbed by another possessing a very different magnetic behavior, considerable shifts of lines should be produced. According to this explanation all bands corresponding to transitions involving perturbed levels in Fig. 2 should show relatively strong Zeeman effects. Unfortunately, among these transitions, only the double band λ3660 was observed by Schmid, since all the others are situated on the long wave-length sides of bands belonging to the progression $v''_1=0$ and are strongly overlapped by the P branch lines of these bands; this was especially unfavorable in the case of Schmid's investigations because the temperature of the discharge was in his case quite considerable.

[8] F. H. Crawford, Rev. Mod. Phys. 6, 90 (1934).

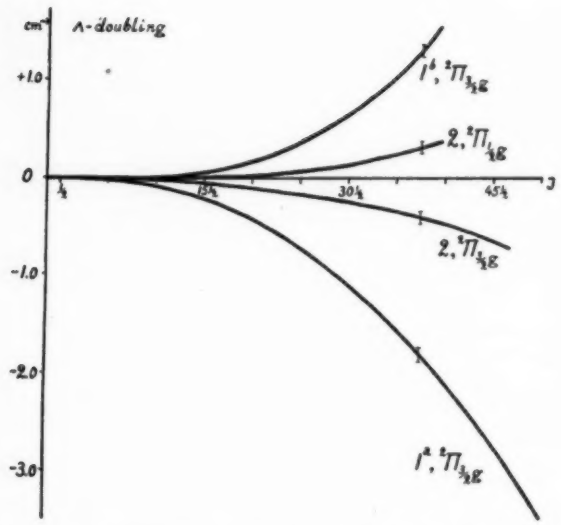

FIG. 4. Λ-doubling of rotational states in the ground state $^2\Pi_g$ of the CO_2^+ molecule for $v''_1=1$ and 2. In each case the uncertainty limits of the doubling are marked by a bar.

The $v_1''=2$ progression of bands

The wave numbers of the lines and the average $\Delta_2F''_2$ values for the levels $v''_1=2$, $^2\Pi_g$ are given in Tables IV and V. The molecular constants obtained from $\Delta_2F''_2$ for the ground state of CO_2^+ with two quanta of the symmetrical vibration ($v''_1=2$) are the following:

$$\begin{aligned} ^2\Pi_{3/2g} \quad & B''_2=0.3769\pm0.0001 \\ & D''_2=-(1.5\pm0.2)\times10^{-7} \\ ^2\Pi_{1/2g} \quad & B''_2=0.3793\pm0.0001 \\ & D''_2=-(1.6\pm0.2)\times10^{-7}. \end{aligned}$$

The Λ-doubling is in both substates anomalous. For the substate $^2\Pi_{3/2g}$ it is negative showing that this level is probably shifted downwards by a perturbation. The same conclusion can be reached by considering the B''_2 value, which appears to be lower than the value 0.3773 calculated on basis of the formula given at the end of this paper. In case of the substate $^2\Pi_{1/2g}$ the sign of the anomalous Λ-doubling and the anomaly in the B''_2 are opposite to those in $^2\Pi_{3/2g}$. The total Λ-doubling for the $^2\Pi_{3/2g}$ substate and the increase of the Λ-doubling relative to the level $v''_1=1$ for the $^2\Pi_{1/2g}$ substate are given in Fig. 4. It is very probable that in the last case the increase is composed of two parts: one linearly dependent on J and corresponding to the increase of the coefficient p'' in passing from $v''_1=0$ to $v''_1=1$ and $v''_1=2$ (probable increase of p'' around 0.0003) and another greater part caused by the perturbation mentioned and increasing approximately proportionally to $J^{2.5}$.

From the data obtained in the analysis of all three progressions $v''_1=0$, $v''_1=1$, and $v''_1=2$ the constants for all excited $^2\Pi_u$ levels so far identified can be calculated. The values obtained for $p'-p''$ in the levels $^2\Pi_{1/2u}$ are:

$p'_0-p''_0=0.0030$	$p'_0-p''_1=0.0027$	$p'_0-p''_2=0.0025$
$p'_1-p''_0=0.0037$	$p'_1-p''_1=0.0033$	$p'_1-p''_2=0.0033$
$p'_2-p''_0=0.0049$	$p'_2-p''_1=0.0046$	$p'_2-p''_2=0.0044$
$p'_3-p''_0=0.0065$	$p'_3-p''_1=0.0061$	
$p'_4-p''_0=0.0087$	$p'_4-p''_1=0.0082$	
	$p'_5-p''_1=0.0110$	$p'_5-p''_2=0.0106$
		$p'_6-p''_2=0.0148.$

The differences $p'_n-p''_2$ were obtained from the staggering for low rotational lines where the influence of the anomalous Λ-doubling cannot be felt. From these values and the value of p''_0 the following Λ-doubling constants are obtained:

$p'_0=0.0077\pm0.0002$	$p'_3=0.0112\pm0.0002$
$p'_1=0.0084\pm0.0002$	$p'_4=0.0133\pm0.0003$
$p'_2=0.0096\pm0.0002$	$p'_5=0.0161\pm0.0004$
	$p'_6=0.0201\pm0.0006.$

The B' constants could now be determined with higher accuracy than the values reported in Part I. Since still better values will be available after the analysis of higher progressions is

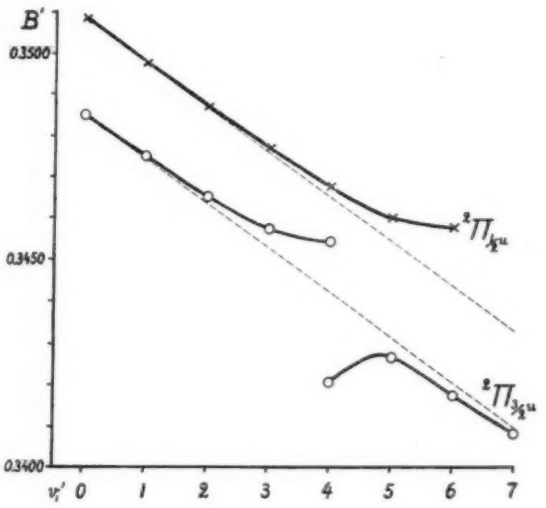

FIG. 5. Graphical presentation of the change of the B' value with vibrational quantum number v'_1 for the excited state $^2\Pi_u$.

completed, the results obtained are presented here only in the form of a graph in Fig. 5, where for $^2\Pi_{3/2u}$ a point found from the analysis of the sub-band (7, 3) has been added. The increasing perturbation of the $^2\Pi_{1u}$ substates with increasing v'_1 is clearly indicated; up to now, however, the expected double level $v'_1=7$ has not been identified. For the double substate $^2\Pi_{3/2u}$, 4 as in the case of the double level $^2\Pi_{3/2g}$, 1, we find that the average value of the B's obtained is smaller than the value calculated assuming a linear decrease of the B's in both substates. This can be explained if the perturbing state possesses a smaller value of B than the substates given. On the contrary, for the substates possessing two quanta of bending vibration, a B value greater than that for the lowest level is expected. In fact, this relation has been confirmed in the cases of CS_2 and CO_2.[9] On the other hand, the perturbation by the double bending vibration seems to offer the only possibility of explanation of the existence of the described perturbation in the ground state $^2\Pi_g$, $v''_1=1$. Since the ground state of the CO_2^+ molecule is different from the molecules of CS_2 and CO_2 and represents a more complicated case a thorough theoretical examination of this case seems to be necessary. The general discussion of Λ-doublings, perturbations, and their probable causes is postponed until all data concerning the $^2\Pi_u \rightarrow {}^2\Pi_g$ system of bands are available.

In view of the perturbations present in higher vibrational levels of both states $^2\Pi_g$ and $^2\Pi_u$ formulas for unperturbed values of B's and the unperturbed energy levels as functions of the quantum number of the symmetrical vibration can be calculated on the basis of data already obtained. These values will not be improved by the subsequent extension of the analysis of the $^2\Pi_u \rightarrow {}^2\Pi_g$ system of bands. The formulas are found by assuming the spin doubling to be independent of the vibrational energy of the molecule, which for the lowest levels should represent at least a fair approximation.

$$^2\Pi_g: \quad B''_v = B''_0 - 0.0012v''_1;$$
$$T''(v_1) = T''_0(0) + 1280v''_1 - 7.25v''_1(v''_1+1)$$
$$^2\Pi_u: \quad B'_v = B'_0 - 0.0011v'_1;$$
$$T'(v_1) = T'_0(0) + 1131v'_1 - 3.0v'_1(v'_1+1).$$

The equilibrium constants and the origins of both subsystems cannot be found since the dependence on the two other vibrational quantum numbers v_2 and v_3 is not known. The spin-orbit coupling constant A for $^2\Pi_u$ is -95.4 cm^{-1}.

The author is very much indebted to Professor R. S. Mulliken for many discussions and suggestions and to Messrs. J. B. Coon and T. J. Kinyon for assistance in computations.

[9] L. S. Liebermann, Phys. Rev. 60, 496 (1941).

The Problem of the Rotating Disk

CARLTON W. BERENDA
College of the City of New York, New York, New York

(Received May 29, 1942)

In Part I of this paper, the spatial geometry of the surface of a rotating disk is examined from the standpoint of general relativity theory. Eddington's argument for a homaloidal surface is shown to be in error, and Einstein's "relative" geometry is correlated with the "intrinsic" geometry of the disk (i.e., the geometry as determined by an observer at rest on the rotating disk). The Gaussian measure of hypercurvature of the surface, at any point on the disk at radius r is found to be $-3\frac{\omega^2}{c^2}\left(1-\frac{\omega^2 r^2}{c^2}\right)^{-2}$. In Part II, the temporal aspects of the rotating disk are examined and a new test of general relativity, by use of the cyclotron, is proposed: an artificially radioactive element of low atomic weight is revolved, as ions, within the cyclotron. Upon being brought to rest, the element should be found *more radioactive* than an equivalent sample of that element remaining at rest.

PART I. GEOMETRY

THE problem of the rotating disk, in relativity theory, is associated with the names of Ehrenfest, Einstein, Lorentz, and Eddington.

Einstein's Geometry

Einstein and Infeld have argued that a rigid disk under uniform angular velocity ω relative to a galilean frame, will exhibit a non-euclidean geometry in the definite sense that the circumference of the disk will no longer equal $2\pi r$, where r is the radius of the disk. More precisely, we fix small rigid rods along the entire disk's periphery at right angles to the radii of the disk. We also surround the edge of the disk with similar, small, rigid rods at rest, in galilean space, with respect to the disk's center. Let us measure such a rod $\bar{P}$ fixed on the disk at r as it passes any rod P' fixed in galilean space. Then relative to the G (galilean) observer, who uses the rod P', the measured length of the adjacent rod on the disk is

$$\bar{P}=P'\left(1-\frac{v^2}{c^2}\right)^{\frac{1}{2}},$$

where $v=\omega r$. Hence $\bar{P}<P'$. This is in accordance with the special theory, and appears to be correct, even though, as we shall see, the complete analysis of the problem requires the formulae of the general theory and superimposes an *additional* effect upon the measurement of $\bar{P}$. Rods at right angles to P (i.e., rods directed along the radius) will not contract, by the special theory, since r is at right angles to the line of motion (v). Hence the measured radius is not affected by the rotation. Each G observer finds the adjacent rod on the disk to have the length $\bar{P}$. If we now add up the measuremental results of the G observers all around the disk, we find

$$\bar{C}=\sum\bar{P}=\sum P'\left(1-\frac{v^2}{c^2}\right)^{\frac{1}{2}}=C'\left(1-\frac{v^2}{c^2}\right)^{\frac{1}{2}}<C',$$

where

$$\sum P'=C'=2\pi r$$

which is the circumference of the disk when it is at rest in the G frame; and $\bar{C}$ is the circumference of the rotating disk relative to the G observers. Then

$$\bar{C}=2\pi r\left(1-\frac{v^2}{c^2}\right)^{\frac{1}{2}}<2\pi r,$$

so that the geometry of the rotating disk is apparently non-euclidean.[1]

Opposed to this point of view are A. S. Eddington, H. A. Lorentz, and H. Levy who contend that the geometry of the rotating disk remains euclidean.[2]

The first part of this paper will attempt to demonstrate the error in Eddington's argument, as well as to distinguish between the "relative"

[1] Cf. A. Einstein and L. Infeld, *Evolution of Physics*, pp. 240–42; also Infeld's review, in *Science and Society* **4**, 236 (1940), of H. Levy's *Modern Science* (p. 595).

[2] A. Eddington, *Mathematical Theory of Relativity* (1923), §4 and p. 36; *Space, Time and Gravitation*, p. 75. H. Lorentz, *Nature* **106**, 795; *Collected Papers*, Vol. 7 (1934), pp. 171–72.

geometry of Einstein and an "intrinsic" geometry obtained by an observer at rest on the rotating disk. It is shown that the intrinsic geometry of the disk is one whose Gaussian measure of surface hypercurvature is negative and variable. Superimposed on the intrinsic geometry there is, for a galilean observer, the relative geometry such that

$$\bar{C}=C_0\left(1-\frac{v^2}{c^2}\right),$$

where C_0 is the circumference of the rotating disk as measured by an observer at rest on the disk.

$$C_0=2\pi r\left(1-\frac{v^2}{c^2}\right)^{-\frac{1}{2}}>2\pi r.$$

Transformation Equations

To deal with the problem systematically, we may proceed as follows: Allow a G observer to assign cartesian or polar coordinates fixed on the rotating disk, with the center O of the disk as the origin of the coordinates. To make this assignment, we have to consider the relation of our galilean measures x', y' to the rotating coordinates x, y. The constant angular velocity of the disk is $\omega=d\theta'/dt'$. Now $d\theta'$ is the measured angle element swept out by a radial coordinate on the disk, as measured from some base line fixed in G space and originating at O. The time dt' is the time required for sweeping out $d\theta'$, and is measured at O. We then take

$$\begin{aligned} x'&=x\cos\omega t-y\sin\omega t \\ y'&=x\sin\omega t+y\cos\omega t \quad t'=t, \end{aligned} \tag{1}$$

to which we may add $z'=z$, since the rotation is around the z axis at O. These equations *define* the cartesian coordinates on the disk. They are the equations of motion of a point fixed on the disk rotating in G space.

We must briefly consider the time coordinate. We may place a clock at O in G space. In assigning a coordinate time to events fixed on the disk, we do not correct for the time light requires to pass from the event to the clock at O. We simply assign time coordinate values to events on the disk as observed at O, using the G clock. If we call t the coordinate time of an event anywhere on the disk, then we identify the coordinate time t with the time t' of the event's observation as measured by the G clock at O. Hence the above equation $t'=t$. It follows from these equations that

$$x'^2+y'^2=x^2+y^2,$$

so that the radial cartesian coordinate vector r equals the galilean measured value r'.

We now employ the rule that G space and time readings satisfy the relation

$$ds^2=dt'^2-\frac{1}{c^2}[dx'^2+dy'^2+dz'^2],$$

where $|ds|$ is an invariant with the dimensions of seconds. From our transformation equations we obtain:

$$\begin{aligned} dx'&=\cos\omega t\cdot dx-\sin\omega t\cdot dy-\omega(x\sin\omega t+y\cos\omega t)dt \\ dy'&=\sin\omega t\cdot dx+\cos\omega t\cdot dy+\omega(x\cos\omega t-y\sin\omega t)dt \\ dz'&=dz;\quad dt'=dt. \end{aligned}$$

Substituting these values in the space-time equation we find that

$$ds^2=\left[1-\frac{\omega^2}{c^2}(x^2+y^2)\right]dt^2-\frac{1}{c^2}[-2\omega ydxdt +2\omega xdydt+dx^2+dy^2+dz^2]. \tag{2}$$

This may also be written in centimeters as $d\bar{s}^2=c^2ds^2$.

Eddington's Geometry

I shall now present Eddington's argument apparently demonstrating that both the radius and the circumference of a rotating disk contract by the same amount; we therewith obtain, or assume, homaloidal space. The following argument appears legitimate up to a certain point where objections will be raised.

Consider a disk having absolute rigidity, i.e., it is incompressible under duress of force, or, its moduli of elasticity are infinitely great. Thus, such a disk, resting in a G frame, if subjected to any external forces upon its rim, would undergo no contraction, extension, or torsion.

We now apply an equation obtained from a theorem of Jacobi, showing that between fixed

limits of integration we have

$$\int\int\int\int(-g')^{\frac{1}{2}}\cdot dx'_1dx'_2dx'_3dx'_4 = \int\int\int\int(-g)^{\frac{1}{2}}\cdot dx_1dx_2dx_3dx_4,$$

where $x_4=ct$ and g is negative and is the determinant of $g_{\lambda\mu}$ in the line element of four dimensions

$$ds^2=g_{\alpha\beta}dx_\alpha dx_\beta.$$

In infinitesimal regions this gives

$$dT=(-g)^{\frac{1}{2}}dx_1dx_2dx_3dx_4,$$

where dT is an invariant four-dimensional volume element that can be written in proper measures as

$$dT=dx_0dy_0dz_0d\bar{s}_0,$$

where the proper time, in centimeters, is

$$d\bar{s}_0=(g_{44})^{\frac{1}{2}}\cdot dx_4.$$

We then obtain

$$dx_0dy_0dz_0=(-g/g_{44})^{\frac{1}{2}}dx_1dx_2dx_3. \qquad (A)$$

Now in the expression (from which $d\bar{s}_0$ is obtained):

$$d\bar{s}^2=\left[1-\frac{\omega^2}{c^2}(x^2+y^2)\right]dx_4{}^2-\left[-\frac{2\omega y}{c}dxdx_4+\frac{2\omega x}{c}dydx_4+dx^2+dy^2+dz^2\right]$$

we have

$$g=\begin{vmatrix} -1 & 0 & 0 & \frac{\omega y}{c} \\ 0 & -1 & 0 & \frac{-\omega x}{c} \\ 0 & 0 & -1 & 0 \\ \frac{\omega y}{c} & \frac{-\omega x}{c} & 0 & \left[1-\frac{\omega^2}{c^2}(x^2+y^2)\right] \end{vmatrix}$$

from which $g=-1$ and

$$g_{44}=\left[1-\frac{\omega^2}{c^2}(x^2+y^2)\right]=\left(1-\frac{\omega^2r^2}{c^2}\right).$$

From (A) we then obtain

$$dx_0dy_0dz_0=\left(1-\frac{\omega^2r^2}{c^2}\right)^{-\frac{1}{2}}dxdydz. \qquad (B)$$

It is now convenient to transform to polar coordinates. The element of area is

$$dxdy=rd\theta dr.$$

Then in (B):

$$r_0d\theta_0dr_0dz_0=\left(1-\frac{\omega^2r^2}{c^2}\right)^{-\frac{1}{2}}rd\theta drdz.$$

Since there is no motion along the z axis, $z=z_0$. Hence

$$r_0d\theta_0dr_0=\left(1-\frac{\omega^2r^2}{c^2}\right)^{-\frac{1}{2}}rd\theta dr. \qquad (C)$$

It is at this point that our objection to Eddington's argument begins. Eddington sets

$$r_0dr_0=\left(1-\frac{\omega^2r^2}{c^2}\right)^{-\frac{1}{2}}rdr. \qquad (C')$$

Then

$$\int_0^{r_0}r_0dr_0=\int_0^r\left\{1-\frac{\omega^2r^2}{c^2}\right\}^{-\frac{1}{2}}rdr$$

or

$$\tfrac{1}{2}r_0{}^2=\frac{c^2}{\omega^2}\left\{1-\left(1-\frac{\omega^2r^2}{c^2}\right)^{\frac{1}{2}}\right\}$$

or finally

$$r=r_0\left(1-\frac{\omega^2r_0{}^2}{4c^2}\right)^{\frac{1}{2}}. \qquad (C'')$$

This gives, to a first approximation

$$r=r_0\left(1-\frac{\omega^2r_0{}^2}{8c^2}\right),$$

which is the result obtained by Eddington and Lorentz.

Up to and including Eq. (C), there seems to be no valid objection to the argument, but in stating (C'), Eddington is assuming that $d\theta_0=d\theta$. This, however, is the whole point at issue, since the latter assumption is equivalent to the postulate that angular measures are unaffected by rotation, i.e., that the geometry remains euclidean. In fact, Eddington and Lorentz show that circumference and radius both contract in

the same ratio relative to a G observer. Thus, an element of the relative circumference would be

$$dC = r d\theta.$$

Likewise, an element of the proper circumference would be

$$dC_0 = r_0 d\theta_0.$$

But from the Eddington argument $\theta = \theta_0$ and

$$C = r\int_0^{2\pi} d\theta,$$

then

$$C = \left(1 - \frac{\omega^2 r_0^2}{4c^2}\right)^{\frac{1}{2}} r_0 \int_0^{2\pi} d\theta_0 = \left(1 - \frac{\omega^2 r_0^2}{4c^2}\right)^{\frac{1}{2}} C_0.$$

Now it is true that the necessary and sufficient condition for "flat" or homaloidal space-time is the vanishing of the Riemann-Christoffel tensor, that is

$$R^{\tau}_{\mu\nu\sigma} = 0 \quad \text{where} \quad \mu, \nu, \sigma, \tau = 1, 2, 3, 4.$$

And this condition is satisfied when one can transform away the *entire* gravitational field. This is implicit in the *integral* transformation Eqs. (1) for x, y, z, t.[3]

However, this argument is valid only for the geometry of space-time—it is not necessarily valid for a sub-space such as the surface of the rotating disk. In general, the condition for homaloidality in n space, namely,

$$R^{\tau}_{\mu\nu\sigma} = 0 \quad \text{where} \quad \mu, \nu, \sigma, \tau = 1, 2, \cdots, n$$

is not always applicable to a space of $n-m$ dimensions, where $m \leqslant n-1$. Of course, the conditions

$$R_{\mu\nu} = R^{\alpha}_{\mu\nu\alpha} = 0$$

and

$$R = g^{\alpha\beta} R_{\alpha\beta} = 0$$

are also satisfied for the space-time ($n=4$) of the disk, but not necessarily for the surface space ($n=2$) of the disk.

Intrinsic Geometry

Another confusion that appears to arise, in arguing for homaloidal space on the disk, is the improper inference that, to obtain the proper spatial geometry, it is sufficient to take t as constant in the equation

$$d\bar{s}^2 = c^2\left[1 - \frac{\omega^2}{c^2}(x^2+y^2)\right]dt^2 - [-2\omega y dx dt + 2\omega x dy dt + dx^2 + dy^2 + dz^2],$$

thereby obtaining

$$d\bar{s}_1{}^2 = -[dx^2 + dy^2 + dz^2].$$

Defining the proper spatial interval as

$$dl = i d\bar{s}_1,$$

we have

$$dl = (dx^2 + dy^2 + dz^2)^{\frac{1}{2}},$$

therewith apparently indicating euclidean geometry once more.

The error in this argument was pointed out by M. von Laue.[4] In order to obtain the purely spatial geometry of the disk, one must select a vector at *right angles* to the world lines of points fixed on the disk. It is not sufficient, for this purpose, to set x_4 equal to a constant and therefore $dx_4 = 0$. The latter is permissible only when $g_{a4} = 0$ for $a = 1, 2, 3$—that is, *if the time axis is everywhere at right angles to the spatial extension*. Parenthetically, it should be remarked that while it is a quite natural geometrical requirement to obtain the three-dimensional sub-space from space-time through this orthogonality condition, it does not follow logically from this, that we may identify rigid metric rod readings on the disk with spatial dimensions and geometry derived from such orthogonality. The identification is a matter of assumption—a convenient one no doubt. This assumption appears related to a fundamental arbitrary feature in the definition of a rigid body that I have dealt with more fully elsewhere.[5]

To return to the basic argument, let us transform our line element $d\bar{s}$ through the equations

$$x = r\cos\theta \quad \text{and} \quad y = r\sin\theta.$$

[3] See R. Tolman, *Relativity, Thermodynamics and Cosmology*, pp. 185–86; R. Lindsay and H. Margenau, *Foundations of Physics*, pp. 360–63.

[4] M. von Laue, *Die Relativitätstheorie*, Vol. 2, pp. 142–43.

[5] Carlton B. Weinberg, Phil. Sci. **8**, No. 4, pp. 506–532; 618–623.

Then we may write

$$-d\bar{s}^2=dr^2+r^2d\theta^2+dz^2+\frac{r^2\omega}{c}d\theta dct$$
$$+\frac{r^2\omega}{c}dctd\theta-\left(1-\frac{\omega^2r^2}{c^2}\right)dc^2t^2$$

or

$$-d\bar{s}^2=dx_1^2+r^2dx_2^2+dx_3^2$$
$$+\frac{2r^2\omega}{c}dx_2dx_4-\left(1-\frac{\omega^2r^2}{c^2}\right)dx_4^2$$
$$=g_{11}dx_1^2+g_{22}dx_2^2+g_{33}dx_3^2$$
$$+2g_{24}dx_2dx_4+g_{44}dx_4^2.$$

Now the angles between the various coordinates are given by the direction cosines

$$\cos(\mu,\nu)=\frac{g_{\mu\nu}}{(g_{\mu\mu}\cdot g_{\nu\nu})^{\frac{1}{2}}},$$

where (μ,ν) is the angle between the x_μ and x_ν coordinates.[6] We can readily see that the angles $(\mu,4)$ equal 90° except for $\mu=2$. Thus we have

$$\cos(2,4)=\frac{g_{24}}{(g_{22}\cdot g_{44})^{\frac{1}{2}}}=\frac{r^2\omega/c}{\left[r^2\left[-\left(1-\frac{\omega^2r^2}{c^2}\right)\right]\right]^{\frac{1}{2}}}$$

or

$$i\cos(2,4)=\frac{r\omega}{c}\left(1-\frac{\omega^2r^2}{c^2}\right)^{-\frac{1}{2}},$$

which gives an imaginary angle between x_2 and x_4 that is a function of r and is equivalent to 90° only when $r=0$.

Hence we find that in $d\bar{s}^2$ the time axis is not everywhere at right angles to the spatial dimensions. We must therefore choose a (four-component) vector which does satisfy this condition.

We take a contravariant vector Δx_μ and the covariant vector $g_{\nu\beta}dx_\beta$ at right angles to each other, so that their scalar product is zero:

$$g_{\alpha\beta}dx_\beta\Delta x_\alpha=0. \tag{3}$$

The vector $g_{\nu\beta}dx_\beta$ is the vector in the world line element $(-d\bar{s}^2)$ where dx_ν defines the infinitesimal coordinate path of a point along its world line. Using the same coordinates, we define Δx_μ as the vector standing at right angles to the world lines of any two points fixed on the disk, so that Δx_μ is an infinitesimal difference in the coordinates between two points at rest on the rotating disk. In other words, this is the vector of the spatial extension. Then, by our assumption, we have

$$g_{ab}\Delta x_adx_b+g_{a4}\Delta x_adx_4+g_{4a}\Delta x_4dx_a+g_{44}\Delta x_4dx_4=0$$
$$a,\ b=1,\ 2,\ 3.$$

But, for any points fixed on the disk

$$\frac{dx_a}{d\bar{s}}=\frac{dx_b}{d\bar{s}}=0,$$

then

$$(g_{a4}\Delta x_a+g_{44}\Delta x_4)dx_4=0$$

or

$$\Delta x_4=-\frac{1}{g_{44}}\cdot g_{a4}\Delta x_a.$$

The invariant (proper) *spatial* interval between two points at rest on the disk is therefore obtained from the scalar product

$$dl^2=g_{\alpha\beta}\Delta x_\alpha\Delta x_\beta,\quad \alpha,\beta=1,\cdots,4 \tag{4}$$

where dl is the proper length of the spatial element between points whose coordinates are separated by the coordinate vector Δx_μ. Then

$$dl^2=g_{ab}\Delta x_a\Delta x_b+g_{a4}\Delta x_a\Delta x_4+g_{4a}\Delta x_4\Delta x_a+g_{44}\Delta x_4^2$$
$$=g_{ab}\Delta x_a\Delta x_b+g_{a4}\Delta x_a\left(-\frac{1}{g_{44}}\cdot g_{a4}\Delta x_a\right)$$
$$+g_{a4}\Delta x_a\left(-\frac{1}{g_{44}}\cdot g_{a4}\Delta x_a\right)$$
$$+g_{44}\cdot\left(-\frac{1}{g_{44}}\right)^2\cdot(g_{a4}\Delta x_a)^2.$$

Now write $\Delta x_a=\delta x_a$. Then

$$dl^2=g_{ab}\delta x_a\delta x_b-\frac{1}{g_{44}}(g_{a4}\delta x_a)^2$$
$$-\frac{1}{g_{44}}(g_{a4}\delta x_a)^2+\frac{1}{g_{44}}(g_{a4}\delta x_a)^2$$
$$=g_{ab}\delta x_a\delta x_b-\frac{1}{g_{44}}\cdot(g_{a4}\delta x_a)^2.$$

[6] Cf. T. Levi-Civita, *The Absolute Differential Calculus* (1929), p. 128.

But we may write

$$(g_{a4}\delta x_a)^2 = g_{a4}\delta x_a g_{b4}\delta x_b.$$

Then

$$dl^2 = \frac{1}{g_{44}}\{g_{44}g_{ab} - g_{a4}g_{b4}\}\delta x_a \delta x_b, \quad a, b = 1, 2, 3. \quad (5)$$

It will be noted that when $g_{a4} = 0$,

$$dl^2 = g_{ab}\delta x_a \delta x_b,$$

which is, of course, the ordinary expression for the spatial line element.

Now in the rotating disk, we obtain from the polar coordinate expression for $-ds^2$:

$$g_{11} = +1; \quad g_{33} = +1; \quad g_{24} = g_{42} = +\frac{r^2\omega}{c}$$

$$g_{22} = +r^2; \quad g_{44} = -\left(1 - \frac{\omega^2 r^2}{c^2}\right);$$

$$g_{12} = g_{13} = g_{14} = g_{23} = g_{24} = 0.$$

With these values, we have

$$dl^2 = \frac{1}{g_{44}}\{(g_{11}g_{44} - g_{14}g_{14})\delta x_1^2 + (g_{22}g_{44} - g_{24}g_{24})\delta x_2^2 + (g_{33}g_{44} - g_{34}g_{34})\delta x_3^2\},$$

$$dl^2 = dr^2 + \left(1 - \frac{\omega^2 r^2}{c^2}\right)^{-1} r^2 d\theta^2 + dz^2, \quad (6)$$

which is the spatial line element for the rotating disk.

We may note in passing that

$$\Delta x_4 = \frac{r\omega/c}{\left(1 - \frac{\omega^2 r^2}{c^2}\right)} \cdot rd\theta = \frac{v/c}{1 - \frac{v^2}{c^2}} \cdot rd\theta$$

or approximately

$$\Delta x_4 = \frac{v}{c} \cdot rd\theta,$$

which gives us a measure of the fourth component of the spatial vector Δx_μ.

Manifestly, the element dl exhibits a non-euclidean geometry on the surface of the disk. Setting z as a constant, we have

$$dl^2 = dr^2 + \left(1 - \frac{r^2\omega^2}{c^2}\right)^{-1} r^2 d\theta^2. \quad (7)$$

If we identify dl with actual measures (with a rigid rod element) by an observer D at rest on the rotating disk, then the proper (measured) length along the radial coordinate element, determined by a D observer, is $dl_r = dr$. The proper length along the disk at right angles to r is

$$dl_c = \frac{rd\theta}{\left(1 - \frac{r^2\omega^2}{c^2}\right)^{\frac{1}{2}}} \quad \text{so} \quad rd\theta < dl_c,$$

where dr and $rd\theta$ are the coordinate lengths of elements. The proper circumference is

$$C_0 = \int_0^{C_0} dl_c = \frac{r}{\left(1 - \frac{\omega^2 r^2}{c^2}\right)^{\frac{1}{2}}} \int_0^{2\pi} d\theta = \frac{2\pi r}{\left(1 - \frac{\omega^2 r^2}{c^2}\right)^{\frac{1}{2}}},$$

where $2\pi r = C$ is the coordinate circumference. Then

$$C_0 = C\left(1 - \frac{\omega^2 r^2}{c^2}\right)^{-\frac{1}{2}} \quad \text{or} \quad C_0 > 2\pi r.$$

Correlation of the Geometries

Returning to the original Einstein argument, and noting that r is the same radius of the rotating disk as in the above equations, we can relate the measures of a G observer directly to those of a D observer. We have $C = C' = 2\pi r$, then

$$C' = C_0\left(1 - \frac{v^2}{c^2}\right)^{\frac{1}{2}} = \bar{C}\left(1 - \frac{v^2}{c^2}\right)^{-\frac{1}{2}},$$

whence

$$\bar{C} = C_0\left(1 - \frac{v^2}{c^2}\right),$$

where $\bar{C}$ is the circumference of the rotating disk measured by a G observer and C_0 is its circumference as measured by a D observer. We should note that *if it were not for the change in the intrinsic geometry* of the disk, as given by the relation

$$C_0 = C\left(1 - \frac{v^2}{c^2}\right)^{-\frac{1}{2}},$$

the Einstein relation

$$\bar{C} = C'\left(1 - \frac{v^2}{c^2}\right)^{\frac{1}{2}}$$

would be a purely relative one, in that an observer D on the disk would find a disk (of radius r) at rest in galilean space (and therefore moving relative to the D observer) to have a non-euclidean geometry satisfying the equivalent relation

$$\bar{C}_D = C_D'\left(1-\frac{v^2}{c^2}\right)^{\frac{1}{2}},$$

where $\bar{C}_D$ would be the circumference of the galilean disk relative to the D observer and $C'_D = 2\pi r$ would be its circumference when at rest in D's space (we assume the galilean disk to have the same axis of relative rotation as the D disk). *But actually* we would have

$$C'_D = C_0 = 2\pi r\left(1-\frac{v^2}{c^2}\right)^{-\frac{1}{2}},$$

from which we must conclude that

$$\bar{C}_D = 2\pi r$$

or the geometry of the galilean disk, relative to a D observer, would remain euclidean.

In connection with Eddington's argument we should note that, in our notation $dr_0 = dl_r = dr$ and

$$r_0 d\theta_0 = dl_c = \left(1-\frac{\omega^2 r^2}{c^2}\right)^{-\frac{1}{2}} r d\theta,$$

from which we obtain

$$d\theta_0 = \left(1-\frac{\omega^2 r^2}{c^2}\right)^{-\frac{1}{2}} d\theta$$

rather than Eddington's $d\theta_0 = d\theta$. Our equation merely shows that, in measuring angles originating from the disk's center O, the measured ratio of an element of arc length to the radius changes as one proceeds outward along the radii.

Hypercurvature of the Surface

We may now inquire into the values of the Riemann-Christoffel tensor $R^{\kappa}_{\lambda\mu\nu}$, the contracted symmetrical form $R_{\lambda\mu} = R^{\alpha}_{\lambda\mu\alpha}$, and the scalar invariant $R = g^{\alpha\beta}R_{\alpha\beta}$, for the rotating disk where we confine our attention to two dimensions ($\lambda, \mu, \nu, \kappa = 1, 2$). Taking

$$dl^2 = dr^2 + \left(1-\frac{\omega^2 r^2}{c^2}\right)^{-1} r^2 d\theta^2$$
$$= g_{11}dx_1^2 + 2g_{12}dx_1dx_2 + g_{22}dx_2^2,$$

where $dx_1 = dr$; $dx_2 = d\theta$ and

$$|g_{\mu\nu}| = \begin{vmatrix} g_{11} & g_{21} \\ g_{12} & g_{22} \end{vmatrix} = \begin{vmatrix} +1 & 0 \\ 0 & +r^2\left(1-\frac{\omega^2 r^2}{c^2}\right)^{-1} \end{vmatrix}$$

we find

$$R_{11} = \frac{3\omega^2}{c^2}\left(1-\frac{\omega^2 r^2}{c^2}\right)^{-2},$$

$$R_{12} = R_{21} = 0,$$

$$R_{22} = \frac{3\omega^2 r^2}{c^2}\left(1-\frac{\omega^2 r^2}{c^2}\right)^{-3}.$$

We also find that

$$R = g^{11}R_{11} + g^{22}R_{22} = \frac{6\omega^2}{c^2}\left(1-\frac{\omega^2 r^2}{c^2}\right)^{-2}.$$

The tensor $R_{\lambda\mu\nu\kappa} = g_{\kappa\beta}R^{\beta}_{\lambda\mu\nu}$ has certain components and relations of interest to us. We find that $R_{1212} = R_{2121} = -R_{1221} = -R_{2112}$ and all others vanish for two dimensions. Now $R = g^{\alpha\beta}R_{\alpha\beta}$ (conversely, we have $R_{\mu\nu} = \frac{1}{2}g_{\mu\nu}R$) and $R_{\mu\nu} = g^{\gamma\delta}R_{\gamma\mu\nu\delta}$ whence

$$R = g^{\gamma\delta}g^{\alpha\beta}R_{\gamma\alpha\beta\delta} = g^{12}g^{21}R_{1212}$$
$$+ g^{21}g^{12}R_{2121} + g^{11}g^{22}R_{1221} + g^{22}g^{11}R_{2112},$$

$$\therefore\quad R = g^{12}g^{12}R_{1212} + g^{12}g^{12}R_{1212} - g^{11}g^{22}R_{1212}$$
$$- g^{11}g^{22}R_{1212} = 2(g^{12}g^{12} - g^{11}g^{22})R_{1212}.$$

But we can show that

$$g^{11}g^{22} - g^{12}g^{12} = g^{-1},$$

then

$$R_{1212} = -\frac{g}{2}R.$$

For the rotating disk, we find that

$$R_{1212} = -\frac{3\omega^2 r^2}{c^2}\left(1-\frac{\omega^2 r^2}{c^2}\right)^{-3}.$$

Now Gauss shows R_{1212}/g to be the measure of curvature of the surface at any point x_1, x_2, so that $R_{1212}/g = 1/r_1r_2 = -R/2$ where r_1 and r_2 are the principal radii of curvature at that point. Then

$$\frac{1}{r_1r_2} = -\frac{3\omega^2}{c^2}\left(1-\frac{\omega^2 r^2}{c^2}\right)^{-2}.$$

Hence, the surface hypercurvature of the rotating disk is negative and variable.

PART II. TIME

This brings us to the last part of our paper: the behavior of clocks at rest on the rotating disk. It seems that in this connection, a new experimental test is now theoretically possible for Einstein's general theory—a test which I shall now discuss.

Events in a Gravitational Field

It has been shown that the periods of clocks or events are, in general, related as follows:[7]

$$\frac{\delta t_2^0}{\delta t_1^0}=\frac{dt_2\left[g_{\alpha\beta}\frac{dx_\alpha}{dx_4}\frac{dx_\beta}{dx_4}\right]^{\frac{1}{2}}_{(x_1)_2(x_2)_2(x_3)_2(x_4)_2}}{dt_1\left[g_{\alpha\beta}\frac{dx_\alpha}{dx_4}\frac{dx_\beta}{dx_4}\right]^{\frac{1}{2}}_{(x_1)_1(x_2)_1(x_3)_1(x_4)_1}},$$

where $x_4=t=$coordinate time, where

$$\delta t_1^0=dt_1\left[g_{\alpha\beta}\frac{dx_\alpha}{dx_4}\frac{dx_\beta}{dx_4}\right]^{\frac{1}{2}}_{(x_1)_1(x_2)_1(x_3)_1(x_4)_1}$$

is the proper period of a light emitting source measured by an observer at rest with respect to that source which has a coordinate velocity $(dx_1/dx_4,\ dx_2/dx_4,\ dx_3/dx_4)_1$ at the point $(x_1)_1$, $(x_2)_1$, $(x_3)_1$ at the time $(x_4)_1$, and where

$$\delta t_2^0=dt_2\left[g_{\alpha\beta}\frac{dx_\alpha}{dx_4}\frac{dx_\beta}{dx_4}\right]^{\frac{1}{2}}_{(x_1)_2(x_2)_2(x_3)_2(x_4)_2}$$

is the proper period of the light from the source as observed by an observer located at the point $(x_1)_2$, $(x_2)_2$, $(x_3)_2$ at the time $(x_4)_2$, and moving with a coordinate velocity $(dx_1/dx_4,\ dx_2/dx_4,\ dx_2/dx_4)_2$. Also dt_1 is the coordinate period of light emitting source, while dt_2 is that period for the observer at $(x_1)_2$, $(x_2)_2$, $(x_3)_2$. Since we have for light, $ds=0$, we can easily show that $t_2=f(t_1)$ which gives the coordinate time t_2 of the observer's reception of the light signal from the source in terms of the coordinate time t_1 of the signal's emission. Whence

$$\frac{dt_2}{dt_1}=\frac{df(t_1)}{dt_1}.$$

[7] R. Tolman, *Relativity, Thermodynamics and Cosmology*, pp. 288–290.

Since $f(t_1)$ is a function of the $g_{\mu\nu}$ values, then where $g_{\mu\nu}$ is not a function of t, we will have $dt_2=dt_1$ or the coordinate periods of emission and observation of successive signals are equal in their intervals.

We should note that while this deduction (used for the generalized Doppler effect) is made in terms of light frequency from radiating atoms, it can be applied to proper times of periodic processes other than radiating atoms. Light will still be the means of observation, but the periods will be those of "clocks" in various parts of the gravitational field, and the time (t_2-t_1) will be the coordinate interval required for a light signal to pass over the distance to the observer, while dt_1 will be the coordinate interval between clock beats at the source and dt_2 will be such an interval for the observer. δt_1^0 and δt_2^0 will be the corresponding proper values.

Clocks on the Disk

In the case of two clocks at rest at different places on the rotating disk, our equation reduces to

$$\frac{\delta t_2^0}{\delta t_1^0}=\frac{[g_{44}]^{\frac{1}{2}}_{(x_1)_2(x_2)_2}}{[g_{44}]^{\frac{1}{2}}_{(x_1)_1(x_2)_1}}$$

but, in polar coordinates, this is

$$\frac{\delta t_2^0}{\delta t_1^0}=\frac{[g_{44}]^{\frac{1}{2}}_{r_2,\theta_2}}{[g_{44}]^{\frac{1}{2}}_{r_1,\theta_1}}$$

and since

$$g_{44}=1-\frac{\omega^2 r^2}{c^2},$$

then

$$\delta t_2^0=\frac{\left(1-\frac{\omega^2 r_2^2}{c^2}\right)^{\frac{1}{2}}}{\left(1-\frac{\omega^2 r_1^2}{c^2}\right)^{\frac{1}{2}}}\delta t_1^0.$$

If the observer is at $r_2=0$, and the clock at r_1, then

$$\delta t_2^0=\left(1-\frac{\omega^2 r_1^2}{c^2}\right)^{-\frac{1}{2}}\delta t_1^0.$$

We note that δt_1^0 corresponds to the proper time ds_0 in our notation.

The point $r_2=0$ is a singular point in the

gravitational field of the rotating disk and is at rest in some galilean space. If a clock is placed anywhere in galilean space and the observer is anywhere on the disk, the G clock will appear to have an angular velocity equal but opposite to that of the disk relative to the observer. We then have

$$\frac{\delta t_2^0}{\delta t_1^0}=\frac{[g_{44}]_{r_2}^{\frac{1}{2}}}{\left[g_{22}\frac{d\theta^2}{dt^2}+\cdots+g_{44}\right]_{r_1}^{\frac{1}{2}}},$$

where

$$ds^2=\left[1-\frac{\omega^2r^2}{c^2}\right]dt^2-\frac{1}{c^2}[\omega r^2 d\theta dt + \omega r^2 dt d\theta + dr^2 + r^2 d\theta^2],$$

which gives us the $g_{\mu\nu}$ values. But $d\theta/dt=-\omega$, then

$$\frac{\delta t_2^0}{\delta t_1^0}=\frac{\left[1-\frac{\omega^2r_2^2}{c^2}\right]^{\frac{1}{2}}}{\left[\frac{r_1^2}{c^2}\omega^2-\frac{\omega r_1^2}{c^2}(-\omega)-\frac{\omega r_1^2}{c^2}(-\omega)+1-\frac{\omega^2r_1^2}{c^2}\right]^{\frac{1}{2}}}$$

(the G clock is assumed at rest relative to the z axis of rotation), hence

$$\delta t_2^0=\left[1-\frac{\omega^2r_2^2}{c^2}\right]^{\frac{1}{2}}\delta t_1^0.$$

From all of this we may infer that clocks on the disk will run slow relative to clocks in G space at rest with respect to the rotational axis of the disk. Such slowing down is absolute, not in the sense that the principle of relativity of motion is not followed, for it can be shown that it is, but we see that the presence of the gravitational field on the disk introduces a gravitational potential for clocks on the disk—a potential not existing for the G clocks. This is another form of the well-known "clock paradox" dealt with so carefully by Richard Tolman as well as by Kopff.[8]

Our conclusion is that a clock, after being isochronized with a galilean clock and then set in rotation with respect to the latter clock, will, after rotating for some time and then being brought to rest again, no longer be isochronous, but will indicate earlier time than the G clock. It is assumed that the time required to bring the clock up to the curvilinear speed ωr is short compared with the time during which it remains at that speed. Similarly, the deceleration period should be short.

In the case of a disk of uniform angular acceleration $d\omega/dt=k$, the line element (for a system initially at rest) would be

$$ds^2=\left[1-\frac{k^2t^2(x^2+y^2)}{c^2}\right]dt^2-\frac{1}{c^2}[-2kty\,dx\,dt + 2ktx\,dy\,dt + dx^2+dy^2]$$

$$=\left[1-\frac{k^2t^2r^2}{c^2}\right]dt^2-\frac{1}{c^2}[2ktr^2\,d\theta\,dt+dr^2+r^2d\theta^2]$$

and where t is small, the $g_{\mu\nu}$ values obviously assume approximately their galilean values.

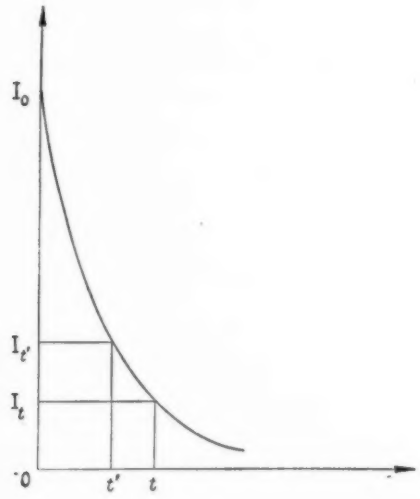

FIG. 1. The relationship between the radioactivities of two identical samples of an element of initial activity I_0, one sample remaining at rest in our space for the time t and the other being revolved in the cyclotron at constant curvilinear speed for the same time t, where t' is the corresponding relative time of the revolving sample. Then I_t is the activity of the resting sample and $I_{t'}$ is that of the revolving sample.

Experimental Test through the Cyclotron

Now it is clear that the highest curvilinear velocities to be obtained on a solid rotating disk must be limited by the elastic constants and

[8] R. Tolman, reference 7, pp. 194–197; A. Kopff, *Mathematical Theory of Relativity* (1921), pp. 125–27.

breaking strengths of the materials of such disks. It can be shown that the limiting speed, under these conditions, is about 10^5 cm/sec. Obviously this is too small when we realize that we are dealing with a factor of v^2/c^2. There remains, however, the use of the cyclotron with (artificial) radioactive ions utilized as our moving clocks. The degree of radioactivity would be a measure of proper time. We know, of course, that the radioactivity of an element is not modified by mechanical, electric, or magnetic forces, or thermal effects. The force holding these ions fixed at a particular radius from the center of the cyclotron would be simply the magnetic field force, once the ions were accelerated out to that radius by the electric field forces (which would then be removed while the ions continued to revolve at fixed radii). The ions at the limiting radius of the cyclotron would eventually (after a period of constant revolution) be brought to rest once more and tested for their activity per unit mass. If our deductions are correct, these ions will be more radioactive than a sample of such atoms which remained at rest—the atoms remaining at rest would have less radioactivity per unit mass.

In a cyclotron, the force exerted by the magnetic field on a charged particle revolving with a speed of v cm/sec. is

$$F=BQv=mv^2/r,$$

where F is in dynes, B is the magnetic field flux density (gauss), Q is the charge (e.m.u.) on the particle of mass m (grams), and r is the radius of path curvature (cm). Whence $BQr=mv$. Where v approaches light speed c, we should introduce the relativistic mass change

$$m=m_0\left(1-\frac{v^2}{c^2}\right)^{-\frac{1}{2}},$$

where m_0 is the proper mass of the particle. Then

$$\frac{BQr}{m_0}=\frac{v}{\left(1-\frac{v^2}{c^2}\right)^{\frac{1}{2}}}=\varphi,$$

whence

$$v=\varphi\left(1+\frac{\varphi^2}{c^2}\right)^{-\frac{1}{2}}$$

or approximately

$$v=\varphi\left(1-\frac{1}{2}\frac{\varphi^2}{c^2}\right).$$

We see, therefore, that to obtain speeds approaching that of light we need ions of highest

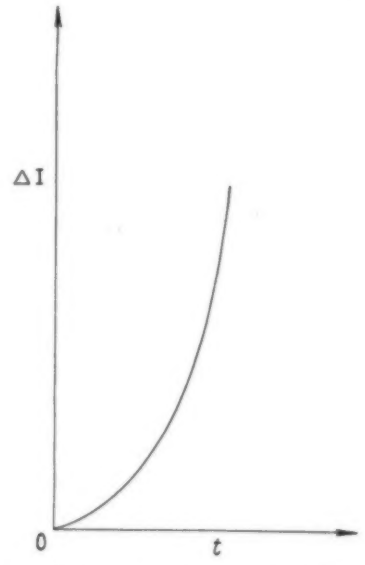

FIG. 2. The relationship between the fractional difference ΔI in activity of a resting and revolving sample of a radioactive element and the duration of revolution t determined by a resting clock.

charge and lowest mass possible in a cyclotron of large radius and high magnetic flux density. The duration of acceleration out to ωr and the corresponding deceleration of the ions of low atomic weight radioactive elements must be as brief as possible, while the duration of constant $v=\omega r$ for the ions should approximate their half-life.

Taking two samples of the same radioactive element having the same initial activity I_0, we may write for the sample at rest

$$I_t=I_0e^{-\lambda t}$$

and for the sample at radius r revolving in the cyclotron

$$I_{t'}=I_0e^{-\lambda t'},$$

where, approximately,

$$t-t'=\frac{1}{2}\frac{v^2}{c^2}t'$$

and t is the duration of the experiment in our time. See Fig. 1. This result may be written

$$\Delta I=\frac{I_{t'}-I_t}{I_t}=\exp\left(\frac{1}{2}\frac{v^2}{c^2}\lambda t\right)-1.$$

See Fig. 2. To obtain velocities approaching c with the large cyclotron now under construction in California appears possible even for radioactive ions of atomic weights as high as ten. But the actual testing of our deductions must await further investigations.

In conclusion, it is worthwhile noting that such an experiment, aside from being a new test of the general theory of relativity, would provide an application of that theory to nuclear physics of the atom.[9]

I am grateful to Professor H. P. Robertson of Princeton University for his suggestions, and to Professors H. Semat, J. D. Shea, H. C. Wolfe, and M. W. Zemansky of New York City College for their helpful discussions. To my colleague, Dr. A. Wundheiler, I am deeply indebted for his careful criticisms, especially on differential geometry.

[9] Of course, as Professor Einstein has kindly pointed out to me, the mesotron decomposition rate, at high speeds, gives results equivalent to those that would be obtained in the cyclotron for radioactive ions *while they are in motion*. One obviously can use the special theory to obtain the relation between t and t', but this formula is here shown to be a logical consequence of the general theory in the non-trivial sense that it makes unequivocal what the special theory alone would leave equivocal. Tolman's argument for the effect of the gravitational potential difference $d\Psi=v^2r^{-1}dr$ is here operative.

Letters to the Editor

PROMPT publication of brief reports of important discoveries in physics may be secured by addressing them to this department. The closing date for this department is the third of the month. Because of the late closing date for the section no proof can be shown to authors. The Board of Editors does not hold itself responsible for the opinions expressed by the correspondents. Communications should not in general exceed 600 words in length.

Electron Reflections in MgO Crystals with the Electron Microscope

ROBERT D. HEIDENREICH
The Dow Chemical Company, Midland, Michigan
August 10, 1942

IN a recent paper, Hillier and Baker[1] have reported observations on Bragg reflections of electrons in crystals of $Al_2O_3 \cdot 3H_2O$. Their results were obtained with no limiting aperture in the microscope, and hence the reflected beam was recorded on the plate as well as the regions in which the reflections took place. A somewhat similar phenomenon has been observed in this laboratory, in the use of a Type B, RCA electron microscope, with cubic crystals of MgO. The arrangement differed from that of Hillier and Baker in that the small objective aperture was employed. Consequently, electrons scattered through angles greater than 3×10^{-3} radian were stopped by the aperture and hence the singly reflected beam did not reach the photographic plate.

Figure 1 is an electron micrograph of MgO crystals

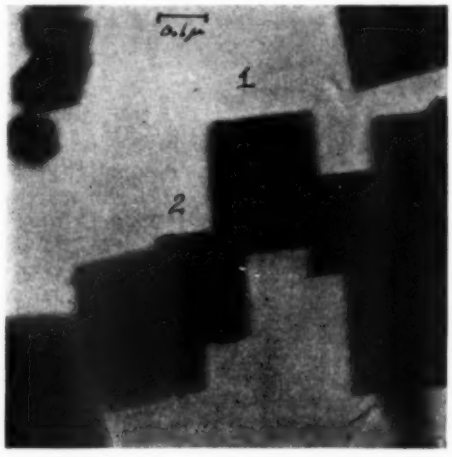

FIG. 1. Reflection bands in images of MgO crystals.

resting on a thin plastic support where they deposited from the smoke of burning magnesium metal. The alternate light and dark bands are evident and are in contrast to those of Hillier and von Ardenne[2] in that they are uniformly spaced. Measurements on the image of Fig. 1 will

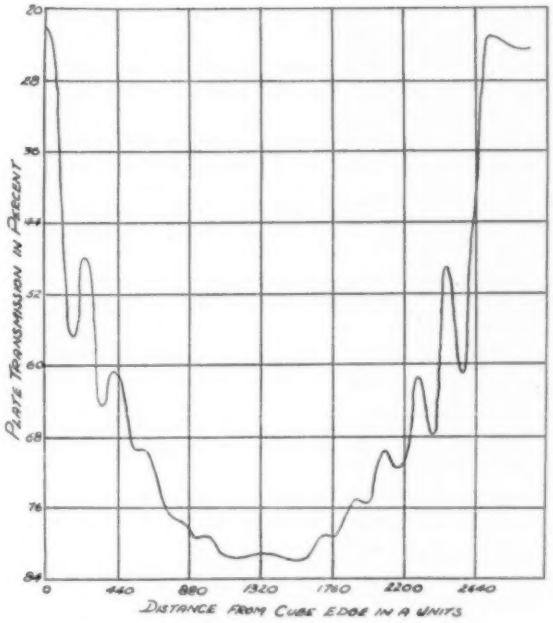

FIG. 2. Microphotometer trace of cube 1 of Fig. 1.

show that the bands occur in cubes which are oriented with the plane of two opposing edges normal to the paper. Numerous micrographs of fields containing such crystals have indicated that the bands appear only in the image of a crystal with approximately this orientation. Bands have never been observed in cubes with a facet in the plane of the image.

The appearance of such bands has been found to depend upon the angle at which the incident electrons enter the crystal as determined by varying the condenser lens current. This fact in conjunction with the orientation requirements of the crystal has led to the conclusion that the phenomenon is a result of multiple electron reflections from the crystallographic planes. If the path length for an electron traversing the crystal is such that it suffers an odd number of reflections, then it will leave the crystal at approximately the Bragg angle and so be stopped by the aperture. If the path length be such that an even number of reflections is suffered, then the electron will leave with the same direction as when it entered and hence contribute to the final image. It follows immediately that a uniform variation of crystal thickness will yield path lengths alternating in the probability that there will be an even or odd number of reflections.

Intensity maxima should thus occur in the image for values of the thickness given by

$$t = ky \quad k = 2, 4, 6, 8, \cdots, \tag{1}$$

where "y" is the distance between successive reflections and "k" is the number of reflections. If "j" is the average number of interplanar spacings traversed between successive reflections, then from the Bragg law (1) becomes

$$t \simeq kj(2d^2/\lambda) \quad k = 2, 4, 6, \cdots, \tag{2}$$

where "d" is the interplanar spacing and "λ" the electronic wave-length. For the diagonal (220) plane of MgO, $d=1.48$A and $\lambda=0.05$A for 60-kv electrons. The average spacing of intensity maxima obtained from Fig. 2 is about 200A. For the crystal orientation of Fig. 2, the crystal thickness at a given maximum is just twice the distance from the maximum to the cube edge and so the maxima are located by simply dividing Eq. (2) by 2. The value of "j" is not known, but in order to obtain the correct spacing, a value of "j"$=2.17$ (± 20 percent) was determined from (2), which is of the correct order of magnitude for penetration of electrons in diffraction from surfaces. It is possible to make some calculations regarding "j," but these must wait on more urgent problems.

It follows from what has been said that with a limiting aperture in the microscope, the plate density of images of crystals oriented with a facet in the plane of the image should vary periodically with the thickness of the crystal. An attempt was made to substantiate this, but the plate densities ranged so widely due to slight variations in orientation of crystal and electron beam[3] that no correlation could be made.

It was learned in a recent conversation with Dr. Hillier that he had observed this phenomenon in MgO crystals and the maxima spacings roughly check those of Fig. 1.

[1] J. Hillier and R. F. Baker, Phys. Rev. **61**, 722 (1942).
[2] M. von Ardenne, Zeits. f. Physik **116**, 736 (1940).
[3] Cf. B. von Borries and E. Ruska, Naturwiss. **28**, 366 (1940).

Electron Microscope Study of Surface Structure

R. D. Heidenreich and V. G. Peck
The Dow Chemical Company, Midland, Michigan
August 28, 1942

THE application of the electron microscope to the study of fine surface structure of opaque bodies depends either upon the ability of an electron optical system to view[1] directly the surface through emission or reflection or a technique of reproducing the surface structure into a thin film suitable for study in the transmission electron microscope. Several methods of producing such replicas have appeared in the literature, chief among which are the natural oxide films of Mahl,[2] the direct Formvar films of Schaefer and Harker,[3] and the silver-collodion process of Zworykin and Ramberg.[4]

It is the purpose of this communication to report yet another technique of reproduction developed in these laboratories which depends upon first forming an impression of the surface to be studied in a thermoplastic by the normal molding technique. Several plastics have been tried and polystyrene was concluded to be the best suited, because of the combination of moldability, dimensional stability, and chemical inertness. The plastic molding is removed from the specimen, either by mechanical shock or dissolution of the metal in an appropriate acid. A thin film replica is then made from the molding by evaporating onto it a film of silica and subsequently removing the silica by means of ethyl bromide solvent.

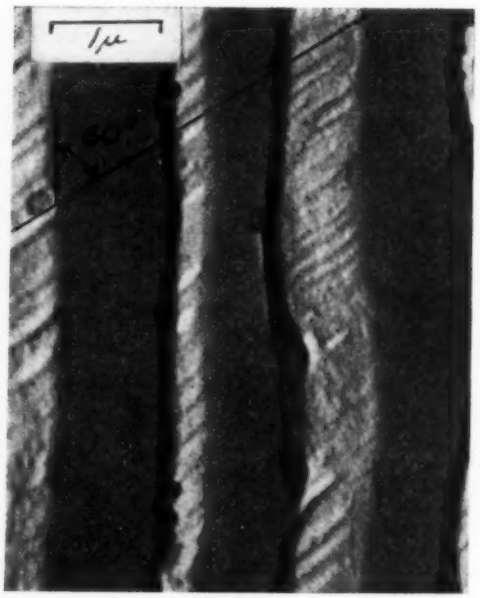

FIG. 1. Deformation striae in calcite crystal.

It has been found that silica condensing from a molecular beam onto a polystyrene surface possesses great mobility upon both the styrene and its own condensing surface. A beam only a few thousandths of an inch in cross section incident upon a styrene block will result in a film completely surrounding the block. If the surface of the styrene is "electron microscopically" smooth a film structureless to the electron microscope is so obtained which will serve as a temperature-stable support for microscope specimens and is capable of being heated to 1000°C without notice-

FIG. 2. Illustrating resolution in silica replica.

able effect. Electron diffraction shows these films to be vitreous silica. Aluminum oxide also tends to be quite mobile on polystyrene during condensation.

If the styrene surface is a molded replica, it is observed that the evaporated silica film tends to fill in the irregularities to a certain degree and yield a positive replica film of the original surface suitable for use in the transmission electron microscope. The extent to which these irregularities are filled in is now under investigation.

Figure 1 is an electron micrograph[5] of a silica replica prepared as just described from a freshly cleaved surface of a calcite crystal. During molding, the crystal was deformed and gave rise to the striae observed in Fig. 1. The light regions in this micrograph are "valleys" in the original surface. The slip lines within the bands are quite visible, making an angle of 60° with the axis of the band, and are particularly interesting because of their curvature. Families of bands were observed, similar to those of Fig. 1, which had the appearance of a sine wave with an amplitude of 0.2–0.3μ and a period of 2–3μ. In a single group, the individual bands exhibited a phase difference of 60° from band to band and this phase difference seemed to be generally in the same direction throughout the group. The curvature of slip lines illustrated in Fig. 1 may well be a demonstration of the local curvature[6] giving rise to shear hardening.

Excellent contrast and resolution can be obtained with these replicas as evidenced in Fig. 2, which was taken from the same replica as Fig. 1, but a different part of the field showing slip on a larger scale. A resolution of 40A is estimated in this replica.

Full details of the technique and applications will appear elsewhere.

[1] V. K. Zworykin, J. Hillier, and R. L. Snyder, A.S.T.M. Bull. No. 117, pp. 15–23 (1942).
[2] H. Mahl, Zeits. f. tech. Physik **22**, 93 (1941).
[3] V. J. Schaefer and D. Harker, J. App. Phys. **13**, 427 (1942).
[4] V. K. Zworykin and E. G. Ramberg, J. App. Phys. **12**, 692 (1941).
[5] Taken with an RCA electron microscope, Type B.
[6] Cf. R. Houwink, *Elasticity, Plasticity, and Structure of Matter* (Cambridge University Press, 1937), pp. 96–97.

Proceedings of the American Physical Society

MEETING AT STATE COLLEGE, PENNSYLVANIA, JUNE 26–27, 1942

THE 249th meeting of the American Physical Society was held in the buildings of The Pennsylvania State College at State College, Pennsylvania, on Friday and Saturday the twenty-sixth and twenty-seventh of June, 1942. The fourth of our meetings since Pearl Harbor, it showed the now-familiar pattern of a marked decline in the number of contributed papers as compared with the summer meeting of the previous year. This, however, was amply compensated by several distinguished physicists and chemists who acceded to requests that they give invited papers. The attendance was higher than in the previous year (there were about 120 at the dinner) but this happy event must be credited in part to our sister societies which were holding meetings on the Thursday and part of the Friday. These were the American Association of Physics Teachers and the Society for the Promotion of Engineering Education, of which the joint symposium "The War and Problems of Physics Teaching" attracted much attention, and will presumably be reported in another journal.

The circumstances of the meeting were remarkably pleasant, and it was evident that the members of the physics staff and even some of the chemistry staff of State College had expended time and pains without stint in making the arrangements for the sessions, while their wives had labored equally in preparing entertainment for visiting ladies. It is difficult to guess whom to single out for special mention, but it should be recalled that Professor D. C. Duncan was Chairman of the Local Committee and that Dean F. C. Whitmore gave a reception on the Thursday evening for all members and guests of the three societies. Special mention should assuredly be made of the enlightened liberality of the local gasoline-rationing board (Chairman, Mr. Maurice Baum) who allowed to all visiting members sufficient gasoline to get to their homes or to the boundary of the rationed area, and was even willing to allow gasoline enough for the round trip. This was a highly valued tribute to the singular importance of physics and of the teaching thereof to the war effort.

The dinner was held on the Friday evening at the Nittany Lion Inn. President Bridgman presided; the three societies were welcomed to State College in the name of its President by Mr. Morse; officials of the other two societies spoke briefly; but the major feature of the after-dinner programme was the brilliant speech of Dean Whitmore, deviating somewhat but not too much from the subject indicated by the title quoted below, and pertaining largely to the problem of synthetic rubber. Another outstanding event was the description of the cryogenic laboratory and the demonstration of liquid hydrogen by J. G. Aston on the following day, which may be described as matchless.

The invited speakers and the titles of their papers were the following, speakers not otherwise designated being of the Pennsylvania State College:

J. G. ASTON AND M. SAGENKAHN: **Production of Low Temperatures at Pennsylvania State College (with demonstrations of liquid hydrogen)**

J. G. ASTON AND S. C. SCHUMANN: **Thermochemical and Thermodynamical Research on Organic Compounds at Pennsylvania State College**

P. DEBYE (*Cornell University*): **Coagulation of Colloids**

J. E. MAYER (*Columbia University*): **Electron Affinity**

D. H. RANK AND R. J. PFISTER: **Direct Photoelectric Method of Measuring Wave-Lengths and Intensities in Raman Spectra**

J. H. SIMONS AND H. T. FRANCIS: **Measurement of the Scattering of Low Velocity Ions in Gases at Low Pressures**

J. A. VAN HORN AND D. H. RANK: **Isotopic Fine Structure in Raman Spectra**

F. C. WHITMORE: **Organic Chemistry for Physicists**

The contributed papers are listed below with the abstracts submitted for them; number 10 was read by title.

At the Council meeting which was held on the Friday, one Member of the Society was advanced to Fellowship, and 27 candidates were elected to Membership; their names are the following:

Elected to Fellowship: J. R. Hirsh.

Elected to Membership: Abraham, George; Atlee, Zed J.; Booge, James Eliot; Boyer, Keith; Burns, Loren V.; Debeau, David Edmund; De Pangher, John; Drake, William Robert; Ekstein, Hans; Fagen, Morton D.; Greenwood, Ivan A., Jr.; Herscher, Leonard O. W.; Lavatelli, Leo Silvio; Linder, Benedict M.; Longini, Richard L.; Maltby, Frederick Lathrop; Peterson, E. L.; Pinkham, Raymond A.; Saby, John S.; Salisbury, W. W.; Spangenberg, Karl; Spatz, Wilber D. B.; Sprengnether, W. F., Jr.; Weinstock, Robert; Weltin, Hans; Winkler, Stanley; Wong, Ming S.

Only one death in the Society has to be reported by the Secretary, that of M. F. Manning, known for his work on the theory of electrons in metals.

The Treasurer and Secretary recall with gratitude the seventeen years of skilful, loyal, and laborious service of Margaret Herod Tilton (now Mrs. Bernard Titche) as secretary in general charge of all routines of the office of the Society at Columbia University.

KARL K. DARROW
Secretary, American Physical Society
Columbia University

ABSTRACTS OF CONTRIBUTED PAPERS

1. The Method of Thin Films. HOWARD S. COLEMAN AND HENRY L. YEAGLEY, *The Pennsylvania State College.*—A simple method for observing intermetallic diffusion rates has been devised. This method involves the deposition from the vapor phase first of one metal than another on top of it. A microscope slide is used as a film base. The diffusion rates are then observed at various temperatures. This is done by noting the change in reflectivity at one surface as the metals diffuse. The apparatus consists essentially of an automobile headlight source maintained at constant voltage, the bi-metallic reflecting film, and a photronic cell connected to a recording microammeter. The recorder draws a record of the change in reflectivity automatically as the diffusion progresses. This new method makes possible the study of diffusion rates of metals through metals and, in some cases, gases through metals at temperatures as low as 50°C and in lengths of time as little as 5 minutes, depending upon the metals involved, the thickness of the metals, and the temperatures. The activation energies determined by the method of thin films are in agreement with values obtained by others. For example the activation energy for the diffusion of gold into lead has been found to be $-13{,}700 \pm 300$ cal.

2. The Surface Layer of Sheet Glass. F. L. BISHOP, JR., *American Window Glass Company.*—There has been considerable speculation as to the nature of the fire polish layer on sheet drawn glass. Drude gave equations for determining the thickness of a surface layer when deviations from Fresnel's equations are found. In this research plane polarized light with its plane of polarization 45° from the plane of incidence was reflected from glass at Brewster's angle. Due to the surface layer, the reflected light was found to be slightly elliptically polarized. A new method of photographic recording, using a Polaroid split field analyzer was used to measure this ellipticity. The result showed the probable existence of a crystalline quartz layer on freshly drawn sheet glass. The extreme difficulty of drying the surface once it had been wet was also confirmed; the existence of a high index layer on glass polished with rouge was verified.

3. Stray Magnetic Fields from Cobalt. L. H. GERMER, *Bell Telephone Laboratories.*—Electrons passing near the surface of a demagnetized cobalt single crystal are deflected by the stray fields from the individual magnetic domains. Iron and nickel single crystals show no similar phenomenon; because these metals are cubic they have more than one direction of easy magnetization and external fields are therefore very weak. 40-kv electrons scattered from a hexagonal face of a cobalt crystal produce on a photographic plate an exceedingly complex pattern made up of curves or arcs interlaced in elaborate fashion but all concave toward the primary beam position. The pattern is decreased in size, but not altered in character, if the hexagonal face is covered by a thin layer of electrodeposited copper. By studying crystals covered by different known thicknesses of copper, it has been discovered that the magnetic fields extend to about 0.01 mm above the surface and that the maximum field intensity just at the surface is of the order of 10^4 gauss. In general, hexagonal faces of demagnetized cobalt crystals do not adhere when pressed together, but if they have been flattened with exceptional care, the magnetic attraction can be very great, 4.9 kg weight/cm² in one case.

4. Transitions in Cobalt-Nickel and Iron-Nickel Alloys Determined by Hydrogen Diffusion. F. D. BENNETT, J. R. DOIG, AND W. R. HAM, *The Pennsylvania State College.*—The measurement of the rate of hydrogen diffusion through metals provides a sensitive and accurate method of detecting transition points in the metal lattice. For a homogeneous metal or alloy the diffusion rate is given by

$$R = \text{const. } p^z e^{-b/T},$$

where z is usually $\frac{1}{2}$. An examination of two Ni-Co alloys shows that while the physical magnetic change occurs at 600° and 910°, respectively, the Curie point break for Ni is still present in the diffusion curve. Two Fe-Ni alloys in which the magnetic transformations occur at 340° and 561° both show a marked discontinuity at 769°, the Curie temperature for pure Fe. A Co-Fe alloy shows a transformation at 1112°C regardless of the length of time it has

been heat treated in hydrogen and this is the magnetic transformation temperature for pure cobalt. The presence of an alloying element with Fe, Co, or Ni changes the temperature of the magnetic transformation, but appears always to leave unchanged a transformation at the Curie transformation temperature of pure Fe, Co or Ni. These data might be interpreted as indicating that fundamental electronic transitions occur in ferromagnetic alloys at the Curie temperatures of the elements that are not necessarily associated with any magnetic changes in the alloys. An alternate explanation of the unexpected transitions is that a segregation of one of the elements exists but this appears to the authors very unlikely, considering the heat treatment.

5. The Use of Secondary Electron Emission to Obtain Trigger or Relay Action. A. M. SKELLETT, *Bell Telephone Laboratories.*—The use of secondary electrons to obtain trigger action similar to that of a thyratron is described. An experimental tube and the necessary circuits by which this action is achieved are discussed. This combination gives the features of a triode with a relay or on and off feature, resulting in an amplifier, oscillator, modulator or other vacuum tube device which may be turned on or off abruptly at high or low frequencies. In addition, it can be used to replace thyratrons in many of their circuits where very low impedance is not necessary and is capable of much greater speeds of operation in such applications.

6. An Automatic X-Ray Diffraction Apparatus. S. W. HARDING, F. R. SMITH, AND W. P. DAVEY, *Pennsylvania State College.*—The use of balanced ZrO_2 and SrO filters in x-ray diffraction work with Mo x-rays is well known. When Geiger-Mueller quantum counters are used to detect the diffracted lines, it is possible, by means of a four-pole synchronous motor operating a disk, to insert into the path of the x-ray beam, first a ZrO_2 filter, then a SrO filter. The impulses from the quantum counter are then amplified and passed through a pulse-leveler in the usual way. After further amplification, the impulses are then led to a mechanical double pole-double throw switch on the shaft of the four-pole synchronous motor. This switch feeds the impulse from the Zr-filtered beam into a "tank condenser" with one polarity, and feeds the impulse from the Sr-filtered beam into the same tank condenser with the opposite polarity. A suitable bleeder-leak in series with a recording microammeter is placed across the tank condenser. The recording meter then registers the difference between the counts made through the two filters. A proper choice of circuit constants gives a useable and reasonably accurate measurement of x-ray intensities provided the original x-ray beam is strong enough.

7. Diffraction of X-Rays by Argon in the Liquid, Vapor and Critical Regions. A. EISENSTEIN AND N. S. GINGRICH, *University of Missouri.*—Rocksalt reflected Mo $K\alpha$ radiation was used to obtain diffraction patterns of argon at twenty-six different conditions of pressure and temperature. Argon gas was compressed in a flat beryllium window cell under pressures of from 0.8 to 51.1 atmospheres and its temperature was held constant at values between 84.35°K and 168°K. The diffracted x-ray intensity was measured by means of a Geiger-Mueller counter. The liquid pattern at 84.35°K (triple point 83.99°K) is considerably sharper than those at any higher temperature, including, particularly, that at 91.8°K. Series of patterns were obtained at temperatures of 126.7°K, 144.1°K and 154°K covering both the vapor and liquid phases in each case. One series was obtained at a pressure of 51.1 atmospheres, somewhat above the critical pressure. The general characteristics of the patterns are largely dependent on the density of the argon, although increase of temperature alone tends to shift the main peak to smaller angle while for the vapor, increase of pressure alone tends to shift it to larger angle. When these curves are fitted to structure factor curves, it is found that at high pressure and temperature and near the vapor-liquid line, considerable excess scattering occurs at small angle.

8. A Diffraction Adapter for the Electron Microscope. J. HILLIER, R. F. BAKER, AND V. K. ZWORYKIN, *RCA Manufacturing Company.*—As part of a program to extend the usefulness of the electron microscope as a scientific tool, an adapter has been developed which allows a conventional electron microscope to be used interchangeably as an electron diffraction camera or an electron microscope. The adapter comprises a unit which takes the place of the projection lens unit of the microscope, and includes a newly designed microscope projection lens, a specimen holder, and a focusing lens. To transform the instrument from a microscope to a diffraction camera (or vice versa) it is only necessary to transfer the specimen from the adapter to the regular object chamber. Diffraction patterns may be obtained by either reflection or transmission. As a result of the excellent reproducibility of voltages and currents from the regulated power supplies used in the electron microscope, the diffraction camera holds its calibration to within 0.1 percent over long periods. Using a calibration determined by measurements of gold patterns, lattice spacings of a number of common materials were determined and found to agree with x-ray values to within 0.5 percent. A number of such transmission-diffraction patterns have been made during the testing of the equipment.

9. The Direct Measurement of the Ionization Potentials of the Free Radicals, Methyl and Ethyl. JOHN A. HIPPLE AND D. P. STEVENSON,[1, 2] *Westinghouse Research Laboratories.*—The lead tetra-alkyls, $Pb(CH_3)_4$ and $Pb(C_2H_5)_4$, were decomposed to yield free methyl and ethyl radicals in a specially designed furnace built into the ionization chamber of a 180° mass-spectrometer tube. From the initial breaks of the ionization efficiency curves of the ions, CH_3^+ and $C_2H_5^+$, we have found the ionization potentials of the methyl and ethyl radicals to be $I_{vert}(CH_3) = 10.0 \pm 0.1$ ev and $I_{vert}(C_2H_5) = 8.6_0 \pm 0.1$ ev. These values are in excellent agreement with those found by indirect calculations from other electron impact data. Fraser and Jewitt,[3] by a molecular beam technique, obtained 11.2 ± 0.8 volts and 10.6 ± 0.8 volts for the corresponding ionization potentials.

The reason for this difference will be discussed. An energy diagram is constructed which represents the present states of combination of a carbon and four hydrogen atoms. It has been found that the thermal decomposition of these lead compounds, even at these low pressures ($\sim 10^{-5}$ mm) yields predominantly stable molecules rather than free radicals. The yield of methyl radicals relative to other decomposition products is critically dependent on the furnace temperature, passing through a sharp maximum.

[1] Westinghouse Research Fellow.
[2] Present Address—Shell Development Company, Emeryville, California.
[3] Fraser and Jewitt, Proc. Roy. Soc. **160A**, 563 (1937).

10. Sensitized Fluorescence of Iron Vapor. J. G. WINANS AND STANLEY BREEN, *University of Wisconsin.*—The sensitized fluorescence of iron vapor in mercury vapor has been obtained by using the simplified form of apparatus.[1] A fused quartz tube containing electrolytic iron dust and mercury was heated at one point to 1100°C with a hydrogen-air flame. This point was illuminated by light of wave-length 2536 from a SC 2537 discharge tube using a focal isolator. The spectrum of the fluorescence showed thirty iron lines at low mercury pressure (about 0.5 cm) and approximately ten iron lines at high mercury pressure (about 10 cm). At medium mercury pressure, a low voltage Tesla discharge showed the same iron lines as the fluorescence at medium pressure, but at low mercury pressure the Tesla discharge showed many more iron lines than appeared in fluorescence at the same pressure.

[1] J. G. Winans and R. W. Williams, Phys. Rev. **52**, 930 (1937).

11. Radioactive Tellurium from Antimony. C. V. KENT AND J. M. CORK, *University of Michigan.*—Antimony exists in nature as isotopes of mass 121 (56 percent) and 123 (44 percent). On bombarding antimony with deuterons, tellurium isotopes of mass 122, 124, 121, and 123 might be produced; the first two by the (d, n) reaction and the latter two by the less probable $(d, 2n)$ process. The separated tellurium fraction has been found to yield several radiations. A positron radiation probably due to Te (121) has been observed. An activity of half-life thirty days consists of several gamma-rays. On the beta-spectrometer the resolution is sufficient to show clearly the K, L, and M peaks for two of the converted gamma-radiations of energy 82.0 kev and 88.3 kev. Both have K–L–M differences characteristic of tellurium and hence must be associated with excited states in the similar stable isotopes of mass 122 and 124. Other gamma-rays have energies of 136, 157.3, 210.8, and 615 kev.

12. The Solution of Maxwell's Equations for Certain Diffraction Problems. ROBERT A. WOODSON, *University of Rochester.**—Particular solutions of Maxwell's electromagnetic field equations are obtained which approximately satisfy the boundary conditions for the diffraction of plane waves normally incident upon an aperture in a plane opaque screen situated in an isotropic transparent medium. The following cases of Fraunhofer diffraction are solved: the infinite plane grating, the single slit, multiple slits, and the rectangular aperture. The problem is solved by an original application of Fourier analysis. Plane waves are combined by pairs into "corrugated waves." Such corrugated waves are periodic both in the direction of propagation and also in the wave front. Coplanar corrugated waves are superimposed in the plane of the aperture in such a way that the Fourier series of their amplitudes gives the amplitude of the incident wave in the plane of the aperture. Thus the boundary conditions are satisfied. This theory is based directly upon Maxwell's equations, and does not depend upon Huygens' principle. The phenomenon of diffraction is shown to be a natural result of limiting the extent of the wave front. Perhaps the most valuable contribution of the corrugated wave theory is its simplicity, by which it readily explains phenomena predicted by much more complicated theories.

* Work done at Rensselaer Polytechnic Institute.

13. Departures from Ohm's Law in Solids. H. OSTERBERG, *Spencer Lens Company* (*Introduced by A. H. Bennett*).—The writer has attempted to ascertain whether there exists in crystalline or isotropic solids a volume effect which obeys Neumann's hypothesis and in which the resistance varies as a power series in the components of the applied electrical field. Crystals of 21 classes allow linear terms different from zero and may exhibit rectification. Quadratic terms are allowed by all crystal classes. Higher terms of the above tensor were not studied. Parallel crystal plates of carborundum, zincite and galena with evaporated metal electrodes were immersed in constant temperature baths and found to exhibit current-voltage characteristics consistent with the above linear and quadratic tensors when the applied electrical fields were small. At higher fields the behavior, especially of galena, became complicated. With repeated grinding and resurfacing the direction of rectification in single crystals of carborundum and zincite remained the same. Consistent with the above volume effect, the resistance changes in isotropic resistors varied quadratically with the field over wide ranges in the applied voltage. These observations together with those made by other observers provide good but not yet indisputable evidence for the above volume effect and indicate that rectification effects in crystals are due only in part to surface effects.

14. The Kinetic Energy Correction in Viscosity Measurements. M. R. CANNON AND EDWARD NADRO,* *The Pennsylvania State College* (*Introduced by W. P. Davey*).—The kinetic energy correction in viscosity measurements appears in the C' term in the equation: $\text{K.V.} = Ct - C'/t$ where K.V. is the kinematic viscosity, t efflux time in seconds, C a constant dependent upon the dimensions of the viscometer and C' an alleged constant which depends upon the kinetic energy coefficient "m" and the dimensions of the viscometer. In this paper extensive data are presented and indicate that C' is not a constant for a given viscometer but is a variable. Therefore, the common practice of assuming C' to be a constant may introduce appreciable errors in viscosity measurements. For example, in some types of viscometers C' changes by 60 percent over a sixfold range in Reynolds number. Eleven different types

of viscometers were used in this investigation. Some of them were designed to make the kinetic energy correction high (20 percent or more) and, therefore, accurately measurable over a wide range of Reynolds numbers. It is apparent that it is necessary to maintain the term C'/t very small in relation to Ct in accurate viscosity measurements. This can be done by proper selection of viscometer dimensions and the C'/t term may be reduced to 0.1 percent or less of the Ct term. The equation then reduces to: $K.V. = Ct$.

* Present address: Socony-Vacuum Oil Company, Paulsboro, New Jersey.

15. An Ultraviolet Recording Photoelectric Spectrophotometer. R. J. PFISTER AND D. H. RANK, *The Pennsylvania State College.*—A large F-4 plane grating monochromator has been built to feed light from a water-cooled hydrogen discharge to a split beam photometer. The photocurrents from two F.J.-405 (General Electric) tubes are separately amplified by two RH-507 (Westinghouse) electrometer tubes and the currents are supplied to a pair of galvanometers whose deflections are continuously recorded while the monochromator moves through the spectrum. The monochromator employs two 8-inch parabolic mirrors used 11 degrees off the axis in such a way that the astigmatism produced by the collimating mirror is partially corrected by the focusing mirror. An 8-inch plane grating containing 26 square inches of ruling with 15,000 lines per inch on aluminum is used in the second-order ultraviolet. The grating is motor driven so that the spectrum moves at a rate of approximately 47A per minute across the exit slit. The source is a π type hydrogen tube with large aluminum electrodes. The complete assembly yields records showing a resolving power of about 5A and sufficient intensity down to about 2350A.

16. Impurities in Certain Arc Carbons Sold for Spectrographic Work. R. H. COTTON, *Pennsylvania State College* (*Introduced by W. P. Davey*).—Arc carbons can be bought from the manufacturers in various degrees of purity. The two most commonly used brands (*A* and *B*) of the less pure type have been examined spectrographically. In some cases chemical methods have been tried to improve the purity. Both *A* and *B* were found to contain Ca, Si, Ti, and B. Ca was removed from brand *A* by Soxhlet extraction with either HCl or HNO_3. Calcium is materially reduced from brand *B* by Soxhlet extraction with HNO_3. As might have been expected, Si was present and did not yield to chemical treatment. Ti was removed from brand *A* by Soxhlet extraction with HCl, but was not completely removed from brand *B* by Soxhlet extraction with HNO_3. B was not removed from either brand by Soxhlet extraction with HCl or HNO_3 or by three one-hour boilings with 29 percent NH_4OH. The following elements were looked for in both *A* and *B* but were not found:

Al	Fe	Mo	Tl
Bi	K	Na	V
Cb	Li	Ni	
		P	W
Co	Mg (doubtful trace)	Pb	
Cr	Mn	Pt	Zn.

17. Near Infra-Red Absorpton by Water Vapor. C. C HAWORTH, JR. AND F. C. TODD, *The Pennsylvania State College.*—The radiation of 1.87 microns absorbed by water vapor has been measured by employing a carefully jacketed, absorption cell. Adsorption on the windows is found negligible by use of a removable glass plate.[1] The absorption cell is filled by saturating it at the temperature of the thermostat. Measurements show that the integrated absorption per unit mass of water is constant for saturated water vapor at 35, 25 and 15°C, but perhaps increases for 0°C. The absorption at atmospheric pressure of air varies from 1.7 to 2.6 times that of water vapor alone, increasing with decreasing temperature. The variation of the integrated absorption with the pressure was measured at 25°C for the 1.4 and the 1.87 micron band. The increased absorption by the pure water at 0°C and the decrease in absorption with increasing temperature at atmospheric pressure, indicates that the Lorentz boradening may not be the sole effect.[2] Association is known to increase the absorption[3] and is indicated here.

[1] F. C. Todd and A. W. Gauger, Proc. A. S. T. M. p. 1134 (1941).
[2] H. Margenau and W. W. Watson, Rev. Mod. Phys. **8**, 40 (1936).
[3] J. J. Fox and A. E. Martin, Proc. Roy. Soc. **A174**, 234 (1940).

18. The Long Wave-Length Absorption of Saturated Carboxylic Acids and Esters. HENRY L. MCMURRY, *Rensselaer Polytechnic Institute.*—Electron configurations for the COOR group (R denotes an alkyl group or an H atom) expressed in terms of localized MO's are like those for the carbonyl group[1] with, however, the inclusion of MO's representing electrons in the added R−O and C−O bonds. A pair of nonbonding electrons are localized on each oxygen atom. Excitation of one of these electrons to the lowest excited MO which has a node in the OCO plane should produce the longest wave-length absorption. This excited MO is largely localized in the C=O part of the COOR group but must cover all three atoms in the COO^- ion. The calculated intensity for these transitions is low except when the excited electron starts from an MO having a node in the OCO plane. This occurs in the ion where a large intensity is predicted. When it occurs in the COOR group the intensity may be very low. The longest wave-length absorptions near $\lambda 2100$ in the unionized COOR group is weak but becomes very strong and appears at somewhat shorter wave-lengths in the ionized salts of the acids. This agrees with predictions.

[1] H. L. McMurry, J. Chem. Phys. **9**, 231 (1941).

19. Effect of Mass on the Shift in Absorption Regions in Conjugated Organic Molecules. GLADYS A. ANSLOW AND EVANS VAUGHAN, *Smith College.*—Attempts to correlate the position of absorption bands in the spectra of conjugated hydrocarbons with the number of conjugated groups have met with considerable success, although the cause of the shift of the bands toward higher wave-lengths with additional groups is not immediately apparent. The increase in the intensity of the bands with the number of groups is undoubtedly the result of the increase in the number of absorbing centers in the molecule. If it be assumed that the energy absorbed in these groups is transferred to the central member of the conjugated

groups, causing vibration of the molecule about the center of gravity of this member and resulting in dissociation, the energy of the exciting photon must be proportional to the inverse square root of the reduced mass of the molecule about this center. This hypothesis is tested from data in the literature. The symmetrically formed molecules such as diphenyl-polyenes, bixin and lycopin form a group of molecules with the same force constant; the metyl- and furyl-carboxylic acids and aldehydes form other groups. Hence the spectral shift occurring in conjugated organic molecules must result from the stretching of the bonds in the conjugated groups by the increased weight of the molecule.

20. Fluctuations of Cosmic-Ray Ionization Data Obtained with Proportional Geiger Counters. PAUL WEISZ AND W. F. G. SWANN, *Bartol Research Foundation of The Franklin Institute.*—Two identically built proportional Geiger counters were operated in such a way that any ray passing through the same length of path in both counters, as defined by an additional coincidence arrangement, would yield a record of the pulse size supplied by each proportional counter. The counters were surrounded by 10 cm of lead on all sides to prevent simultaneous rays from producing disturbing records. The six hundred dual records so far obtained have been analyzed as to the relative fluctuations between the two data of each pair. The analysis shows that the probability for obtaining two data identical within 10 percent is greatest, as should be expected. If the frequency of such identical pairs be F, pairs of data differing from each other by 50 percent are obtained in about $1/2\ F$ cases, differences of 100 percent in $1/10\ F$ cases. One of us[1] has pointed out that such fluctuations should be expected, since the ionization does not occur in individual pairs of ions only, but in form of ionization blobs of different sizes, some of which may contain great numbers of ions. Their number is infrequent enough to be subject to appreciable fluctuations.

[1] W. F. G. Swann, Paper No. 15, Am. Phys. Soc. Meeting at Baltimore, Maryland, May, 1942.

AUTHOR INDEX TO ABSTRACTS OF PAPERS PRESENTED AT THE STATE COLLEGE MEETING

Anslow, Gladys A. and Evans Vaughan—No. 19

Baker, R. F.—see Hillier, J.
Bennett, F. D., J. R. Doig, and W. R. Ham—No. 4
Bishop, F. L., Jr.—No. 2
Breen, Stanley—see Winans, J. G.

Cannon, M. R. and Edward Nadro—No. 14
Coleman, Howard S. and Henry L. Yeagley—No. 1
Cork, J. M.—see Kent, C. V.
Cotton, R. H.—No. 16

Davey, W. P.—see Harding, S. W.
Doig, J. R.—see Bennett, F. D.

Einstein, A. and N. S. Gingrich—No. 7

Germer, L. H.—No. 3
Gingrich, N. S.—see Einstein, A.

Ham, W. R.—see Bennett, F. D.
Harding, S. W., F. R. Smith, and W. P. Davey—No. 6
Haworth, C. C., Jr. and F. C. Todd—No. 17
Hillier, J., R. F. Baker, and V. K. Zworykin—No. 8
Hipple, John A. and D. P. Stevenson—No. 9

Kent, C. V. and J. M. Cork—No. 11

McMurry, Henry L.—No. 18

Nadro, Edward—see Cannon, M. R.

Osterberg, H.—No. 13

Pfister, R. J. and D. H. Rank—No. 15

Rank, D. H.—see Pfister, R. J.

Skellett, A. M.—No. 5
Smith, F. R.—see Harding S. W.
Stevenson, D. P.—see Hipple, John A.
Swann, W. F. G.—see Weisz, Paul

Todd, F. C.—see Haworth, C. C., Jr.

Vaughan, Evans—see Anslow, Gladys A.

Weisz, Paul and W. F. G. Swann—No. 20
Winans, J. G. and Stanley Breen—No. 10
Woodson, Robert A.—No. 12

Yeagley, Henry L.—see Coleman, Howard S.

Zworykin, V. K.—see Hillier, J.

Proceedings of the American Physical Society

MEETING AT BERKELEY, CALIFORNIA, JULY 11, 1942

THE 250th meeting of the American Physical Society was held in Berkeley, at the University of California, on Saturday, July 11, 1942. The attendance at the two sessions varied from 60 to 75, and 34 members and guests had luncheon together at the Faculty Club. Of the 27 papers of which the abstracts are given below, Nos. 14, 19, and 23 were read by title.

This meeting would normally have been held at Salt Lake City in June, in conjunction with the A.A.A.S., but the war conditions seemed to make a change imperative. In spite of the fact that the great majority of both professional physicists and graduate students on the Pacific Coast are now engaged in war work, the number of contributed papers was only 20 to 25 percent below normal, and the attendance was fully up to normal. Dr. Darrow, national secretary, was present at the meeting, and he assisted in presiding.

R. T. BIRGE
Local Secretary for the Pacific Coast

ABSTRACTS OF CONTRIBUTED PAPERS

1. Some Isotope Shifts in the Atomic Spectrum of Nitrogen. J. R. HOLMES, *University of California.* (*Introduced by F. A. Jenkins.*)—The line spectrum of a mixture of N^{15} and N^{14} kindly furnished by Professor H. C. Urey was photographed with a Fabry-Perot interferometer. A liquid-air cooled quartz tube with external electrodes excited by a 12-meter oscillator was used as a source. The tube was charged with helium at a few mm pressure containing about 0.03 mm of a mixture of the nitrogen isotopes. The lines from this discharge were so sharp that it was possible to resolve completely the two components due to N^{14} and N^{15} in nine infra-red lines. No nitrogen lines were found in this discharge in the visible and ultraviolet. The oscillator excitation produced a remarkably high intensity in the lines found. The lines of $^4P \rightarrow {}^4P$ and $^4S \rightarrow {}^4P$ transitions showed a negative isotope shift of the order of 0.06 cm^{-1}. $^2P \rightarrow {}^2P$ transitions showed a positive shift of the order of 0.07 cm^{-1}. The variations in the isotope shifts within the $^2P \rightarrow {}^2P$ multiplets indicate some deviation from Russell-Saunders coupling No. hyperfine structure in either component was observed in any of the lines. The directions of the shifts were checked by obtaining the abundance ratio of the isotopes in the discharge from the intensities of the isotopic heads in the second positive N_2 bands.

2. The Criterion for Streamer Formation. GERHARD L. WEISSLER AND LEONARD B. LOEB. *University of California.*—Meek's criterion for streamer formation is that the positive space charge tip field of an electron avalanche exceed $1 > K > 0.1$ times the impressed field. Evaluation of K is influenced by electron diffusion. Estimates of K had come from uncertain values of sparking potentials. A careful study of streamer onset in confocal paraboloid gaps in moist and dry air and H_2 at various pressures with evaluations of the diffusion correction have been made. It was observed that between atmospheric pressure and pressures where streamers cease, >200 mm, the value of K changes by factors of 2, 15, and 25 in dry air, room air, and H_2. The effect also appears if consistent sparking potential data are used. Errors due to method of calculation of space charge fields, while modifying, are not responsible. Though interpretation is not complete, present indications are that density of photoionization is more important than tip field in streamer propagation. Despite these observations, Meek's criterion for spark breakdown still applies in practice with $K \sim 0.1$ for air, within experimental error.

3. Electrical Breakdown in Vacuum Between Electrodes of Large Area. HOWARD S. SEIFERT, *Westinghouse Research Laboratories.*—Studies of vacuum sparks have been made heretofore with small electrodes. An increase in electrode area increases the probability of breakdown and permits examination of its statistical distribution. Concentric steel cylinders with an area of about 500 cm^2 and a spacing of 7 mm were mounted in a Pyrex envelope which was evacuated to pressures between 10^{-5} and 10^{-6} mm of Hg. Voltages to about 100 kv were applied in an effort to determine frequency of breakdown as a function of applied voltage. Voltage at which breakdown occurred depended in a complex manner upon the following factors: (1) number of previous breakdowns, (2) energy dissipated per breakdown, (3) electrode smoothness, cleanliness, and outgassing, (4) geometrical disposition of insulation with respect to high field stress, and surface condition of insulation, (5) geometry and polarity of electrodes, with special reference to bombardment of insulators by electrons, (6) gas pressure and rate of pumping. Irregular background currents of the order of 0.1 ma were observed at voltages above

60 kv, usually accompanied by fluorescence on the quartz insulating supports. It is believed that removal of all insulation from regions of strong electric field should increase the voltage limits attainable before breakdown. Experiments are under way to test this assumption.

4. Determination of Toluene by Ultraviolet Absorption Spectrophotometry. L. R. ZUMWALT, R. R. BRATTAIN, AND O. BEECK, *Shell Development Company, Emeryville, California.*—Hydrocarbon mixtures of narrow boiling range are analyzed for toluene by ultraviolet absorption spectrophotometry. Analytical samples are suitably diluted with *n*-heptane and the optical density of the solution at the toluene absorption band (268.3 mμ) is measured with a Beckman photoelectric spectrophotometer.[1] The measurement allows the determination of the toluene content of a sample to be made with an accuracy of about one percent. Conjugated diolefins which often are present in the hydrocarbon mixtures absorb strongly in this region. Therefore, a treatment of the diluted sample with aqueous alkaline potassium permanganate has been devised to remove diolefins in order to eliminate interference with the analysis. If the hydrocarbon mixtures contain olefins or if the toluene content is very low, the spectrophotometric method is found to be superior to all other known physical or chemical methods for the determination of toluene.

[1] H. H. Cary and A. O. Beckman, J. Opt. Soc. Am. **31**, 682 (1941).

5. A New Band in the Infra-Red Absorption Spectrum of Ethylene. R. S. RASMUSSEN, *Shell Development Company, Emeryville, California.* (*Introduced by O. Beeck.*)—Several absorption maxima not previously reported were found in the infra-red absorption spectrum of ethylene in the region 12.5 to 14.5μ. The spacing is correct for maxima of an ethylene perpendicular type band, and all other indications point to the band not being due to impurity. The band is weak, requiring a fairly high pressure to bring it out. Only ^{P}Q maxima were observed, since the ^{R}Q side and the center are overlain by the strong 950 cm^{-1} band. There is no ^{Q}Q branch, indicating that the band is of the B_{1u} type.[1] From the intensity distribution the origin is at 800$\pm$5 cm^{-1}. The band cannot be interpreted as a difference band between any known frequencies. Assuming it to be the fundamental ν_9^2 places ν_{10} at *circa* 1247 cm^{-1}, from the combination band at 2047 cm^{-1}. These values for ν_9 and ν_{10} explain the observed combinations in C_2H_4 and C_2D_4 in a more satisfactory way than previous assignments.[2] To fit the observed C_p data,[1] the torsional frequency must have a value of about 950 cm^{-1}.

[1] E. J. Burcik, E. H. Eyster, and D. M. Yost, J. Chem. Phys. **9**, 118 (1941).
[2] W. S. Gallaway and E. F. Barker, J. Chem. Phys. **10**, 88 (1942).

6. Possible Assignment of the Long-Lived Yttrium. A. C. HELMHOLZ, *Radiation Laboratory, University of California.*—Dubridge and Marshall[1] tentatively assigned the 100-day yttrium to Y^{86}. Because of the large yield of this radioactive isotope from Sr+16-Mev deuterons,[2] it is suggested that Y^{88}, formed from Sr^{88} $(d, 2n)$ rather than Y^{86} formed from the eight times less abundant Sr^{86} is responsible. To test this hypothesis Y was bombarded with fast neutrons for four months. The sample then showed an activity of half-life approximately 100 days and a γ-ray absorption curve similar to that from the long-lived yttrium. The reaction would be Y^{89} $(n, 2n)$ Y^{88}. Y^{86} could be formed only from Y $(n, 4n)$. The weakness of the activity and the possibility of other rare earth contaminations, however, make the assignment uncertain. If it is correct, the long-life yttrium would be an isomer of the 2-hr. Y^{88} and at least 0.5 Mev higher in energy. A measurement of the half-life on a sample from deuteron bombardment gave 87$\pm$6 days.

[1] L. A. Dubridge and J. Marshall, Phys. Rev. **58**, 7 (1940).
[2] A. C. Helmholz, C. Pecher, and P. R. Stout, Phys. Rev. **59**, 902 (1941).

7. A Cloud-Chamber Study of Heavy Particles Accelerated in the Cyclotron. RICHARD CONDIT, *Radiation Laboratory, University of California.* (*Introduced by E. O. Lawrence.*)—It has been found possible to produce $^{12}C^{6+}$ of energy 85 Mev and $^{16}O^{8+}$ of energy 113 Mev with the 60″ Berkeley cyclotron. Very small beams of these high speed particles were led from the cyclotron through a thin window into a Wilson cloud chamber of conventional design. Range-velocity measurements have been made for carbon at three new points, extending the known relation from a range of 0.8 cm normal air to a range of 20 cm. Two new points for oxygen have also been obtained, and the range-velocity relation extended from 5 mm to 18 mm normal air. Pictures have been obtained of the carbon and oxygen beam penetrating Cellophane and gold targets in the cloud chamber. Typical examples have thus been obtained of the scattering and straggling of these heavy particles. Many interesting chance collisions of the accelerated particles with gas atoms and with target atoms have been photographed. Some insights into the cyclotron appeared in the course of the research. A variation of heavy particle range with dee voltage was observed. Harmonic acceleration, the simultaneous appearance of accelerated ions with $e/m = \frac{1}{2}, \frac{1}{6}, \frac{1}{10}$, etc., have been demonstrated.

8. Determination of h/e by Means of the Short Wave Length Limit of the Continuous X-Ray Spectrum at 20 kv. W. K. H. PANOFSKY, J. W. M. DUMOND, AND A. E. S. GREEN, *California Institute of Technology.*—A final value of $1.3786 \cdot 10^{-17}$ erg sec./e.s.u. is obtained for the value of h/e by the method of isochromats as applied to the continuous x-ray spectrum. The accuracy of the experiment is materially improved by: (1) large primary x-ray intensity, (2) the use of a high resolving power 2-crystal spectrometer in conjunction with a set of balanced filters; (3) improved accuracy in voltage measurement and voltmeter standardization; (4) cleaning of the x-ray tube target in vacuum. The result is shown to be in fair, though not complete, agreement with other determinations of functions of the atomic constants. The probable error of the result is estimated as 1.6 parts in 10^4.

9. The Properties of Certain Crystals and the Value of the Avogadro Number N_0. R. T. BIRGE, *University of California.*—The value adopted for N_0 is normally one based solely on the properties of calcite—its density ρ, molecular weight M, structure constant ϕ, and lattice con-

stant d. (The value of d is obtained from ruled grating wave-lengths of x-rays, and corresponding Bragg reflection angles.) In the case of any other crystal, it is customary to use an assumed value of N_0, in order to evaluate ρ, *or* d, *or* M for the crystal. But recent accurate measurements by Johnston and Hutchison of the density of LiF and NaCl, and by Bearden of the density of diamond, make possible new precision determinations of N_0 from the properties of these three crystals. A detailed study has been made of the experimental values of ρ, d, and M for calcite, rocksalt, diamond, and LiF. The *best* crystals of these substances show little variation in either d or ρ, and the resulting values of N_0 form the consistent set—6.02276 ($CaCO_3$), 6.02392 (NaCl), 6.02323 (LiF), and 6.02335 (C), all $\times 10^{23}$. The unweighted average, 6.02331, is only nine parts in 10^5 above the calcite value, and the results, taken collectively, furnish strong evidence that selected specimens of these four types of crystals may be considered geometrically perfect to at least one part in 10^4.

10. Preparation of Ross Filters. PAUL KIRKPATRICK, *Stanford University.*—Ross filters for x-ray monochromatization have usually consisted of metal sheets. For some frequency regions no metals exist. Often rolling to the required thinness is impracticable. For intensity measurements on nickel lines, copper, nickel, cobalt, iron, and manganese filters were required. Nickel was rolled to 0.0090 cm and a copper filter balanced to it by electroplating. Manganese was condensed on aluminum leaf in vacuum, and cobalt and iron were brought to balance with it by electroplating on aluminum from ferrous and cobaltous ammonium sulfate solutions. In another case a tantalum filter was brought accurately to balance against tungsten by grinding. For the highest frequencies aqueous solutions of thorium and uranyl nitrates in special cells have been used. Elements available in fine powders but not in thin sheets have been made into filters by kneading the powder uniformly into warm paraffin wax of high melting point and pressing the mixture between spaced glass plates. The balance error resulting from dissimilarity of K jumps may be corrected by perforation of one filter or by reduction of the effective area of one. Theoretically two filters may be brought to balance at any number of wave-lengths by giving one the proper thickness distribution.

11. Absolute K-Ionization Cross Section of the Nickel Atom under Electron Bombardment. A. E. SMICK, *Stanford University.* (*Introduced by P. Kirkpatrick.*)—Nickel targets about 5×10^{-6} cm in thickness, prepared by evaporation in vacuum and condensation upon thin cellulose acetate films, were bombarded with 70-kv electrons. The frequency of K-ionization was calculated from the observed intensity of emitted $K\alpha$ radiation. In the measurement of this radiation the lines were isolated by Ross filters of copper and nickel, the continuous background correction being evaluated by the use of filters of cobalt, iron, and manganese. (See Abstract No. 10.) A large standard ionization chamber connected to a calibrated electrometer received the radiation. The effects of absorption of the K radiation in the target, the various windows, the atmospheric air, and the gas (air) in the ionization chamber were duly considered and evaluated. Further corrections were applied for (a) electron retardation in the target, (b) single and multiple scattering of electrons within the target, (c) rediffusion by the cellulose backing and adjacent metals, (d) excitation of fluorescence radiation in the target, (e) scattering and fluorescence in the ion chamber, (f) ion current saturation deficiency. Results from different targets agreed closely and yielded as the most probable cross section 3.49×10^{-22} cm². Existing theories are not sufficiently precise for useful comparison, but Bethe's order-of-magnitude theory is not inconsistent with this result.

12. Energy Expended in Ionizing Argon by X-Rays. DAVID B. NICODEMUS, *Stanford University.* (*Introduced by P. Kirkpatrick.*)—A new method suggested by P. Kirkpatrick for making absolute intensity measurements of monochromatic x-rays has been used to determine the average energy expended in producing a pair of ions in a gas. This quantity ϵ is obtained by dividing the energy flux in a beam of x-rays by the rate at which it forms ions. X-rays are monochromatized by a calcite crystal and pass through a cloud chamber which produces photoelectron tracks that are recorded photographically. Since each track represents the true absorption of one quantum, the energy flux in the x-ray beam can be expressed as $Nhc/t\lambda f$ where N is the average number of tracks produced for an exposure time t, λ is the wave-length of the x-rays, and f is the fraction of the beam photoelectrically absorbed in the cloud chamber. The cloud chamber is replaced by a standard ionization chamber connected to a calibrated Compton electrometer that measures the rate at which ions are produced by the same x-ray beam. For argon at wave-lengths of 0.709A and 1.54A the measured values of ϵ are identical to within experimental error and give $\epsilon=27.4$ electron volts per ion pair.

13. The Effect of Temperature on the Production of the Afterglow of Active Nitrogen. DAVID E. DEBEAU, *University of California.* (*Introduced by Leonard B. Loeb.*)—The effect of liquid air temperature on active nitrogen has been studied. An electrodeless discharge in N_2 at a pressure of 0.5 mm of Hg gives rise to the afterglow and nearly doubles the pressure, with but a slight increase in temperature of the glass walls. Application of liquid air to less than one percent of the area of the system reduces the pressure to its original value. The afterglow is first intensified at the cold surface, then disappears, reappearing first near the cold surface after the liquid air evaporates. The pressure changes are too great to be explained by temperature changes alone, but can be attributed to the nearly complete dissociation of the N_2 in the discharge. This conclusion also follows from the results on the energy of active N_2 recently published by Rayleigh. J. J. Thomson believed that these intensity changes proved that liquid air condensed an active component of the afterglow. However, if it is assumed that the active N_2 precursor, molecular nitrogen in the B state, is one of the products of the recombination of nitrogen atoms, the observed intensity effects can be explained by the changes in the rates of the reaction involved.

14. The Orientation of Ellipsoidal Spores while Falling in Air. C. E. YARWOOD AND W. E. HAZEN, *University of California.* (*Introduced by R. B. Brode.*)—The spores of the powdery mildew *Erysiphe graminis D. C.* are one-celled, smooth-surfaced prolate ellipsoids (13×32 microns) with a large central nucleus and have a terminal velocity of 1.2 cm per second in air. When caught on glass slides after falling through air confined in a large can or a glass tube, many of the spores are found standing on end. Spores which had fallen at least 50 cm in a 7-mm glass tube were observed and photographed with a horizontal microscope (100× magnification) and 45-degree illumination from a commercial adaption of the Edgerton flash apparatus. Six-hundred spores were observed visually and sixty-five photographically. About one-half were oriented vertically and the other half horizontally. Hydrodynamic theory gives $3mv^2 \sin 2\theta$ for the restoring torque tending to orient the axis of the spore perpendicular to the direction of motion in the case of non-viscous motion. About 0.1 sec. after starting from rest this torque (for $\theta = 45°$) is so small that a displacement of the center of gravity by one percent of the spore length would orient half the spores vertically if they were randomly oriented at that time. When the air is undisturbed the spores would continue indefinitely with horizontal or vertical orientation.

15. Radioactive Sulfur from Neutron Activation of Chlorine Isotopes. M. D. KAMEN, *Radiation Laboratory, University of California.*—Samples of silver chloride, identical except for relative abundance of the two chlorine isotopes, were exposed to neutrons from the 60-inch Berkeley cyclotron. Due to the low weight (~10 mg) of the samples, a bombardment of four months was needed to obtain sufficiently active samples of the long-lived sulfur produced by the (n, p) reaction on chlorine.[1] Carrier sulfur in various valence forms was added and the samples assayed quantitatively by identical chemical procedures. From the relative activities obtained in this fashion, it was found that the amount of active sulfur produced was proportional to the Cl^{35} and not Cl^{37} present. Hence the assignment of the 88-day activity of sulfur is unambiguously fixed as S^{35} in agreement with that previously found by cross section arguments.[2] A detailed report will be published later.

[1] E. B. Anderson, Zeits. f. physik. Chemie **B32**, 237 (1936).
[2] M. D. Kamen, Phys. Rev. **60**, 537 (1941).

16. Neutron Polarization and Ferromagnetic Saturation. F. BLOCH, M. HAMERMESH, AND H. STAUB, *Stanford University.*—Measurements have been made to establish a quantitative connection between the transmission of magnetized iron for thermal neutrons and its magnetization. The change of transmission was obtained by observing the intensity of a well-collimated beam of thermal neutrons from the cyclotron, having passed through a plate of hot-rolled steel which in alternate runs was magnetized and demagnetized. The small deviations of the magnetization from its saturation value were then measured by the usual isthmus method, determining the change of B-H for values of H between about 500 and 4000 gauss. Two sets of data were taken with a total thickness of iron of 1.91 and 3.82 cm, respectively. The results strongly support the depolarization theory of Halpern and Holstein. We have verified over a fairly wide range the following dependence of the increase of transmission E upon the thickness d of the iron and the percentage deviation ϵ from saturation $E \sim d^2 f(\epsilon d)$. The theoretical form of the function f fits our data within the statistical error. By extrapolation we obtain for the increase of transmission through one cm iron on magnetizing it to complete saturation, 1.1 ± 0.2 percent.

17. A Study of Velocity-Selected Neutrons. E. M. FRYER, *Stanford University.* (*Introduced by F. Bloch.*)—The measurements have been made by means of a neutron-velocity selector similar to that of Baker and Bacher[1] and originally suggested by Alvarez.[2] The method consists in modulating the cyclotron arc with short pulses and applying similar short pulses displaced in phase to a discriminating stage in the amplifier of the counting circuit. A 2½-Mev deuteron beam and a beryllium target are used to obtain the neutrons, which are slowed to thermal velocities by paraffin. A collimated beam of thermal neutrons 2½″ in diameter and 10′ long is used. Neutrons with energies corresponding to a temperature range of 50°K to 400°K have been studied. Absorption measurements have been made with an absorption cell 20 cm long filled with BF_3 under two atmospheres pressure and the $1/v$ law for the cross section of boron verified within five percent. A distribution curve of the thermal neutrons shows a maximum at an energy corresponding to 300°K, and a half-width of roughly 200°K.

[1] C. P. Baker and R. F. Bacher, Phys. Rev. **59**, 332 (1941).
[2] L. W. Alvarez, Phys. Rev. **54**, 609 (1938).

18. A Method of Cooling Hydrogen Discharge Tubes.* CHAO-WANG HSUEH, *California Institute of Technology.* (*Introduced by W. V. Houston.*)—Most workers on the fine structure of Balmer lines have used the Wood's discharge tube and cooled it in liquid air at ordinary atmospheric pressure. Spedding, Shane, and Grace tried to cool their tube with liquid hydrogen, which proved to be unsatisfactory. To reduce the heat generated in the discharge, an electrodeless tube excited by a short-wave (68–81 meters) oscillator has been used in our laboratory. We have tried a great number of experiments to cool our hydrogen discharge tube by means of liquid air evaporated rapidly with fast vacuum pumps. The main difficulties encountered were the leakage and the heat insulation of the system. The temperatures of the liquid air were measured with a copper-constantan thermocouple, which was calibrated at the boiling points of liquid hydrogen, nitrogen, and oxygen, the sublimation point of carbon dioxide, and the freezing points of mercury and of other organic compounds. The usual procedure is to pump the liquid air until the lowest temperature is reached. Then the oscillator is started to excite the discharge tube, while the pumping is going on. In one of our measurements, the lowest temperature attained was 55.6°K and the temperature rose slowly to 55.9°K after the discharge tube was run for 45 minutes and longer.

* Aided by a grant from the Sigma Xi Alumni Research Fund.

19. On the Lack of Saturation of Exchange Tensor Forces. G. M. VOLKOFF, *University of British Columbia.*—Nuclear models based on *non-exchange* interactions between elementary particles lead to excessive nuclear binding energies; consequently *spherically symmetrical exchange* forces were originally introduced to account for the observed saturation. Recent suggestions of additional *tensor* forces find support in the discovery of the deuteron quadrupole moment, and in the results of various field theories of nuclear forces. The contribution to the nuclear binding energy made by these tensor forces was estimated by the Hartree method. If the tensor term, whether of the ordinary or of the exchange type, is assumed to be the dominant one in the interaction between a pair of nuclear particles, it will not lead to saturation, but will permit the existence of nuclei with excessive values of binding energy, spin, and isotopic number. A sufficiently strong spherically symmetrical exchange term in the interaction seems to be required to counteract this effect of the tensor forces. The feature of exchange tensor forces responsible for their lack of saturation is that a reversal of sign produced by the exchange operator may be compensated by a change in the distribution of the particles composing the nucleus from prolate to oblate.

20. Assay of Organic Molecules in Tissue from Absorption Spectra Using a Baly Tube and Densitometer. LOUIS A. STRAIT, *University of California.*—Ultraviolet spectrophotometers measure extinction coefficient or concentration of a solution within one percent. However, in analytical practice the unknown is rarely in a pure solution, being a product of preliminary extraction from a complex matrix. The unavoidable errors of extraction procedures may be tenfold the photometric error. A method which needs only a Baly tube, densitometer, and constant light source has been found convenient and sufficiently accurate. Cocaine assay from brain tissue and body fluids and assay of an estrogen from breast, tumor, and other tissues have been made. The extracted cocaine or estrogen in a quartz Baly tube was spectrographed in absorption with light from a hydrogen discharge tube. A standard solution of the cocaine or estrogen of appropriate concentration was photographed through a series of path lengths which would "map out" the absorption band over a range of densities. Transparencies of the unknown and standard concentrations were measured at wave-length of maximum absorption. From a graph (preferably log-log) of path length of known concentration *versus* transparency (Fig. 1) the corresponding path length of the unknown and, by application of Beer's law, its concentration may be evaluated. Significant data describing the permeability property of the blood-brain barrier are evidenced in Fig. 2, the relationship of estrogen to tumor formation in Fig. 3.

21. On Fitting Data with Polynomial Functions by the Method of Least Squares. J. WEINBERG, *University of California.* (*Introduced by R. T. Birge.*)—A general formula is derived for the coefficients of an nth degree polynomial $p_n(x)$ fitted by the method of least squares to data $y(x)$ for $x=0, 1, \cdots(N-1)$, where one uses the factorial form

$$p_n(x)=\sum_{m=0}^{n}(-)^m\binom{2m}{m}a_{mn}\binom{x+m}{m}\Big/\binom{N+m}{m}.$$

In particular,

$$a_{nn}=(2n+1/N)\binom{N-1}{n}^{-1}\sum_{x=0}^{N-1}y(x)$$

$$\times\sum_{k=0}^{n}(-)^k\binom{n+k}{k}\binom{N-k-1}{n-k}\binom{x}{k},$$

which confirms the expression obtained empirically by Birge and Shea[1] for the coefficient of x^n. For $m<n$, the general formula leads to

$$a_{mn}=\sum_{k=m}^{n}\binom{m+k}{2k}a_{kk}.$$

This corresponds to the rapid and direct mode of solution found by Birge and Shea, who, however, give explicit formulas only for $n\leqslant 5$.

[1] R. T. Birge and J. D. Shea, University of California Publication in Mathematics **2**, No. 5 (1927).

22. Theory of the Spread of Cosmic-Ray Showers. JANE ROBERG, *Duke University.* (*Introduced by L. W. Nordheim.*)—In continuation of the work reported at the Baltimore meeting the following results have been obtained. The mean square angular and lateral spreads of both shower electrons and photons above the critical energy have been obtained as function of energy for all substances. They have also been computed for air for the low energy range down to four Mev. The root mean square lateral deviation for electrons of all energies above four Mev is found to be 63 meters in normal air. In these calculations close approximations to the true probabilities for radiative effects have been used, and both pair production and Compton effects have been taken into account at low energies.

23. Multiple Scattering of Fast Electrons. C. W. SHEPPARD, *California Institute of Technology.*—The multiple scattering of B^{12} electrons has been studied in carbon and lead scatterers using G.M. coincidence counters. Comparison was made of scattering in two laminae of equal NTZ^2. The ratio of the arithmetical mean angles of scattering was nearly the same experimentally as given by the theoretical expression of Williams. The difference in transmission of carbon and lead scatterers was compensated for by placing the carbon scatterer between the counters when the lead was scattering, and vice versa. The mean error in the measured scattering ratio was estimated to be ten percent.

24. Measurement of the Ionization of Fast Mesotrons with a High Pressure Ionization Chamber. W. C. DUNLAP, *University of California.*—An ionization chamber and a pulse amplifier have been used to measure the ionization in argon of mesotrons capable of penetrating 8 cm of lead.

A pair of counters was mounted above and below the chamber so that a mesotron tripping the counter passed between two rectangular plates, one of which was the collector. A block of lead 7.5 cm thick was also inserted between the counters. Results were obtained by having the counters trip the sweep of an oscillograph connected to the output of the amplifier, so that the pulse size could be observed visually or from a photographic film. The amplifier was made after the design of Waddell, and was calibrated by means of an audiofrequency generator and with polonium α-particles. The apparatus was sensitive enough to detect cosmic-ray particles at atmospheric pressure. Measurements were made at pressures from 10 to 70 atmospheres. Calculations for a run at 25 atmospheres show an average ionization of 46 ions/cm at one atmosphere assuming all pulses due to single particles. These observations are being continued and extended.

25. Reduction of the Problem of Arbitrary Spin to That of Spin 1/2. F. BLOCH, *Stanford University.*—It has been shown by Majorana[1] and is implied in the usual group theoretical methods that the wave mechanics of a system with arbitrary angular momentum j (in units $h/2\pi$) can be reduced to that of a system with $j=\frac{1}{2}$. These rather abstract methods can be seen to be equivalent to the well-known vector model in which an angular momentum j can be represented as the sum of $2j$ angular momenta of value $\frac{1}{2}$. The mathematical expression of this fact is obtained by the symmetrized product of $2j$ arbitrary wave functions, each representing a system with spin $\frac{1}{2}$ and by showing that this yields the description of the most general state of a system with spin j. The transformation which a state of a system with arbitrary spin j undergoes under given physical conditions can be derived in an elementary way from that which a system with spin $\frac{1}{2}$ undergoes under the same conditions.

[1] E. Majorana, Nuovo Cimento **9**, 43 (1932).

26. A Simple Excitation Source for Quantitative Spectrochemical Analysis—Analysis of Pb in Tissues. LOUIS A. STRAIT, *University of California.*—A source of excitation suitable for quantitative spectrochemical analysis must vaporize the sample in a representative manner and must readily excite the components of the sample to give off characteristic radiations reproducibly. The reproducibility of excitation conditions in the condensed spark source previously described here[1] was limited by the degree of uniformity of the deposition of the sample on a lower moveable copper cylindrical electrode. The following modifications have simplified this source and extended its usefulness: I. Preparation of the sample: The sample is deposited on a thin paper (e.g., lens paper) and after drying the paper is wrapped around the lower cylindrical electrode. II. Excitation of the sample: The contents of the paper are vaporized and excited by feeding the paper covered cylinder into the electrical discharge between the upper point electrode and the cylinder. The discharge is uncondensed and is excited by the secondary of a 3-kva, 5000-volt transformer. The secondary current is 150 milliamperes. The source has been applied to the analysis for Pb of ashed samples of tissues and organs of mice. The customary procedure of analysis was followed using internal standard (Cd in this case) and "working" curves.

[1] Louis A. Strait, Phys. Rev. **56**, 855 (1939).

27. Application of the Edgerton Lamp to Droplet Counting. W. M. POWELL, *Kenyon College.**—A Wilson cloud chamber fourteen inches deep and eight inches in diameter is illuminated by two beams of light which enter the chamber at the base of the cylinder and cross in the middle. The chamber is surrounded by Helmholz coils which give a magnetic field of 2500 oersteds. The light source consists of two rectangular tubes ten cm long and 3.2 by 0.8 cm in cross section. The electrodes are 40-mil tungsten T's 8.2 cm apart. Two of these tubes are connected in series with a 150-μf condenser which is charged to 2000 volts. They stand behind condenser lenses 4.5 inches in diameter and 3 inches in focal length. The tubes are filled with a very small amount of hydrogen and 3.5 cm of argon. Two pieces of chromium plated brass are pressed against the back of the two tubes. They perform the double service of mirrors and tickler electrodes. Droplets were photographed 0.15 sec. or less after expansion of the chamber with an F number of 9 and appeared to be overexposed by about four times. The illumination appears to be quite uniform.

* Guggenheim Memorial Fellow now at the University of California.

AUTHOR INDEX TO ABSTRACTS OF PAPERS PRESENTED AT THE BERKELEY MEETING

Beeck, O.—see Zumwalt, L. R.
Birge, R. T.—No. 9
Bloch, F.—No. 25
Bloch, F., M. Hamermesh, and H. Staub—No. 16
Brattain, R. R.—see Zumwalt, L. R.

Condit, Richard—No. 7

Debeau, David E.—No. 13
DuMond, J. W. M.—see Panofsky, W. K. H.

Dunlap, W. C.—No. 24

Fryer, E. M.—No. 17

Green, A. E. S.—see Panofsky, W. K. H.

Hamermesh, M.—see Bloch, F.
Hazen, W. E.—see Yarwood, C. E.
Helmholz, A. C.—No. 6

Holmes, J. R.—No. 1
Hsueh, Chao-Wang—No. 18

Kamen, M. D.—No. 15
Kirkpatrick, Paul—No. 10

Loeb, Leonard B.—see Weissler, Gerhard L.

Nicodemus, David B.—No. 12

Panofsky, W. K. H., J. W. M. DuMond, and A. E. S. Green—No. 8
Powell, W. M.—No. 27

Rasmussen, R. S.—No. 5
Roberg, Jane—No. 22

Seifert, Howard S.—No. 3
Sheppard, C. W.—No. 23
Smick, A. E.—No. 11
Staub, H.—see Bloch, F.
Strait, Louis A.—Nos. 20 and 26

Volkoff, G. M.—No. 19

Weinberg, J.—No. 21
Weissler, Gerhard L. and Leonard B. Loeb—No. 2

Yarwood, C. E. and W. E. Hazen—No. 14

Zumwalt, L. R., R. R. Brattain, and O. Beeck—No. 4

Information For Contributors

THE Editors of THE PHYSICAL REVIEW would be aided in their task if the following items were used as a guide by all contributors.

MANUSCRIPTS

Send manuscripts to J. W. Buchta, Department of Physics, University of Minnesota, Minneapolis, Minnesota.

Papers must be in English, typewritten double spaced with wide margins on a durable white paper, preferably lettersize. The original copy, not the carbon, should be submitted.

For general style, spellings, abbreviations and form, recent issues of this journal should be consulted.

ABSTRACTS

An abstract must accompany each article. It should be adequate as an *index* and as a *summary*. As an index it should give all subjects, major and minor, concerning which new information is presented. As a summary it should give the conclusions of the article and all numerical results of general interest.

MATHEMATICAL EXPRESSIONS

Make all expressions clear to the typesetter. Identify in the margin of the manuscript Greek letters and unusual symbols.

Use fractional exponents instead of root signs.

Avoid complicated exponents and subscripts. Should it be necessary to repeat a complicated expression a number of times it should be represented by some convenient symbol.

The solidus (/) should be used wherever possible for fractions.

REFERENCES

References should appear as footnotes, numbered consecutively, and arranged thus:

[1] A. B. Smith, Phys. Rev. **41**, 852 (1932).
[2] G. R. Harrison, *Atoms in Action* (William Morrow & Company, New York, 1939), first edition, p. 30.

FIGURES AND TABLES

Legends for figures must accompany manuscript. Each table should have a caption. These in all cases should be complete in themselves so as to make the data intelligible to the reader without reference to the text. Each figure and table should be cited in sequence in the text.

LINE DRAWINGS AND PHOTOGRAPHS

Plan figures for reduction to one third or one fourth the original size. Wherever possible arrange figures so that after reduction they will not be wider than three inches. Lettering must be large enough to be readable (about 3 mm high) after reduction. The figures should be so arranged that the space is used efficiently.

Line drawings must be made with India ink on white paper or tracing cloth. Coordinate paper is not desirable, but if used must be blue-lined and all coordinates to be reproduced drawn with India ink.

Drawings which cannot be used will be returned to the author.

Photographs of drawings seldom are satisfactory. They often do not show clear black and white contrasts and are not suitable for relettering which is sometimes necessary. Photographs of apparatus seldom give as much information as drawings.

Please avoid round or oval photographs.

ALTERATIONS

Take great care that each manuscript is typographically accurate. A limited number of alterations in proof are unavoidable, but the cost of making extensive alterations after the article has been set in type will be charged to the author.

Proof and all correspondence concerning papers in the process of publication should be addressed to the Publications Manager, American Institute of Physics, 175 Fifth Avenue, New York, New York.